Preparation, Separation, Characterization and Hydrogenation of Endohedral Metallofullerenes

Wujun Fu

Dissertation submitted to the Faculty of Virginia Polytechnic Institute and State University in partial fulfillment of the requirements for the degree of

Doctor of Philosophy
in
Chemistry

Harry C. Dorn, Chair
Harry W. Gibson
John R. Morris
James R. Heflin
Alfred L. Ritter

December 10, 2009

Blacksburg, Virginia

Keywords: Yttrium-based, Endohedral, Di-metallic, Metal-carbide, Metallofullerene , Metalloheterofullerene, Hydrogenation

Preparation, Separation, Characterization and Hydrogenation of Endohedral Metallofullerenes

Wujun Fu

Abstract

Endohedral metallofullerenes (EMFs) have attracted increasing attention during past decades due to their novel structures and potential applications in a variety of fields such as biomedical applications and molecular electronics. This dissertation addresses the structural characterization and hydrogenation of EMFs.

A family of novel large cage yttrium-based TNT EMFs $Y_3N@C_{2n}$ (n=40-44) was prepared, separated, and structurally characterized for the first time. The structure of $Y_3N@C_{2n}$ (n=40-44) is proposed by the experimental and computational ^{13}C NMR studies. The first ^{89}Y NMR results for $Y_3N@I_h$-$C_{80,}$ $Y_3N@C_s$-C_{84} and $Y_3N@D_3$-C_{86} reveal a progression from isotropic to restricted $(Y_3N)^{6+}$ cluster motional processes.

The *di*-metallic EMF Y_2C_{94} is distinguished as a metal-carbide based EMF, $Y_2C_2@D_3$-C_{92}. The carbide within the cage is successfully detected by ^{13}C NMR. The scalar $J_{Y\text{-}C}$ coupling between the yttrium atoms and the C_2 unit within the C_{92} cage is successfully observed, suggesting the C_2 unit rotates rapidly around the yttrium atoms.

Two paramagnetic endohedral metalloheterofullerenes, $Y_2@C_{79}N$ and $Gd_2@C_{79}N$, were also synthesized and characterized. The EPR study demonstrated that the spin density is mainly localized between the two metallic ions. A spin-site exchange system could be constructed between $Y_2@C_{79}N$ and the organic donor TMPD. Being a

unique paramagnetic material, $Gd_2@C_{79}N$ displays an unusual stability over a wide temperature range, which could be very useful in optical and magnetic areas.

Functionalization of EMFs is another point of interest in this dissertation. Hydrogenated $Sc_3N@C_{80}$ was synthesized and characterized. Our study demonstrated that the $Sc_3N@C_{80}$ can be fully hydrogenated and the pristine $Sc_3N@C_{80}$ can be recovered from $Sc_3@C_{80}H_{80}$ after being heated in vacuum. The hydrogenated EMFs could be potential hydrogen storage materials.

Acknowledgements

The completion of my doctoral degree would have never been possible without the advice and encouragement of many people.

First, I would like to thank my Ph.D. advisor, Professor Harry C. Dorn, for his guidance, inspiration and support during my entire Ph.D. period at Virginia Tech. I have earnest respect to his great personality, serious academic manner, profound knowledge and dedication to science. His continual patience and encouragement make me less stressful and more confident to face the challenges. I am so fortunate to carry out this research under his guidance.

I would also like to express my sincere appreciation to my committee members, Professor Harry W. Gibson, Professor John Morris, Professor Randy Heflin and Professor Jimmy Ritter. Without their insightful and supportive supervision, this dissertation could not have been completed and I would never achieve this degree.

There are several other faculty members and staff that I would like to acknowledge. I thank Professor Paul Deck for allowing me to use the glove box in his laboratory and his guidance with departmental policies. I thank Professor James E Mahaney (Edward via Virginia College of Osteopathic Medicine) for allowing me to use his EPR instrument. I thank Professor Tatsuhisa Kato (Josai University, Japan) for his help in low temperature EPR measurements. I would like to thank Dr. Hugo Azurmendi and Tom Glass in timely analytical support in running NMR samples. I thank Dr. Jerry Dallas and Dr. Daniel Bearden (Hollings Marine Laboratory) for their NMR measurements at 800 MHz instrument. I thank Dr. Carla Slebodnick for her

help in single crystal X-ray crystallography studies. I thank Mr. Frank Cromer for his help to perform XPS analyses. I also thank Mr. Kim Harich for his help to perform mass spectrometric analyses.

My great appreciation also goes to all my group members, Professor James Duchamp (Emory and Henry College), Tim Fuhrer, Liaosa Xu, Hunter Champion, Jianfei Zhang, Jianyuan Zhang, Dr. Chunying Shu, Dr. Jiechao Ge and Stephanie J. Hurt. I especially would like to thanks to my colleague Tim and Liaosha for their collaboration on the DFT computation studies. I also thank Hunter for his help on electrochemical measurements and Dr. Ge's help on material supply. I also thank Professor James Duchamp for all his helpful discussion and suggestions over the past few years. I would also like to thanks those past group members, Tianming Zuo, Ting Cai, Xuelei Wang, Jonathan Reid and Jenny Russ.

Finally, I would like to thank my family for their selfless love and support. I can't image how can I went through the tough times without their company. They were always there for me whenever I needed them.

List of Figures

Chapter 1

Chapter 3

Chapter 4

Chapter 5

Chapter 6

List of Tables

Chapter 1

Chapter 4

Chapter 1

Introduction and Background

1.1. Introduction

Fullerenes, the third allotrope of carbon after graphite and diamond, were first discovered in 1985 by Kroto and co-workers[1] when they investigated the carbon clusters generated from laser vaporization of graphite in a high-pressure supersonic nozzle. In order to explain the prominent intensity of peak *m/z*=720 of stable carbon cluster in mass spectra, the truncated icosahedral (I_h) symmetry of the C_{60} molecule was proposed. The truncated I_h structure is a polygon which has 60 vertices, 32 faces and 90 edges and each carbon atom is placed on each vertex in a C_{60} molecule. Of the 32 faces, 12 faces must be pentagons and others are hexagons. It is much easier to visualize by comparing a soccer ball with an I_h-C_{60} fullerene cage (Figure 1.1). Both of them have the ball structure, which is composed of 12 pentagons and 20 hexagons, with each hexagon surrounded by 5 pentagons. Because of the empty soccer-ball-shaped cage of a C_{60} molecule, the term "buckyballs" has evolved as an interesting designation of this type of carbonaceous materials.[2]

The I_h symmetry of C_{60} was identified by four-band infrared (IR) vibrational absorption spectrum,[3] which is perfectly consistent with the theoretical prediction of I_h-C_{60} fullerene. Soon afterwards, the one-line ^{13}C NMR spectrum,[4] which is consistent with only one type of carbon atom in the C_{60} molecule, confirmed the I_h symmetry of

C_{60}. The latter paper reported the synthesis and separation of a series of empty fullerene cages, such as C_{70},[4] C_{76},[5] C_{78},[6, 7] C_{84}[7] and higher. "Fullerene" became the comprehensive name of this family of carbon molecules.

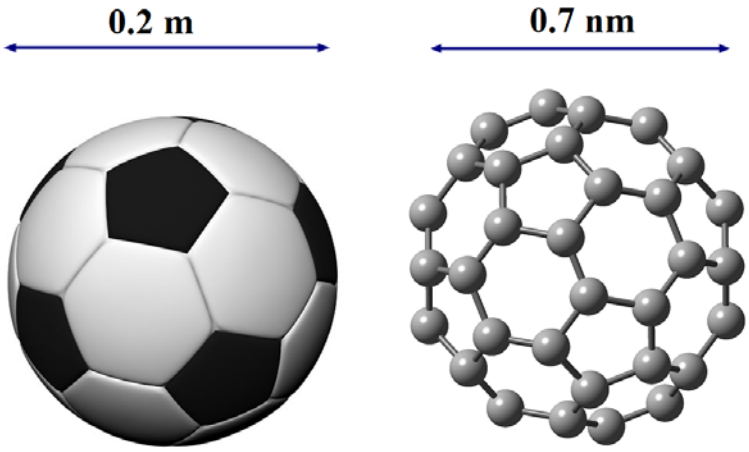

Figure 1.1. Comparison of structures of a soccer ball and an I_h-C_{60} fullerene.

The discovery of C_{60} attracted wide attention of scientists throughout the world. However, fullerene research was limited to theoretical studies in the early stage because only tiny amounts of materials were available in the 1980's.[8] In 1990, another exciting breakthrough in fullerene history was achieved by Krätschmer and Huffman.[3, 9] They reported a simple method that allowed the preparation of macroscopic quantities of fullerenes from the vaporization of inexpensive graphite rods – the so called Krätschmer and Huffman arc-discharge method.[9]

The availability of macroscopic amounts of fullerenes led to expanded research in the fullerene area, which widely spread throughout chemistry, biochemistry, physics, and materials science.

1.2. Preparation, Extraction and Separation

1.2.1 Preparation of Fullerenes

There are two methods that have been routinely used to prepare macroscopic amounts of fullerenes and metallofullerenes. They are the Krätschmer and Huffman arc-discharge method [9] and the laser ablation method.[6, 10]

The most popular method to produce the fullerenes and metallofullerenes is the AC/DC arc-evaporation technique by using a Krätschmer and Huffman generator (Figure 1.2). In the Krätschmer-Huffman method, a voltage is applied across two graphite rods by an AC/DC power supply. The carbon rods are vaporized at above 4000 °C by electric arc-discharge between two electrodes under helium flow. The vaporized small carbon clusters are annealed to form fullerenes at the outer sphere of the arcing plasma. The carbon soot generated in the arc condenses onto the bottom of the cylinder. For endohedral metallofullerenes (EMFs) production, the desired metal-oxide/graphite is packed into a hollow graphite rod, which is normally used as a positive electrode in the arc-vaporization process. The prime soot is collected for the further extraction.

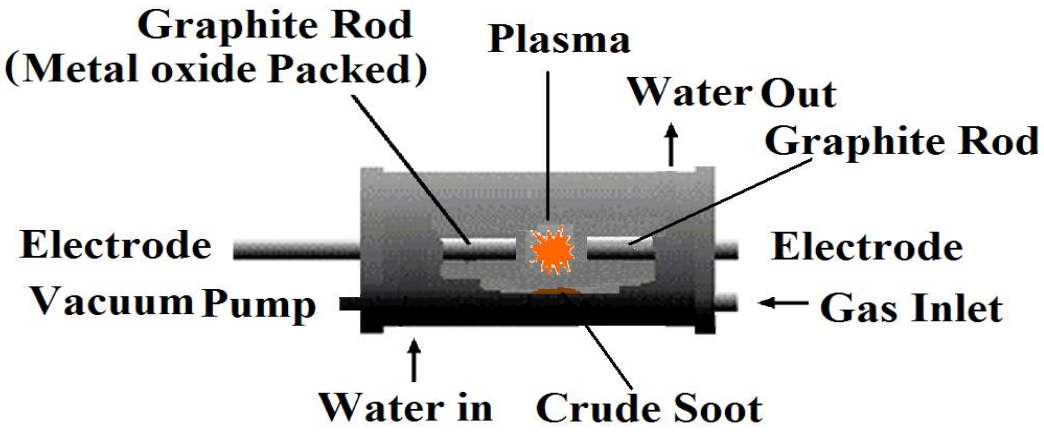

Figure 1.2. Krätschmer and Huffman generator for the production of fullerenes

The laser ablation technique is a less commonly used method, which is considered to be a valuable technique to investigate the formation mechanism of fullerenes.[11] In this method, a graphite rod is placed in a tube furnace and heated to 1200 °C. Then a Nd:YAG laser at 532 nm is focused on the rod. In order to get a fresh surface, the rod should be rotating in an argon gas flow (100-200 Torr). After the rod is consumed, the crude soot will be carried by argon gas and get trapped at the end of the quartz tube (Figure 1.3). The advantage of the laser ablation method is that it is easier to connect with the analytical instruments required for further characterizations, such as the mass spectrometer, etc. A similar method has been applied for the production of single-wall carbon nanotubes.[12]

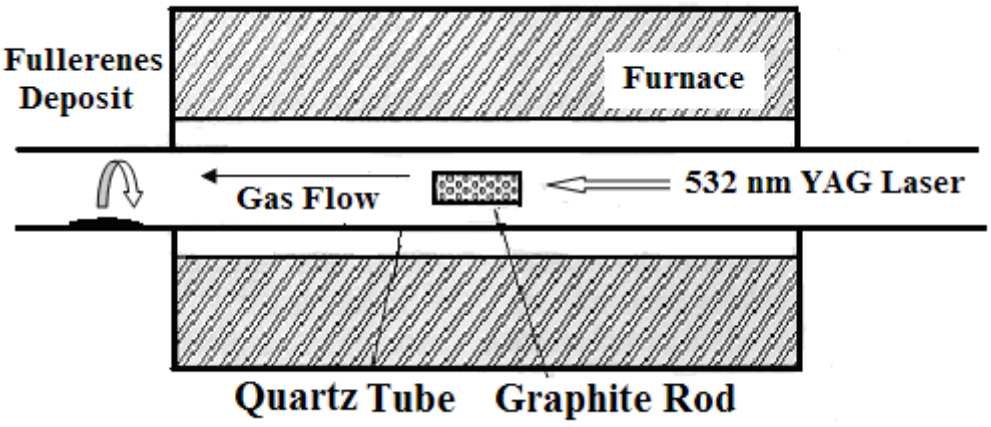

Figure 1.3. Schematic diagram of laser ablation apparatus

1.2.2. Extraction

The fullerenes are obtained by extracting the crude soot with organic solvents through a porous cellulose thimble. The fullerene mixture is soluble in some non-polar solvents,[13] such as benzene, toluene, carbon disulfide (CS_2), chlorobenzene and hexane. It is noted that the extraction efficiency is dependent on the solvent used for extraction.

Toluene is the most commonly used one because it has good solubility for fullerenes and is less toxic than CS_2 and benzene. Khemani's research group[14] reported that Soxhlet extraction with hot solvent can increase the efficiency of the solvent extraction. In comparison with a 14% yield by simple reflux, a 26% yield of soluble material can obtained. Parker *et al.*[15] reported a multi-step extraction using a combination of solvents that can increase the yield up to 44%. Non-soluble materials including amorphous carbon, graphite, and a small amount of carbon nanotube remain in the thimble after extraction.

Sublimation is the other method reported to isolate the fullerenes from the crude soot,[6] in which the raw soot is heated in helium atmosphere or under vacuum up to 400 °C for fullerenes to sublime. The advantage of sublimation is that it is solvent-free and suitable for large-scale extraction.

1.2.3. Separation and Purification

1.2.3.1. Separation by High Pressure Liquid Chromatography (HPLC)

Separation of individual fullerenes from crude soot extract is an important step for further applications. In 1990, Whetten *et al.* [13] first developed the separation of C_{60} and C_{70} molecules through column chromatography by using hexanes on silica and alumina gels. To date, the purification of an individual component from the fullerene mixture normally involves LC (Liquid Chromatography) and HPLC (High Pressure Liquid Chromatography) processes. Many novel stationary phases have been designed and applied in fullerene separations.

Octadecyl silica (ODS) is commonly used in the LC separation.[16] Being one of the most conventional stationary phase, ODS is commercially available and widely used. It is reported the polymeric ODS phases have good selectivity for the fullerene isomers.[17] However, the low separation efficiency limited its application. Therefore, several other novel stationary phases were developed and reported. [18-21]

PYE (2-(1-pyrenyl)ethylsilyl)[18] and Buckyprep (3-(1-pyrenyl)propylsilyl)[19] silica columns, as shown in Figure 1.4, are the most commonly used for high efficiency fullerene separation. PYE and Buckprep have the electron-donating pyrenyl moiety and have strong π-π stacking interactions with fullerenes in the mobile phase, which may be responsible for their high efficiency in fullerene separation. The structures of PYE and Buckyprep are similar. The only difference is that the Buckyprep has one more -CH_2- group than the PYE in the chain connecting the silica supporting material and pyrene group, indicating that the Buckyprep is more hydrophobic than the PYE column.

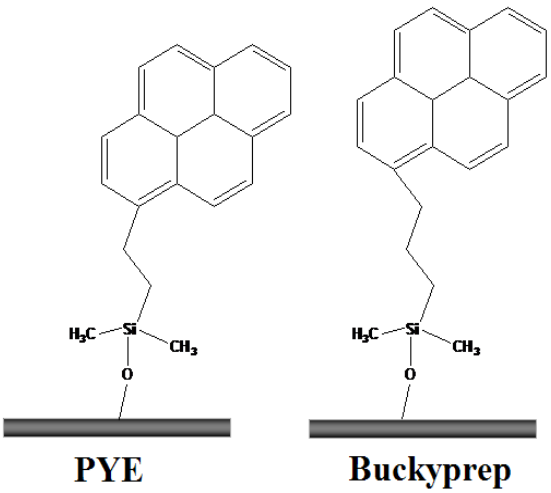

Figure 1.4. 2-(1-pyrenyl)ethylsilyl) (PYE) and 3-(1-pyrenyl)propylsilyl) (Buckyprep) stationary phase

The Buckyclutcher (tripodal 2,4-dinitrophenyl ether) (Figure 1.5) was developed by

Pirkle and Welch.[20, 21] The stationary phase has very polar moieties consisting of two electron-withdrawing nitro substituents on phenyl rings, which allow electron donor-acceptor interactions between the fullerenes and polar moieties. Because of this interaction, EMFs have longer retention times than empty cage fullerenes on the Buckyclutcher column. Thus, the Buckyclutcher is very useful for the separation of EMFs from empty cage fullerenes.

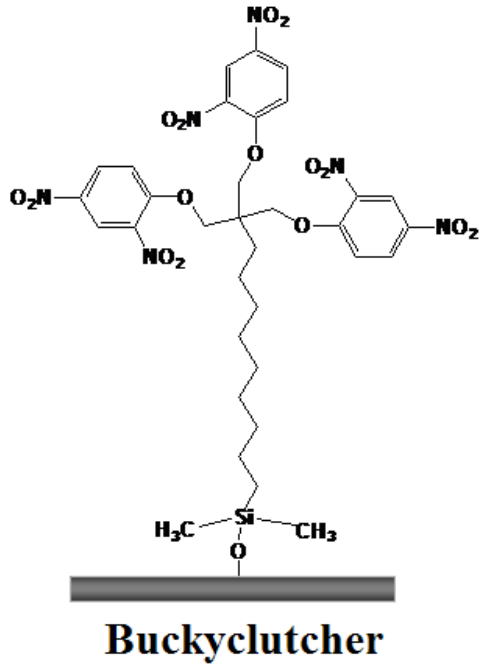

Figure 1.5. Tripodal 2,4-dinitrophenyl ether (Buckyclutcher) stationary phase

PBB (3-[(pentabromobenzyl)oxy]propylsilyl)[22] (Figure 1.6) is another effective stationary packing material for fullerene separations. The stationary phase of the PBB column contains five bromine atoms, which possibly result in longer retention of the fullerenes. One advantage of the PBB column is its higher loading capacity.[23] Therefore, the PBB column can be used in preparative separation. The other interesting property of the PBB column is that the retention behavior of a fullerene is proportional to its cage size. This property is extremely helpful in determining the size of a fullerene cage.

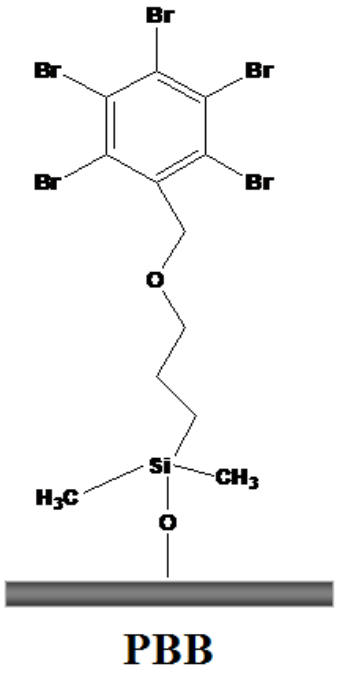

Figure 1.6. 3-[(pentabromobenzyl)oxy]propylsilyl (PBB) stationary phase

Stationary phases applied in separation of fullerenes have different absorption mechanisms. Therefore, in a specific separation process, based on the fullerene size, shape, molecular weight and polarity, a combination of these columns is desirable. For all metallofullerene purifications, a two- or three-phase sequence of HPLC columns with different absorption mechanisms is generally utilized.

1.2.3.2. Chemical Separation Approaches

Although over the years HPLC is the most powerful technique for fullerene separation, the poor solubility of fullerenes limits the sample loading and the separation process is usually time consuming. The preparation of microgram quantities of purified samples needs many days' labor. Thus, alternative purification methods are highly desirable and efforts have been made by several groups.

Aihara *et al.*[24, 25] predicted that the trimetallic nitride template endohedral metallofullerenes (TNT EMFs) are kinetically much more stable than empty cage fullerenes by calculating the minimum bond resonance energies for numerous fullerenes and metallofullerenes. Based on this prediction, two chemical separation approaches using Diels-Alder cycloaddition reactions have been developed by Dorn's group at Virginia Tech.[26, 27] The principles of these two methods are the same: C_{60} and other empty fullerenes are electron deficient and more reactive than EMFs in many reactions.

The first one is cyclopentadiene-functionalized Merrifield's peptide resin (CPDE-MPR) method,[26] which uses a CPDE-MPR stationary phase. When the mixture of empty cages and EMFs passes through the resin, the most stable TNT EMFs do not react with the CPDE-MPR and they are eluted out with the mobile phase. Other empty cages and endohedral fullerenes are more reactive and are covalently connected to the CPDE-MPR (Figure 1.7).

The other method is a support-free chemical separation by Diels-Alder cycloaddition of 9-methylanthracene with empty cage fullerenes.[27] After heating 9-methylanthracene with and Sc- and Lu-based soot extracts, most of empty fullerenes reacted with 9-methylanthracene and the derivatives can be removed by washing with ether. The remaining unreacted TNT EMFs can be easily purified by one-stage HPLC. This method is inexpensive and suitable for large scale separations.

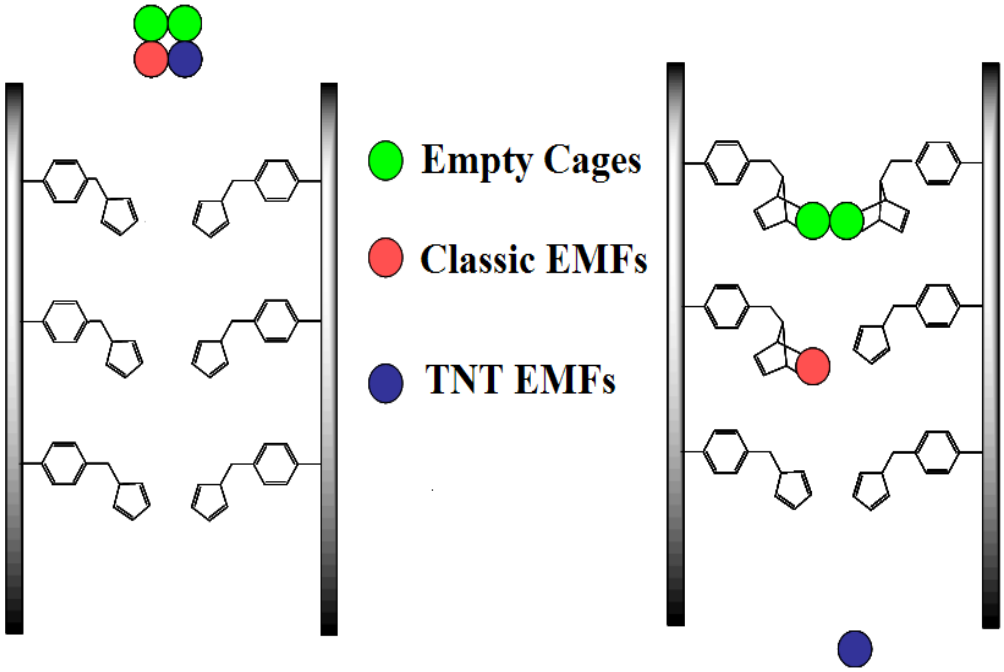

Figure 1.7. Schematic illustration of the strategy for separation of TNT EMFs from empty cage fullerenes by CPDE-MPR method [26]

1.2.3.3. Other Separation Approaches

A selective electrochemical reduction of the EMFs from carbon soot extracts was reported by Akasaka's research group.[28] $La@C_{82}$ and $La_2@C_{82}$ were selectively reduced to anions from carbon soot extracts. These anions were soluble in polar solvents and insoluble in non-polar solvents, which was in contrast with the high solubility of the neutral empty fullerenes in non-polar solvents. Thus, the reduced EMFs and empty fullerenes were separated based on their different solubilities.

Electrochemical methods also can be applied in separation of the EMFs isomers. Echegoyen *et al.*[29] reported a simple method of separation of the $Sc_3N@I_h$-C_{80} isomer from $Sc_3N@C_{80}$ by an electrochemical process. Since the first oxidation potential of D_{5h} is 270 mV, which is lower than the I_h isomer, the selective chemical oxidation of

$Sc_3N@D_{5h}$-C_{80} using a suitable agent leaves $Sc_3N@I_h$-C_{80} in the neutral state. Pure $Sc_3N@I_h$-C_{80} can be obtained by subsequent removal of the $Sc_3N@D_{5h}$-C_{80} cation.

Host-guest complexing behavior between EMFs and an azacrown ether was applied for the selective separation of EMFs from the empty cage fullerenes.[30] The complex formed by EMFs with an azacrown ether precipitated out of toluene, whereas empty cages did not. The EMFs can be recovered by sonication of precipitates in CS_2.[30]

1.3. Empty Cage and Endohedral Fullerenes

1.3.1. Empty Cage Fullerenes

The most abundant fullerene extractable from arc-processed soot is the soccer-ball shaped C_{60}. Among 1812 C_{60} isomers,[31] the one with I_h symmetry is the only isomer isolated experimentally, which means I_h-C_{60} must be thermodynamically and kinetically stable compared to other isomers of C_{60}.[32, 33] I_h-C_{60} fullerene has a soccer-ball structure composed of 12 pentagons and 20 hexagons and obeys the "isolated pentagon rule" (IPR).[33, 34] IPR states that the most stable fullerenes are those in which all pentagons on the cage are surrounded by five hexagons. In other words, there are no fused pentagons in those stable fullerenes.

The second most abundant fullerene is C_{70}, which is also an IPR-satisfying fullerene. Whetten *et al.*[13] reported that the ratio for chromatographic separation yields of C_{60} and C_{70} is 85:15. The ^{13}C NMR spectrum of C_{70} consists of five lines with 3×10, 2×20 pattern (number of NMR lines × relative intensity), suggesting there are five types of carbon atoms in the C_{70} cage and the C_{70} molecule possesses D_{5h} symmetry.

Crystallographic characterization of C_{70} was reported by Balch *et al.* and was consistent with previous ^{13}C NMR experiments.[35]

The fullerene C_{84} is the third most abundant empty cage fullerene extractable from fullerene soot. Among the 24 IPR-satisfying isomers of $C_{84,}$ only a few isomeric C_{84} structures are found to be stable enough to be separated from the fullerene soot. The early theoretical calculations suggested $D_{6h}(24)$, $T_d(20)$ and $D_2(21)$ as possible candidates for the most stable isomers.[36] The number in the bracket is the isomer number in the sequence proposed by Fowler and Manolopoulos.[37] However, ^{13}C NMR studies indicate that the C_{84} fraction of the fullerene soot consists mainly of two major isomers, $D_2(22)$ and $D_{2d}(23)$ with a 2:1 abundance ratio.[38] Interestingly, the most symmetrical isomer does not always represent the greatest stability. In the C_{84} case, a D_2 isomer is the most abundant isomer, instead of the D_{6h} isomer.[39]

C_{86} is another large cage fullerene obtained from fullerene soot. In 2000, Miyake *et al.*[40] isolated two isomers of C_{86} using the multi-stage HPLC method. The ^{13}C NMR study indicated that these two isomers have C_2 and C_s symmetry. Soon after, Kertesz and co-workers[41] predicted these two isomers were $C_s(16)$ and $C_2(17)$ because these two isomers had low total energies and large HOMO-LUMO gaps by employing density functional theory (DFT) calculations.

With the increase in numbers of carbons, the number of fullerene isomers grows greatly. For example, the total number of isomers ranges from 1812 for C_{60} to 1,674,171 for C_{120}.[31] For the larger fullerenes beyond C_{96}, because of their limited solubility in common solvents and extreme difficulty in purification, detailed

characterization of properties of individual isomers of large fullerenes has rarely been reported.[42] In order to identify thermodynamically favorable isomers of large fullerenes cages, theoretical calculations on the structures of large fullerenes were performed widely.[43-47] Zhao *et al.* [44-46] investigated the full set of the IPR-satisfying isomers of the fullerenes from C_{90} to C_{100} by various semi-empirical and quantum chemical approaches. Cai and co-workers[42] predicted the top five low-energy isomers of C_{132} to C_{160} by using a topological scheme as a prescreening tool to select candidate isomers.

The IPR condition is an important filter that has been found to limit the numbers of possible fullerenes isomers. So far, the isolated and well characterized empty cage fullerenes are all IPR-satisfying structures. However, external derivatization of empty fullerene cages make possible the synthesis of IPR-violating empty cage fullerenes. For example, Xie and co-workers[48, 49] prepared $C_{50}Cl_{10}$ and $C_{64}Cl_4$ by a modified graphite arc-discharge process in the helium atmosphere by introducing a small amount of carbon tetrachloride (CCl_4). The single X-ray crystal structures indicated both cages are IPR-violating, D_{5h}(271)-C_{50} and C_{3v}(1911)-C_{64}, as shown in Figure 1.8. IPR-violating fullerenes also can be stabilized by encapsulation with metal atoms or their carbide/nitride clusters. There are several IPR-violating endohedral fullerenes that have been reported, such as $Sc_3N@C_{68}$,[50] $La@C_{72}$,[51] $Gd_3N@C_{82}$,[52] $M_3N@C_{84}$,(M= Tb, Gd, Tm),[53, 54] and $Sc_2C_2@C_{66}$.[55]

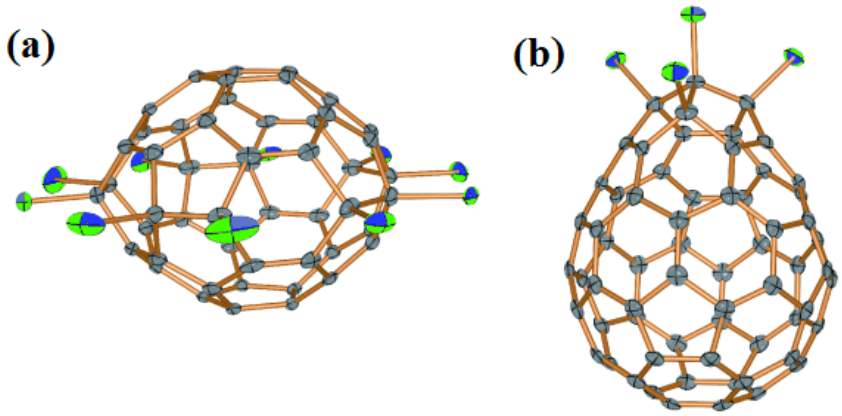

Figure 1.8. X-ray crystal structures of (a) $C_{50}Cl_{10}$, (b) $C_{64}Cl_4$ (Reprinted with permission from Ref. 49. Copyright 2008 Wiley-VCH Verlag GmbH & Co. KGaA.)

1.3.2. Endohedral Fullerenes

1.3.2.1. Monometallofullerenes

Several days after the discovery of C_{60}, the Smalley group[5] observed a series of C_n^+ and LaC_n^+ ions along with LaC_{60}^+ and $La_2C_{60}^+$ in the laser ablation of La-doped graphite rods experiment. Therefore, they proposed that the lanthanide atoms were encapsulated in the fullerene cages. Chai *et al.*[6] reported the observation of La@C_{60}, La@C_{70} and La@C_{82} in 1991; however, only La@C_{82} was air stable and extractable from the soot. Since then, M@C_{82} (M = group III metals and lanthanides) have been recognized as a prototype of the mono-metallofullerene family since many M@C_{82} can be isolated and purified in macroscopic quantities.

There are nine IPR-satisfying isomers for the C_{82} fullerene cage.[37] The theoretical calculations have predicted that the M atom is mainly encapsulated inside the C_{2v}-C_{82} cage.[56] This prediction has been confirmed by several groups.[57-63] Akasaka *et al.*[57, 58] prepared the diamagnetic anion of La@C_{82} by bulk potential controlled electrolysis. By analysis of the ^{13}C NMR spectra of the La@C_{82} anion, they verified the

C_{2v} structure of the major isomer of La@C_{82}. Yang and co-workers[59] reported the near-infrared (NIR) absorption spectrum of Ce@C_{82}, which is similar to those of La@C_{2v}-C_{82}, suggesting that Ce@C_{82} and La@C_{82} have a common C_{2v}-C_{82} cage. The C_{2v} symmetry of Ce@C_{82} is verified by the ^{13}C NMR spectrum[60] of the diamagnetic anion of Ce@C_{82}, which exhibits 17 distinct lines of nearly equal intensities and 7 half-intensity lines (Figure 1.9a). So far, the C_{2v} cage structure of M@C_{82} has been confirmed for metals including Sc,[61] Y, [62] La,[57, 58] Ce[60] and Pr.[63]

By the MEM (maximum entropy method)/Rietveld analysis of synchrotron powder diffraction data of Sc@C_{82},[61] Y@C_{82}[64] and La@C_{82},[65] Shinohara and co-workers determined that the metal atom was located at an off-center position adjacent to a hexagonal ring along the C_2 axis of C_{2v}-C_{82} cage, which was consistent with early theoretical predictions.[56] The paramagnetic NMR spectral analysis and theoretical calculation of Ce@C_{82} cation also indicated that Ce atom had the same position within the C_{2v}-C_{82} cage (Figure 1.9b).[66]

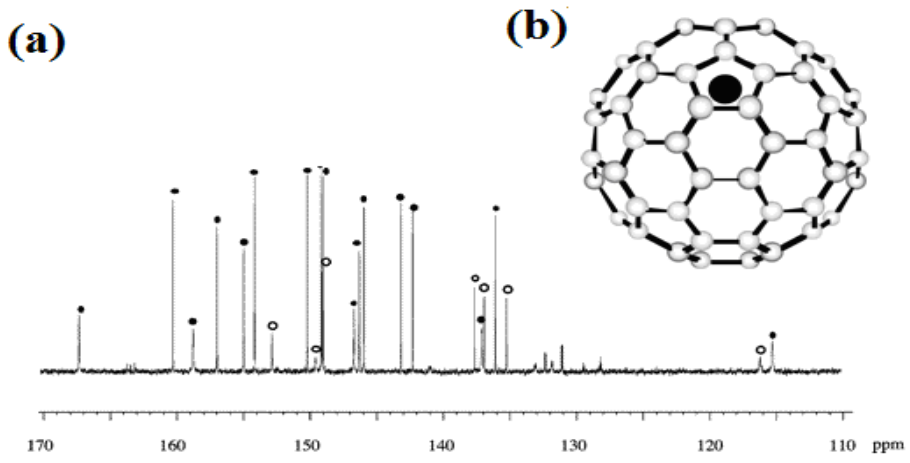

Figure 1.9. (a) ^{13}C NMR of [Ce@C_{2v}-C_{82}]$^-$ without ^{1}H decoupling (303 K) (b) Optimized Structure of Ce@C_{2v}-C_{82} (Reprinted with permission from Ref. 60. Copyright 2004 American Chemical Society.)

$M@C_{82}$ (M= Sc, Y, La) are paramagnetic metallofullerenes, which provide important information on their electronic structures. Because of the electron transfer from the M atom to the C_{82} cage, the electronic states of $M@C_{82}$ can be described as $(M^{2+})@C_{82}^{2-}$ and $(M^{3+})@C_{82}^{3-}$.[67-70] In the case of $La@C_{82}$, the latter electronic state leads to an open-shell electronic structure and the unpaired electron delocalized on the surface of the carbon cage. The observation of eight equally spaced lines (Figure 1.10)[71] confirms the isotropic electron-nuclear hyperfine coupling (hfc) to ^{139}La (I=7/2). The spin site exchange behavior between paramagnetic $La@C_{82}$ and organic donor N,N,N',N'-tetramethyl-*p*-phenylendiamine (TMPD) was reported by Nagase and co-workers.[71] As shown in Figure 10, in the presence of TMPD, the intensity of EPR signals of $La@C_{82}$ is weakened and the signals of $[TMPD]^{\bullet+}$ appear, suggesting that a spin-site exchange system constructed from $La@C_{82}$ and TMPD.

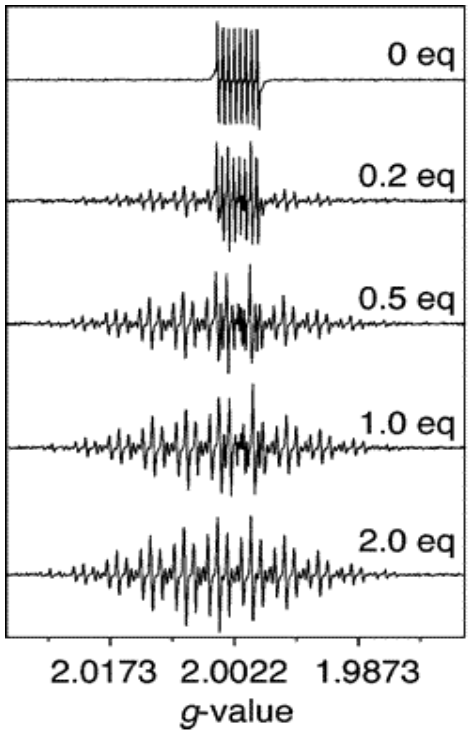

Figure 1.10. EPR spectra of $La@C_{82}$ in the presence of 0−2 equiv of TMPD in nitrobenzene at 296 K (Reprinted with permission from Ref. 71. Copyright 2006 American Chemical Society.)

1.3.2.2. Dimetallofullerenes

In 1994, $Sc_2@C_{84}$ was prepared and characterized by the Dorn group at Virginia Tech, together with two other research groups from IBM and CalTech.[72] Strong evidence of the endohedral nature of $Sc_2@C_{84}$ was suggested by electron diffraction and high-resolution transmission electron microscopy (TEM). There are 24 IPR-satisfying isomers for C_{84} cage [37] and there are three isomers mainly produced by arc-discharge of carbon rods.[38, 73] These three structural isomers of $Sc_2@C_{84}$ (I, II, III) were assigned as C_s, C_{2v} and D_{2d} symmetry by ^{13}C NMR.[74] Each Sc atom transfers 2 electrons to the C_{84} cage, leading to a formal electronic structure $(Sc^{2+})_2@C_{84}^{4-}$.[74, 75] However, Nagase *et al.*[76] re-characterized $Sc_2@C_{84}$ (III) isomer by improved ^{13}C NMR and suggested $Sc_2@C_{84}$ (III) as a scandium carbide metallofullerene, $Sc_2C_2@C_{3v}$-C_{82}.

$La_2@C_{80}$ is the other dimetallofullerene that has attracted special attention during recent years. The progress on the separation and purification in macroscopic quantities made it possible to investigate their interesting structural and electronic properties. Based on ^{13}C NMR and ^{139}La NMR studies, Akasaka *et al.*[77] suggested an I_h symmetry of $La_2@C_{80}$ cage, in which two La atoms were not stationary but circulated inside the round cage. This prediction was confirmed by the MEM/Rietveld analysis of the high resolution X-ray powder diffraction data.[78] Kobayashi *et al.*[79] showed that the two La were located on the C_2 axis, resulting in the symmetry reduction to a D_{2h} configuration. Each encapsulated La atom transferred three electrons to the cage and the electronic configuration of the molecule was described as $(La^{3+})_2@C_{80}^{6-}$.[79]

1.3.2.3. Trimetallic Nitride Template (TNT) Endohedral Metallofullerenes (EMFs)

In 1999, a novel family of EMFs, TNT EMFs, were discovered by Dorn and co-workers[80] at Virginia Tech by introducing N_2 gas into the generator during arc vaporization of composite (scandium oxide/graphite) rods. These novel endohedral fullerenes attracted great interest immediately because of their unique properties, such as outstanding yields compared with traditional mono- and dimetallofullerens, high thermal stability and long term stability in air.[81] Until now, the family of TNT EMFs has been expanded to group III metals (Sc, Y),[80, 81] lanthanides (Er,[80] Ho,[82, 83] Lu,[84] Tm,[85, 86] Gd,[87, 88] Dy,[89] Tb[90, 91]), and mixed metal clusters.[92, 93]

1.3.2.3.1. Scandium based TNT EMFs, $Sc_3N@C_{2n}$ (n=34, 39, 40)

1.3.2.3.1.1. $Sc_3N@C_{80}$ (I_h and D_{5h})

$Sc_3N@C_{80}$ (I_h) is a representative member in the TNT EMF family, not only because it is the first TNT EMF discovered, but also it has outstanding abundance in the soot.[80] Currently, $Sc_3N@C_{80}$ represents the third most abundant fullerene species just behind C_{60} and C_{70}. The molecule was found to have a mass-to-charge ratio (*m/z*) of 1109, and a two-line ^{13}C NMR spectrum with a 3:1 ratio, suggesting I_h symmetry of the C_{80} cage. The C_{80} cage is composed of two types of carbon atoms, 20 corannulene-type carbon atoms (intersection of one five-membered and two six-membered rings) and 60 pyrene-type carbons atoms (intersection of three six-membered rings). The I_h-C_{80} is different from that of C_{60}, where there is only one type of carbon atom: 60 corannulene-type carbon atoms.

The ^{13}C NMR data suggest that the Sc_3N cluster provides an averaged chemical environment for all 80 carbon atoms on the NMR time scale. Based on this observation, Dorn and co-workers proposed that the Sc_3N cluster was dynamic and rotated as a wheel inside the I_h-C_{80} cage (Figure 12b). This prediction was confirmed by ^{45}Sc NMR spectrum, in which there was only a single symmetric line.[80] A single-crystal X-ray diffraction study[80] of $Sc_3N@C_{80}\cdot CoII(OEP)\cdot 1.5CHCl_3\cdot 0.5C_6H_6$ (OEP is the dianion of octaethylporphyrin) confirmed the proposed $Sc_3N@I_h$-C_{80} structure (Figure 1.11). However, the major occupation of Sc_3N cluster in the C_{80} cage has not been found yet even with good quality *co*-crystals.

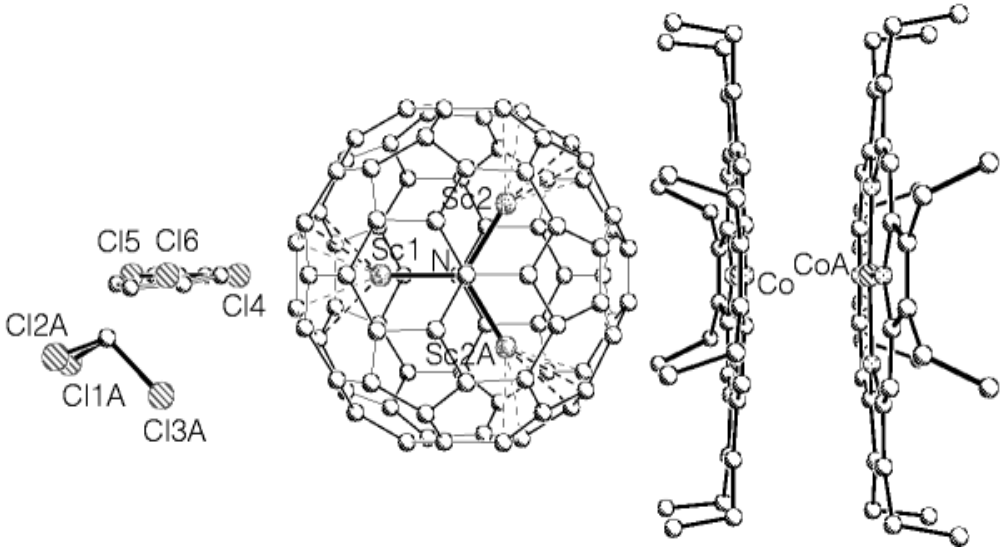

Figure 1.11. The crystal structure of $Sc_3N@I_h$-$C_{80}\cdot CoII(OEP)\cdot 1.5CHCl_3\cdot 0.5C_6H_6$ (Reprinted by permission from Macmillan Publisher Ltd:[Nature](Ref. 80), copyright 1999)

The theoretical calculations show that neutral I_h-C_{80} has only two electrons in its four-fold degenerate HOMO and has an open-shell electronic structure.[94] Thus, the neutral I_h-C_{80} has a very small HOMO-LUMO gap and is not stable. Analogous to the electronic structure of $La_2@C_{80}$ mentioned before, each of three Sc atoms donates two electrons to the I_h-C_{80} cage and one electron to the central N atom within I_h-C_{80} cage

(Figure 1.12a). After accommodation of six electrons, the four-fold degenerate HOMOs are fully occupied and form a closed-shell electronic structure with a large HOMO-LUMO gap. Thus, $Sc_3N@I_h$-C_{80} is thermodynamically stable and its formal electronic structure can be expressed as $(Sc_3N)^{6+}@C_{80}^{6-}$. [94]

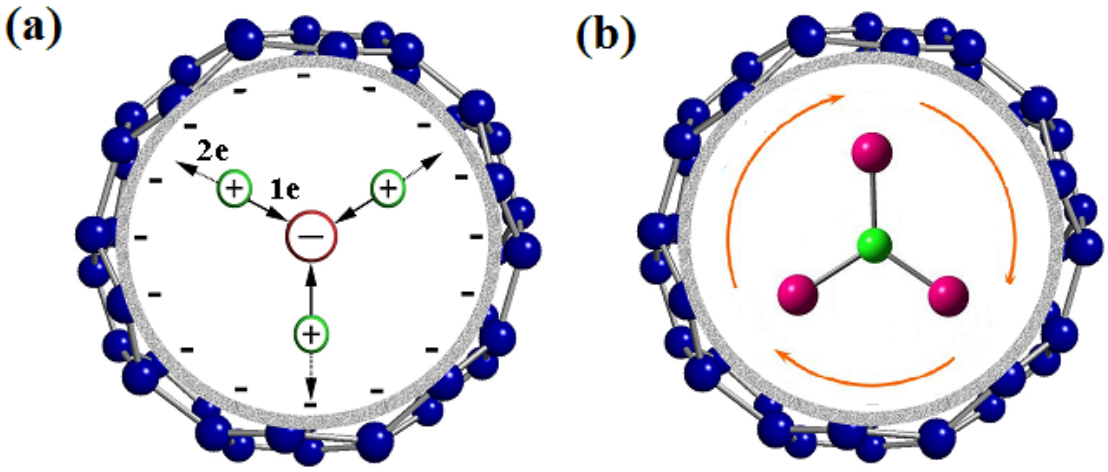

Figure 1.12. (a) Charge transfer model for $Sc_3N@C_{80}$; (b) Dynamic rotation of Sc_3N cluster inside the I_h-C_{80} cage

There are seven IPR-satisfying isomers for C_{80} cage, (D_{5d}, D_2, C_{2v}, D_3, C_{2v}, D_{5h}, I_h).[37] The $Sc_3N@D_{5h}$-C_{80} is the other isolated and well characterized isomer.[95] The yield of D_{5h} isomer is about 10% of $Sc_3N@I_h$-C_{80} formed during the electric-arc synthesis. The ^{13}C NMR shows 6 lines with ratio of 1:2:2:1:1:1, which allows conclusive assignment of the D_{5h} isomer (20 × 2, 10 × 4). The experimental and calculated ^{13}C NMR shifts with their corresponding carbon sites are shown in Table 1.1. Possible explanations of the difference between experimental and calculated shifts are the inherent difficulty in calculating the chemical shielding of large molecules and averaging of the values for the symmetry related carbon atoms.

Table 1.1. The assignment of the ^{13}C NMR peaks of $Sc_3N@D_{5h}$-C_{80}[95]

Experimental (ppm)	Theoretical calculation (ppm)	Site
149.8	150.7	Corannulene
145.0	149.8	Corannulene
143.9	148.2	Pyracylene
139.3	145.7	Corannulene
138.5	141.6	Pyrene
135.2	141.4	Pyrene

The $Sc_3N@D_{5h}$-C_{80} was further confirmed by the single crystal X-ray diffraction measurement,[96] as shown in Figure 1.13. Because of the presence of the pyracylene carbon (absent on $Sc_3N@I_h$-C_{80}), the D_{5h} isomer of $Sc_3N@C_{80}$ is more reactive than the I_h isomer. The theoretical calculation shows that the I_h isomer is 19.4 kcal/mol lower in energy than the D_{5h} isomer, which is qualitatively consistent with the yield ratio (9:1) for these two isomers.[95]

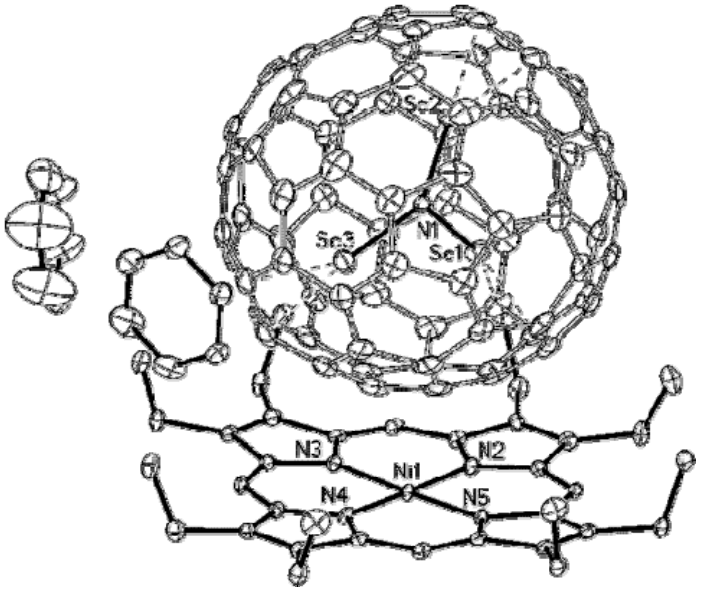

Figure 1.13. The crystal structure of $Sc_3N@D_{5h}$-C_{80}·Ni(OEP)·$2C_6H_6$ (Reprinted with permission from Ref. 96. Copyright 2006 American Chemical Society.)

1.3.2.3.1.2. $Sc_3N@D_3$(6140)-C_{68}

The first non-IPR TNT EMF, $Sc_3N@C_{68,}$ was discovered when a mass of m/z= 965 was observed for a scandium metallofullerene extractable soot.[50] As the second member of the Sc based TNT EMFs family, $Sc_3N@C_{68}$ is different from $Sc_3N@C_{80,}$ not only due to its smaller cage but also because it contains adjacent pentagons, which are also known as pentalenes. The identification of $Sc_3N@C_{68}$ is based on information obtained by ^{13}C and ^{45}Sc NMR measurements,[50] theoretical chemistry,[97] and X-ray diffraction study.[98] The ^{13}C NMR pattern contains 12 singlet peaks, with 11 having full intensity and one with one-third intensity. The ^{45}Sc NMR contains only single broad peak (Figure 1.14b), suggesting that the three scandium atoms are equivalent on the NMR time scale. Of the 6332 possible isomers, only 11 isomers have either D_3 or S_6 symmetry that match the ^{13}C NMR pattern shown in Figure 1.14 (a).

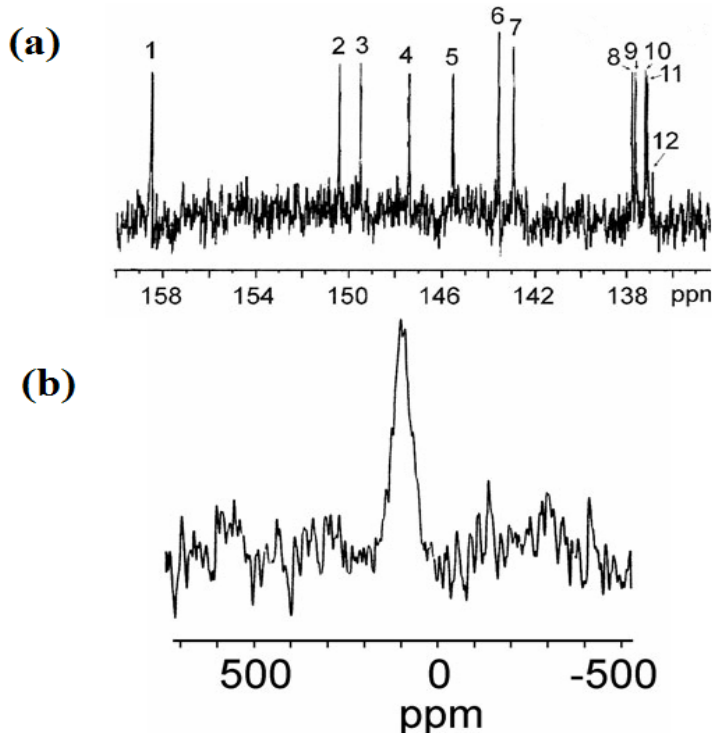

Figure 1.14. (a) 150 MHz ^{13}C NMR of $Sc_3N@C_{68;}$ (b) 121.5 MHz ^{45}Sc NMR of $Sc_3N@C_{68}$ (Reprinted by permission from Macmillan Publisher Ltd:[Nature](Ref. 50), copyright 2000)

Out of these 11 isomers, two of them (D_3(6140)-C_{68} and D_3(6275)-C_{68}) have the minimum number of three fused pentagons. The minimum number of fused pentagons was one important argument for the reduction of the set of possible isomer candidates of non-IPR fullerenes cages as a fused pentagon is connected with an energy penalty of 70−90 kJ/mol for a fullerene cage. DFT calculations suggest that the D_3(6140)-C_{68} is 120 kJ/mol more stable than isomer D_3(6275)-C_{68} when the six electrons transfer from the cluster to the cage. As a result, $Sc_3N@D_3$(6140)-C_{68} becomes the most favored one over 11 other isomers of the C_{68} set, as shown in Figure 1.15. This result was confirmed by an XRD study, which indicates each Sc atom of the Sc_3N cluster sits on a fused pentagon patch of the C_{68} cage (orthogonal to the C_3 axis).[98]

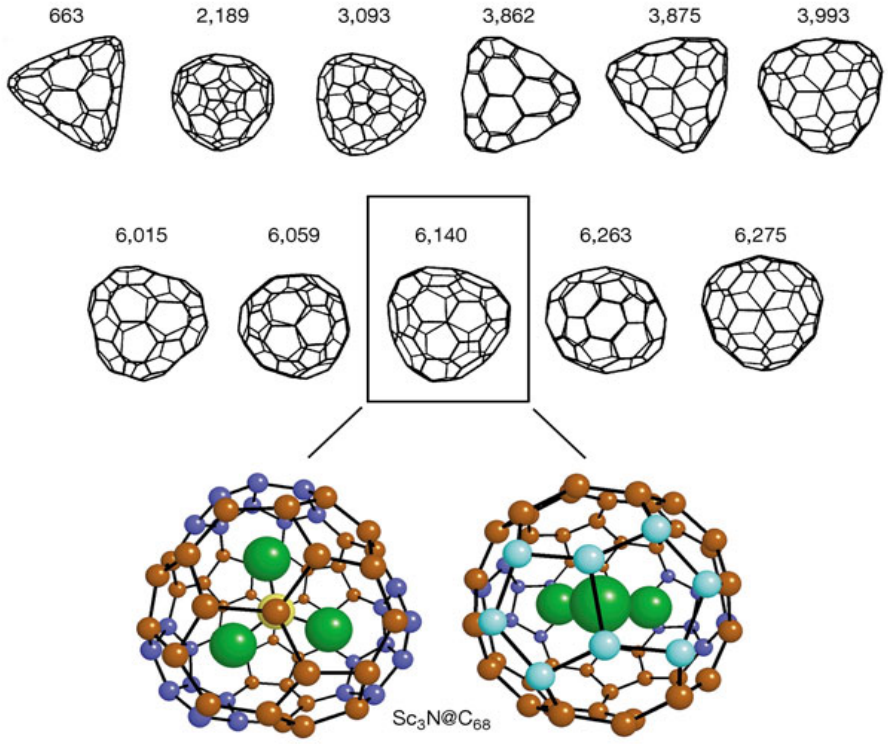

Figure 1.15. The structures of the eleven C_{68} isomers with 3-fold symmetry and the proposed structure of $Sc_3N@D_3$(6140)-C_{68} (Reprinted by permission from Macmillan Publisher Ltd:[Nature](Ref. 50), copyright 2000)

1.3.2.3.1.3. $Sc_3N@D_{3h}(5)$-C_{78}

The third species discovered in Sc-based TNT EMFs is $Sc_3N@C_{78}$, which has a mass of 1085.[99] There are a total of five IPR-satisfying isomers for the empty C_{78} cage.[37] The stability of these five empty cage isomers are listed in the order of: $D_3(1)$-C_{78}> $C_{2v}(2)$-C_{78}> $C_{2v}(3)$-C_{78}> $D_{3h}(4)$-C_{78}> $D_{3h}(5)$-C_{78}.[43, 100] The three most stable isomers, $D_3(1)$-C_{78}, $C_{2v}(2)$-C_{78}, $C_{2v}(3)$-C_{78}, have been separated and characterized, while the two highest energy isomers with D_{3h} structure have not been reported yet. However, the crystal structure of the $Sc_3N@C_{78}$ (Figure 1.16) reveals that the Sc_3N cluster is encapsulated in a $D_{3h}(5)$-C_{78} cage,[99] which is the least stable IPR-satisfying empty cage structure. The planar Sc_3N cluster lies on the horizontal mirror plane of the C_{78} cage with the scandium atoms localized over three pyracylene patches. In a similar fashion to $Sc_3N@I_h$-C_{80}, the unstable $D_{3h}(5)$-C_{78} cage is stabilized by filling three LUMOs and exists as a closed-shell electronic structure with a large HOMO-LUMO gap. The formula $(Sc_3N)^{6+}@C_{78}^{6-}$ has been widely accepted as the formal charge distribution of $Sc_3N@D_{3h}(5)$-C_{78}.[101]

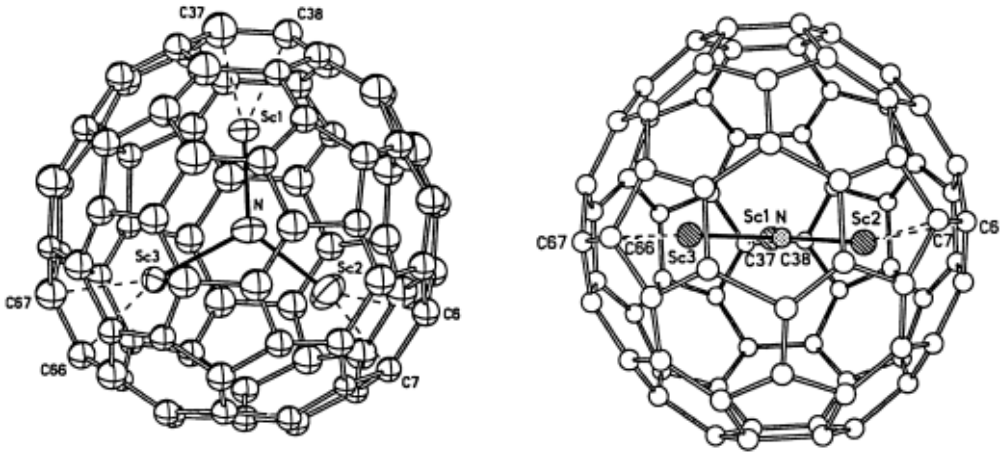

Figure 1.16. Two orthogonal views of $Sc_3N@D_{3h}(5)$-C_{78} structure (Reprinted with permission from Ref. 99. Copyright 2001 Wiley-VCH Verlag GmbH & Co. KGaA.)

Unlike the $Sc_3N@I_h$-C_{80} isomer, in which the Sc_3N cluster is not trapped in a specific position and can rotate freely inside the C_{80} cage, the Sc_3N cluster in the C_{78} cage is strongly bonded to the three 6,6 ring junctions of three different pyracylene patches. Such bonding restricts the Sc_3N unit from freely rotating inside the cage. Instead the Sc_3N unit rotates within the two-dimensional horizontal mirror plane.[101]

1.3.2.3.2. Terbium (Tb) based TNT EMFs, $Tb_3N@C_{2n}$ (n=40, 42-44)

So far, C_{80} is the largest fullerene cage for Sc-based TNT EMFs. When larger metal atom ions, such Gd, Dy, Nd and Tb, are employed in TNT process, new families of TNT EMFs including larger carbon cage are produced in significantly lower abundance.[85, 88, 91] As the size of fullerene cage increases, the possibility of additional isomers also increases. The definitive structural characterization of these endohedrals with larger fullerene cages is very difficult. Recently, six members of the $Tb_3@C_{2n}$ (n=40, 42-44) family of endohedrals were prepared and examined by single-crystal XRD by Zuo *et al.*,[91] which expanded the TNT EMFs family to much larger fullerene cages.

In a similar fashion to $Sc_3N@C_{80}$, there are two isomers of $Tb_3N@C_{80}$, $Tb_3N@I_h$-C_{80} and $Tb_3N@D_{5h}$-C_{80} (Figure 1.17). In contrast to the planar Sc_3N cluster in the $Sc_3N@C_{2n}$ (n = 34, 36 and 40) and $Lu_3N@C_{80}$ molecules, the Tb_3N unit is significantly pyramidalized. The differences in pyramidalization of the M_3N cluster within the C_{80} cage were interpreted based on the sizes of the metal ions. Thus, M_3N clusters with small metal ions, such as Sc^{3+} (0.88 Å) and Lu^{3+} (1.00 Å) are planar M_3N

cluster in the C_{80} cage. Metal ions with significantly larger radii, such as Gd^{3+} (1.08 Å) and Tb^{3+} (1.06 Å), exhibit pyramidal M_3N clusters in the C_{80} cage.[87, 91]

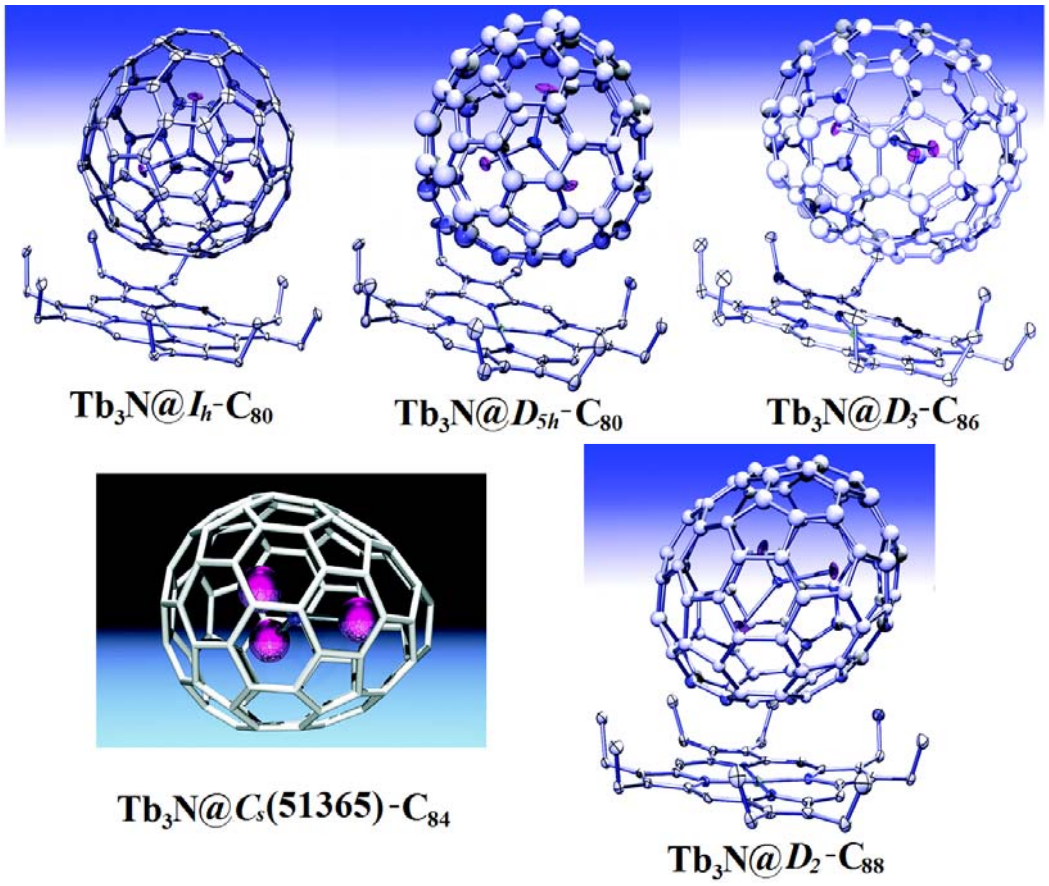

Figure 1.17. The crystal structures of Tb-based TNT EMFs, $Tb_3N@C_{2n}$ (n=40, 42-44) (Reprinted with permission from Ref. 91. Copyright 2007 American Chemical Society.)

The crystal structure of $Tb_3N@C_s(51365)$-C_{84} (Figure 1.17) demonstrates that the C_{84} cage is egg-shaped with a non-IPR C_s symmetry. There are a total of 51,592 isomers for the C_{84} cage.[37] Twenty-four isomers are IPR-satisfying structures, and the other 51,568 isomers are non-IPR isomers. It is remarkable that $Tb_3N@C_{84}$ adopts No. 51,365 among the possible 51,568 non-IPR isomers.[91] This finding suggests that the Isolated Pentagon Rule (IPR) may not be the only criteria for the selection of larger EMFs and fullerene structures. In contrast with the C_{80} cage, the Tb_3N unit is planar in

both major sites and minor sites within C_{84} cage. One Tb atom is situated within the fold of the pentalene unit formed by the fused pentagon pair, which is similar to that of the scandium atoms within three pentalene units of the D_3 symmetric $Sc_3N@C_{68}$.[98] Among all the non-IPR EMFs reported so far, it seems that the pentalene fold always coordinates with a metal ion inside the cage.

The single-crystal XRD studies indicate that both $Tb_3N@C_{86}$ and $Tb_3N@C_{88}$ have IPR-satisfying structures (Figure 1.17). $Tb_3N@D_3$-C_{86} is the isomer of number 19 of the total 19 IPR isomers of C_{86} in the sequence proposed by Fowler and Manolopoulos,[37] whereas $Tb_3N@D_2$-C_{88} is the No. 35 isomer. The Tb_3N cluster in these two cages is planar. Thus, it is clear that there is a correlation between the cage size and the structure of the Tb_3N cluster in the cage. For the larger cage (C_{84}, C_{86}, C_{88}), the Tb_3N cluster is planar; for the smaller C_{80} (I_h and D_{5h}) cage, the Tb_3N cluster is pyramidal.

Although $Tb_3N@C_{82}$ was detected in the mass spectra, the scarcity of sample hampered definitive structural characterization. Echegoyen and co-workers[52] reported the first separation and structural characterization of the Gd-counterpart, $Gd_3N@C_{82}$. Single-crystal XRD studies indicated that the carbon cage in $Gd_3N@C_{82}$ is non-IPR with a C_s symmetry. Among the 9 IPR-satisfying isomers and 39709 non-IPR isomers, $Gd_3N@C_{82}$ adopts isomer No.39663 among the 39709 non-IPR isomers, as shown in Figure 18. One of the Gd atoms is situated within the fold of the pentalene unit formed by the fused pentagon pair, which is consistent with the other non-IPR EMFs reported.

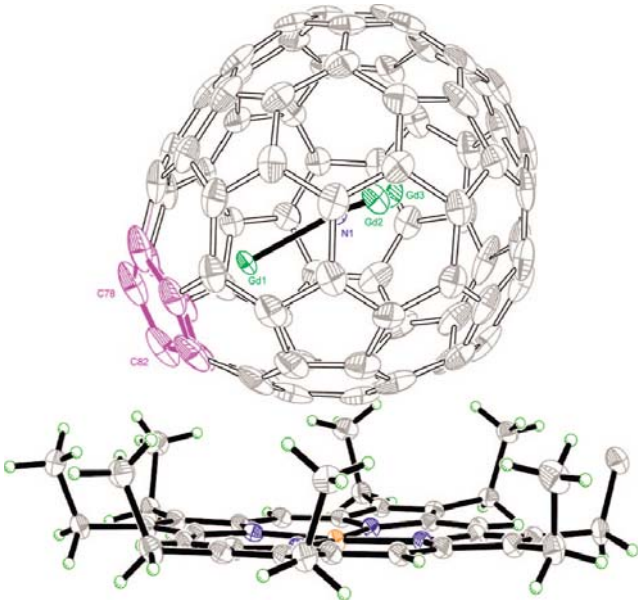

Figure 1.18. The crystal structure of $Gd_3N@C_s(39663)\text{-}C_{82}\cdot NiII(OEP)\cdot 2C_6H_6$.The pair of fused pentagons is highlighted in purple (Reprinted with permission from Ref. 52. Copyright 2008 American Chemical Society.)

1.3.2.3.3. Other TNT EMFs, $M_3N@C_{2n}$ (M = Nd, Pr, Ce)

Since the discovery of the first TNT EMF, $Sc_3N@I_h\text{-}C_{80}$, a series of TNT EMFs have been isolated and characterized with different metallic cluster inside, such as Sc, Y, Er, Ho, Lu, Tm, Gd, Dy and Tb. Each metal-based TNT EMF has a wide distribution of cage sizes, which could range from C_{68} to C_{98}. However, the yield of TNT EMFs decreases dramatically when the fullerene cage size increases. The $M_3N@I_h\text{-}C_{80}$ always has the highest yield in the series of $M_3N@C_{2n}$ and it appears that $M_3N@I_h\text{-}C_{80}$ is the preferential template for the formation of TNT EMFs.

Recently, Echegoyen and co-workers reported the preparation and separation of Nd, Pr and Ce based TNT EMF families,[102, 103] which were characterized by mass spectrometry, HPLC, UV/Vis-NIR spectroscopy and cyclic voltammetry. Results indicate that these three families all exhibit the same preferential templating of the C_{88}

cage and the yield of $M_3N@C_{88}$ is much higher than $M_3N@C_{80}$. In addition, as the metal size increases, the larger fullerene cage, C_{96}, is greatly favored and the yield of $M_3N@C_{96}$ is improved significantly.

1.3.2.4. Metal Carbide Endohedral Fullerenes, $M_xC_2@C_{2n}$ (x=1-3, n=34-46),

With the development of structural characterization techniques, several originally reported as di- or tri- EMFs, such as $Sc_2@C_{86}$,[104] $Sc_3@C_{82}$[105, 106] and $Sc_2@C_{84}$[107] were re-characterized as metal carbide endohedral fullerenes- $Sc_2C_2@C_{84}$,[108] $Sc_3C_2@C_{80}$[109, 110] and $Sc_2C_2@C_{82}$.[76, 111] The observation of the metal carbide M_xC_2 cluster inside the fullerene has attracted wide interest because of the unique electronic properties and potential applications.

1.3.2.4.1. $Sc_2C_2@D_{2d}$-C_{84}

The first isolation and characterization of a metal carbide encapsulated metallofullerene was $Sc_2C_2@D_{2d}$-C_{84}, which was previously reported as $Sc_2@C_{86}$ (I).[104, 108] The relative yield of $Sc_2C_2@C_{84}$ is about 2% of that of C_{60}, which is abundant enough for the study of its structural and electronic properties. The ^{13}C NMR spectrum of $Sc_2C_2@D_{2d}$-C_{84} exhibits a series of ten distinct lines with equal intensity, one line with 1/2 intensity and the additional one line with 1/4 intensity. The NMR pattern 10×8, 1×4, 1×2 (number of NMR lines × number of carbons) can be assigned to D_{2d}-C_{84} cage if line 12 (the line with 1/4 intensity, as shown in Figure 1.19) is attributed to the carbide in the C_{84} cage. Among the 24 IPR-satisfying isomers of C_{84}, D_{2d}-C_{84} is No. 23 in the sequence proposed by Fowler and Manolopoulos.[37] This assignment was confirmed by synchrotron X-ray structural/ maximum entropy method (MEM) analysis.

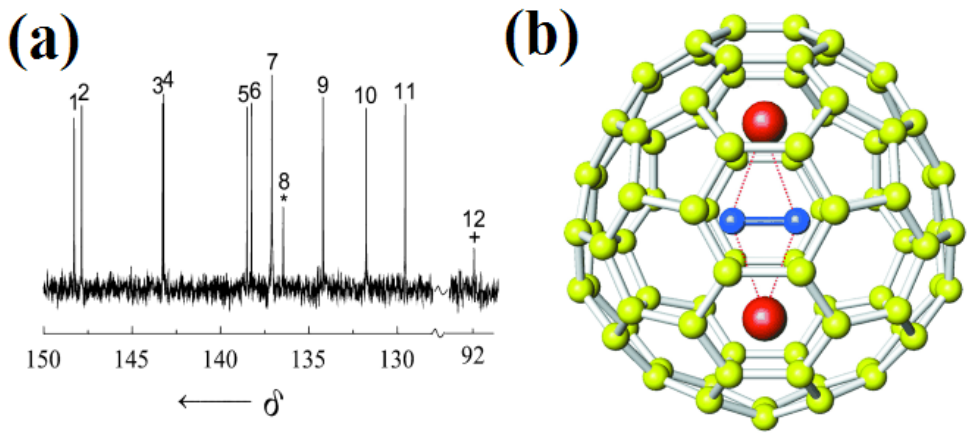

Figure 1.19. (a) ^{13}C NMR spectrum of $(Sc_2C_2)@D_{2d}$-C_{84} in CS_2; (b) Schematic representation of the $(Sc_2C_2)@D_{2d}$-C_{84} molecule (Reprinted with permission from Ref. 108. Copyright 2001 Wiley-VCH Verlag GmbH & Co. KGaA.)

1.3.2.4.2. $Sc_2C_2@C_{3v}$-C_{82}

Among the three isomers of Sc_2C_{84} that have been isolated, Sc_2C_{84} (III) is the most abundant one. Similar to other metal carbide endohedrals, Sc_2C_{84} (III) was first proposed as a dimetallofullerene, $Sc_2@C_{84}$.[112] Nagase *et al.*[76] reported an improved ^{13}C NMR spectrum of Sc_2C_{84}(III) that shows a total of 17 lines (11 full-intensity signals, five 1/2-intensity signals and one 1/6-intensity signal). However, the ^{13}C NMR pattern cannot be explained by any of the IPR-satisfying isomers of the C_{84} cage. Instead if two Sc atoms and two C atom are placed inside a C_{3v}-C_{82} cage, the ^{13}C NMR pattern of $Sc_2C_2@C_{3v}$-C_{82} will match the observed spectrum well, while the carbide inside the cage is invisible in this ^{13}C NMR spectrum.

This prediction was verified by the X-ray single-crystal analysis of the adamantylidene carbene (Ad) cycloadduct of this Sc_2C_{84} isomer.[113] The single-crystal structure (Figure 1.20) clearly showed the C_{3v}-C_{82} cage with metal carbide inside.

DFT calculations suggested the electronic structure of $Sc_2C_2@C_{3v}$-C_{82} is $(Sc_2C_2)^{4+}C_{82}^{4-}$ as a result of four-electron transfer from the Sc_2C_2 cluster to the C_{82} cage. The unstable C_{3v}-C_{82} cage is stabilized by the transfer of four electrons to the cage.

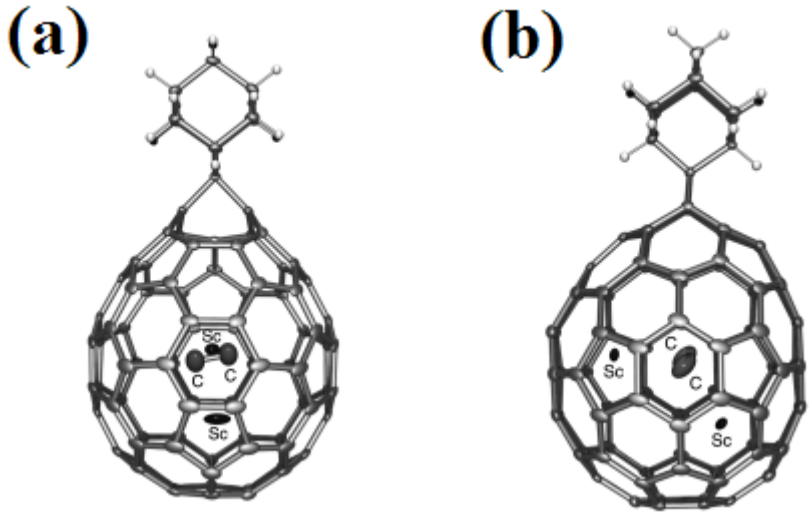

Figure 1.20. The crystal structure of $Sc_2C_2@C_{3v}$-C_{82}(Ad) (a) front view (b) side view (Reprinted with permission from Ref. 113. Copyright 2007 Wiley-VCH Verlag GmbH & Co. KGaA.)

Although the X-ray single-crystal analysis of $Sc_2C_2@C_{3v}$-C_{82}(Ad) provide direct evidence that the carbide is inside the fullerene cage, it is important to study the ^{13}C NMR shift of the carbide. However, because the carbide may rotate rapidly inside carbon cage, the spin-rotation interaction makes it very difficult to detect by ^{13}C NMR spectroscopy.[114] The carbide in $Sc_2C_2@D_{2d}$-C_{84} was assigned as line 12 (δ = 91.99 ppm) by Wang *et al.* (Figure 1.19).[108] However, it was proved that signal was just an impurity.[115]

Very recently, Nagase and co-workers[115] reported the first detection of the ^{13}C NMR chemical signals of the carbide unit in $Sc_2C_2@C_{3v}$-C_{82}, $Sc_2C_2@D_{2d}$-C_{84} and $(Sc_3C_2@I_h$-$C_{80})^-$ by using ^{13}C-enriched samples. As shown in Figure 1.21, the ^{13}C NMR shift of the C_2 unit in $Sc_2C_2@C_{3v}$-C_{82} is around δ= 253.2 ppm, which is consistent with

the calculated ^{13}C NMR shift value. Due to the low signal to noise ratio, the carbide cannot be observed for the sample without ^{13}C isotopic labeling.

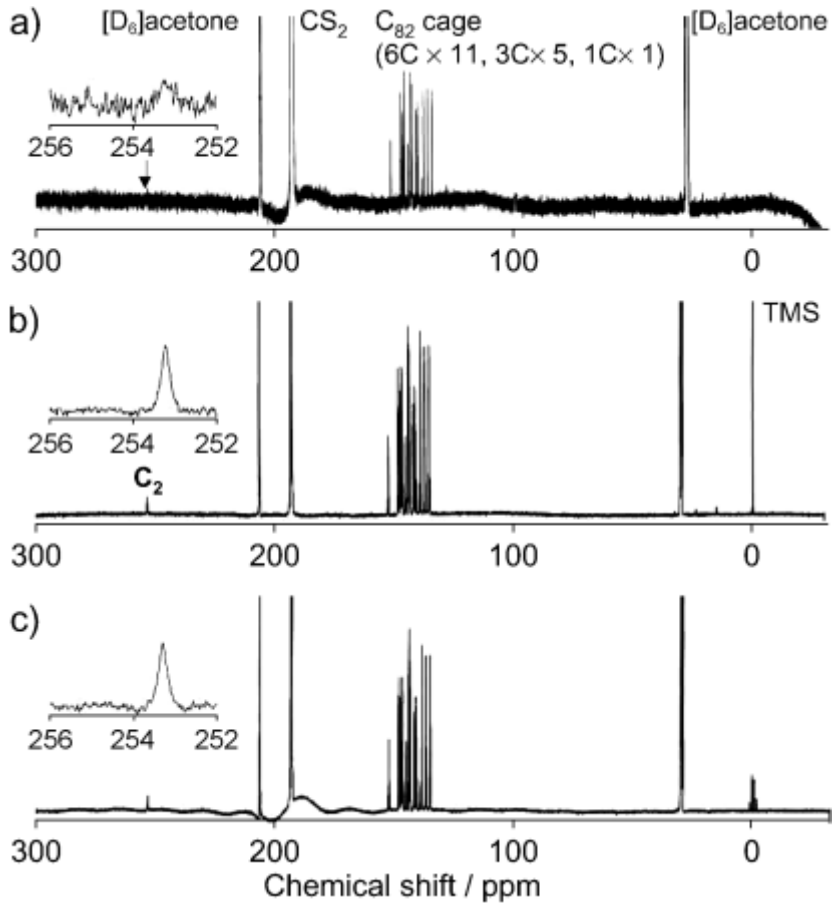

Figure 1.21. ^{13}C NMR (125 MHz) spectra of (a) $Sc_2C_2@C_{3v}$-C_{82} in proton-decoupled mode, (b) ^{13}C-enriched $Sc_2C_2@C_{3v}$-C_{82} in proton-decoupled, (c) ^{13}C-enriched $Sc_2C_2@C_{3v}$-C_{82} in proton-coupled modes (Reprinted with permission from Ref. 115. Copyright 2008 Wiley-VCH Verlag GmbH & Co. KGaA.)

1.3.2.4.3. $Gd_2C_2@D_3(85)$-C_{92}

Recently, Liu *et al.*[116] reported the detection of a family of gadolinium (Gd) containing EMFs, which extended from Gd_2C_{90} to Gd_2C_{124}. Detailed structural characterization was made for one member-Gd_2C_{94}. The crystallographic results indicated that Gd_2C_{94} contains a Gd_2C_2 unit inside a cage of 92 carbon atoms (Figure 1.22). The C_{92} cage is an IPR-satisfying cage and it is in No.85 of 86 IPR-satisfying

isomers of C_{92}. Like other M_2C_2 units in fullerene cages, Gd_2C_2 unit also appears to have a butterfly shape. So far, $Gd_2C_2@D_3(85)$-C_{92} is the largest well characterized metal carbide EMF.

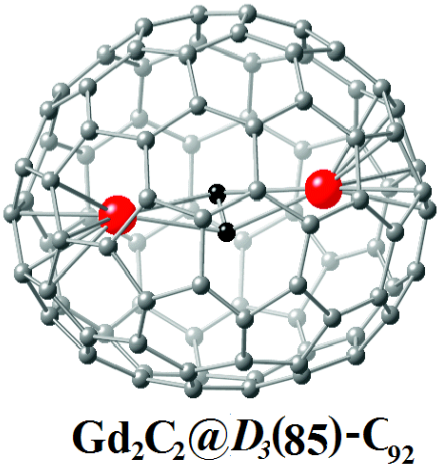

Figure 1.22. The crystal structure of $Gd_2C_2@D_3(85)$-C_{92} (Reprinted with permission from Ref. 116. Copyright 2008 American Chemical Society.)

1.3.2.5. Endohedral Metalloheterofullerenes

Heterofullerenes are those fullerenes in which one or more carbon atoms on the fullerene cage are replaced by non-carbon atoms, such as nitrogen, boron, silicon, etc.[117] Arranging heteroatoms into the fullerene cage significantly changes its physico-chemical properties, thus leading to new applications.[118]

Several heterofullerenes derived from empty cages have been reported,[119] such as the well characterized heterofullerene $C_{59}N$ derived from C_{60} by substitution of a nitrogen atom.[120] However, endohedral metalloheterofullerenes have been rarely discussed. Akasaka *et al.*[121] reported the observation of $La@C_{81}N$ and $La_2@C_{79}N$ signals via fast atom bombardment mass (FABMS) fragmentation. No endohedral metalloheterofullerenes have ever been separated and characterized until Dorn and co-workers[122] reported the first preparation, isolation and characterization of $Y_2@C_{79}N$

and $Tb_2@C_{79}N$ recently. The single crystal X-ray diffraction crystallography of $Tb_2@C_{79}N$ indicated that the fullerene cage of $M_2@C_{79}N$ is an I_h eighty-atom (seventy-nine carbon atoms and one nitrogen atom) cage. [122]

1.4. Hydrogenation of Fullerenes

Diatomic hydrogen is a light, convenient and potential fuel source which can easily be converted to other energy forms without producing harmful byproducts. Hydrogen storage is an interesting subject that has attracted considerable attention in recent years.[123] Carbon-based hydrogen adsorption materials are a topic of special interest. Due to their unique molecular structure, fullerenes have been considered as a form of carbon which can be hydrogenated and dehydrogenated reversibly.[124] Based on theoretical calculations, the C-H bond is 68 kcal/mol, which is 15 kcal/mol weaker than a C-C bond (83 kcal/mol).[124] Thus, the C-H bond will generally break more readily than the C-C bond. For the case of fullerenes, the cage will remain intact when hydrogen is released at elevated temperatures.

1.4.1. Hydrogenation of C_{60}

1.4.1.1. $C_{60}H_2$ and $C_{60}H_4$

The simplest fullerene hydride, $C_{60}H_2$, was synthesized and characterized by Henderson and Cahill in 1993.[125] The reaction of C_{60} with BH_3: tetrahydrofuran(THF) in dry toluene followed by hydrolysis gave the $C_{60}H_2$ in 10-30 % yield. HPLC using a buckyclutcher column was employed to separate and purify the $C_{60}H_2$ from unreacted C_{60} and $C_{60}O$. A sharp singlet at δ= 5.93 was observed in the ^{1}H NMR spectrum of

$C_{60}H_2$ in [D_8]-toluene. This sharp singlet remained at temperatures between - 80 °C and 100 °C, suggesting a static structure of $C_{60}H_2$ on the NMR time scale. There are two possible ways of H_2 addition: either across the 6,6 ring fusion or across the 6,5-ring fusion. Theoretical calculations suggested that the addition across the 6,6-ring fusion was energetically favored (Figure 1.23).[126]

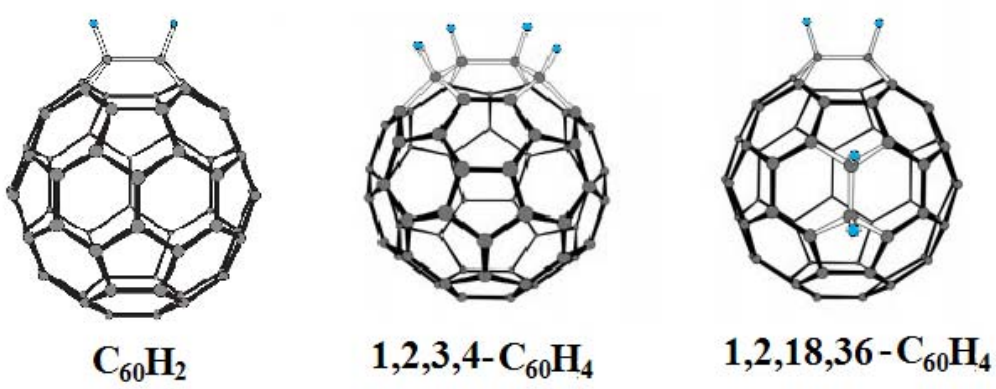

Figure 1.23. Structures of $C_{60}H_2$, 1,2,3,4-$C_{60}H_4$ and 1,2,18,36-$C_{60}H_4$ [127] modes (Reprinted with permission from Ref. 127. Copyright 2001 Wiley-VCH Verlag GmbH & Co. KGaA.)

Synthesis and separation of $C_{60}H_4$ was soon reported by the same group.[128] By reduction of $C_{60}H_2$ with the reducing agent borane, a 10% yield of $C_{60}H_4$ mixture isomers were isolated. With the increase in number of hydrogen additions, the number of fullerene isomers increases rapidly. In contrast to the single isomer of $C_{60}H_2$, there are eight possible isomers that would result from hydrogenation of two 6,6-double bonds. The major isomer, 1,2,3,4-$C_{60}H_4$, is approximately 50% of the crude isomer mixture. An AA'BB' spin system centered at δ= 5.03 can be easily assigned to 1,2,3,4-$C_{60}H_4$, which has two pairs of hydrogen atoms attached to adjacent 6,6-ring fusions. The second most abundant isomer, 1,2,18,36-$C_{60}H_4$, was also separated and identified by its ^{1}H NMR data.

1.4.1.2. $C_{60}H_{36}$

$C_{60}H_{36}$, a buff-colored solid, is the most abundant hydrogenated fullerene that was first prepared through Birch reduction (Scheme 1) by Smalley and co-workers in 1990.[129] The mass spectrum of the buff-colored solid product obtained from Birch reduction exhibits a *m/z*=756 peak, suggesting the formation of $C_{60}H_{36}$. When the crude product was treated with 2,3-dichloro-5,6-dicyanobenzoquinone (DDQ) in refluxing toluene, the red color of the DDQ-toluene complex was rapidly discharged and a dark brown solution formed. Mass spectral analysis confirmed that the product was C_{60}, indicating that the fullerene skeleton did not change by Birch reduction.

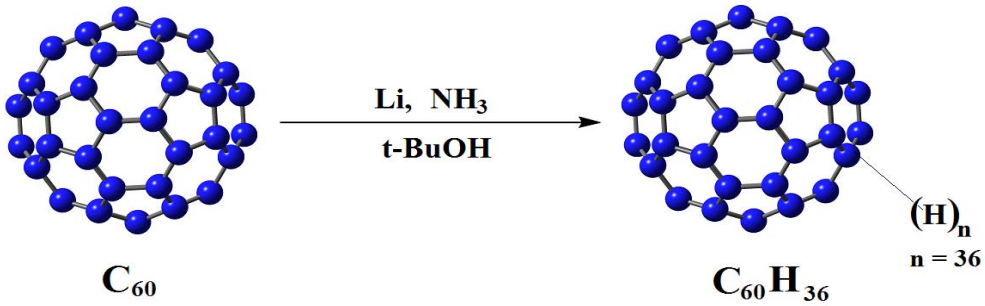

Scheme 1.1. Birch reduction of C_{60}

Despite considerable skepticism,[130] this result was repeated successfully in several laboratories.[131, 132] Many routes have been established for the hydrogenation of the fullerenes, such as solid phase hydrogenation,[133] transfer hydrogenation,[134] dissolving metal reduction,[135] hydrozirconation,[136] hydrogen radical induced hydrogenation[137] as well as electrochemical reduction,[138] and Benkeser reduction[139]. The $C_{60}H_{36}$ produced is the main product for most of the hydrogenation routes.

However, characterization of $C_{60}H_{36}$ is very difficult since a large number of isomers are formed. Indeed, Balasubra-manian[140] estimated that there are $6.0*10^4$

isomers of $C_{60}H_{36}$, and Clare and Kepert[141] have catalogued over 100 $C_{60}H_{36}$ isomers as reasonable candidates. Furthermore, highly reduced fullerenes are unstable toward light and air, especially when in solution.[132, 142, 143] The spectra obtained by using ^{1}H and ^{13}C NMR spectroscopy were broad, featureless and uninformative.[132] Bensasson and co-worker predicted the products of transfer hydrogenation of C_{60} are a mixture of D_{3d} **2** isomer and S_6 **3** isomer (Figure 1.24) by comparison with experimental and simulated infrared and Raman spectra of five $C_{60}H_{36}$ isomers.[144, 145]

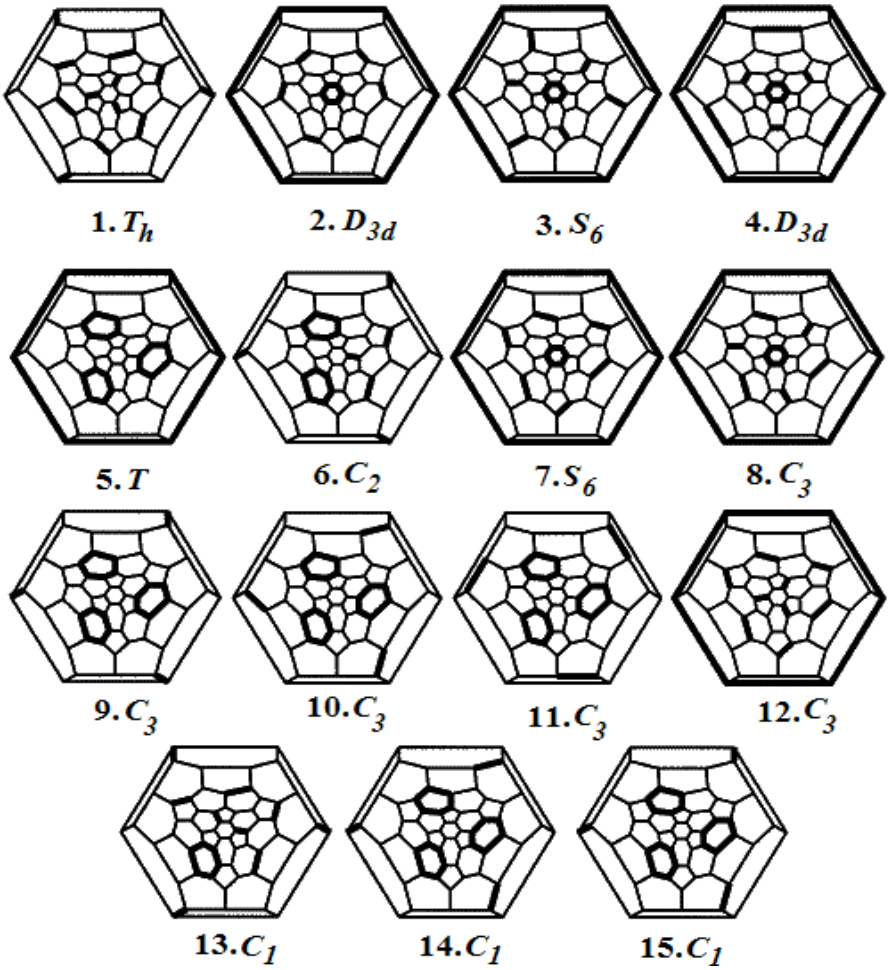

Figure 1.24. Schlegel diagrams of 15 isomers of $C_{60}H_{36}$. Isolated heavy lines indicated C=C bonds. A hexagon outlined in heavy lines indicates a benzene ring. The intersection of three light lines represents a methane carbon with three C-C bonds (Reprinted with permission from Ref. 132. Copyright 2001 American Chemical Society.)

A major advance in the identification of highly reduced fullerene was proposed by Saunders and co-workers.[146] As an excellent NMR nucleus, ^{3}He has a nuclear spin 1/2 and a high gyromagnetic ratio and the ^{3}He NMR spectrum of each product will yield a single sharp peak. He@C_{60} and its derivatives can be examined by ^{3}He NMR spectroscopy. Nossal *et al.*[132] reported the ^{3}He NMR spectra of the mixture of ^{3}He@$C_{60}H_{36}$ from Birch reduction. The ^{3}He spectra of different fractions showed slightly broadened but different signals. When compared with computationally determined ^{3}He chemical shift values, the major two fractions of ^{3}He@$C_{60}H_{36}$ included S_6 **3**, C_2 **6,** S_6 **7**, C_3 **8**, D_{3d} **2**, C_3 **9** and C_3 **11** (shown in Figure 1.24). The theoretical calculation predicted that all isomers are among the most stable isomers of $C_{60}H_{36}$.

Thermogravimetric analyses (TGA)[147] of $C_{60}H_{36}$ indicated a weight loss of around 6.8 % at 480-500 °C, which is significantly larger than the theoretical weight loss, 4.8 %. This may be due to release of not only hydrogen but also hydrocarbon solvent species trapped in the crystal lattice.

1.4.2. Hydrogenation of C_{70}

In comparison with one type of carbon in C_{60}, there are five types of carbon atoms in C_{70},[148] so the number of possible isomers of hydrogen addition increases dramatically. For example, 23 possible exohedral isomers may exit for $C_{60}H_2$, whereas there are 143 possible structures for $C_{70}H_2$.[149]

The methods that have been used to hydrogenate C_{60} are normally applied for hydrogenation of C_{70}. There are two isomers of $C_{70}H_2$, 1,2–$C_{70}H_2$ and 5,6-$C_{70}H_2$, that have been synthesized and characterized.[150, 151] Theoretical calculations suggest that

these two isomers are the two lowest-energy isomers; however, the 1,2–$C_{70}H_2$ isomer is about 0.2-1.3 kcal/mol more favored than the 5,6-$C_{70}H_2$ isomer.[149, 150] The calculation is consistent with the experimental result. Hydrogenation of C_{70} by diimide produces both isomers and the ratio between the 1,2–$C_{70}H_2$ and 5,6-$C_{70}H_2$ isomers in the product mixture is 8:1.[151]

More highly hydrogenated C_{70}, such as $C_{70}H_{36}$ and a mixture of hydrogenated $C_{70}H_{38\text{-}44}$, can be prepared by Zn/HCl reduction method.[152] The ^{1}H NMR spectrum of these hydrides displays a wide band between δ= 2.4-4.0, which resembles the spectrum of the $C_{60}H_{36}$.[152] However, due to the instability and multiple isomers, the structure of $C_{70}H_{36}$ has not been determined to date.

1.5. Applications of Fullerenes and EMFs

1.5.1. Medicinal Applications

1.5.1.1. HIV-P Inhibitor

The protease of human immunodeficiency virus (HIV-P) is a key enzyme of the human immunodeficiency virus I.[153] Identification and characterization of novel inhibitors of HIV-P is a key step to develop new anti-AIDS drugs. The active site of HIV-P is an open-ended cylindrical hydrophobic cavity. Two amino acids reside on the surface of the cavity. They are ASP 25 and ASP 125, which catalyze the hydrolysis of the substrate.[153] Inhibition of amino acids may suppress the replicate viral cycle.

In 1993, Friedman and co-workers[154, 155] reported the first C_{60} derivative which could be employed as an HIV-P inhibitor. By molecular modeling, they recognized that

the C_{60} spheroid can fit into the cavity of the protease, where the hydrophobic end (the fullerene cage) can fit into the active site through strong van der Waals interactions, while the water-soluble arms extend out of the cage into the solvent. They predicted that when applying a fullerene diamino derivative as an inhibitor, extremely strong electrostatic or hydrogen bond interactions may take place between the inhibitor and ASP 25 and ASP 125. The optimum distance between the two amino groups is 5.5 Å.

Based on the prediction of Friedman, Prato *et al.*[156] reported the design and synthesis of the water-soluble C_{60} derivatives via 1,3-dipolar cycloaddition of an azomethine to C_{60}. As shown in Figure 1.25a, the distance between the two ammonium functional groups is 5.1 Å, which is close to 5.5 Å, the optimum distance to allow the electrostatic and /or hydrogen bond interactions between functional groups with the amino acids. The modeling study showed that the C_{60} derivatives nicely fits into the HIV-P cavity and the H-bond interactions between the neutral -COOH aspartic group with the $-NH_2$ group could help by stabilizing the complex.[156]

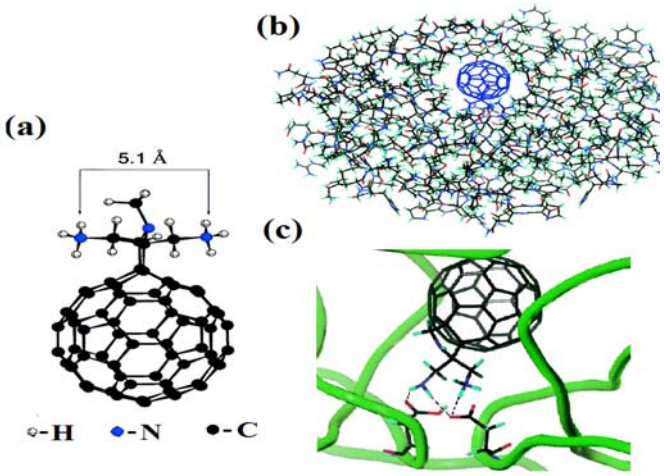

Figure 1.25. (a) Fullerene as an inhibitor for HIV-P, (b) Computer-designed accommodation of fullerene inhibitor in the cavity of HIV-P, (c) Closer view of fullerene inhibitor in the cavity of HIV-P (Reprinted with permission from Ref. 156. Copyright 2000 American Chemical Society.)

1.5.1.2. Neuroprotective Agents

Modern medical science[157] suggests that free radicals are associated with a number of neurodegenerative diseases, such as Parkinson's disease, Huntington's disease and stroke. These extremely reactive un-paired electrons may attack lipid, protein and deoxyribonucleic acids, and lead to neuronal cell death.[157, 158] C_{60} has high affinity towards free radicals and is capable of being reversibly reduced by up to 6 electrons.[159] As a "free radical sponge", C_{60} has drawn considerable attention as a potential novel neuroprotecting agent.[160-162] It has been reported that several water soluble C_{60} derivatives, such as carboxyfullerenes,[160] hexa(sulfobutyl)fullerenes[161] and fullerenols,[162], have strong ability to scavenge reactive free radicals. In addition, neuroprotective effects of the water soluble C_{60} derivatives on oxidative injuries have also been widely studied.[163,164]

In 1997, Dugan *et al.*[163] synthesized and characterized two regioisomers with C_3 or D_3 symmetry of water-soluble carboxylic acid C_{60} derivatives (Figure 1.26). By EPR analysis, both isomers were able to effectively scavenge hydroxyl radical (·OH) and super-oxide radical (O_2^{-}·). *In vitro* studies have shown that both isomers have the ability to prevent neuronal death induced by NMDA (*N*-methyl-*D*-aspartae). It was also reported that the C_3 isomer was more effective than the D_3 isomer. It was suggested that the C_3 isomer is more polar and enters the lipid membranes easier.

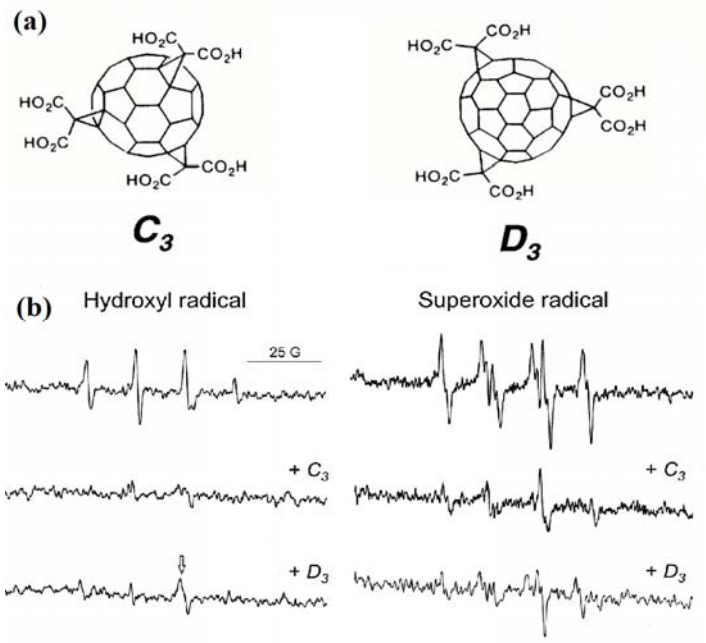

Figure 1.26. (a) Structures of carboxyfullerenes with paired carboxyl groups on the C_{60} cage; (b) Water-soluble carboxylic C_{60} compounds are effective free radical savengers (Reprinted with permission from Ref. 163. Copyright 1997 National Academy of Sciences, U.S.A.)

Recently, Liu and co-workers[164] reported a new C_{60}-based ebselen derivative by a cycloaddition reaction between C_{60} and ebselenyl azide. It was found that the C_{60}-based ebselen derivative showed enhanced neuroprotective potency in comparison with the parent C_{60} or ebselen derivative alone and it could be a more biologically effective neuroprotective agent.

1.5.1.3. Magnetic Resonance Imaging (MRI) Contrast Agents

Magnetic Resonance Imaging (MRI) is one of the most powerful tools used in biomedical diagnostics and has become increasingly important in recent years. By enhancing the relaxation rate of protons in human tissue in the presence of an MRI agent, the resolution and the brightness of the MRI images can be improved. The Gd^{3+} ion has a high paramagnetic moment because of its seven unpaired 4f electrons and has a long electron-spin relaxation time.[165] One of the most popular and commercial used

the MRI contrast agents is Gd^{3+} chelate of DTPA (diethylenetriaminepentaacetate), also known as Magnevist.[166] As a widely used MRI contrast agent, Gd-DTPA is highly water-soluble and has a good relaxivity. However, Gd-DTPA can dissociate and release the toxic Gd^{3}+ ions, which can be embedded in the surrounding tissue. Furthermore, it was reported that Gd-DTPA is not stable in acidic conditions.[167]

The advantages of using EMFs as MRI contrast agents have been well recognized.[168] Unlike the traditional Gd-chelate, the encapsulation of metals greatly reduces the possibility of metal-ion loss to organisms, which make them less toxic and safer. Furthermore, their ability to reduce the spin relaxation time of water protons is better than the commercial Gd-DTPA. With these special properties, water-soluble EMFs are considered as potential replacements for the commercial MRI contrast agents utilized today.

Shinohara and co-workers[169] prepared and characterized a series of water soluble lanthanoid metallofullerenols, $M@C_{82}(OH)_n$ (M=La, Ce, Gd, Dy, and Er) and found that both the R_1 (longitudinal relaxivity) and R_2 (transverse relaxivity) values of these metallofullerenols are much higher than those of the corresponding free ions and lanthanoid-DTPA compounds. Among these lanthanoid metallofullerenes, $Gd@C_{82}(OH)_n$ showed an extremely strong signal enhancement compared with the other compounds, which only showed a slight enhancement at the same concentration (Figure 1.27a). Based on the previous *in vivo* and *in vitro* evaluation of water soluble $Gd@C_{82}(OH)_n$, $Gd@C_{82}(OH)_{40}$ exhibited the highest water proton relaxivity: R_1= 81 $mM^{-1}s^{-1}$, R_2=108 $mM^{-1}s^{-1}$ at 1.0 T and 25 °C, which is around 20-times higher than that

of the commercial MRI contrast agents Gd-DTPA (R_1= 4.4 $mM^{-1}s^{-1}$, R_2=5.5 $mM^{-1}s^{-1}$).[170] Thus, a significant enhancement was observed as shown in Figure 1.27b.

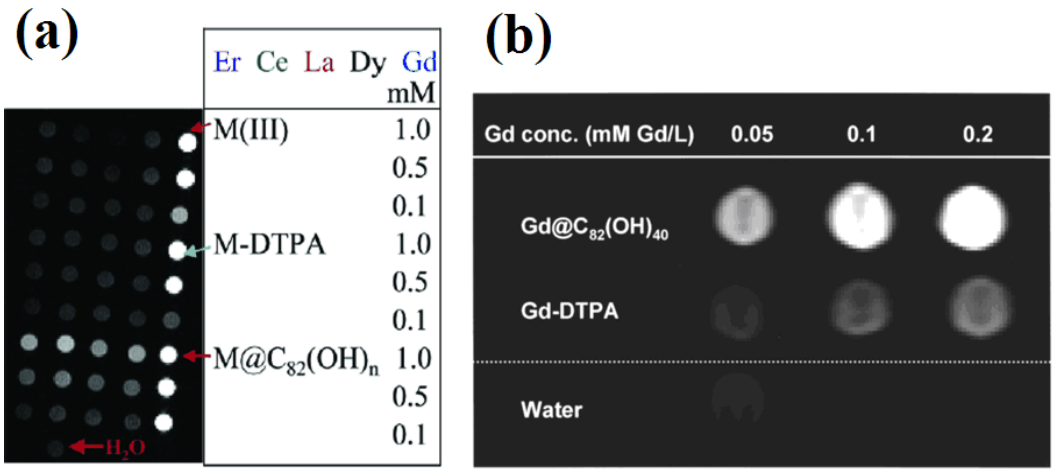

Figure 1.27. (a) Phantom NMR images of various lanthanoid ions, DTPA complex and metallofullerenols at different concentration (Reprinted with permission from Ref. 169. Copyright 2003 American Chemical Society.) (b) Enhancement of the MRI signals by $Gd@C_{82}(OH)_{40}$ compared to Gd-DTPA and water (Reprinted with permission from Ref. 170. Copyright 2001 American Chemical Society.)

So far, most of the studies involve derivatives of mono metallofullerenes, such as $Gd@C_{2n}$.[170] The better relaxivities of TNT EMFs derivatives are expected not only because of the higher number of paramagnetic ions but also due to the functionality of TNT EMFs, which can influence the interactions between water and the paramagnetic metals.[171] More recently, Fatouros**,** Dorn and Gibson *et al.*[172] reported the watersoluble poly(ethylene glycol) (PEG) functionalized and hydroxylated $Gd_3N@C_{80}$, $Gd_3N@C_{80}[DiPEG_{5000}(OH)_x]$, which has better water solubility and bio-distribution. The measured R_1 values for $Gd_3N@C_{80}[DiPEG_{5000}(OH)_x]$ were 102, 143, and 32 $mM^{-1}s^{-1}$ at 0.35, 2.4, and 9.4 T, respectively, significantly higher than that of gadodiamide. In studies of *in vitro* agarose gel infusion, when the image intensities

were equivalent, the concentrations for the $Gd_3N@C_{80}$[DiPEG5000$(OH)_x$] agent are at least 30-times smaller than gadodiamide (Figure 1.28). Impressively, with direct infusion of $Gd_3N@C_{80}$[DiPEG5000$(OH)_x$] and gadodiamide into live normal rat brain, comparable contrast enhancement was obtained with 0.013 mM^{-1} $Gd_3N@C_{80}$[DiPEG5000$(OH)_x$] and 0.50 mM^{-1} gadodiamide. These results indicate $Gd_3N@C_{80}$[DiPEG5000$(OH)_x$] as a potential new MRI contrast agent.

However, the extremely low production yield of $Gd_3N@C_{80}$ is a major limitation to its commercial development. The improvement of the yield of the $Gd_3N@C_{80}$ will be a major concern in the future.

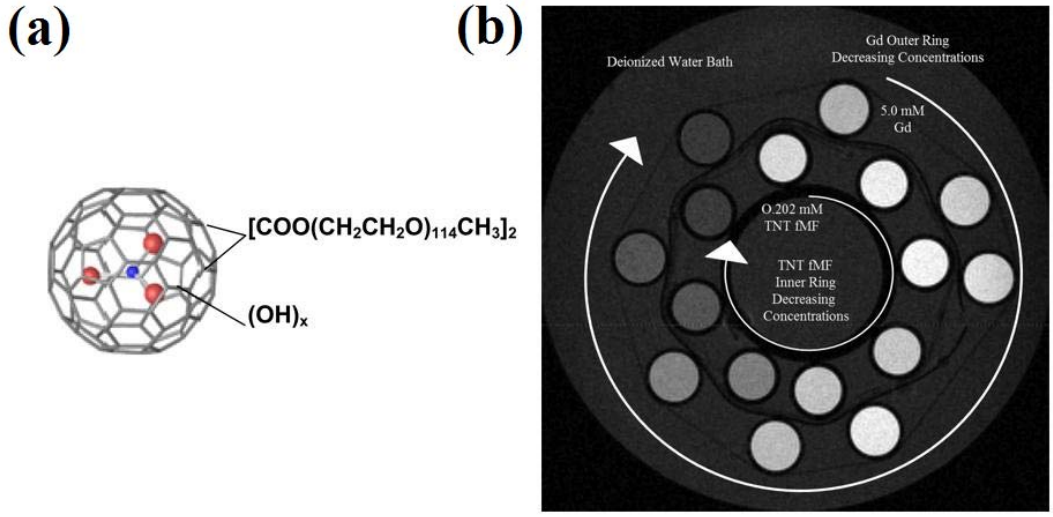

Figure 1.28. (a) PEGylated-hydroxylated EMFs: $Gd_3N@C_{80}$[DiPEG5000$(OH)_x$], (b) T_1-weighted MRI image (700/10) of aqueous solutions of $Gd_3N@C_{80}$[DiPEG5000$(OH)_x$] (inner ring, concentration decreasing in clockwise direction: 0.2020, 0.0101, 0.0505, 0.0252, 0.0126, 0.0063, 0.0032, and 0.0016 mM^{-1}) and gadodiamide (outer ring, concentration decreasing in clockwise direction: 5.0, 3.0, 1.0, 0.70, 0.50, 0.30, 0.10, and 0.050 mM^{-1}). Note the substantially lower concentrations required for $Gd_3N@C_{80}$[DiPEG5000$(OH)_x$] for achieving equivalent image intensities to gadodiamide (Reprinted with permission from Ref. 172. Copyright 2006 The Radiological Society of North America.)

1.5.2. Polymer-fullerene Photovoltaic Devices

Solar energy as a fossil fuel alternative has attracted wide attention in recent years. Organic photovoltaic devices are moving to the forefront of the energy related area because of lower cost and light weight.[173-175] Polymer based photovoltaic systems usually take the form of the bulk heterojunction (BHJ) devices, which contain an active photoactive layer with donor and acceptor. Many semiconducting polymers are applied as donor and fullerenes are considered to be the ideal acceptor for organic solar cells for their unique properties, such as their high electron affinity relative to the numerous organic donors and superior ability to transport charge. Figure 1.29 lists examples of the donors/acceptors which are commonly used in BHJ solar cells.[173]

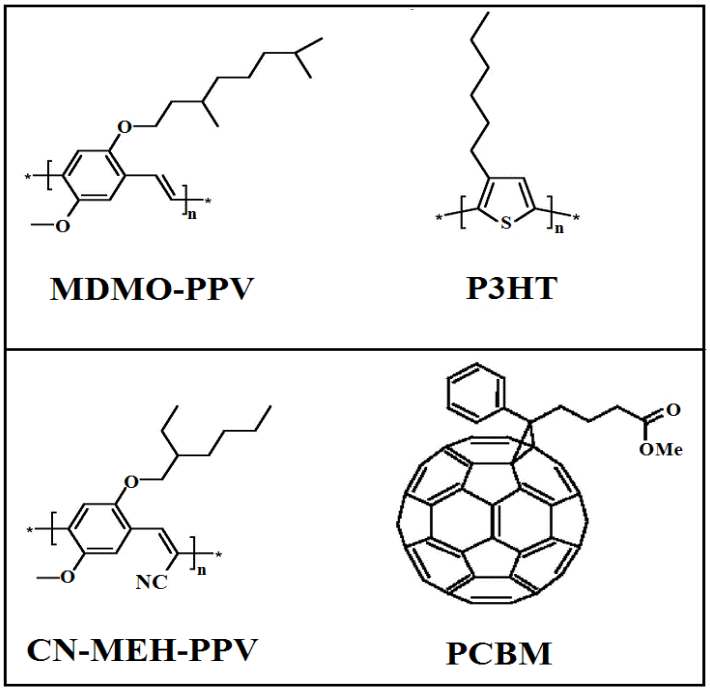

Figure 1.29. Several donors/acceptors used in organic solar cells. Upper row (donor polymers): MDMO-PPV (poly[2-methoxy-5-(3,7-dimethyloctyloxy)]-1,4-phenylenevinylene), P3HT (poly(3-hexylthiophene-2,5-diyl). Lower row (acceptors): CN-MEH-PPV (poly-[2-methoxy-5-(2'-ethylhexyloxy)-1,4-(1-cyanovinylene)phenylene) and C_{60}-PCBM (Phenyl C_{61} butyric acid ethyl ester) [173]

The most commonly and successfully employed fullerene derivative in polymer-fullerene BHJ solar cells is C_{60}-PCBM (Figure 1.29), which was first synthesized and reported by Wudl *et al.* in 1995.[176] Polymer-fullerene BHJ solar cells are generally fabricated in a "sandwich" geometry (Figure 1.30). Transparent glass or plastic covered with indium tin oxide (ITO) are used as the cathode. The active layer is the polymer-fullerene composite as the donor and acceptor components, which can be spin coated or vacuum deposited from solutions. The evaporated alumina on the top of the "sandwich" is the anode. The energy conversion of light into electricity by BHJ solar cell has three steps: (1) Absorption of light leading to formation of an electron-hole pair; (2) Electron transfer between donor (conjugated polymer) and acceptor (C_{60}-PCBM), so charge separation occurs; (3) Charge transport to anode (AI) and cathode (ITO), so a direct electric current form.[175]

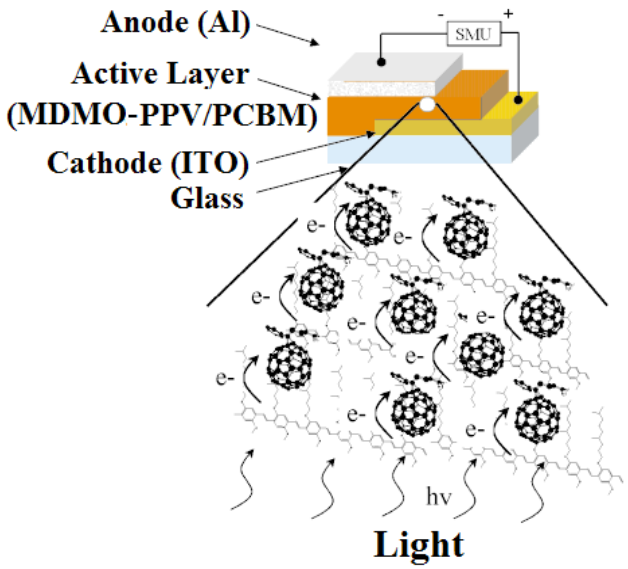

Figure 1.30. Schematic illustration of a polymer-fullerene (MDMO-PPV/C_{60}-PCBM) BHJ solar cell modes (Reprinted with permission from Ref. 175. Copyright 2001 Wiley-VCH Verlag GmbH & Co. KGaA.)

In 2001, Shaheen and co-workers[177] reported a MDMO-PPV/C_{60}-PCBM BHJ solar cell with 2.5% power conversion efficiency. The weight ratio of MDMO−PPV:C_{60}-PCBM was 1:4 and solvent for spin casting is chlorobenzene. When using toluene as solvent, the efficiency dramatically decreased to 0.9 %. This result indicated that the effect of the solvent adversely impacted the performance of the device. Compared with C_{60}, C_{70} has an unsymmetrical structure with significantly improved light absorption through the visible region.[178] Replacing the C_{60} moiety of C_{60}-PCBM by the C_{70} fullerene derivative could improve the performance of polymer-fullerene BHJ solar cell. This prediction was proved by Hummelen *et al.*,[178] as their study suggested that power conversion efficiency of MDMO−PPV:C_{70}-PCBM BHJ solar cell can reach 3.0% with significantly improved short circuit current density. However, the best efficiency was achieved with a ratio 1:4.6 of MDMO−PPV:C_{70}-PCBM and the solvent for spin casting was *o*-dichlorobenzene.

P3HT/C_{60}-PCBM (Figure 1.29) is another polymer-fullerene combination for BHJ solar cell that has been widely studied.[179, 180] When the weight ratio between P3HT and C_{60}-PCBM is 1:1[179] or 1:0.8[180] ratio, the performance of photovoltaic device was optimized with efficiency up to 5 %. Chlorobenze is commonly used as the solvent because both P3HT and C_{60}-PCBM have good solubility in it.[180]

One of the major limitations of polymer-fullerene BHJ solar cell efficiency is the mismatch of LUMOs of the polymer donor and fullerene acceptor.[174] As shown in Figure 1.31, the optimum energy difference between donors and acceptors is 0.3 eV. The LUMO energy of C_{60}-PCBM is 4.2 eV and there is 1.0 eV difference between

C_{60}-PCBM and the most commonly used polymer donor (P3HT and MDMO-PPV), which have 3.2 eV of LUMO energy. Obviously, there is a gap between optimum and actual energy difference. One of the effective ways to reduce the gap is to pick an acceptor having a higher LUMO energy. Theoretical[101] and experimental[181] data suggested that TNT EMFs have much higher LUMO energies than that of the empty cage fullerenes; thus, TNT EMFs may be promising acceptors for BHJ solar cell. Very recently, Drees *et al.*[182] reported that BHJ solar devices using P3HT/$Lu_3N@C_{80}$-PCBX (X=M, B, H, O) as electron donor/acceptors. The device using $Lu_3N@C_{80}$-PCBH has one of the highest reported open circuit voltage (V_{oc}), 890mV, which is a 260 mV enhancement compared with the P3HT/C_{60}-PCBM solar device. And the power conversion efficiency of P3HT/ $Lu_3N@C_{80}$-PCBH is higher than 4 %. This work suggests that TNT EMF derivatives are a new class of acceptor materials for solar cells that may ultimately clear the path toward commercially used devices.[182]

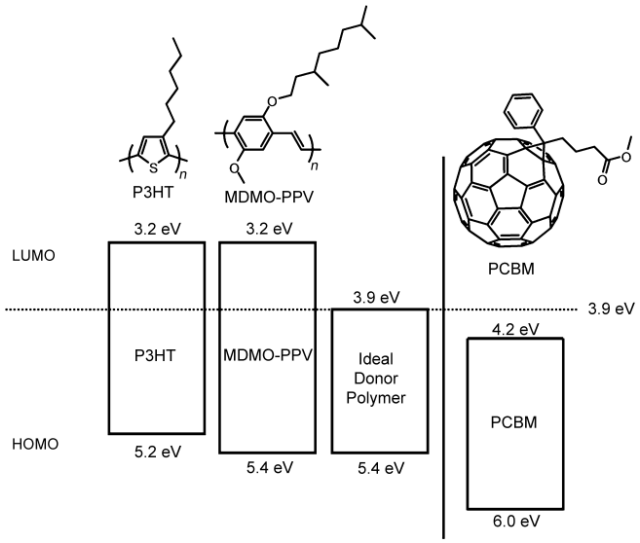

Figure 1.31. Band structure diagram illustrating the HOMO and LUMO energies of MDMO-PPV, P3HT, and an "ideal" donor relative to the band structure of C_{60}-PCBM. (Energy values are reported as absolute values relative to a vacuum) (Reprinted with permission from Ref. 174. Copyright 2008 Wiley-VCH Verlag GmbH & Co. KGaA.)

References:

(1) Kroto, H. W.; Heath, J. R.; Obrien, S. C.; Curl, R. F.; Smalley, R. E., C_{60}-Buckminsterfullerene. *Nature* **1985,** *318* (6042), 162-163.

(2) Hammond, G. S.; Kuck, V.; Editors, *ACS Symposium Series, Vol. 481: Fullerenes. Synthesis, Properties, and Chemistry of large Carbon Clusters. [Developed from a Symposium at the 201st National Meeting of the American Chemical Society, Atlanta, Georgia, April 14-19, 1991]*. 1992; p 195 pp.

(3) Kratschmer, W.; Lamb, L. D.; Fostiropoulos, K.; Huffman, D. R., Solid C_{60} - a New Form of Carbon. *Nature* **1990,** *347* (6291), 354-358.

(4) Taylor, R.; Hare, J. P.; Abdulsada, A. K.; Kroto, H. W., Isolation, Separation and Characterization of the Fullerenes C_{60} and C_{70} - the 3rd Form of Carbon. *J. Chem. Soc., Chem. Commun.* **1990,** (20), 1423-1424.

(5) Heath, J. R.; Obrien, S. C.; Zhang, Q.; Liu, Y.; Curl, R. F.; Kroto, H. W.; Tittel, F. K.; Smalley, R. E., Lanthanum Complexes of Spheroidal Carbon Shells. *J. Am. Chem. Soc.* **1985,** *107* (25), 7779-7780.

(6) Chai, Y.; Guo, T.; Jin, C. M.; Haufler, R. E.; Chibante, L. P. F.; Fure, J.; Wang, L. H.; Alford, J. M.; Smalley, R. E., Fullerenes with Metals Inside. *J. Phys. Chem.* **1991,** *95* (20), 7564-7568.

(7) Wudl, F.; Smalley, R. E.; Smith, A. B.; Taylor, R.; Wasserman, E.; Godly, E. W., Nomenclature and terminology of fullerenes: A preliminary survey. *Pure Appl. Chem.* **1997,** *69* (7), 1412-1434.

(8) Anthony, T. R.; Bradley, J. C.; Horoyski, P. J.; Thewalt, M. L. W., Graphite rod precursors for isotopically pure fullerenes and diamond. *Carbon* **1996,** *34* (11), 1323-1328.

(9) Kratschmer, W.; Fostiropoulos, K.; Huffman, D. R., The Infrared and Ultraviolet-Absorption Spectra of Laboratory-Produced Carbon Dust - Evidence for the Presence of the C_{60} Molecule. *Chem. Phys. Lett.* **1990,** *170* (2-3), 167-170.

(10) Smalley, R. E., Self-Assembly of the Fullerenes. *Acc. Chem. Res.* **1992,** *25* (3), 98-105.

(11) Shinohara, H., Endohedral metallofullerenes. *Rep. Prog. Phys.* **2000,** *63* (6), 843-892.

(12) Thess, A.; Lee, R.; Nikolaev, P.; Dai, H. J.; Petit, P.; Robert, J.; Xu, C. H.; Lee, Y. H.; Kim, S. G.; Rinzler, A. G.; Colbert, D. T.; Scuseria, G. E.; Tomanek, D.; Fischer, J. E.; Smalley, R. E., Crystalline ropes of metallic carbon nanotubes. *Science* **1996,** *273* (5274), 483-487.

(13) Ajie, H.; Alvarez, M. M.; Anz, S. J.; Beck, R. D.; Diederich, F.; Fostiropoulos, K.; Huffman, D. R.; Kratschmer, W.; Rubin, Y.; Schriver, K. E.; Sensharma, D.; Whetten, R. L., Characterization of the Soluble All-Carbon Molecules C_{60} and C_{70}. *J. Phys. Chem.* **1990,** *94* (24), 8630-8633.

(14) Khemani, K. C.; Prato, M.; Wudl, F., A Simple Soxhlet Chromatographic

Method for the Isolation of Pure C_{60} and C_{70}. *J. Org. Chem.* **1992,** *57* (11), 3254-3256.

(15) Parker, D. H.; Wurz, P.; Chatterjee, K.; Lykke, K. R.; Hunt, J. E.; Pellin, M. J.; Hemminger, J. C.; Gruen, D. M.; Stock, L. M., High-Yield Synthesis, Separation, and Mass-Spectrometric Characterization of Fullerenes C_{60} to C_{266}. *J. Am. Chem. Soc.* **1991,** *113* (20), 7499-7503.

(16) Jinno, K.; Saito, Y., Separation of fullerenes by liquid chromatography: Molecular recognition mechanisms in liquid chromatographic separation. *Adv. Chromatogr.* **1996,** *36*, 65-125.

(17) Saito, Y.; Ohta, H.; Jinno, K., Chromatographic separation of fullerenes. *Anal. Chem.* **2004,** *76* (15), 266a-272a.

(18) Yamamoto, K.; Funasaka, H.; Takahashi, T.; Akasaka, T.; Suzuki, T.; Maruyama, Y., Isolation and Characterization of an ESR-Active La@C_{82} Isomer. *J. Phys. Chem.* **1994,** *98* (49), 12831-12833.

(19) Suetsuna, T.; Dragoe, N.; Shimotani, H.; Takeda, A.; Ito, S.; Cross, R. J.; Saunders, M.; Takagi, H.; Kitazawa, K., Chromatographic purification of Kr@C_{60}. *Fullerenes, Nanotubes, Carbon Nanostruct.* **2002,** *10* (1), 15-21.

(20) Pirkle, W. H.; Welch, C. J., An Unusual Effect of Temperature on the Chromatographic Behavior of Buckminsterfullerene. *J. Org. Chem.* **1991,** *56* (25), 6973-6974.

(21) Welch, C. J.; Pirkle, W. H., Progress in the Design of Selectors for Buckminsterfullerene. *J. Chromatogr.* **1992,** *609* (1-2), 89-101.

(22) Kimata, K.; Hirose, T.; Moriuchi, K.; Hosoya, K.; Araki, T.; Tanaka, N., High-Capacity Stationary Phases Containing Heavy-Atoms for HPLC Separation of Fullerenes. *Anal. Chem.* **1995,** *67* (15), 2556-2561.

(23) Jinno, K., *Sep. Fullerene Liq. Chromatogr.* 1999; p 179 pp.

(24) Aihara, J., Kinetic stability of carbon cages in non-classical metallofullerenes. *Chem.Phys. Lett.* **2001,** *343* (5-6), 465-469.

(25) Aihara, J., Kinetic stability of metallofullerenes as predicted by the bond resonance energy model. *Phys. Chem. Chem. Phys.* **2001,** *3* (8), 1427-1431.

(26) Ge, Z. X.; Duchamp, J. C.; Cai, T.; Gibson, H. W.; Dorn, H. C., Purification of endohedral trimetallic nitride fullerenes in a single, facile step. *J. Am. Chem. Soc.* **2005,** *127* (46), 16292-16298.

(27) Angeli, C. D.; Cai, T.; Duchamp, J. C.; Reid, J. E.; Singer, E. S.; Gibson, H. W.; Dorn, H. C., Purification of trimetallic nitride templated endohedral metallofullerenes by a chemical reaction of congeners with eutectic 9-methylanthracene. *Chem. Mater.* **2008,** *20* (15), 4993-4997.

(28) Tsuchiya, T.; Wakahara, T.; Shirakura, S.; Maeda, Y.; Akasaka, T.; Kobayashi, K.; Nagase, S.; Kato, T.; Kadish, K. M., Reduction of endohedral metallofullerenes: A convenient method for isolation. *Chem. Mater.* **2004,** *16* (22), 4343-4346.

(29) Elliott, B.; Yu, L.; Echegoyen, L., A simple isomeric separation of D_{5h} and I_h $Sc_3N@C_{80}$ by selective chemical oxidation. *J. Am. Chem. Soc.* **2005,** *127* (31), 10885-10888.

(30) Tsuchiya, T.; Sato, K.; Kurihara, H.; Wakahara, T.; Nakahodo, T.; Maeda, Y.; Akasaka, T.; Ohkubo, K.; Fukuzumi, S.; Kato, T.; Mizorogi, N.; Kobayashi, K.; Nagase, S., Host-guest complexation of endohedral metallofullerene with azacrown ether and its application. *J. Am. Chem. Soc.* **2006,** *128* (20), 6699-6703.

(31) Brinkmann, G.; Dress, A. W. M., PentHex puzzles - A reliable and efficient top-down approach to fullerene-structure enumeration. *Adv. Appl. Math.* **1998,** *21* (3), 473-480.

(32) Hawkins, J. M.; Meyer, A.; Lewis, T. A.; Loren, S.; Hollander, F. J., Crystal-Structure of Osmylated C_{60} - Confirmation of the Soccer Ball Framework. *Science* **1991,** *252* (5003), 312-313.

(33) Schmalz, T. G.; Seitz, W. A.; Klein, D. J.; Hite, G. E., Elemental Carbon Cages. *J. Am. Chem. Soc.* **1988,** *110* (4), 1113-1127.

(34) Kroto, H. W., The Stability of the Fullerenes C_{24}, C_{28}, C_{32}, C_{36}, C_{50}, C_{60} and C_{70}. *Nature* **1987,** *329* (6139), 529-531.

(35) Balch, A. L.; Catalano, V. J.; Lee, J. W.; Olmstead, M. M.; Parkin, S. R., (Eta-2-C_{70})Ir(Co)Cl(Pph_3)$_2$ - the Synthesis and Structure of an Organometallic Derivative of a Higher Fullerene. *J. Am. Chem. Soc.* **1991,** *113* (23), 8953-8955.

(36) Negri, F.; Orlandi, G.; Zerbetto, F., Prediction of the Structure and the Vibrational Frequencies of a C_{84} Isomer of D_2 Symmetry. *Chem. Phys. Lett.* **1992,** *189* (6), 495-498.

(37) Fowler, P. W.; Manolopoulos, D. E., *An Atlas of fullerenes*. Oxford University: New York: 1995.

(38) Dennis, T. J. S.; Kai, T.; Asato, K.; Tomiyama, T.; Shinohara, H.; Yoshida, T.; Kobayashi, Y.; Ishiwatari, H.; Miyake, Y.; Kikuchi, K.; Achiba, Y., Isolation and characterization by ^{13}C NMR spectroscopy of [84]fullerene minor isomers. *J. Phys. Chem. A* **1999,** *103* (44), 8747-8752.

(39) Kikuchi, K.; Nakahara, N.; Wakabayashi, T.; Suzuki, S.; Shiromaru, H.; Miyake, Y.; Saito, K.; Ikemoto, I.; Kainosho, M.; Achiba, Y., Nmr Characterization of Isomers of C_{78}, C_{82} and C_{84} Fullerenes. *Nature* **1992,** *357* (6374), 142-145.

(40) Miyake, Y.; Minami, T.; Kikuchi, K.; Kainosho, M.; Achiba, Y., Trends in structure and growth of higher fullerenes isomer structure of C_{86} and C_{88}. *Mol. Cryst. Liq. Cryst.* **2000,** *340*, 553-558.

(41) Sun, G. Y.; Kertesz, M., ^{13}C NMR spectra for IPR isomers of fullerene C_{86}. *Chem. Phys.* **2002,** *276* (2), 107-114.

(42) Cai, W. S.; Xu, L.; Shao, N.; Shao, X. G.; Guo, Q. X., An efficient approach for theoretical study on the low-energy isomers of large fullerenes C_{90}-C_{140}. *J. Chem. Phys.* **2005,** *122* (18), 184318-184327.

(43) Osawa, E.; Ueno, H.; Yoshida, M.; Slanina, Z.; Zhao, X.; Nishiyama, M.; Saito, H., Combined topological and energy analysis of the annealing process in fullerene formation. Stone-Wales interconversion pathways among IPR isomers of higher fullerenes. *J. Chem. Soc., Perkin Trans. 2* **1998,** (4), 943-950.

(44) Zhao, X.; Slanina, Z.; Goto, H.; Osawa, E., Theoretical investigations on

relative stabilities of fullerene C_{94}. *J. Chem. Phys.* **2003,** *118* (23), 10534-10540.

(45) Zhao, X.; Goto, H.; Slanina, Z. C_{100} IPR fullerenes: temperature-dependent relative stabilities based on the Gibbs function. *Chem. Phys.* **2004,** *306* (1-3), 93-104.

(46) Zhao, X.; Slanina, Z.; Goto, H., Theoretical studies on the relative stabilities of C_{96} IPR fullerenes. *J. Phys. Chem. A* **2004,** *108* (20), 4479-4484.

(47) Achiba, Y.; Fowler, P. W.; Mitchell, D.; Zerbetto, F., Structural predictions for the C_{116} molecule. *J. Phys. Chem. A* **1998,** *102* (34), 6835-6841.

(48) Xie, S. Y.; Gao, F.; Lu, X.; Huang, R. B.; Wang, C. R.; Zhang, X.; Liu, M. L.; Deng, S. L.; Zheng, L. S., Capturing the labile fullerene[50] as $C_{50}Cl_{10}$. *Science* **2004,** *304* (5671), 699-699.

(49) Han, X.; Zhou, S. J.; Tan, Y. Z.; Wu, X.; Gao, F.; Liao, Z. J.; Huang, R. B.; Feng, Y. Q.; Lu, X.; Xie, S. Y.; Zheng, L. S., Crystal structures of Saturn-like $C_{50}Cl_{10}$ and pineapple-shaped $C_{64}Cl_4$: Geometric implications of double- and triple-pentagon-fused chlorofullerenes. *Angew. Chem. Int. Ed.* **2008,** *47* (29), 5340-5343.

(50) Stevenson, S.; Fowler, P. W.; Heine, T.; Duchamp, J. C.; Rice, G.; Glass, T.; Harich, K.; Hajdu, E.; Bible, R.; Dorn, H. C., A stable non-classical metallofullerene family. *Nature* **2000,** *408* (6811), 427-428.

(51) Wakahara, T.; Nikawa, H.; Kikuchi, T.; Nakahodo, T.; Rahman, G. M. A.; Tsuchiya, T.; Maeda, Y.; Akasaka, T.; Yoza, K.; Horn, E.; Yamamoto, K.; Mizorogi, N.; Slanina, Z.; Nagase, S., La@C_{72} having a non-IPR carbon cage. *J. Am. Chem. Soc.* **2006,** *128* (44), 14228-14229.

(52) Mercado, B. Q.; Beavers, C. M.; Olmstead, M. M.; Chaur, M. N.; Walker, K.; Holloway, B. C.; Echegoyen, L.; Balch, A. L., Is the isolated pentagon rule merely a suggestion for endohedral fullerenes? The structure of a second egg-shaped endohedral fullerene-$Gd_3N@C_s$(39663)-C_{82}. *J. Am. Chem. Soc.* **2008,** *130* (25), 7854-7855.

(53) Beavers, C. M.; Zuo, T.; Duchamp, J. C.; Harich, K.; Dorn, H. C.; Olmstead, M. M.; Balch, A. L., $Tb_3N@C_{84}$: an improbable, egg-shaped endohedral fullerene that violates the isolated Pentagon rule. *J. Am. Chem. Soc.* **2006,** *128* (35), 11352-11353.

(54) Zuo, T.; Walker, K.; Olmstead, M. M.; Melin, F.; Holloway, B. C.; Echegoyen, L.; Dorn, H. C.; Chaur, M. N.; Chancellor, C. J.; Beavers, C. M.; Balch, A. L.; Athans, A. J., New egg-shaped fullerenes: non-isolated pentagon structures of $Tm_3N@C_s$(51365)C_{84} and $Gd_3N@C_s$(51365)-C_{84}. *Chem. Commun.* **2008,** (9), 1067-1069.

(55) Shi, Z. Q.; Wu, X.; Wang, C. R.; Lu, X.; Shinohara, H., Isolation and characterization of $Sc_2C_2@C_{68}$: A metal-carbide endofullerene with a non-IPR carbon cage. *Angew. Chem., Int. Ed.* **2006,** *45* (13), 2107-2111.

(56) Kobayashi, K.; Nagase, S., Structures and electronic states of M@C_{82} (M = Sc, Y, La and lanthanides). *Chem. Phys. Lett.* **1998,** *282* (3-4), 325-329.

(57) Akasaka, T.; Wakahara, T.; Nagase, S.; Kobayashi, K.; Waelchli, M.;

Yamamoto, K.; Kondo, M.; Shirakura, S.; Okubo, S.; Maeda, Y.; Kato, T.; Kako, M.; Nakadaira, Y.; Nagahata, R.; Gao, X.; Van Caemelbecke, E.; Kadish, K. M., La@C_{82} anion. An unusually stable metallofullerene. *J. Am. Chem. Soc.* **2000,** *122* (38), 9316-9317.

(58) Akasaka, T.; Wakahara, T.; Nagase, S.; Kobayashi, K.; Waelchli, M.; Yamamoto, K.; Kondo, M.; Shirakura, S.; Maeda, Y.; Kato, T.; Kako, M.; Nakadaira, Y.; Gao, X.; Van Caemelbecke, E.; Kadish, K. M., Structural determination of the La@C_{82} isomer. *J. Phys. Chem. B* **2001,** *105* (15), 2971-2974.

(59) Ding, J. Q.; Weng, L. T.; Yang, S. H., Electronic structure of Ce@C_{82}: An experimental study. *J. Phys. Chem.* **1996,** *100* (26), 11120-11121.

(60) Wakahara, T.; Kobayashi, J.; Yamada, M.; Maeda, Y.; Tsuchiya, T.; Okamura, M.; Akasaka, T.; Waelchli, M.; Kobayashi, K.; Nagase, S.; Kato, T.; Kako, M.; Yamamoto, K.; Kadish, K. M., Characterization of Ce@C_{82} and its anion. *J. Am. Chem. Soc.* **2004,** *126* (15), 4883-4887.

(61) Nishibori, E.; Takata, M.; Sakata, M.; Inakuma, M.; Shinohara, H., Determination of the cage structure of Sc@C_{82} by synchrotron powder diffraction. *Chem. Phys. Lett.* **1998,** *298* (1-3), 79-84.

(62) Feng, L.; Wakahara, T.; Tsuchiya, T.; Maeda, Y.; Lian, Y. F.; Akasaka, T.; Mizorogi, N.; Kobayashi, K.; Nagase, S.; Kadish, K. M., Structural characterization of Y@C_{82}. *Chem. Phys. Lett.* **2005,** *405* (4-6), 274-277.

(63) Wakahara, T.; Okubo, S.; Kondo, M.; Maeda, Y.; Akasaka, T.; Waelchli, M.; Kako, M.; Kobayashi, K.; Nagase, S.; Kato, T.; Yamamoto, K.; Gao, X.; Van Caemelbecke, E.; Kadish, K. M., Ionization and structural determination of the major isomer of Pr@C_{82}. *Chem. Phys. Lett.* **2002,** *360* (3-4), 235-239.

(64) Takata, M.; Umeda, B.; Nishibori, E.; Sakata, M.; Saito, Y.; Ohno, M.; Shinohara, H., Confirmation by X-Ray-Diffraction of the Endohedral Nature of the Metallofullerene Y@C_{82}. *Nature* **1995,** *377* (6544), 46-49.

(65) Nishibori, E.; Takata, M.; Sakata, M.; Tanaka, H.; Hasegawa, M.; Shinohara, H., Giant motion of La atom inside C_{82} cage. *Chem. Phys. Lett.* **2000,** *330* (5-6), 497-502.

(66) Yamada, M.; Wakahara, T.; Lian, Y. F.; Tsuchiya, T.; Akasaka, T.; Waelchli, M.; Mizorogi, N.; Nagase, S.; Kadish, K. M., Analysis of lanthanide-induced NMR shifts of the Ce@C_{82} anion. *J. Am. Chem. Soc.* **2006,** *128* (5), 1400-1401.

(67) Weaver, J. H.; Chai, Y.; Kroll, G. H.; Jin, C.; Ohno, T. R.; Haufler, R. E.; Guo, T.; Alford, J. M.; Conceicao, J.; Chibante, L. P. F.; Jain, A.; Palmer, G.; Smalley, R. E., Xps Probes of Carbon-Caged Metals. *Chem. Phys. Lett.* **1992,** *190* (5), 460-464.

(68) Laasonen, K.; Andreoni, W.; Parrinello, M., Structural and Electronic-Properties of La@C_{82}. *Science* **1992,** *258* (5090), 1916-1918.

(69) Nagase, S.; Kobayashi, K., Theoretical-Study of the Lanthanide Fullerene CeC_{82} - Comparison with ScC_{82}, YC_{82} and LaC_{82}. *Chem. Phys. Lett.* **1994,** *228* (1-3), 106-110.

(70) Poirier, D. M.; Knupfer, M.; Weaver, J. H.; Andreoni, W.; Laasonen, K.;

Parrinello, M.; Bethune, D. S.; Kikuchi, K.; Achiba, Y., Electronic and Geometric Structure of La@C_{82} and C_{82} - Theory and Experiment. *Phy. Rev. B* **1994,** *49* (24), 17403-17412.

(71) Tsuchiya, T.; Sato, K.; Kurihara, H.; Wakahara, T.; Maeda, Y.; Akasaka, T.; Ohkubo, K.; Fukuzumi, S.; Kato, T.; Nagase, S., Spin-site exchange system constructed from endohedral metallofullerenes and organic donors. *J. Am. Chem. Soc.* **2006,** *128* (45), 14418-14419.

(72) Beyers, R.; Kiang, C. H.; Johnson, R. D.; Salem, J. R.; Devries, M. S.; Yannoni, C. S.; Bethune, D. S.; Dorn, H. C.; Burbank, P.; Harich, K.; Stevenson, S., Preparation and Structure of Crystals of the Metallofullerene Sc_2@C_{84}. *Nature* **1994,** *370* (6486), 196-199.

(73) Dennis, T. J. S.; Kai, T.; Tomiyama, T.; Shinohara, H., Isolation and characterisation of the two major isomers of [84]fullerene (C_{84}). *Chem. Commun.* **1998,** (5), 619-620.

(74) Inakuma, M.; Yamamoto, E.; Kai, T.; Wang, C. R.; Tomiyama, T.; Shinohara, H.; Dennis, T. J. S.; Hulman, M.; Krause, M.; Kuzmany, H., Structural and electronic properties of isomers of Sc_2@C_{84} (I, II, III): ^{13}C NMR and IR/Raman spectroscopic studies. *J. Phys. Chem. B* **2000,** *104* (21), 5072-5077.

(75) Nagase, S.; Kobayashi, K., Structural study of endohedral dimetallofullerenes Sc_2@C_{84} and Sc_2@C_{74}. *Chem. Phys. Lett.* **1997,** *276* (1-2), 55-61.

(76) Iiduka, Y.; Wakahara, T.; Nakajima, K.; Tsuchiya, T.; Nakahodo, T.; Maeda, Y.; Akasaka, T.; Mizorogi, N.; Nagase, S., ^{13}C NMR spectroscopic study of scandium dimetallofullerene, Sc_2@C_{84} vs. Sc_2C_2@C_{82}. *Chem. Commun.* **2006,** (19), 2057-2059.

(77) Akasaka, T.; Nagase, S.; Kobayashi, K.; Walchli, M.; Yamamoto, K.; Funasaka, H.; Kako, M.; Hoshino, T.; Erata, T., ^{13}C and ^{139}La NMR studies of La_2@C_{80}: First evidence for circular motion of metal atoms in endohedral dimetallofullerenes. *Angew. Chem. Int. Ed.* **1997,** *36* (15), 1643-1645.

(78) Takata, M.; Nishibori, E.; Sakata, M., Charge density studies utilizing powder diffraction and MEM. Exploring of high Tc superconductors, C_{60} superconductors and manganites. *Z. Kristall.* **2001,** *216* (2), 71-86.

(79) Kobayashi, K.; Nagase, S.; Akasaka, T., A Theoretical Study of C_{80} and La_2@C_{80}. *Chem. Phys. Lett.* **1995,** *245* (2-3), 230-236.

(80) Stevenson, S.; Rice, G.; Glass, T.; Harich, K.; Cromer, F.; Jordan, M. R.; Craft, J.; Hadju, E.; Bible, R.; Olmstead, M. M.; Maitra, K.; Fisher, A. J.; Balch, A. L.; Dorn, H. C., Small-bandgap endohedral metallofullerenes in high yield and purity. *Nature* **1999,** *401* (6748), 55-57.

(81) Krause, M.; Kuzmany, H.; Georgi, P.; Dunsch, L.; Vietze, K.; Seifert, G., Structure and stability of endohedral fullerene Sc_3N@C_{80}: A Raman, infrared, and theoretical analysis. *J. Chem. Phys.* **2001,** *115* (14), 6596-6605.

(82) Dunsch, L.; Krause, M.; Noack, J.; Georgi, P., Endohedral nitride cluster fullerenes - Formation and spectroscopic analysis of $L_{3-x}M_xN$@C_{2n} ($0 <= x <= 3$; N=39, 40). *J. Phys. Chem. Solids* **2004,** *65* (2-3), 309-315.

(83) Wolf, M.; Muller, K. H.; Eckert, D.; Skourski, Y.; Georgi, P.; Marczak, R.;

Krause, M.; Dunsch, L., Magnetic moments in $Ho_3N@C_{80}$ and $Tb_3N@C_{80}$. *J. Magn. Mater.* **2005,** *290*, 290-293.

(84) Stevenson, S.; Lee, H. M.; Olmstead, M. M.; Kozikowski, C.; Stevenson, P.; Balch, A. L., Preparation and crystallographic characterization of a new endohedral, $Lu_3N@C_{80}$·5(o-xylene), and comparison with $Sc_3N@C_{80}$·5(o-xylene). *Chem.-Eur. J.* **2002,** *8* (19), 4528-4535.

(85) Krause, M.; Wong, J.; Dunsch, L., Expanding the world of endohedral fullerenes - The $Tm_3N@C_{2n}$ (39 <= n <= 43) clusterfullerene family. *Chem. -Eur. J.* **2005,** *11* (2), 706-711.

(86) Zuo, T. M.; Olmstead, M. M.; Beavers, C. M.; Balch, A. L.; Wang, G. B.; Yee, G. T.; Shu, C. Y.; Xu, L. S.; Elliott, B.; Echegoyen, L.; Duchamp, J. C.; Dorn, H. C., Preparation and structural characterization of the I_h and the D_{5h} isomers of the endohedral fullerenes $Tm_3N@C_{80}$: Icosahedral C_{80} cage encapsulation of a trimetallic nitride magnetic cluster with three uncoupled Tm^{3+} ions. *Inorg. Chem.* **2008,** *47* (12), 5234-5244.

(87) Stevenson, S.; Phillips, J. P.; Reid, J. E.; Olmstead, M. M.; Rath, S. P.; Balch, A. L., Pyramidalization of Gd_3N inside a C_{80} cage. The synthesis and structure of $Gd_3N@C_{80}$. *Chem. Commun.* **2004,** (24), 2814-2815.

(88) Krause, M.; Dunsch, L., Gadolinium nitride $_{Gd3N}$ in carbon cages: The influence of cluster size and bond strength. *Angew. Chem. Int. Ed.* **2005,** *44* (10), 1557-1560.

(89) Yang, S. F.; Dunsch, L., A large family of dysprosium-based trimetallic nitride endohedral fullerenes: $Dy_3N@C_{2n}$ (39 <= n <= 44). *J. Phys. Chem. B* **2005,** *109* (25), 12320-12328.

(90) Wolf, M.; Muller, K. H.; Skourski, Y.; Eckert, D.; Georgi, P.; Krause, M.; Dunsch, L., Magnetic moments of the endohedral cluster fullerenes $Ho_3N@C_{80}$ and $Tb_3N@C_{80}$: The role of ligand fields. *Angew. Chem. Int. Ed.* **2005,** *44* (21), 3306-3309.

(91) Zuo, T. M.; Beavers, C. M.; Duchamp, J. C.; Campbell, A.; Dorn, H. C.; Olmstead, M. M.; Balch, A. L., Isolation and structural characterization of a family of endohedral fullerenes including the large, chiral cage fullerenes $Tb_3N@C_{88}$ and $Tb_3N@C_{86}$ as well as the I_h and D_{5h} isomers of $Tb_3N@C_{80}$. *J. Am. Chem. Soc.* **2007,** *129* (7), 2035-2043.

(92) Olmstead, M. M.; de Bettencourt-Dias, A.; Duchamp, J. C.; Stevenson, S.; Dorn, H. C.; Balch, A. L., Isolation and crystallographic characterization of $ErSc_2N@C_{80}$: an endohedral fullerene which crystallizes with remarkable internal order. *J. Am. Chem. Soc.* **2000,** *122* (49), 12220-12226.

(93) Wang, X. L.; Zuo, T. M.; Olmstead, M. M.; Duchamp, J. C.; Glass, T. E.; Cromer, F.; Balch, A. L.; Dorn, H. C., Preparation and structure of $CeSc_2N@C_{80}$: An icosahedral carbon cage enclosing an acentric $CeSc_2N$ unit with buried f electron spin. *J. Am. Chem. Soc.* **2006,** *128* (27), 8884-8889.

(94) Kobayashi, K.; Sano, Y.; Nagase, S., Theoretical study of endohedral metallofullerenes: $Sc_{3-n}La_nN@C_{80}$ (n=0-3). *J. Comput. Chem.* **2001,** *22* (13), 1353-1358.

(95) Duchamp, J. C.; Demortier, A.; Fletcher, K. R.; Dorn, D.; Iezzi, E. B.; Glass, T.; Dorn, H. C., An isomer of the endohedral metallofullerene $Sc_3N@C_{80}$ with D_{5h} symmetry. *Chem. Phys. Lett.* **2003,** *375* (5-6), 655-659.

(96) Cai, T.; Xu, L.; Anderson, M. R.; Ge, Z.; Zuo, T.; Wang, X.; Olmstead, M. M.; Balch, A. L.; Gibson, H. W.; Dorn, H. C. C., Structure and enhanced reactivity rates of the D_{5h} $Sc_3N@C_{80}$ and $Lu_3N@C_{80}$ metallofullerene isomers: the importance of the pyracylene motif. *J. Am. Chem. Soc.* **2006,** *128* (26), 8581-8589.

(97) Reveles, J. U.; Heine, T.; Koster, A. M., ^{13}C NMR pattern of $Sc_3N@C_{68}$. Structural assignment of the first fullerene with adjacent pentagons. *J. Phys. Chem. A* **2005,** *109* (32), 7068-7072.

(98) Olmstead, M. M.; Lee, H. M.; Duchamp, J. C.; Stevenson, S.; Marciu, D.; Dorn, H. C.; Balch, A. L., $Sc_3N@C_{68}$: Folded pentalene coordination in an endohedral fullerene that does not obey the isolated pentagon rule. *Angew. Chem. Int. Ed.* **2003,** *42* (8), 900-903.

(99) Olmstead, M. H.; de Bettencourt-Dias, A.; Duchamp, J. C.; Stevenson, S.; Marciu, D.; Dorn, H. C.; Balch, A. L., Isolation and structural characterization of the endohedral fullerene $Sc_3N@C_{78}$. *Angew. Chem. Int. Ed.* **2001,** *40* (7), 1223-1225.

(100) Slanina, Z.; Francois, J. P.; Bakowies, D.; Thiel, W., Fullerene C-78 Isomers - Temperature-Dependence of Their Calculated Relative Stabilities. *Theochem.-J. Mol. Struc.* **1993,** *98*, 213-216.

(101) Campanera, J. M.; Bo, C.; Olmstead, M. M.; Balch, A. L.; Poblet, J. M., Bonding within the endohedral fullerenes $Sc_3N@C_{78}$ and $Sc_3N@C_{80}$ as determined by density functional calculations and reexamination of the crystal structure of $\{Sc_3N@C_{78}\}\cdot \{Co(OEP)\}\cdot 1.5(C_6H_6)\cdot 0.3(CHCl_3)$.*J. Phys. Chem. A* **2002,** *106* (51), 12356-12364.

(102) Melin, F.; Chaur, M. N.; Engmann, S.; Elliott, B.; Kumbhar, A.; Athans, A. J.; Echegoyen, L., The large $Nd_3N@C_{2n}$ ($40 <= n <= 49$) cluster fullerene family: preferential templating of a C_{88} cage by a trimetallic nitride cluster. *Angew. Chem. Int. Ed.* **2007,** *46* (47), 9032-9035.

(103) Chaur, M. N.; Melin, F.; Elliott, B.; Kumbhar, A.; Athans, A. J.; Echegoyen, L., New $M_3N@C_{2n}$ endohedral metallofullerene families (M = Nd, Pr, Ce; n=40-53): Expanding the preferential templating of the C_{88} cage and approaching the C_{96} cage. *Chem--Eur. J.* **2008,** *14* (15), 4594-4599.

(104) Wang, C. R.; Inakuma, M.; Shinohara, H., Metallofullerenes $Sc_2@C_{82}$ (I, II) and $Sc_2@C_{86}$ (I, II): isolation and spectroscopic studies. *Chem. Phys. Lett.* **1999,** *300* (3-4), 379-384.

(105) Shinohara, H.; Sato, H.; Ohkohchi, M.; Ando, Y.; Kodama, T.; Shida, T.; Kato, T.; Saito, Y., Encapsulation of a Scandium Trimer in C_{82}. *Nature* **1992,** *357* (6373), 52-54.

(106) Stevenson, S.; Dorn, H. C.; Burbank, P.; Harich, K.; Sun, Z.; Kiang, C. H.; Salem, J. R.; Devries, M. S.; Vanloosdrecht, P. H. M.; Johnson, R. D.; Yannoni, C. S.; Bethune, D. S., Isolation and Monitoring of the Endohedral

Metallofullerenes $Y@C_{82}$ and $Sc_3@C_{82}$ - Online Chromatographic-Separation with Epr Detection. *Anal. Chem.* **1994,** *66* (17), 2680-2685.

(107) Yamamoto, E.; Tansho, M.; Tomiyama, T.; Shinohara, H.; Kawahara, H.; Kobayashi, Y., ^{13}C NMR study on the structure of isolated $Sc_2@C_{84}$ metallofullerene. *J. Am. Chem. Soc.* **1996,** *118* (9), 2293-2294.

(108) Wang, C. R.; Kai, T.; Tomiyama, T.; Yoshida, T.; Kobayashi, Y.; Nishibori, E.; Takata, M.; Sakata, M.; Shinohara, H., A scandium carbide endohedral metallofullerene: $(Sc_2C_2)@C_{84}$. *Angew. Chem. Int. Ed.* **2001,** *40* (2), 397-399.

(109) Iiduka, Y.; Wakahara, T.; Nakahodo, T.; Tsuchiya, T.; Sakuraba, A.; Maeda, Y.; Akasaka, T.; Yoza, K.; Horn, E.; Kato, T.; Liu, M. T. H.; Mizorogi, N.; Kobayashi, K.; Nagase, S., Structural Determination of Metallofullerene Sc_3C_{82} Revisited: A Surprising Finding. *J. Am. Chem. Soc.* **2005,** *127* (36), 12500-12501.

(110) Nishibori, E.; Terauchi, I.; Sakata, M.; Takata, M.; Ito, Y.; Sugai, T.; Shinohara, H., High-resolution analysis of $(Sc_3C_2)@C_{80}$ metallofullerene by third generation synchrotron radiation X-ray powder diffraction. *J. Phys. Chem. B* **2006,** *110* (39), 19215-19219.

(111) Nishibori, E.; Ishihara, M.; Takata, M.; Sakata, M.; Ito, Y.; Inoue, T.; Shinohara, H., Bent $(metal)_2C_2$ clusters encapsulated in $(Sc_2C_2)@C_{82}$(III) and $(Y_2C_2)@C_{82}$(III) metallofullerenes. *Chem. Phy. Lett.* **2006,** *433* (1-3), 120-124.

(112) Takata, M.; Nishibori, E.; Umeda, B.; Sakata, M.; Yamamoto, E.; Shinohara, H., Structure of endohedral dimetallofullerene $Sc_2@C_{84}$. *Phys. Rev. Lett.* **1997,** *78* (17), 3330-3333.

(113) Iiduka, Y.; Wakahara, T.; Nakajima, K.; Nakahodo, T.; Tsuchiya, T.; Maeda, Y.; Akasaka, T.; Yoza, K.; Liu, M. T. H.; Mizorogi, N.; Nagase, S., Experimental and theoretical studies of the scandium carbide endohedral metallofullerene $Sc_2C_2@C_{82}$ and its carbene derivative. *Angew. Chem. Int. Ed.* **2007,** *46* (29), 5562-5564.

(114) Inoue, T.; Tomiyama, T.; Sugai, T.; Shinohara, H., Spectroscopic and structural study of Y_2C_2 carbide encapsulating endohedral metallofullerene: $(Y_2C_2)@C_{82}$. *Chem. Phys. Lett.* **2003,** *382* (3-4), 226-231.

(115) Yamazaki, Y.; Nakajima, K.; Wakahara, T.; Tsuchiya, T.; Ishitsuka, M. O.; Maeda, Y.; Akasaka, T.; Waelchli, M.; Mizorogi, N.; Nagase, S., Observation of ^{13}C NMR chemical shifts of metal carbides encapsulated in fullerenes: $Sc_2C_2@C_{82}$, $Sc_2C_2@C_{84}$, and $Sc_3C_2@C_{80}$. *Angew. Chem. Int. Ed.* **2008,** *47* (41), 7905-7908.

(116) Yang, H.; Lu, C.; Liu, Z.; Jin, H.; Che, Y.; Olmstead, M. M.; Balch, A. L., Detection of a Family of Gadolinium-Containing Endohedral Fullerenes and the Isolation and Crystallographic Characterization of One Member as a Metal-Carbide Encapsulated inside a Large Fullerene Cage. *J. Am. Chem. Soc.* **2008,** *130* (51), 17296-17300.

(117) Cox, D. M.; Reichmann, K. C.; Trevor, D. J.; Kaldor, A., Co Chemisorption on Free Gas-Phase Metal-Clusters. *J. Phys. Chem.* **1988,** *88* (1), 111-119.

(118) Andreoni, W.; Curioni, A.; Holczer, K.; Prassides, K.; KeshavarzK, M.;

Hummelen, J. C.; Wudl, F., Unconventional bonding of azafullerenes: Theory and experiment. *J. Am. Chem. Soc.* **1996,** *118* (45), 11335-11336.

(119) Hauke, F.; Vostrowsky, O.; Hirsch, A.; Quaranta, A.; Leibl, W.; Leach, S.; Edge, R.; Navaratnam, S.; Bensasson, R. V., Monomeric azaheterofullerene derivatives $RC_{59}N$: Influence of the R moiety on spectroscopic and photophysical properties. *Chem.-Eur. J.* **2006,** *12* (18), 4813-4820.

(120) Kim, K. C.; Hauke, F.; Hirsch, A.; Boyd, P. D. W.; Carter, E.; Armstrong, R. S.; Lay, P. A.; Reed, C. A., Synthesis of the $C_{59}N^+$ carbocation. A monomeric azafullerene isoelectronic to C_{60}. *J. Am. Chem. Soc.* **2003,** *125* (14), 4024-4025.

(121) Akasaka, T.; Okubo, S.; Wakahara, T.; Yamamoto, K.; Kobayashi, K.; Nagase, S.; Kato, T.; Kako, M.; Nakadaira, Y.; Kitayama, Y.; Matsuura, K., Endohedrally metal-doped heterofullerenes: $La@C_{81}N$ and $La_2@C_{79}N$. *Chem. Lett.* **1999,** (9), 945-946.

(122) Zuo, T. M.; Xu, L. S.; Beavers, C. M.; Olmstead, M. M.; Fu, W. J.; Crawford, D.; Balch, A. L.; Dorn, H. C., $M_2@C_{79}N$ (M = Y, Tb): Isolation and characterization of stable endohedral metallofullerenes exhibiting M-M bonding interactions inside aza[80]fullerene cages. *J. Am. Chem. Soc.* **2008,** *130* (39), 12992-12997.

(123) Akiba, E., Research and development of hydrogen storage materials. *Shokubai* **2009,** *51* (4), 287-291.

(124) Withers, J. C.; Loutfy, R. O.; Lowe, T. P., Fullerene commercial vision. *Fullerene Sci. Technol.* **1997,** *5* (1), 1-31.

(125) Henderson, C. C.; Cahill, P. A., $C_{60}H_2$ - Synthesis of the Simplest C_{60} Hydrocarbon Derivative. *Science* **1993,** *259* (5103), 1885-1887.

(126) Henderson, C. C.; Cahill, P. A. Semiempirical Calculations of the Isomeric C_{60} Dihydrides. *Chem. Phys. Lett.* **1992,** *198* (6), 570-576.

(127) Nossal, J.; Saini, R. K.; Alemany, L. B.; Meier, M.; Billups, W. E., The synthesis and characterization of fullerene hydrides. *Eur. J. Org. Chem.* **2001,** (22), 4167-4180.

(128) Henderson, C. C.; Rohlfing, C. M.; Assink, R. A.; Cahill, P. A., $C_{60}H_4$ - Kinetics and Thermodynamics of Multiple Addition to C_{60}. *Angew. Chem. Int. Ed.* **1994,** *33* (7), 786-788.

(129) Haufler, R. E.; Conceicao, J.; Chibante, L. P. F.; Chai, Y.; Byrne, N. E.; Flanagan, S.; Haley, M. M.; Obrien, S. C.; Pan, C.; Xiao, Z.; Billups, W. E.; Ciufolini, M. A.; Hauge, R. H.; Margrave, J. L.; Wilson, L. J.; Curl, R. F.; Smalley, R. E., Efficient Production of C_{60} (Buckminsterfullerene), $C_{60}H_{36}$, and the Solvated Buckide Ion. *J. Phys. Chem.***1990,** *94* (24), 8634-8636.

(130) Banks, M. R.; Dale, M. J.; Gosney, I.; Hodgson, P. K. G.; Jennings, R. C. K.; Jones, A. C.; Lecoultre, J.; Langridgesmith, P. R. R.; Maier, J. P.; Scrivens, J. H.; Smith, M. J. C.; Smyth, C. J.; Taylor, A. T.; Thorburn, P.; Webster, A. S., Birch Reduction of C_{60} - a New Appraisal. *J. Chem. Soc., Chem. Commun.* **1993,** (14), 1149-1152.

(131) Billups, W. E.; Luo, W. M.; Gonzalez, A.; Arguello, D.; Alemany, L. B.; Marriott, T.; Saunders, M.; JimenezVazquez, H. A.; Khong, A., Reduction of

C_{60} using anhydrous hydrazine. *Tetrahedron Lett.* **1997,** *38* (2), 171-174.

(132) Nossal, J.; Saini, R. K.; Sadana, A. K.; Bettinger, H. F.; Alemany, L. B.; Scuseria, G. E.; Billups, W. E.; Saunders, M.; Khong, A.; Weisemann, R., Formation, isolation, spectroscopic properties, and calculated properties of some isomers of $C_{60}H_{36}$. *J. Am. Chem. Soc.* **2001,** *123* (35), 8482-8495.

(133) Jin, C. M.; Hettich, R.; Compton, R.; Joyce, D.; Blencoe, J.; Burch, T., Direct Solid-Phase Hydrogenation of Fullerenes. *J. Phys. Chem.* **1994,** *98* (16), 4215-4217.

(134) Ruchardt, C.; Gerst, M.; Ebenhoch, J.; Beckhaus, H. D.; Campbell, E. E. B.; Tellgmann, R.; Schwarz, H.; Weiske, T.; Pitter, S. Transfer hydrogenation and deuteration of buckminsterfullerene C_{60} by 9,10-Dihydroanthracene and 9,9',10,10'-tetradeuterioanthracene. *Angew. Chem. Int. Ed.* **1993,** *32* (4), 584-586.

(135) Spielmann, H. P.; Wang, G.-W.; Meier, M. S.; Weedon, B. R., Preparation of $C_{70}H_2$, $C_{70}H_4$, and $C_{70}H_8$: Three Independent Reduction Manifolds in the Zn(Cu) Reduction of C_{70}. *J. Org. Chem.* **1998,** *63* (26), 9865-9871.

(136) Ballenweg, S.; Gleiter, R.; Kraetschmer, W., Hydrogenation of buckminsterfullerene C_{60} via hydrozirconation: a new way to organofullerenes. *Tetrahedron Lett.* **1993,** *34* (23), 3737-40.

(137) Attalla, M. I.; Vassallo, A. M.; Tattam, B. N.; Hanna, J. V., Preparation of Hydrofullerenes by Hydrogen Radical-Induced Hydrogenation. *J. Phys. Chem.* **1993,** *97* (24), 6329-6331.

(138) Cliffel, D. E.; Bard, A. J., Electrochemical Studies of the Protonation of C_{60}^- and C_{60}^{2-}. *J. Phys. Chem.* **1994,** *98* (33), 8140-8143.

(139) Zhang, J. P.; Wang, N. X.; Yang, Y. X.; Yu, A. G., Hydrogenation of [60]fullerene with lithium in aliphatic amines. *Carbon* **2004,** *42* (3), 675-676.

(140) Balasubramanian, K., Enumeration of isomers of polysubstituted carbon sixty-atom molecule (buckminsterfullerene), and application to NMR. *Chem. Phys. Lett.* **1991,** *182* (3-4), 257-62.

(141) Clare, B. W.; Kepert, D. L., Structures and Stabilities of Hydrofullerenes - Completion of a Tetrahedral Fused Quadruple Crown Structure and a Double Crown Structure at $C_{60}H_{36}$. *Theochem.-J. Mol. Stru.c* **1994,** *110* (3), 181-189.

(142) Darwish, A. D.; Kroto, H. W.; Taylor, R.; Walton, D. R. M., Hydrogenation of [76]-, [78]- and [84]-fullerenes: Cage degradation. *J. Chem. Soc.,Perkin Tran. 2* **1996,** (7), 1415-1418.

(143) Darwish, A. D.; Abdulsada, A. K.; Langley, G. J.; Kroto, H. W.; Taylor, R.; Walton, D. R. M., Polyhydrogenation of [60]-Fullerenes and [70]-Fullerenes. *J. Chem. Soc.,Perkin Tran. 2* **1995,** (12), 2359-2365.

(144) Bensasson, R. V.; Hill, T. J.; Land, E. J.; Leach, S.; McGarvey, D. J.; Truscott, T. G.; Ebenhoch, J.; Gerst, M.; Ruchardt, C., Spectroscopy and photophysics of $C_{60}H_{18}$ and $C_{60}H_{36}$. *Chem. Phys.* **1997,** *215* (1), 111-123.

(145) Bini, R.; Ebenhoch, J.; Fanti, M.; Fowler, P. W.; Leach, S.; Orlandi, G.; Ruchardt, C.; Sandall, J. P. B.; Zerbetto, F., The vibrational spectroscopy of $C_{60}H_{36}$: An experimental and theoretical study. *Chem. Phys.* **1998,** *232* (1-2),

75-94.

(146) Saunders, M.; Jimenezvazquez, H. A.; Bangerter, B. W.; Cross, R. J.; Mroczkowski, S.; Freedberg, D. I.; Anet, F. A. L., ^{3}He NMR - a Powerful New Tool for Following Fullerene Chemistry. *J. Am. Chem. Soc.* **1994,** *116* (8), 3621-3622.

(147) Peera, A. A.; Alemany, L. B.; Billups, W. E., Hydrogen storage in hydrofullerides. *Appl. Phys. A: Mater. Sci. Process.* **2004,** *78* (7), 995-1000.

(148) Hirsch, A., Fullerene chemistry: an overview. *Angew. Chem. Int. Ed.* **1993,** 32(8), 1138-1141.

(149) Henderson, C. C.; Rohlfing, C. M.; Cahill, P. A., Theoretical-Studies of Selected $C_{60}H_2$ and $C_{70}H_2$ Isomers. *Chem. Phys. Lett.* **1993,** *213* (3-4), 383-388.

(150) Henderson, C. C.; Rohlfing, C. M.; Gillen, K. T.; Cahill, P. A., Synthesis, Isolation, and Equilibration of 1,9-$C_{70}H_2$ and 7,8-$C_{70}H_2$. *Science* **1994,** *264* (5157), 397-399.

(151) Avent, A. G.; Darwish, A. D.; Heimbach, D. K.; Kroto, H. W.; Meidine, M. F.; Parsons, J. P.; Remars, C.; Roers, R.; Ohashi, O.; Taylor, R.; Walton, D. R. M., Formation of Hydrides of Fullerene-C_{60} and Fullerene C_{70}. *J. Chem. Soc., Perkin Tran. 2* **1994,** (1), 15-22.

(152) Darwish, A. D.; AbdulSada, A. K.; Langley, G. J.; Kroto, H. W.; Taylor, R.; Walton, D. R. M., Polyhydrogenation of [60]- and [70]fullerenes with Zn/HCl and Zn/DCl. *Synth. Met.* **1996,** *77* (1-3), 303-307.

(153) Bosi, S.; Da Ros, T.; Spalluto, G.; Prato, M., Fullerene derivatives: an attractive tool for biological applications. *Eur. J. Med. Chem.* **2003,** *38* (11-12), 913-923.

(154) Friedman, S. H.; Decamp, D. L.; Sijbesma, R. P.; Srdanov, G.; Wudl, F.; Kenyon, G. L., Inhibition of the Hiv-1 Protease by Fullerene Derivatives - Model-Building Studies and Experimental-Verification. *J. Am. Chem. Soc.* **1993,** *115* (15), 6506-6509.

(155) Sijbesma, R.; Srdanov, G.; Wudl, F.; Castoro, J. A.; Wilkins, C.; Friedman, S. H.; Decamp, D. L.; Kenyon, G. L., Synthesis of a Fullerene Derivative for the Inhibition of Hiv Enzymes. *J. Am. Chem. Soc.* **1993,** *115* (15), 6510-6512.

(156) Marcorin, G. L.; Da Ros, T.; Castellano, S.; Stefancich, G.; Bonin, I.; Miertus, S.; Prato, M., Design and synthesis of novel [60]fullerene derivatives as potential HIV aspartic protease inhibitors. *Org. Lett.* **2000,** *2* (25), 3955-3958.

(157) Beyer, C. E.; Steketee, J. D.; Saphier, D., Antioxidant properties of melatonin-an emerging mystery. *Biochem. Pharmacol.* **1998,** *56* (10), 1265-1272.

(158) Chan, P. H., Reactive oxygen radicals in signaling and damage in the ischemic brain. *J. Cereb. Blood Flow Metab.* **2001,** *21* (1), 2-14.

(159) Xie, Q. S.; Perezcordero, E.; Echegoyen, L., Electrochemical Detection of C_{60}^{6-} and C_{70}^{6-} - Enhanced Stability of Fullerides in Solution. *J. Am. Chem. Soc.* **1992,** *114* (10), 3978-3980.

(160) Cheng, F. Y.; Yang, X. L.; Zhu, H. S.; Sun, J.; Liu, Y., Synthesis of oligoadducts of malonic acid C_{60} and their scavenging effects on hydroxyl radical. *J. Phys. Chem. Solids* **2000,** *61* (7), 1145-1148.

(161) Lee, Y.-T.; Chiang, L.-Y.; Chen, W.-J.; Hsu, H.-C., Water-soluble hexasulfobutyl[60]fullerene inhibit low-density lipoprotein oxidation in aqueous and lipophilic phases (44517). *Proc. Soc. Exp. Biol. Med.* **2000,** *224* (2), 69-75.

(162) Lai, H. S.; Chen, W. J.; Chiang, L. Y., Free radical scavenging activity of fullerenol on the ischemia-reperfusion intestine in dogs. *World J. Surg.* **2000,** *24* (4), 450-454.

(163) Dugan, L. L.; Turetsky, D. M.; Du, C.; Lobner, D.; Wheeler, M.; Almli, C. R.; Shen, C. K. F.; Luh, T.-Y.; Choi, D. W.; Lin, T.-S., Carboxyfullerenes as neuroprotective agents. *Proc. Natl. Acad. Sci. U. S. A.* **1997,** *94* (17), 9434-9439.

(164) Liu, X.-F.; Guan, W.-C.; Ke, W.-S., Synthesis and enhanced neuroprotective activity of C_{60}-based ebselen derivatives. *Can. J. Chem.* **2007,** *85* (3), 157-163.

(165) Bolskar, R. D., Gadofullerene MRI contrast agents. *Nanomed.* **2008,** *3* (2), 201-213.

(166) Caravan, P.; Ellision, J. J.; McMurry, T. J.; Lauffer, R. B., Gadolinium(III) Chelates as MRI Contrast Agents: Structure, Dynamics, and Applications. *Chem. Rev.* **1999,** *99*, 2293-2352.

(167) Cagle, D. W.; Alford, J. M.; Tien, J.; Wilson, L. J., Gadolinium-containing fullerenes for MRI contrast agent applications. *Proc. - Electrochem. Soc.* **1997,** *97-14* (Recent Advances in the Chemistry and Physics of Fullerenes and Related Materials), 361-368.

(168) Hartman, K. B.; Laus, S.; Bolskar, R. D.; Muthupillai, R.; Helm, L.; Toth, E.; Merbach, A. E.; Wilson, L. J., Gadonanotubes as ultrasensitive pH-smart probes for magnetic resonance imaging. *Nano Lett.* **2008,** *8*, 415-419.

(169) Kato, H.; Kanazawa, Y.; Okumura, M.; Taninaka, A.; Yokawa, T.; Shinohara, H., Lanthanoid endohedral metallofullerenols for MRI contrast agents. *J. Am. Chem. Soc.* **2003,** *125* (14), 4391-4397.

(170) Mikawa, M.; Kato, H.; Okumura, M.; Narazaki, M.; Kanazawa, Y.; Miwa, N.; Shinohara, H., Paramagnetic water-soluble metallofullerenes having the highest relaxivity for MRI contrast agents. *Bioconjugate Chem.* **2001,** *12* (4), 510-514.

(171) Yin, J. J.; Lao, F.; Fu, P. P.; Wamer, W. G.; Zhao, Y. L.; Wang, P. C.; Qiu, Y.; Sun, B. Y.; Xing, G. M.; Dong, J. Q.; Liang, X. J.; Chen, C. Y., The scavenging of reactive oxygen species and the potential for cell protection by functionalized fullerene materials. *Biomaterials* **2009,** *30* (4), 611-621.

(172) Fatouros, P. P.; Corwin, F. D.; Chen, Z. J.; Broaddus, W. C.; Tatum, J. L.; Kettenmann, B.; Ge, Z.; Gibson, H. W.; Russ, J. L.; Leonard, A. P.; Duchamp, J. C.; Dorn, H. C., In vitro and in vivo imaging studies of a new endohedral metallofullerene nanoparticle. *Radiology* **2006,** *240* (3), 756-764.

(173) Hoppe, H.; Sariciftci, N. S., Organic solar cells: An overview. *J. Mater. Res.* **2004,** *19* (7), 1924-1945.

(174) Thompson Barry, C.; Frechet Jean, M. J., Polymer-fullerene composite solar cells. *Angew. Chem. Int. Ed.* **2008,** *47* (1), 58-77.

(175) Brabec, C. J.; Sariciftci, N. S.; Hummelen, J. C., Plastic solar cells. *Adv. Funct.*

Mater. **2001,** *11* (1), 15-26.

(176) Hummelen, J. C.; Knight, B. W.; Lepeq, F.; Wudl, F.; Yao, J.; Wilkins, C. L., Preparation and characterization of fulleroid and methanofullerene derivatives. *J. Org. Chem.* **1995,** *60* (3), 532-538.

(177) Shaheen, S. E.; Brabec, C. J.; Sariciftci, N. S.; Padinger, F.; Fromherz, T.; Hummelen, J. C., 2.5% efficient organic plastic solar cells. *Appl. Phys. Lett.* **2001,** *78* (6), 841-843.

(178) Wienk, M. M.; Kroon, J. M.; Verhees, W. J. H.; Knol, J.; Hummelen, J. C.; van Hal, P. A.; Janssen, R. A. J., Efficient methano[70]fullerene/MDMO-PPV bulk heterojunction photovoltaic cells. *Angew Chem Int. Ed.* **2003,** *42* (29), 3371-3375.

(179) Li, G.; Shrotriya, V.; Huang, J. S.; Yao, Y.; Moriarty, T.; Emery, K.; Yang, Y., High-efficiency solution processable polymer photovoltaic cells by self-organization of polymer blends. *Nature Mater.* **2005,** *4* (11), 864-868.

(180) Ma, W.; Yang, C.; Gong, X.; Lee, K.; Heeger, A. J., Thermally Stable, Efficient Polymer Solar Cells with Nanoscale Control of the Interpenetrating Network Morphology. *Adv. Funct. Mater.* **2005,** *15*, 1617-1622.

(181) Cardona, C. M.; Elliott, B.; Echegoyen, L., Unexpected chemical and electrochemical properties of $M_3N@C_{80}$ (M = Sc, Y, Er). *J. Am. Chem. Soc.* **2006,** *128* (19), 6480-6485.

(182) Ross, R. B.; Cardona, C. M.; Guldi, D. M.; Sankaranarayanan, S. G.; Reese, M. O.; Kopidakis, N.; Peet, J.; Walker, B.; Bazan, G. C.; Van Keuren, E.; Holloway, B. C.; Drees, M., Endohedral fullerenes for organic photovoltaic devices. *Nature Mater.* **2009,** *8* (3), 208-212.

Chapter 2

Research Overview

One of the most important properties of fullerenes is their ability to encapsulate atoms or clusters in the carbon cage. Since the first lanthanum-based endohedral metallofullerenes (EMFs) were detected,[1] other endohedrals have also been encapsulated; mainly the metals from group II, III and lanthanides as well as their corresponding metal clusters,[2] metallic nitride clusters,[3] metal carbides,[4] metal oxides,[5] noble gases[6] and nitrogen.[7] In the big fullerene family, the EMF family is one of the most widely studied, not only because of their intriguing electronic properties but also their potential applications in medicine and materials fields.[8-11]

The structures of EMFs are directly related with their electronic properties and chemical funtionalization ability. Thus, the structural characterization of EMFs is a key in fullerene chemistry. Detailed single-crystal X-ray structural information has been obtained for the most abundant $A_{3-x}B_xN@C_{80}$ series, such as $Gd_3N@I_h$-C_{80},[12] $Dy_3N@I_h$-C_{80},[13] $Lu_3N@I_h$-C_{80},[14] $Tm_3N@I_h$-C_{80},[15] $Tm_3N@D_{5h}$-C_{80},[15] $Tb_3N@I_h$-C_{80},[16] $Tb_3N@D_{5h}$-C_{80}[16] as well as $Er_2ScN@I_h$-C_{80}[17] and $CeSc_2N@I_h$-C_{80}.[18] However, for the EMFs with different sizes and endohedrals, structural characterization is very difficult due to the scarcity of purified samples. Herein, my research mainly focuses on the preparation, separation and structural characterization of EMFs.

In Chapter 3, we report a ^{89}Y and ^{13}C NMR study of a new family of TNT EMFs

represented by the diamagnetic yttrium-$Y_3N@C_{2n}$ (n = 40-44) family. This yttrium-based TNT EMF family is an important contrast to previous studies, since high resolution ^{13}C NMR studies are usually not feasible for the paramagnetic lanthanide TNT EMFs and the ^{89}Y nuclide provides a unique opportunity to monitor motional processes of the $(Y_3N)^{6+}$ cluster. Based on experimental and computational ^{13}C NMR studies, we propose cage structures for $Y_3N@I_h$-C_{80} (IPR allowed), $Y_3N@D_{5h}$-C_{80} (IPR allowed), $Y_3N@C_s$-C_{82} (non-IPR), $Y_3N@C_s$-C_{84} (non-IPR), $Y_3N@D_3$-C_{86} (IPR allowed) and $Y_3N@D_2$-C_{88} (IPR allowed). A surprising result is the limited numbers of isomers found for each carbon cage; for example, there are 51,568 non-IPR and 24 isolated pentagon rule (IPR) structures possible for the C_{84} cage, but only one major isomer was found, i.e., $Y_3N@C_s$-C_{84}. This study also represents the first ^{89}Y NMR results for $Y_3N@I_h$-$C_{80,}$ $Y_3N@Cs$-C_{84} and $Y_3N@D_3$-C_{86}, revealing a progression from isotropic to restricted $(Y_3N)^{6+}$ cluster motional processes. A more surprising finding is the sensitivity of the ^{89}Y NMR chemical shift parameters to subtle changes in the electronic environment at each yttrium nuclide in the $(Y_3N)^{6+}$ cluster (a range of over 200 ppm). This ^{89}Y NMR study suggests that ^{89}Y NMR is a powerful tool for cluster motional studies in EMFs. This work appeared as an article in the Journal of the American Chemical Society. (Fu, W. J.; Xu, L.S.; Azurmendi, H.; Ge, J. C.;.Fuhrer, T.; Zuo, T .M.; Reid, J.; Shu, C. Y.; Harich, K.; Dorn, H. C. *J. Am. Chem. Soc.* **2009**, 131, 11762.)

The EMFs with metal carbide inside the fullerene cage have also attracted special interest in recent years. In chapter 4, we report the first preparation, separation and characterization of an yttrium-carbide-based dimetallofullerene, $Y_2C_2@D_3$-C_{92}. The ^{13}C

NMR study suggests that the Y_2C_2 cluster is encapsulated in a C_{92} cage with D_3 symmetry, which is consistent with the DFT calculation. An interesting result is that the scalar $J_{Y\text{-}C}$ coupling between the two yttrium atoms and the C_2 unit within the C_{92} cage was successfully detected, suggesting that the two carbon atoms rotate rapidly around the yttrium atoms. This is the first report of coupling between a metallic atom and carbide within the fullerene cage, providing direct observation of the cluster motion in the fullerene cage. This observation would be very helpful to understand electronic and magnetic properties of these novel endohedral metallofullerenes. The manuscript of this work is in preparation.

In Chapter 5, we discuss the preparation, separation and characterization of two paramagnetic endohedral metalloheterofullerenes, $Y_2@C_{79}N$ and $Gd_2@C_{79}N$. The substitution of a carbon atom in the C_{80} cage by a nitrogen atom leads to a unique heterofullerene structure. The EPR study suggested that the spin density is mainly localized between the two metallic ions in both endohedral metalloheterofullerenes. And $Gd_2@C_{79}N$ is a stable paramagnetic material over a wide temperature range. The electron transfer behavior between $Y_2@C_{79}N$ and an organic donor has also been investigated. The manuscript of this work is in preparation.

Hydrogenation of TNT EMFs is another point of interest in my research. As potential hydrogen storage materials, fullerenes are considered to be the only form of carbon which can be hydrogenated and dehydrogenated reversibly. As discussed in Chapter 1, hydrogenation of empty cage fullerenes, such as C_{60} and C_{70}, has been widely studied. However, there is no reported attempt in the EMF area. In Chapter 6,

we reported the hydrogenation of $Sc_3N@C_{80}$ by Benkeser reduction. Our study suggests that the $Sc_3@C_{80}$ can be fully hydrogenated. The decomposition study shows that the $Sc_3@C_{80}$ can be recovered from hydrogenated product after being heated in vacuum. As a by-product, the water soluble $Sc_3@C_{80}$ derivative containing amino functional group was synthesized and characterized. This work has been published in a patent application, *U.S. Pat. Appl. Publ.* (Dorn, H. C.; Gibson, H. W.; Fu, W. J. *U.S. Pat. Appl. Publ.* **2007,** 12pp).

References:

(1) Heath, J. R.; O'Brien, S. C.; Zhang, Q.; Liu, Y.; Curl, R. F.; Kroto, H. W.; Tittel, F. K.; Smalley, R. E., Lanthanum complexes of spheroidal carbon shells. *J. Am. Chem. Soc.* **1985,** *107* (25), 7779-7780.

(2) Shinohara, H., Endohedral metallofullerenes. *Rep. Prog. Phys.* **2000,** *63* (6), 843-892.

(3) Stevenson, S.; Rice, G.; Glass, T.; Harich, K.; Cromer, F.; Jordan, M. R.; Craft, J.; Hadju, E.; Bible, R.; Olmstead, M. M.; Maitra, K.; Fisher, A. J.; Balch, A. L.; Dorn, H. C., Small-bandgap endohedral metallofullerenes in high yield and purity. *Nature* **1999,** *401* (6748), 55-57.

(4) Wang, C. R.; Kai, T.; Tomiyama, T.; Yoshida, T.; Kobayashi, Y.; Nishibori, E.; Takata, M.; Sakata, M.; Shinohara, H., A scandium carbide endohedral metallofullerene: $(Sc_2C_2)@C_{84}$. *Angew. Chem. Int. Ed.* **2001,** *40* (2), 397-399.

(5) Stevenson, S.; Mackey, M. A.; Stuart, M. A.; Phillips, J. P.; Easterling, M. L.; Chancellor, C. J.; Olmstead, M. M.; Balch, A. L., A distorted tetrahedral metal oxide cluster inside an lcosahedral carbon cage. Synthesis, isolation, and structural characterization of $Sc_4(\mu 3\text{-}O)_2@I_h\text{-}C_{80}$. **2008,** *J. Am. Chem. Soc. 130* (36), 11844-11845.

(6) Saunders, M.; Jimenezvazquez, H. A.; Cross, R. J.; Poreda, R. J., Stable Compounds of Helium and Neon: $He@C_{60}$ and $Ne@C_{60}$. *Science* **1993,** *259* (5100), 1428-1430.

(7) Mauser, H.; Hommes, N. J. R. V.; Clark, T.; Hirsch, A.; Pietzak, B.; Weidinger, A.; Dunsch, L., Stabilization of atomic nitrogen inside C_{60}. **1997,** *Angew. Chem. Int. Ed. 36* (24), 2835-2838.

(8) Thompson Barry, C.; Frechet Jean, M. J., Polymer-fullerene composite solar cells. *Angew. Chem. Int. Ed.* **2008,** *47* (1), 58-77.

(9) Ross, R. B.; Cardona, C. M.; Guldi, D. M.; Sankaranarayanan, S. G.; Reese, M. O.; Kopidakis, N.; Peet, J.; Walker, B.; Bazan, G. C.; Van Keuren, E.; Holloway, B. C.; Drees, M., Endohedral fullerenes for organic photovoltaic devices. *Nature Mater.* **2009,** *8* (3), 208-212.

(10) Shu, C. Y.; Corwin, F. D.; Zhang, J. F.; Chen, Z. J.; Reid, J. E.; Sun, M. H.; Xu, W.; Sim, J. H.; Wang, C. R.; Fatouros, P. P.; Esker, A. R.; Gibson, H. W.; Dorn, H. C., Facile Preparation of a New Gadofullerene-Based Magnetic Resonance Imaging Contrast Agent with High H-1 Relaxivity. *Bioconjugate Chem.* **2009,** *20* (6), 1186-1193.

(11) Shu, C. Y.; Ma, X. Y.; Zhang, J. F.; Corwin, F. D.; Sim, J. H.; Zhang, E. Y.; Dorn, H. C.; Gibson, H. W.; Fatouros, P. P.; Wang, C. R.; Fang, X. H., Conjugation of a water-soluble gadolinium endohedral fulleride with an antibody as a magnetic resonance imaging contrast agent. *Bioconjugate Chem.* **2008,** *19* (3), 651-655.

(12) Stevenson, S.; Phillips, J. P.; Reid, J. E.; Olmstead, M. M.; Rath, S. P.; Balch, A.

L., Pyramidalization of Gd_3N inside a C_{80} cage. The synthesis and structure of $Gd_3N@C_{80}$. *Chem. Commun.* **2004,** (24), 2814-2815.

(13) Yang, C. Y.; Hu, J. G.; Heeger, A. J., Molecular structure and dynamics at the interfaces within bulk heterojunction materials for solar cells. *J. Am. Chem. Soc.* **2006,** *128* (36), 12007-12013.

(14) Stevenson, S.; Lee, H. M.; Olmstead, M. M.; Kozikowski, C.; Stevenson, P.; Balch, A. L., Preparation and crystallographic characterization of a new endohedral, $Lu_3N@C_{80}\cdot 5$(o-xylene), and comparison with $Sc_3N@C_{80}\cdot 5$(o-xylene). *Chem.-Eur. J.* **2002,** *8* (19), 4528-4535.

(15) Zuo, T. M.; Olmstead, M. M.; Beavers, C. M.; Balch, A. L.; Wang, G. B.; Yee, G. T.; Shu, C. Y.; Xu, L. S.; Elliott, B.; Echegoyen, L.; Duchamp, J. C.; Dorn, H. C., Preparation and structural characterization of the I_h and the D_{5h} isomers of the endohedral fullerenes $Tm_3N@C_{80}$: Icosahedral C_{80} cage encapsulation of a trimetallic nitride magnetic cluster with three uncoupled Tm^{3+} ions. *Inorg. Chem.* **2008,** *47* (12), 5234-5244.

(16) Zuo, T. M.; Beavers, C. M.; Duchamp, J. C.; Campbell, A.; Dorn, H. C.; Olmstead, M. M.; Balch, A. L., Isolation and structural characterization of a family of endohedral fullerenes including the large, chiral cage fullerenes $Tb_3N@C_{88}$ and $Tb_3N@C_{86}$ as well as the I_h and D_{5h} isomers of $Tb_3N@C_{80}$. *J. Am. Chem. Soc.* **2007,** *129* (7), 2035-2043.

(17) Olmstead, M. M.; de Bettencourt-Dias, A.; Duchamp, J. C.; Stevenson, S.; Dorn, H. C.; Balch, A. L., Isolation and crystallographic characterization of $ErSc_2N@C_{80}$: an endohedral fullerene which crystallizes with remarkable internal order. *J. Am. Chem. Soc.* **2000,** *122* (49), 12220-12226.

(18) Wang, X.; Zuo, T.; Olmstead, M. M.; Duchamp, J. C.; Glass, T. E.; Cromer, F.; Balch, A. L.; Dorn, H. C., Preparation and structure of $CeSc_2N@C_{80}$: an icosahedral carbon cage enclosing an acentric $CeSc_2N$ unit with buried f electron spin. *J. Am. Chem. Soc.* **2006,** *128* (27), 8884-8889.

Chapter 3

Preparation, Separation and Characterization of Yttrium-based TNT EMFs, $Y_3N@C_{2n}$ (n=40-44)

3.1. Introduction

There is increasing interest in the trimetallic nitride template endohedral metallofullerenes (TNT-EMFs), $M_3N@C_{2n}$ (n=34-50) because of their electronic and structural properties.[1,2] In addition, potential applications of TNT EMFs are emerging in diverse areas including photovoltaic devices[3,4] and MRI contrast agents.[5-11]

It is now clear that the size of the trimetallic cluster $(M_3N)^{6+}$ plays an important role in dictating the formation of TNT EMF isomers. To illustrate, the first protypical scandium member of the TNT EMF family $Sc_3N@C_{80}$, was determined to be $Sc_3N@I_h$-C_{80} with stabilization of the icosahedral (I_h) cage by transfer of six electrons to the fullerene cage (C_{80}).[6-12] However, it was later discovered by ^{13}C NMR analysis[13] that a second isomer, $Sc_3N@D_{5h}$-C_{80} was present in the Krätschmer-Huffman reaction mixture that was later isolated and structurally characterized by single crystal X-ray diffraction analysis. With the smaller scandium ions present in the trimetallic cluster $(Sc_3N)^{6+}$, a smaller non-IPR structure, $Sc_3N@D_3$-C_{68} was also first identified by ^{13}C NMR and later structural characterization by single crystal X-ray diffraction analysis.[14, 15] A second cage smaller than eighty carbons, $Sc_3N@D_{3h}$-C_{78} was also characterized by both ^{13}C NMR and single crystal X-ray studies.[16] More recently, larger lanthanide

trimetallic cluster $(M_3N)^{6+}$ TNT EMFs have been produced and characterized in the laboratories of Balch, Dunsch and Echegoyen, including $Gd_3N@C_{2n}$ (n=40-44),[17, 18] $Tm_3N@C_{2n}$ (n=39-44),[19, 20] $Dy_3N@C_{2n}$ (n=38-44),[20] $Tb_3N@C_{2n}$ (n=40, 42-44),[21, 22] $Nd_3N@C_{2n}$ (n=40-50),[23, 24] $Pr_3N@C_{2n}$ (n=40-52),[24] $Ce_3N@C_{2n}$ (n=43-53)[24] and $La_3N@C_{2n}$ (n=43-55).[25] To illustrate, detailed single-crystal X-ray structural information has been obtained for most of the $M_3N@C_{80}$ family, such as $Gd_3N@I_h$-C_{80},[17] $Dy_3N@I_h$-C_{80},[26] $Lu_3@I_h$-C_{80},[27] $Tm_3N@I_h$-C_{80},[28] $Tm_3N@D_{5h}$-C_{80},[28] $Tb_3N@I_h$-C_{80}[22] and $Tb_3N@D_{5h}$-C_{80},[22] as well as larger cages $Gd_3N@C_s$(39663)-C_{82},[29] $Tb_3N@C_s$(51365)-C_{84},[21] $Gd_3N@C_s$(51365)-C_{84},[30] $Tm_3N@C_s$(51365)-C_{84},[30] $Tb_3N@D_3$-C_{86}[22] and $Tb_3N@D_2$-C_{88}.[22] An unusual result of these latter studies is the limited number of isomers observed for a given cage size. For example, there are 39,709 possible non-IPR and 9 IPR structures for C_{82}; C_s(39663)-C_{82} with a non-IPR structure is the only one reported for a TNT EMF so far.

^{13}C NMR spectroscopy is a powerful probe for structural identification of the fullerenes; it is particularly valuable when the available amounts are simply too small to grow satisfactory diffraction-quality single crystals. Significant progress has been made in applying ^{13}C NMR technique in TNT EMF studies. For example, high field ^{13}C NMR spectra of $Sc_3N@C_{68}$,[14] $Sc_3N@C_{78}$,[16] and $Sc_3N@C_{80}$[12] yield 12, 8, and 2 lines, respectively, consistent with D_3 , D_{3h} , and I_h symmetries for the cages of these representative TNT EMF members (the structures shown in Figure 3.1).

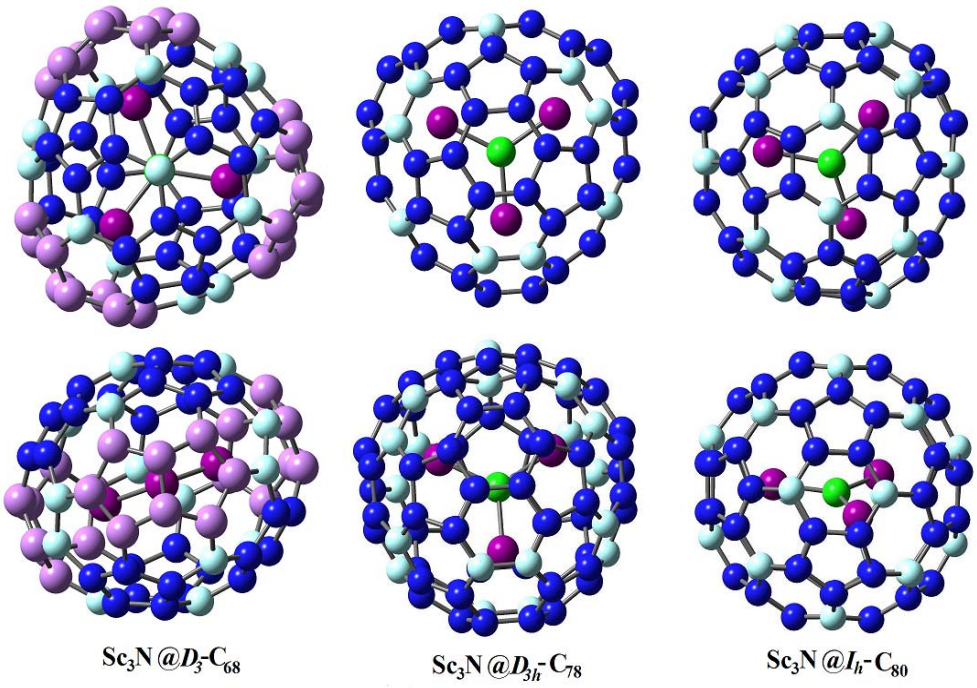

Figure 3.1. Structures of $Sc_3N@D_3(6140)$-C_{68}, $Sc_3N@D_{3h}$-C_{78}, $Sc_3N@I_h$-C_{80}

As illustrated in Figure 3.2, there are several common fullerene and metallofullerene carbon cage motifs that are readily recognized by their characteristic ^{13}C NMR chemical shift ranges. The first three motifs in Figure 2 (a-c) are commonly encountered in IPR fullerenes[13, 22, 31] and the other is the important pentalene motif (2d) found in certain non-IPR metallofullerenes that usually exhibit highly deshielded resonances at 155-165 ppm.[14, 21, 30] For example, the pyracylene 6,6,5 carbon site is identified by the unique fullerene I_h-C_{60} with a single ^{13}C resonance at 142.5 ppm.[32] In contrast, the pyrene motif and specifically 6,6,6 junction carbons are typically more shielded ^{13}C resonances in the range of 130-138 ppm as observed for the belt carbons of D_{5h}-C_{70}, 130.9 ppm.[33]

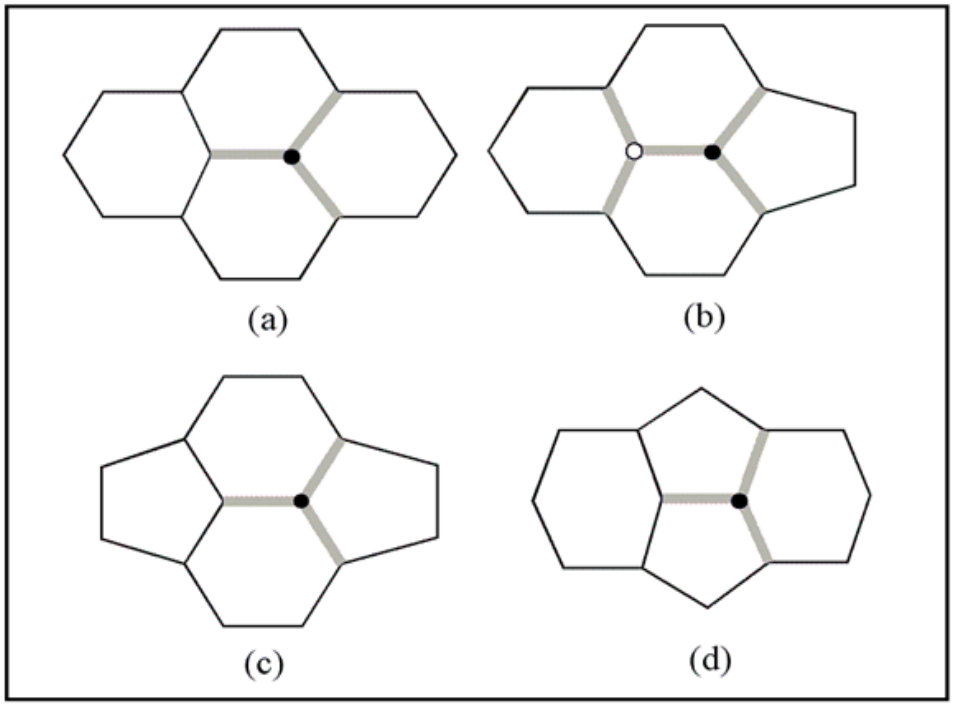

Figure 3.2. (a) Pyrene Motif, 6,6,6 Junction; (b) Corannulene Motif, 6,6,6 (o), and (6,6,5) Junctions; (c) Pyracylene Motif, 6,6,5 Junctions; (d) Pentalene Motif, 6,5,5 Junction

However, high resolution ^{13}C NMR studies are usually not feasible for the paramagnetic lanthanide TNT EMFs. And $(M_3N)^{6+}$ cluster motion in the larger fullerene cage is still unclear. In an attempt to solve these problems, we report preparation, separation and characterization of a new family of endohedral metallofullerenes (EMFs) represented by the diamagnetic yttrium-$Y_3N@C_{2n}$ (n=40-44) family. The size of the $(Y_3N)^{6+}$ cluster is intermediate in comparison with the smaller scandium and generally larger lanthanide clusters. Thus, an interesting question is whether the trimetallic nitride templated Kraschmer-Huffman process will provide smaller fullerene cages analogous to scandium or the larger unique cages observed for the lanthanides (*vide supra).* In addition, The ^{89}Y nuclide provides the unique opportunity to monitor motional processes of the $(Y_3N)^{6+}$ cluster. Although the ^{89}Y nuclide is 100 % abundant, solution

^{89}Y NMR studies have been hampered by the small magnetogyric ratio and corresponding long spin lattice (T_1) relaxation.[35] For the current study, high magnetic fields and long scan times are required; however, this could be alleviated in future studies by utilizing higher fields and dynamic nuclear polarization.[35]

3.2. Experimental Section and Calculation

Preparation of $Y_3N@C_{2n}$: The samples were prepared in a Krätschmer-Huffman generator by vaporizing composite graphite rods containing a mixture Y_2O_3, graphite powder and metallic Cu as catalyst with a weight ratio of 1.1:1.0:2.1 in a dynamic flow of He and N_2 (flow rate ratio of N_2/H_2=3:100). The resulting soot was then extracted with refluxing toluene in a Soxhlet extractor for 24 h to obtain the soluble extract for further purification.

Purification of $Y_3N@C_{2n}$: 45 g of cyclopentadiene-functionized Merrifield resin (CPDE-MPR) was synthesized as previously described[36] and packed in a glass column (22 × 450 mm). The soot extract was applied to the glass column and flushed using toluene at 20 mL/h. The eluent was further separated by two-stage HPLC. The first stage was carried out on a PBB column (4.6 × 250 mm). The different fractions (fraction Y1 to Y7) from this PBB column were collected and further separated with a PYE column (10 × 250 mm). The flow rate for both stages was 2.0 mL/min and the detection wavelength was 390 nm. The HPLC system was the following: Acure series III pump, 757 absorbance detector (Applied Biosystems).

Characterization of the $Y_3N@C_{2n}$: 150 MHz ^{13}C and 29.4 ^{89}Y NMR

spectroscopic measurements of all samples were performed on a Bruker Avance spectrometer (600 MHz, ^{1}H). The samples were dissolved in carbon disulfide (1,2 dichlorobenzene for ^{89}Y NMR) with chromium tris(acetylacetonate, $Cr(acac)_3$) as the relaxation agent and acetone-d_6 (1,2-dichlorobenzene-d_4 for ^{89}Y NMR) as internal lock at 25 ºC. Mass spectrometry was performed on a Kratos Analytical Kompact SEQ LD-TOF mass spectrometer.

Crystal Growth of $Y_3N@C_{80}$: $Y_3N@C_{80}$ and $Ni^{II}(OEP)$ were co-crystallized by diffusion of a benzene solution of the $Y_3N@C_{80}$ into an $Ni^{II}(OEP)$ benzene solution. The black crystals formed over a 15-day period, as shown in Figure 3.3.

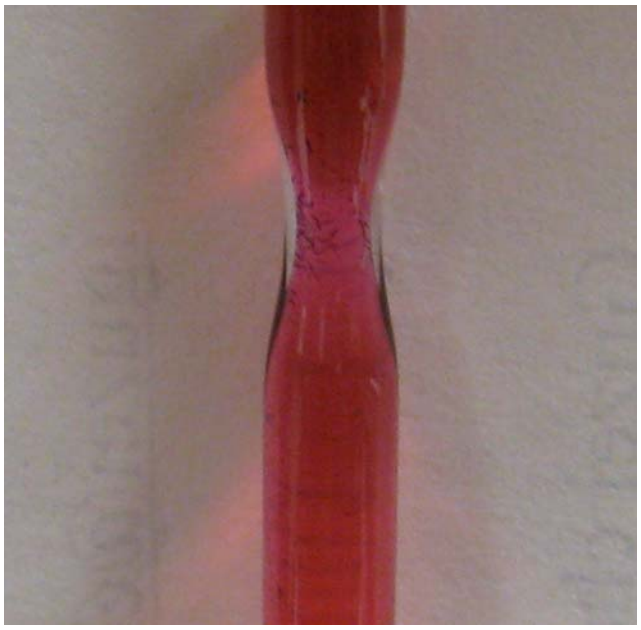

Figure 3.3. Formation of the black crystals of $Y_3N@C_{80}$•$Ni^{II}(OEP)$

X-ray Crystallography and Data collection: The crystal was centered on the goniometer of an Oxford Diffraction Gemini A Ultra diffractometer operating at 100 K with CuKα radiation. The data collection routine, unit cell refinement, and data processing were carried out with the program CrysAlisPro. The Laue symmetry and systematic absences were consistent with the monoclinic space groups Cc and C2/c.

The centric space group *C*2/*c* was chosen. The structure was solved by direct methods and refined using SHELXTL NT. The asymmetric unit of the structure comprises one crystallographically independent $Y_3N@C_{80}$•Ni^{II}(OEP) and two benzene solvates. The final refinement model involved anisotropic displacement parameters for non-hydrogen atoms, except a disordered benzene molecule. A riding model was used for all hydrogen atoms. There was evidence of minor disorder in the Y_3N cluster, but attempt to model this disorder did not improve the model significantly and wreaked havok on the yitrium ADPs. Dr. Carla Slebodnick at Virginia Tech graciously cooperated and undertook the single crystal X-ray crystallography study.

Computational Studies: Density functional theory (DFT) computations were performed using Gaussian 03 program package.[37] All molecules were geometry optimized using the UB3LYP/DZVP level for yttrium and the UB3LYP/6-31G* level for carbon and nitrogen atoms.[38] DFT energy optimized values were obtained starting from the X-ray crystallographic structures of the corresponding $Tb_3N@C_{2n}$ (n=40, 42-44) and $Gd_3N@C_{2n}$ (n=41) EMFs. The energy minimized values and the same level of theory were used to calculate all ^{13}C NMR chemical shifts. Tim Fuhrer and Liaosa Xu in Dorn's group kindly collaborated on the calculation portion of this work.

3.3. Results and Discussion

3.3.1. Preparation of $Y_3N@C_{2n}$ (n=40-44)

The samples were prepared in a Krätschmer-Huffman generator by vaporizing composite graphite rods containing a mixture of Y_2O_3, graphite powder and metallic Cu

as catalyst with a weight ratio of 1.1:1.0:2.1 in a dynamic flow of He and N_2 (flow rate ratio of N_2/H_2=3:100). The resulting soot was then extracted with refluxing toluene in a soxhlet extractor for 24 h to obtain the toluene soluble extract for the further purification. The LD-TOF (laser desorption time-of-flight) mass spectrum of the soot extract is shown in Figure 3.4. The HPLC chromatogram of the toluene soluble soot extract in a PBB column is shown in Figure 5a.

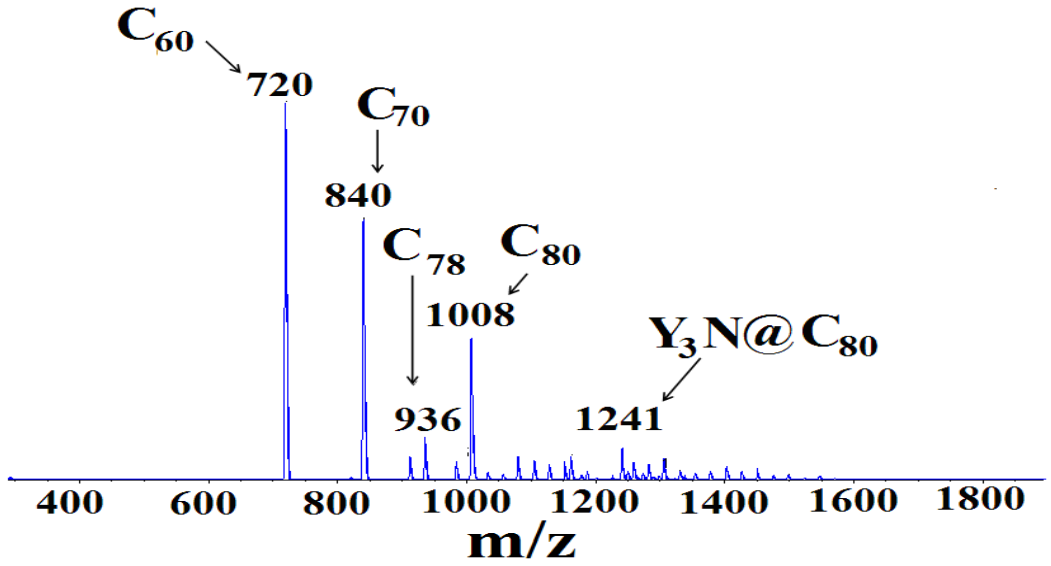

Figure 3.4. LD-TOF mass spectrum of toluene soluble soot extract with positive ionization

3.3.2. Separation of $Y_3N@C_{2n}$ (n=40-44)

The HPLC trace and mass spectrum indicate that the most abundant fullerenes in the soot extract were the empty cages, such as C_{60}, C_{70} and C_{84}. However, simple HPLC chromatographic procedures are repetitive, time-consuming and need a lot labor to purify the TNT EMFs. Thus, a chemical separation described below was applied.

3.3.2.1. Chemical Separation

On the basis of the greater kinetic chemical stability of the EMFs relative to empty cage fullerenes, a CPDE-MPR column was applied as the preliminary separation

as previously described in Chapter 1 (Figure 1.7).[36] 45 g of cyclopentadiene-functionized Merrifield resin (CPDE-MPR) was synthesized and packed in a glass column (22 × 450 mm). The soot extract was applied to the column and flushed using toluene at a rate of 20 mL/h. The HPLC trace of the eluent from CPDE-MPR column is illustrated in Figure 3.5b and the dominant peak in Figure was $Y_3N@C_{80}$. As illustrated, the more reactive empty-cage fullerenes (C_{60}, C_{70} and C_{84}) are strongly attenuated, and the less reactive yttrium TNT EMFs, $Y_3N@C_{2n}$ (n=40-44) family is now significantly concentrated.

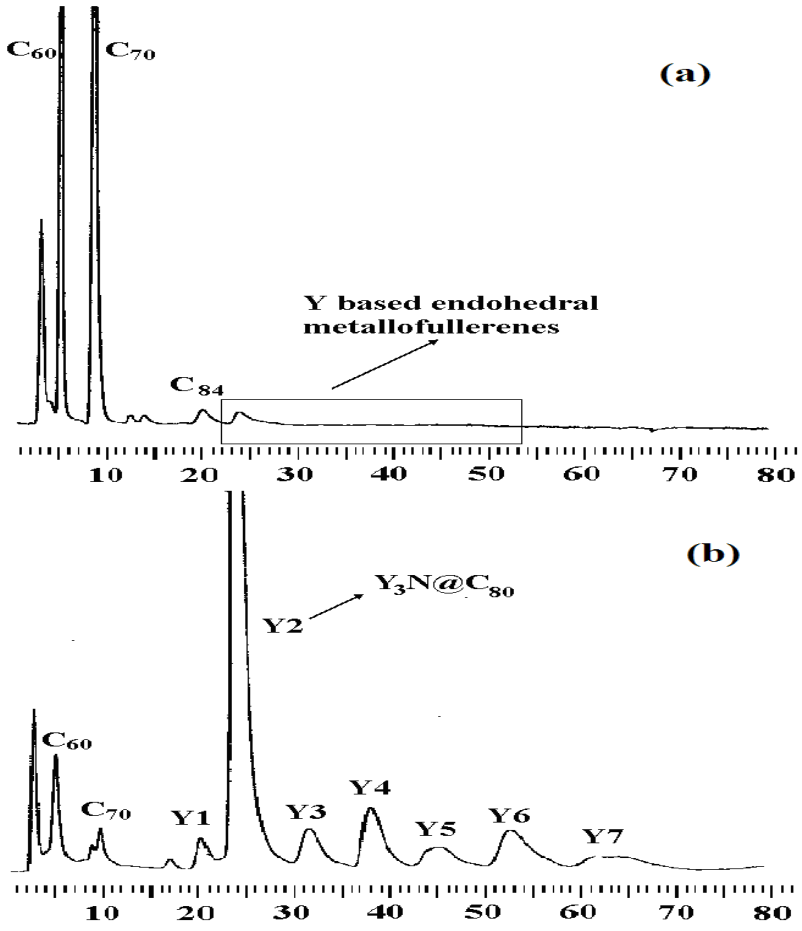

Figure 3.5. (a) HPLC chromatogram of the toluene extract from the raw soot (b) HPLC chromatogram of the eluent from CPDE-MPR column (Both chromatogram on a 4.6 × 250 mm 5PBB column; λ=390 nm; flow rate 2.0 mL/min; toluene as eluent; 25 ºC)

3.3.2.2. Two Stage HPLC Separation

The eluent was further separated by two-stage HPLC. The first stage was carried out on a PBB column (4.6 × 250 mm). Seven major fractions labeled as Y1 to Y7 (Figure 3.5b) from this PBB column were collected and further separated with a PYE column (10 × 250 mm). The LD-TOF mass spectra of Y1 to Y7 fractions (Figure 3.6 to Figure 3.10) gave the tentative identity of each fraction. Specifically, fraction Y1 contains endohedral metalloheterofullerenes $Y_2@C_{79}N$ and empty-cage C_{84}; fraction Y2 contains two $Y_3N@C_{80}$ isomers (I_h and D_{5h}); fraction Y3 contains $Y_3N@C_{82}$; fraction Y4 contains $Y_3N@C_{84}$; fraction Y5 contains $Y_3N@C_{86}$ and Y_2C_{90}; fraction 6 contains $Y_3N@C_{88}$ and Y_2C_{92} and fraction 7 contains metal carbide EMFs.

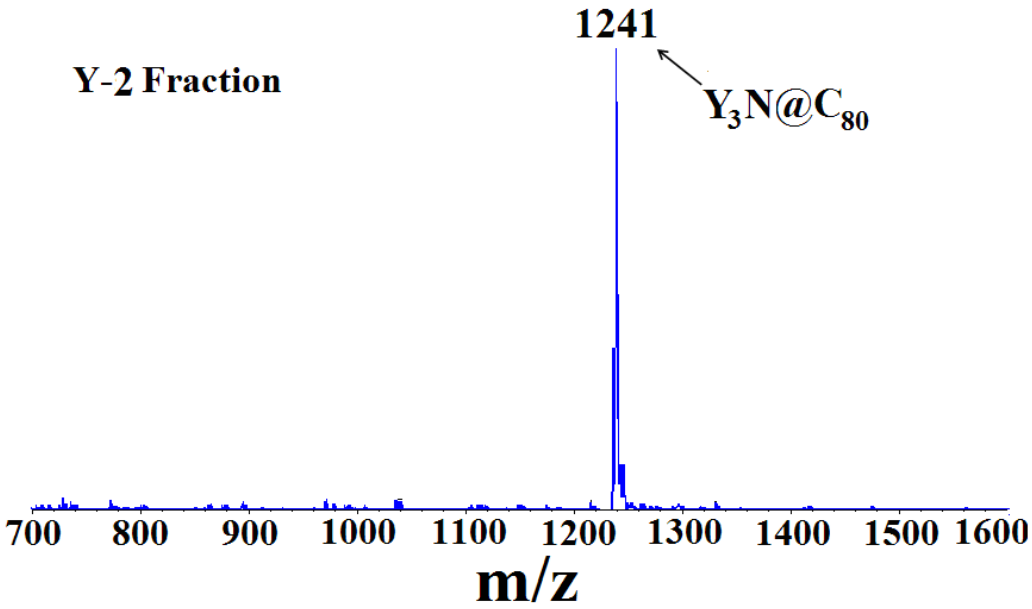

Figure 3.6. The LD-TOF mass spectrum of Y-2 fraction with positive ionization

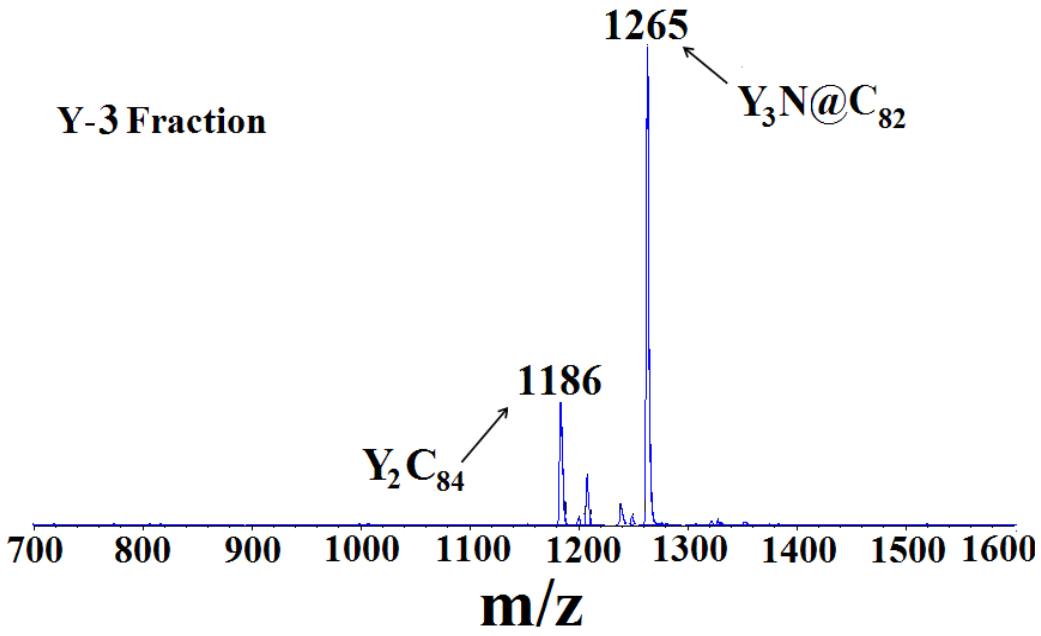

Figure 3.7. The LD-TOF mass spectrum of Y-3 fraction with positive ionization

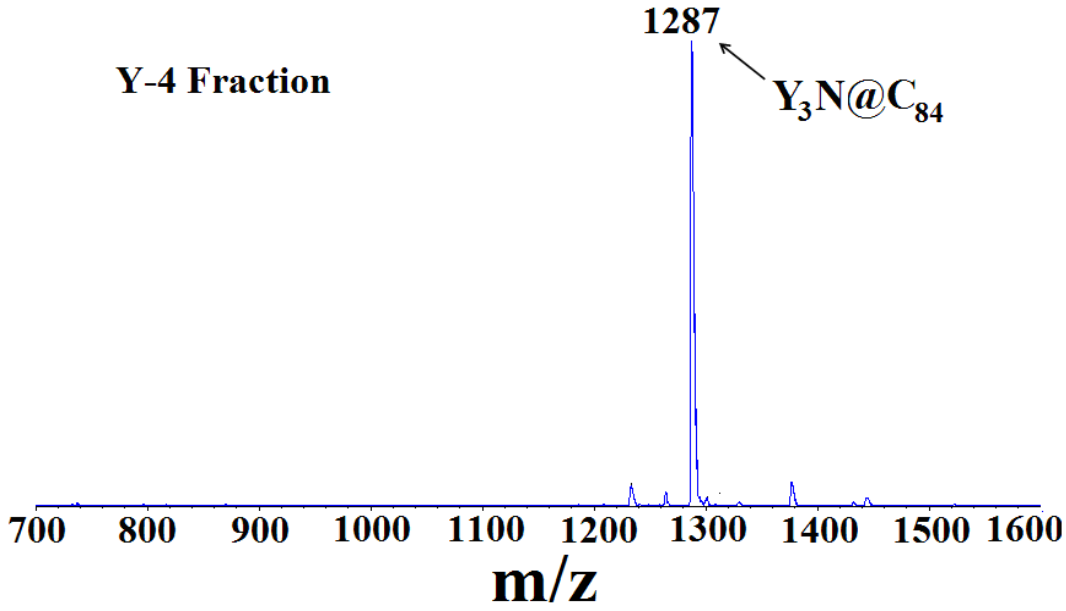

Figure 3.8. The LD-TOF mass spectrum of Y-4 fraction with positive ionization

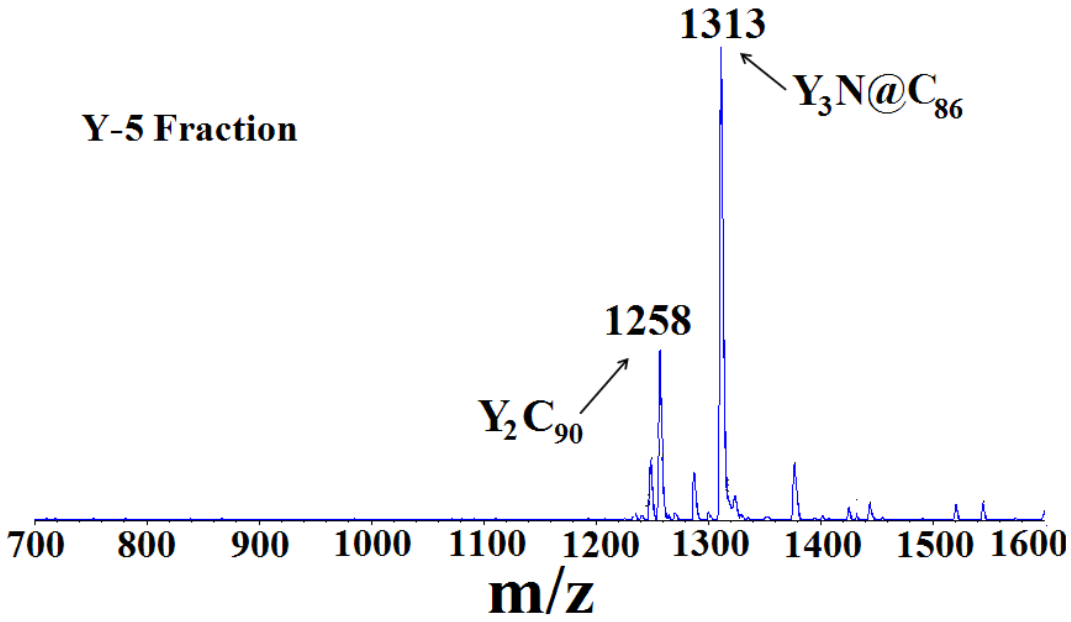

Figure 3.9. The LD-TOF mass spectrum of Y-5 fraction with positive ionization

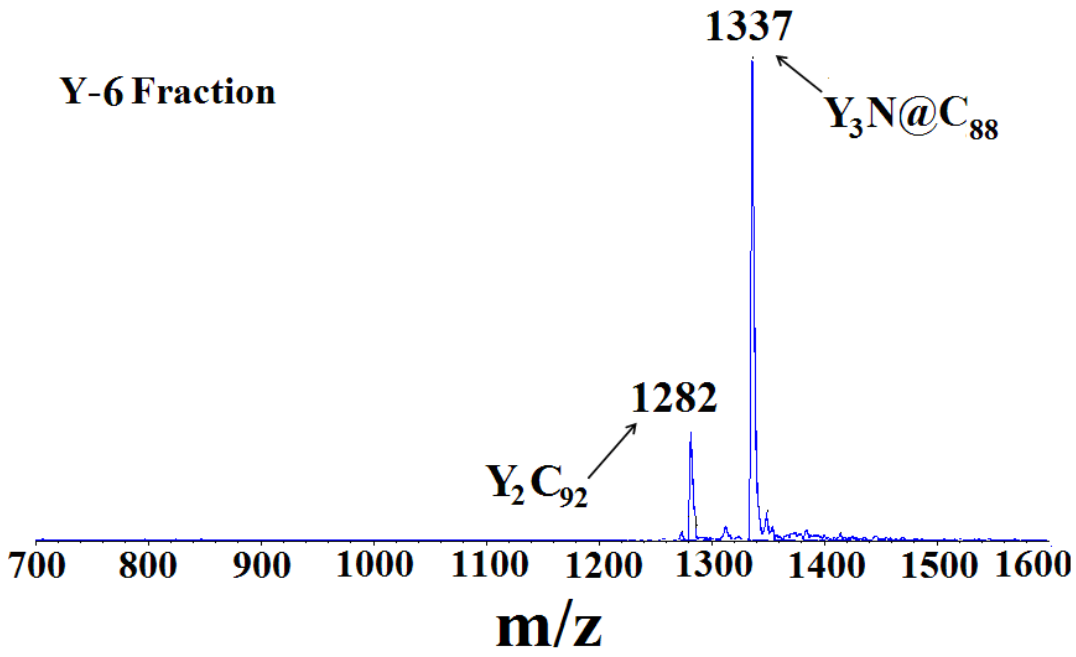

Figure 3.10. The LD-TOF mass spectrum of Y-6 fraction with positive ionization

From the mass spectra, it is clear that each fraction from PBB is still a mixture of EMFs. However, the components of each fraction are not too complicated. The main species of each fraction are TNT EMFs and dimetallic EMFs. In this chapter we will focus on Y2 to Y6 fractions, in which the most abundant components are TNT EMFs.

In order to obtain pure TNT EMFs, these fractions (Y2 to Y6) from the PBB column were further purified using a PYE column (10 ×250 mm). Since each fraction is still a mixture of EMFs and their isomers, the second stage HPLC separation on a PYE column involves repeated cycling processes. HPLC chromatograms of the first cycling process for these fractions are shown from Figure 3.11 to Figure 3.15.

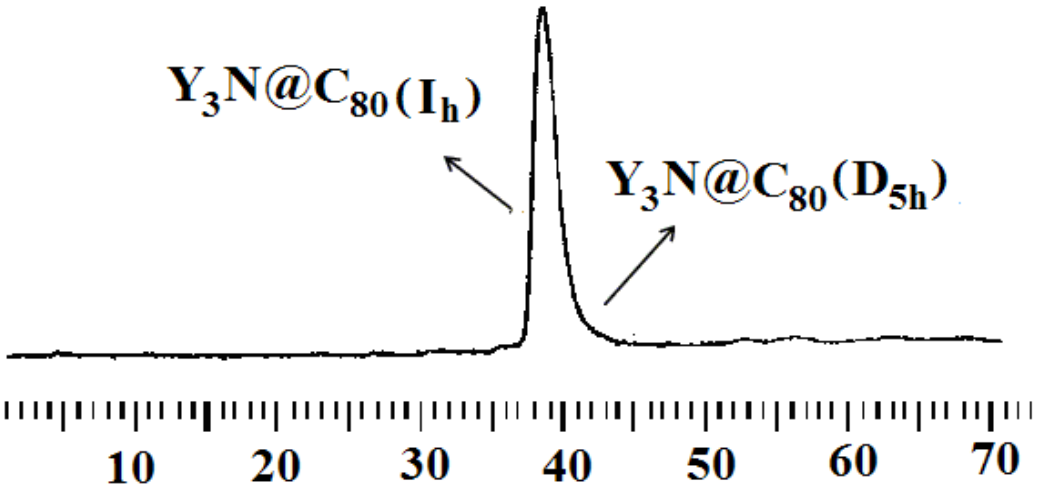

Figure 3.11. HPLC chromatogram of fraction Y2 in the first cycling process on a PYE column. (10 x 250 mm 5PYE column; λ=390 nm; flow rate 2.0 mL/min; toluene as eluent; 25 ºC)

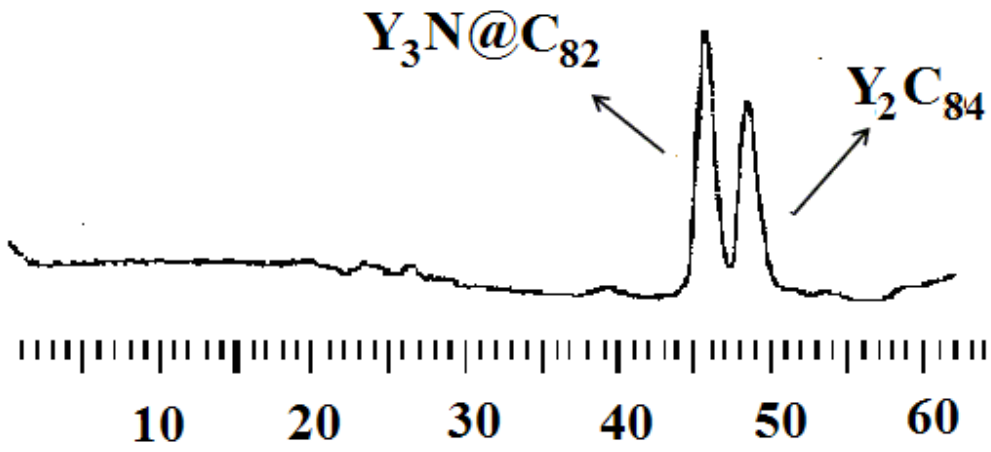

Figure 3.12. HPLC chromatogram of fraction Y3 in the first cycling process on a PYE column. (10 × 250 mm 5PYE column; λ=390 nm; flow rate 2.0 mL/min; toluene as eluent; 25 ºC)

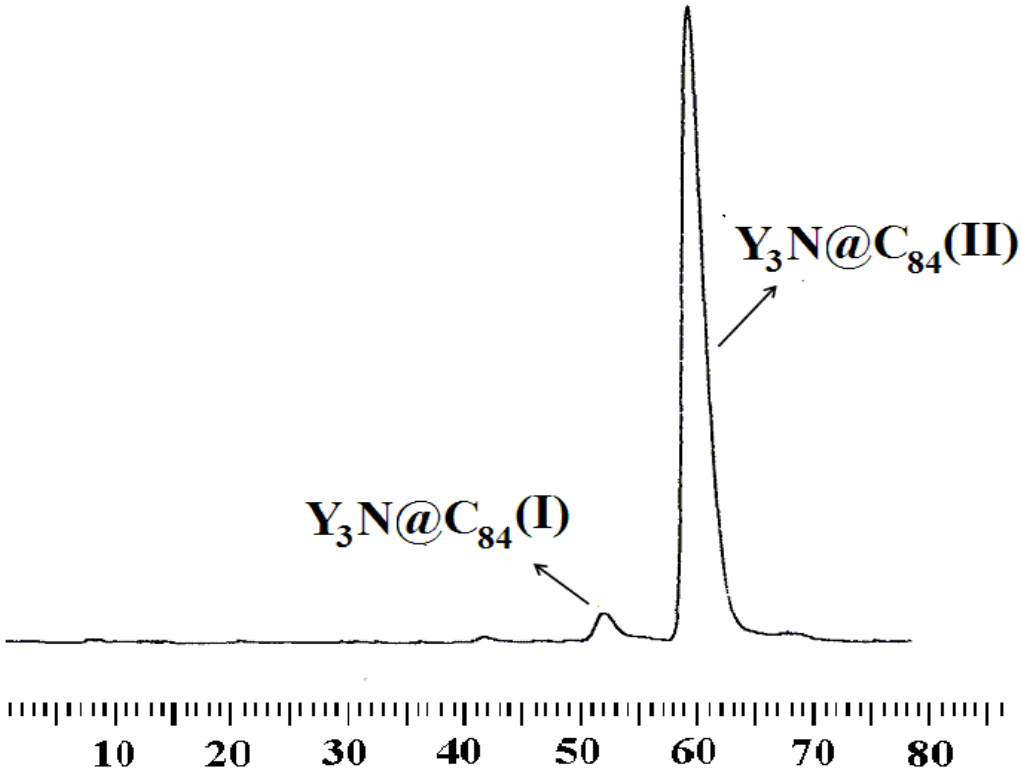

Figure 3.13. HPLC chromatogram of fraction Y4 in the first cycling process on a PYE column. (10 × 250 mm 5PYE column; λ=390 nm; flow rate 2.0 mL/min; toluene as eluent; 25 ºC)

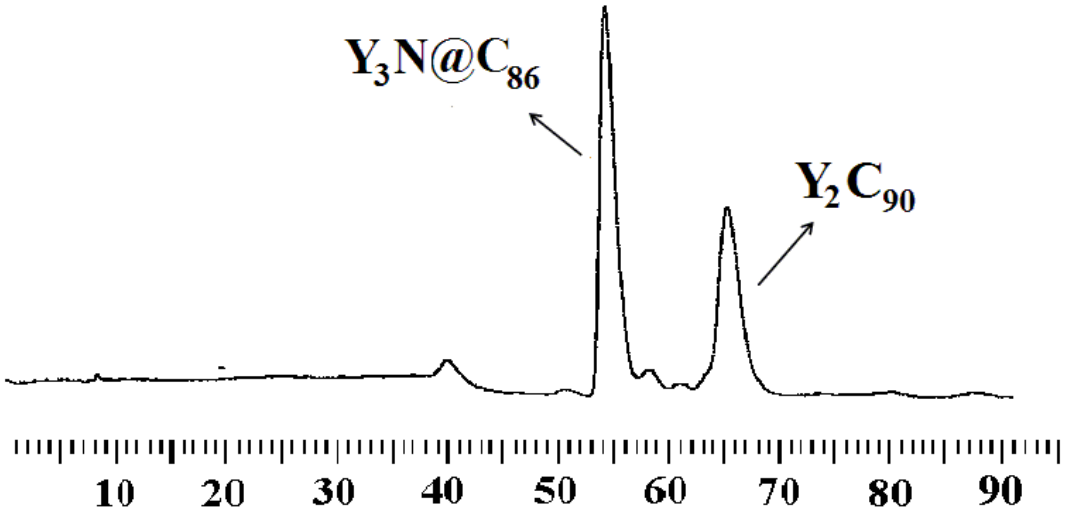

Figure 3.14. HPLC chromatogram of fraction Y5 in the first cycling process on a PYE column. (10 ×250 mm 5PYE column; λ=390 nm; flow rate 2.0 mL/min; toluene as eluent; 25 ºC)

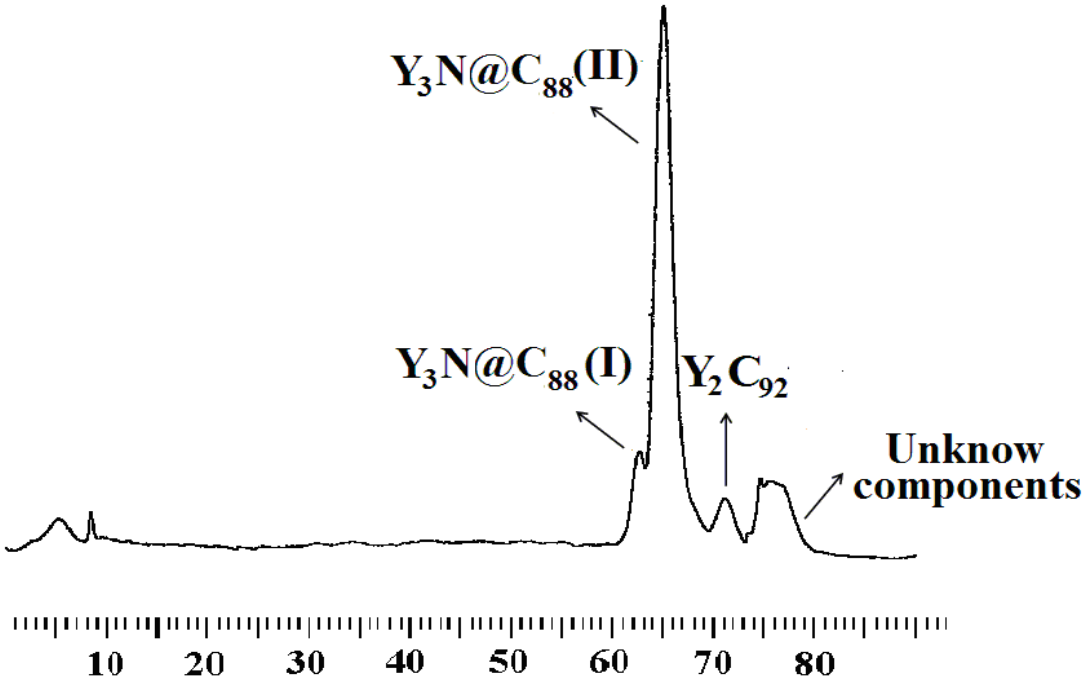

Figure 3.15. HPLC chromatogram of fraction Y6 in the first cycling process on a PYE column. (10 × 250 mm 5PYE column; λ=390 nm; flow rate 2.0 mL/min; toluene as eluent; 25 ºC)

Each peak in the HPLC chromatograms of these fractions was collected and was further cycled on the PYE column until pure samples were obtained. The retention times of the two $Y_3N@C_{80}$ isomers (I_h and D_{5h}) are very close, so we decreased the flow rate to 1.0 mL/min to get a better separation. In a similar fashion to the previously reported $Tm_3N@C_{80}$ isomers (I_h and D_{5h}), repeated chromatographic passages were necessary to separate the Y2 fraction into pure $Y_3N@I_h$-C_{80} and $Y_3N@D_{5h}$-C_{80} samples. Figure 3.16 shows the separation process of two $Y_3N@C_{80}$ isomers.

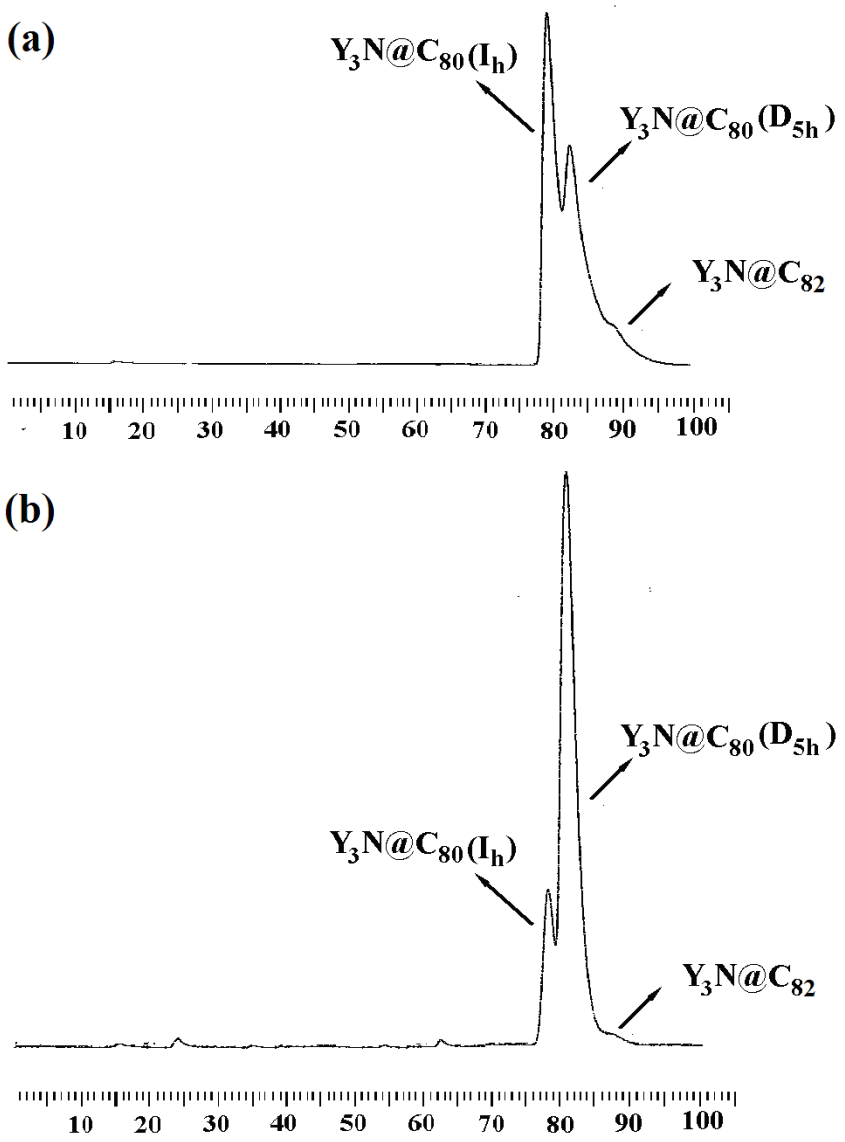

Figure 3.16. HPLC chromatogram of separation of two $Y_3N@C_{80}$ isomers (I_h and D_{5h}) on a PYE column, (a) I_h:D_{5h}=3:2, (b) I_h:D_{5h}=1:5. (10 × 250 mm, PYE column; λ=390 nm; flow rate 1.0 mL/min; toluene as eluent; 25 ºC)

The purity of each TNT EMF (most abundant isomer) was confirmed by HPLC chromatograms (Figure 3.17) and LD-TOF mass spectra (Figure 3.18).

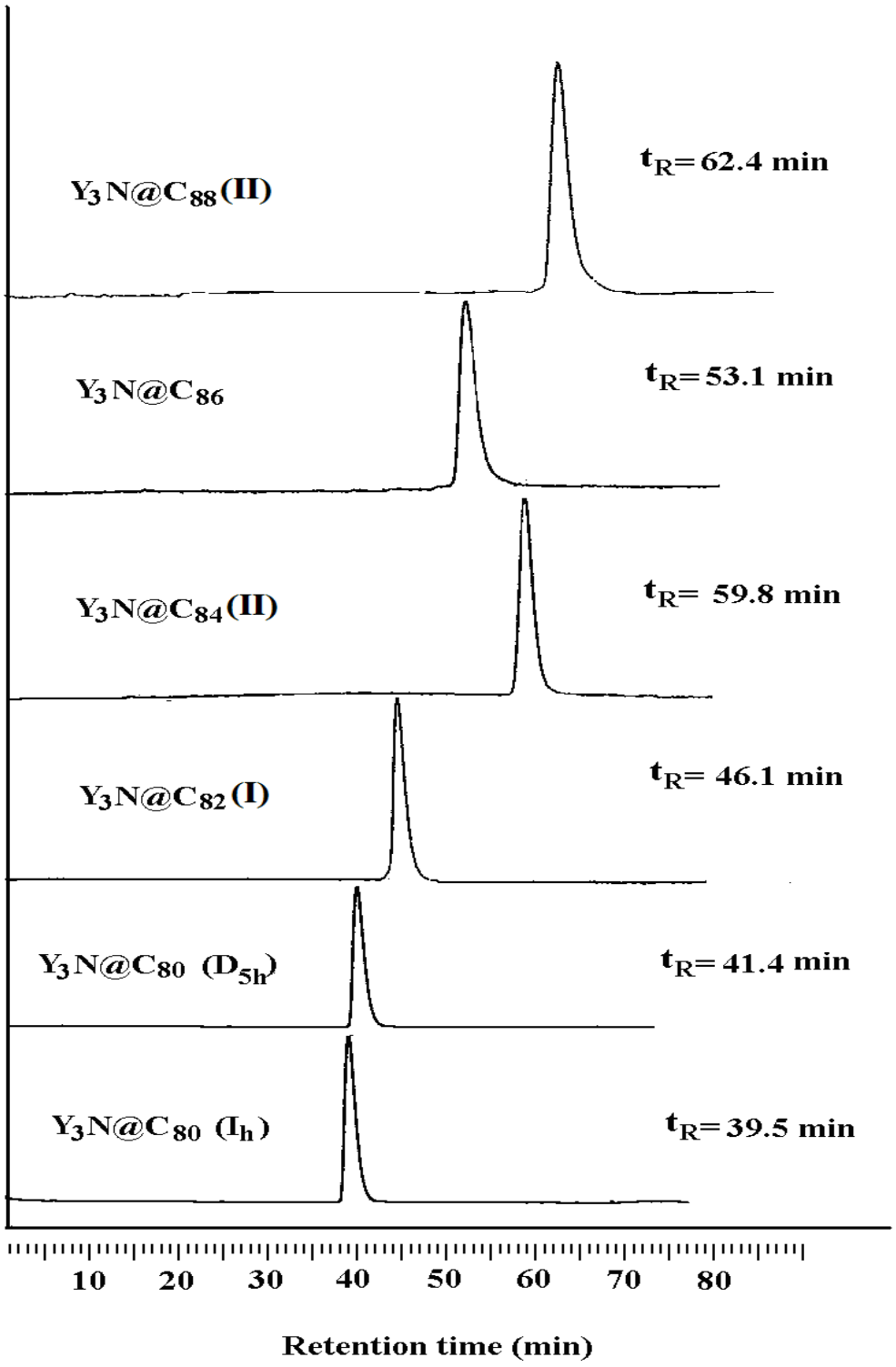

Figure 3.17. HPLC chromatograms of purified yttrium-based TNT EMFs $Y_3N@C_{2n}$ (n=40-44). (10 × 250 mm 5PYE column; λ=390 nm; flow rate 1.0 mL/min; toluene as eluent; 25 ºC)

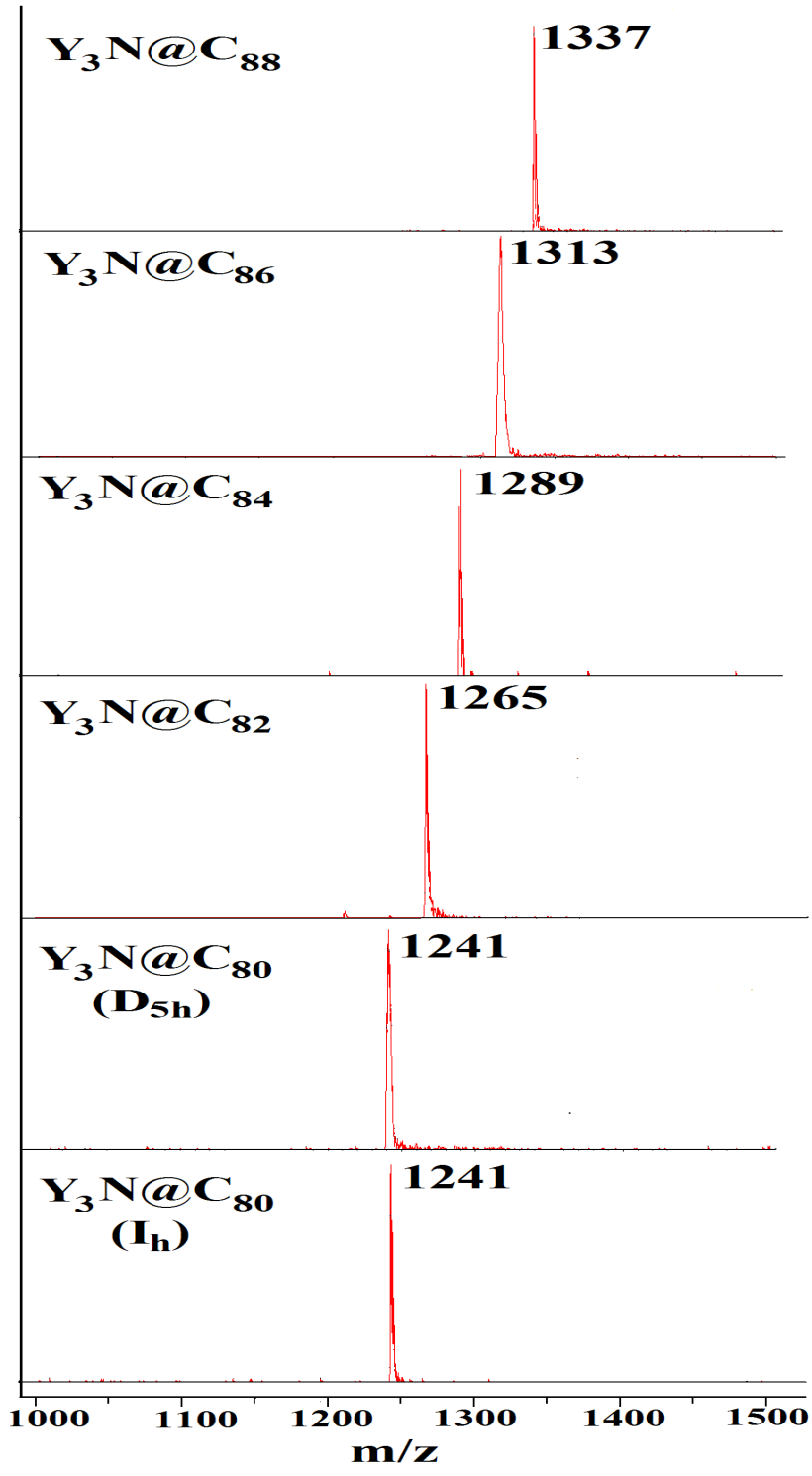

Figure 3.18. LD-TOF mass spectra of yttrium-based TNT EMFs, $Y_3N@C_{2n}$ (n=40-44) with positive ionization

3.3.3. Characterization of $Y_3N@C_{2n}$ (n=40-44)

3.3.3.1. $Y_3N@C_{80}$ Isomers:

3.3.3.1.1. $Y_3N@I_h$-C_{80}

There are a total of 31,917 non-IPR isomers for the C_{80} cage, but only seven isomers obey the isolated pentagon rule (IPR). Of the seven IPR isomers for the C_{80} cage, only the I_h isomer yields a ^{13}C NMR spectrum containing two lines with a 3:1 ratio. The simulated structure of $Y_3N@I_h$-C_{80} is shown in Figure 3.19.

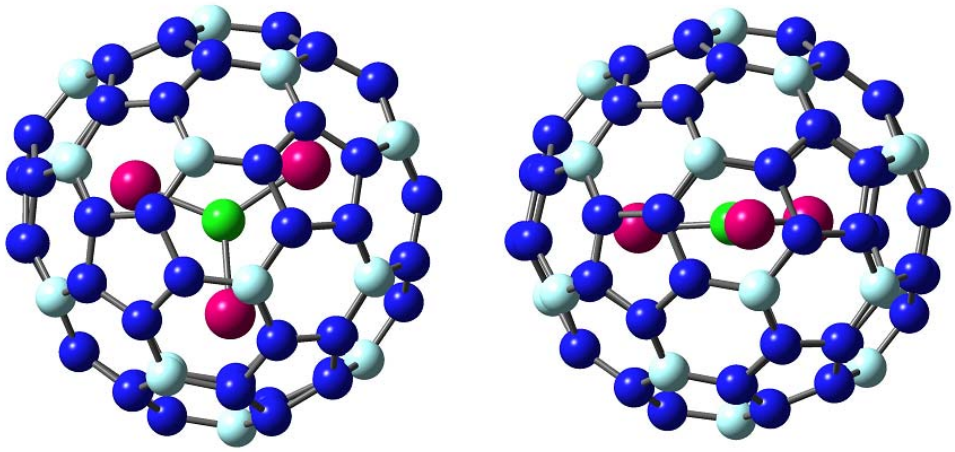

Figure 3.19. Structure of $Y_3N@I_h$-C_{80}

An initial observation for the $M_3N@I_h$-C_{80} family is the relatively small perturbation of the ^{13}C NMR shifts as a function of size and metal differences of the $(M_3N)^{6+}$ clusters. This is illustrated for several diamagnetic $Sc_3N@I_h$-C_{80}[12] and $Lu_3N@I_h$-C_{80}[9] cages as well as mixed clusters, $Lu_2YN@C_{80}$[39] and $LuY_2N@C_{80}$,[39] as previously reported. In the cases cited above, the I_h-C_{80} cage with the corannulene type motif exhibits ^{13}C NMR shifts for the 6,6,5 and 6,6,6 junctions with corresponding ranges from 142.8-144.7 and 135.9-138.2 ppm. These relatively small shift ranges even include the weakly paramagnetic $CeSc_2N@C_{80}$ system.[40] The ^{13}C NMR spectrum for $Y_3N@I_h$-C_{80} (Figure 3.20) supports an electronic distribution of $[Y_3N]^{6+}@[C_{80}]^{6-}$ with a

nearly spherical charge distribution over the fullerene cage, resulting from the corannulene-type carbon atoms (intersection of three hexagons, δ = 138.2 ppm) and the pyrene-type carbon atoms (intersection of a pentagon and two hexagons, δ = 144.6 ppm). These resonances are similar to those of $Sc_3N@I_h$-C_{80} (δ =137.24 and δ =144.57 ppm)[12] and $Lu_3N@I_h$-C_{80} (δ =137.4 and δ =144.0 ppm).[9] The computational values are within 2-3 ppm of the experimental values.

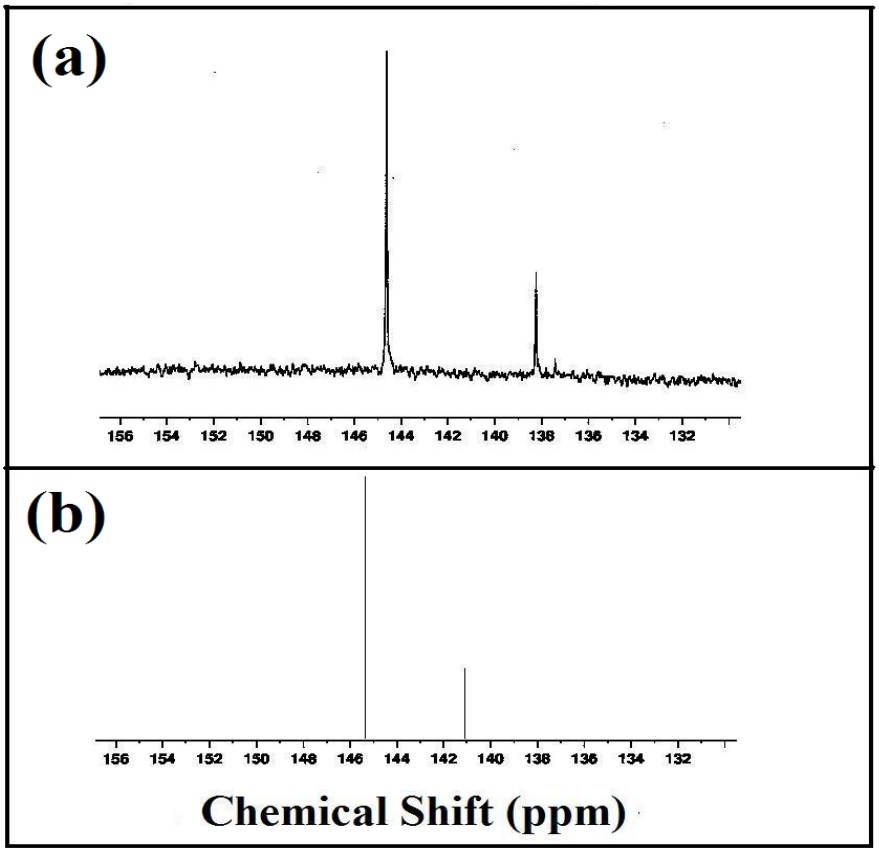

Figure 3.20. (a) ^{13}C NMR spectrum of $Y_3@I_h$-C_{80} in CS_2 with 5 mg $Cr(acac)_3$ relaxant and acetone-d_6 lock after 64,000 scan at 25 ºC, 1× 60, 1×20 pattern (number of NMR lines ×relative intensity). The chemical shifts for the two lines are at δ: 144.62 and 138.24 ppm. (b) Theoretical ^{13}C NMR spectrum of $Y_3N@I_h$-C_{80}

For the case of the internal cluster in the I_h C_{80} cage, we observe a single sharp resonance line for $Y_3N@I_h$-C_{80} at 191.63 ppm in the ^{89}Y NMR spectrum (Figure 3.21),

which is consistent with isotropic rotation of the $(Y_3N)^{6+}$ cluster at ambient temperature. The ^{13}C NMR spectrum at ambient temperature also confirms isotropic motional averaging of the Y_3N cluster inside the I_h cage and is consistent with the ^{89}Y NMR results (*vide infra*).

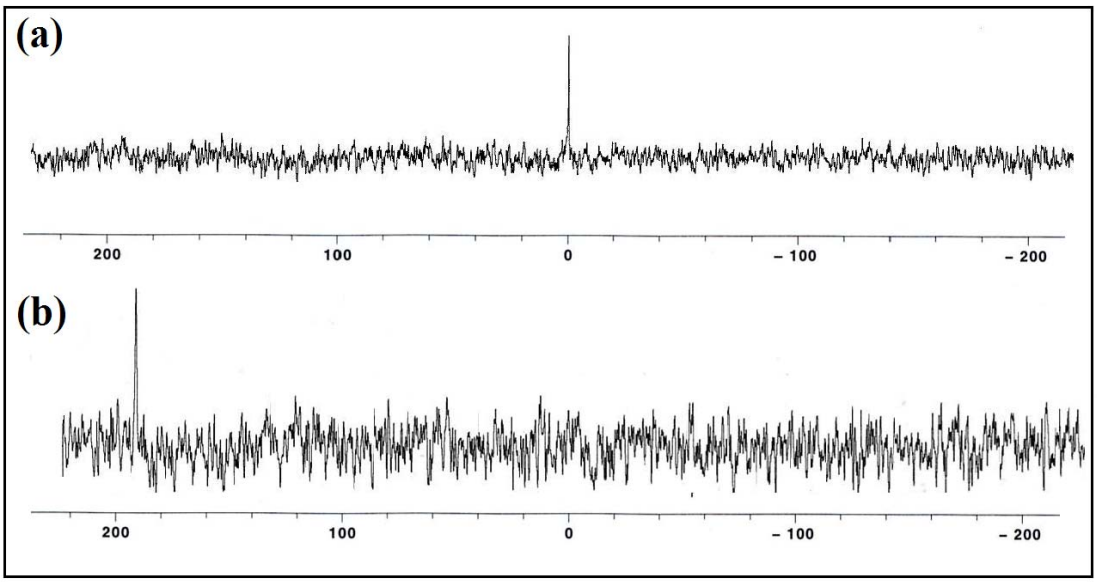

Figure 3.21. (a) ^{89}Y NMR of YCl_3 in D_2O after 32 scans (external reference); (b) ^{89}Y NMR of $Y_3N@I_h$-C_{80} in dichlorobenzene with 20 mg $Cr(acac)_3$ relaxant and 1,2-dichlorobenzene-d_4 lock after 51,520 scans. The chemical shifts for the one line is at δ: 191.63 ppm

The crystal structure of $Y_3N@I_h$-C_{80} is shown in Figure 3.22. It is similar to that previously reported $Sc_3N@I_h$-C_{80} isomer, the sum of three Y-N-Y angles is 359.99°, indicating that Y_3N cluster inside the I_h-C_{80} cage assumes a planar shape. The M_3N cluster geometry within a C_{80} cage depends on the size of the metal ions involved. For example, a planar M_3N unit is formed for small metal ions such as Sc^{3+} (0.88 Å) and Lu^{3+} (1.00 Å),[41] while a pyramidal M_3N cluster is exhibited by larger metal ions such as Tb^{3+} (1.06 Å)[41] and Gd^{3+} (1.08 Å).[17] The planar structure of Y_3N cluster in I_h-C_{80} is consistent with the intermediate size of Y^{3+} (1.04 Å).

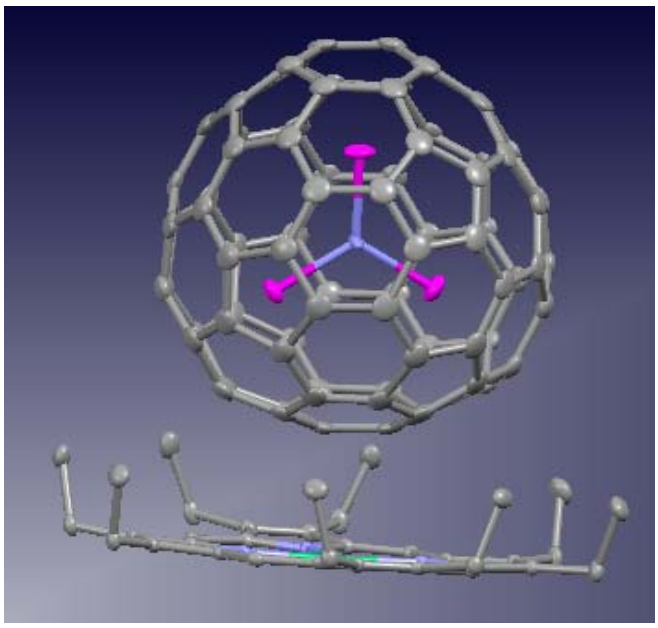

Figure 3.22. A perspective view of the single crystal structure of $Y_3N@I_h$-C_{80}•Ni(OEP)•2.5benzene

3.2.3.1.2. $Y_3N@D_{5h}$-C_{80}

As previously indicated, it has been established that there are two isomers of $Sc_3N@C_{80}$ (I_h and D_{5h}, both obeying the IPR) that have been isolated and characterized. The D_{5h} isomer has also been characterized for other $M_3N@C_{80}$ systems, such as $Tm_3N@D_{5h}$-C_{80}[28] and $Tb_3N@D_{5h}$-C_{80}.[22] The simulated structure of $Y_3N@D_{5h}$-C_{80} is shown in Figure 3.23.

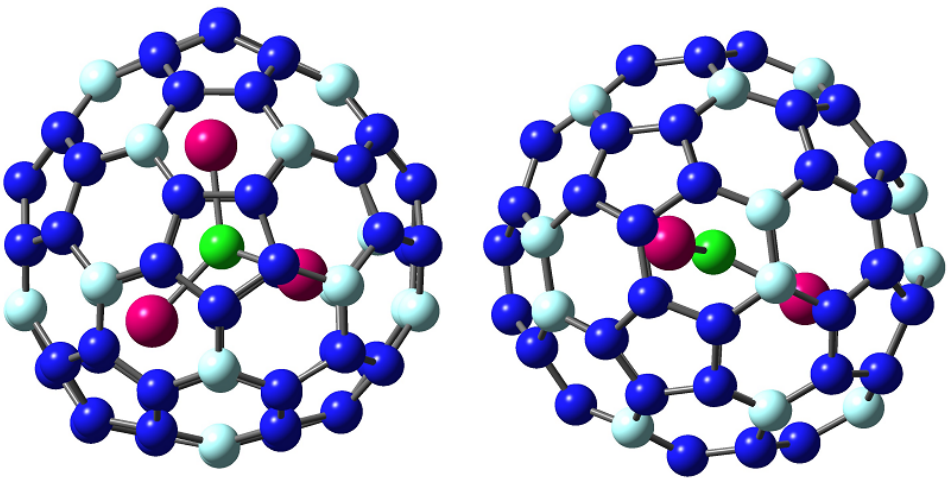

Figure 3.23. Structure of $Y_3N@D_{5h}$-C_{80}

Because of the lower symmetry, there are a total of six kinds of carbon atoms in the D_{5h}-C_{80} carbon cage. Thus, the ^{13}C NMR spectrum (Figure 3.24) is presented for the purified $Y_3N@D_{5h}$-C_{80} isomer with six spectral lines with the intensity ratios of 1:2:2:1:1:1. As expected, ^{13}C NMR data for $Y_3N@D_{5h}$-C_{80} closely matches the ^{13}C NMR data reported for other $M_3N@D_{5h}$-C_{80} isomers and does not significantly deviate as a function of the metal in the $[M_3N]^{6+}$ (M=Lu and Sc) cluster.[12, 13] However, the corannulene-type 6,6,5 carbon atoms (**a** in Figure 24a) are significantly deshielded relative to those for the $Y_3N@I_h$-C_{80} isomer (δ = 149.63 vs 144.62 ppm). In addition, the computed value (Figure 24c) is within ~1 ppm of the experimental value. Although a definitive assignment is not possible for all of the signals for the $Y_3N@D_{5h}$-C_{80} isomer, there appears to be good agreement between the experimental and computational values for **b** and **d**. On the other hand, the pyracylene 6,6,5 carbon site **f** is not definitively assignable, but it must be one of the three most shielded resonances (139.06, 138.82 and 136.58 ppm) with intensity ratios 1:1:1. These values indicate significantly more shielding than for typical pyracylene 6,6,5 carbon sites, such as, I_h-C_{60} at δ = 142.5 ppm[32] or for endcap pyracylene carbons in D_{5h}-C_{70} (δ = 150.7 ppm).[33] The corresponding deshielding and shielding effects observed for carbon sites **a** and **f,** respectively, could result from restricted motion of the $[Y_3N]^{6+}$ cluster in the horizontal plane of D_{5h} isomer. These results deserve further study, but the current results clearly illustrate the importance of the position and motional process of the internal $[M_3N]^{6+}$ cluster in determining ^{13}C NMR chemical shifts. The experimental and computational values match well, as shown in the correlation between them in Figure

3.25.

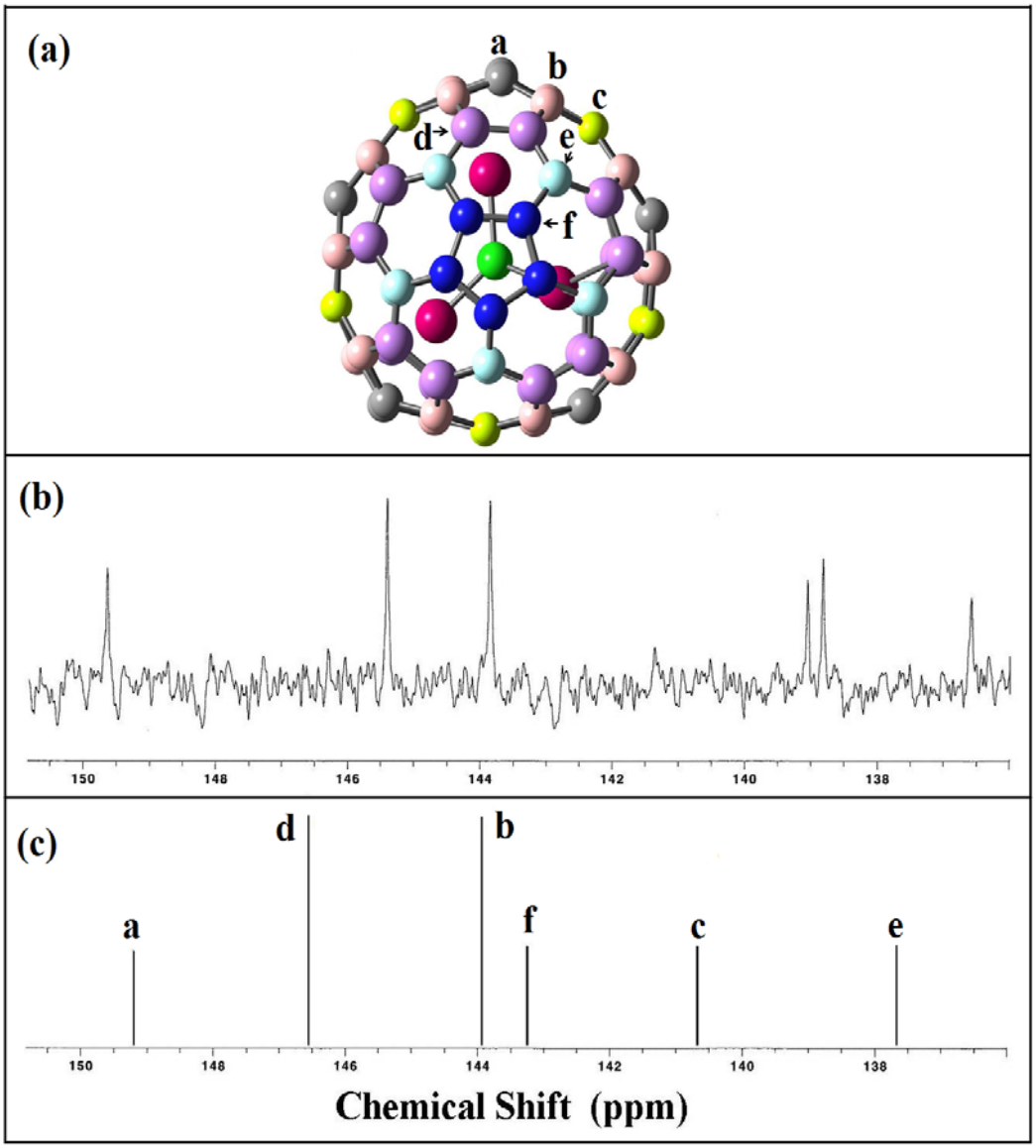

Figure 3.24. (a) Simulated molecular structure of $Y_3N@D_{5h}$-C_{80} with labels for different kinds of carbon atoms based on symmetry considerations; (b) ^{13} C NMR spectrum of $Y_3@D_{5h}$-C_{80} in CS_2 with 12 mg $Cr(acac)_3$ relaxant and acetone-d_6 lock after 75000 scan at 25 ºC, 2x20,4x10 pattern (number of NMR lines x relative intensity). The chemical shifts for the six lines are at δ: 149.63, 145.40 (double intensity), 143.85 (double intensity), 139.06, 138.82 and 136.58 ppm. (c) Theoretical ^{13}C NMR spectrum of $Y_3N@D_{5h}$-C_{80}

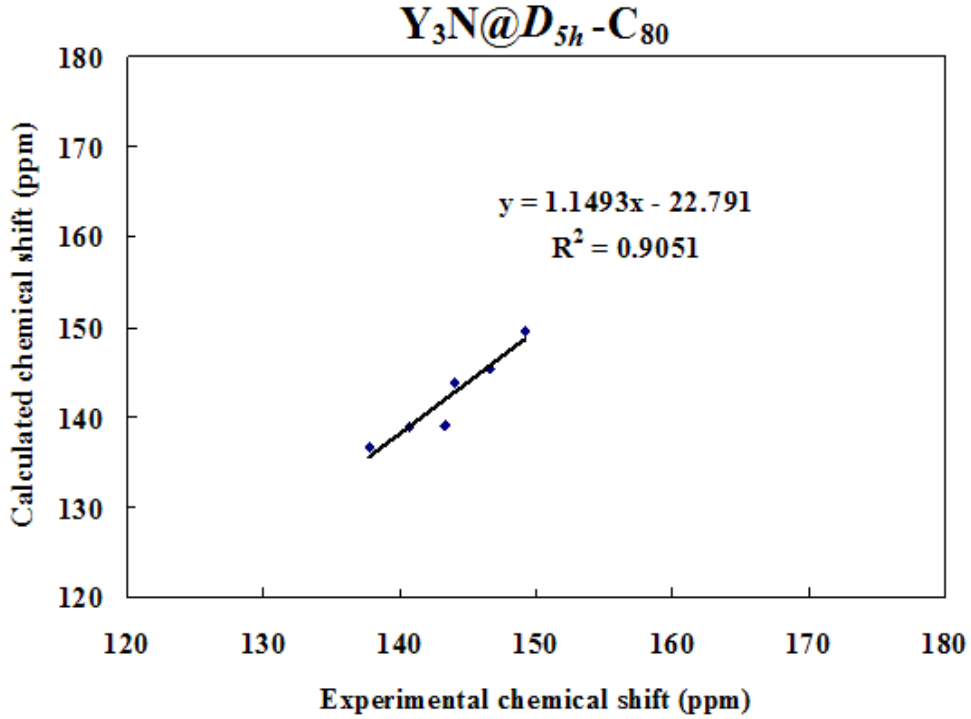

Figure 3.25. Correlation of experimental and computational ^{13}C NMR shifts of $Y_3N@D_{5h}$-C_{80}

Both the D_{5h} and I_h are members of the seven IPR-satisfying isomers for the C_{80} cage and the structures of these two isomers are closely related. By slicing the D_{5h} cage along the horizontal mirror plane and rotating one-half by 36º, then putting the two halves back together, the I_h isomer can be obtained.[13] The UV-Vis spectrum is particularly useful for characterization for fullerene cage structure and charges on it. The structural difference between D_{5h} and I_h is observed by the UV-Vis measurement (Figure 3.26).

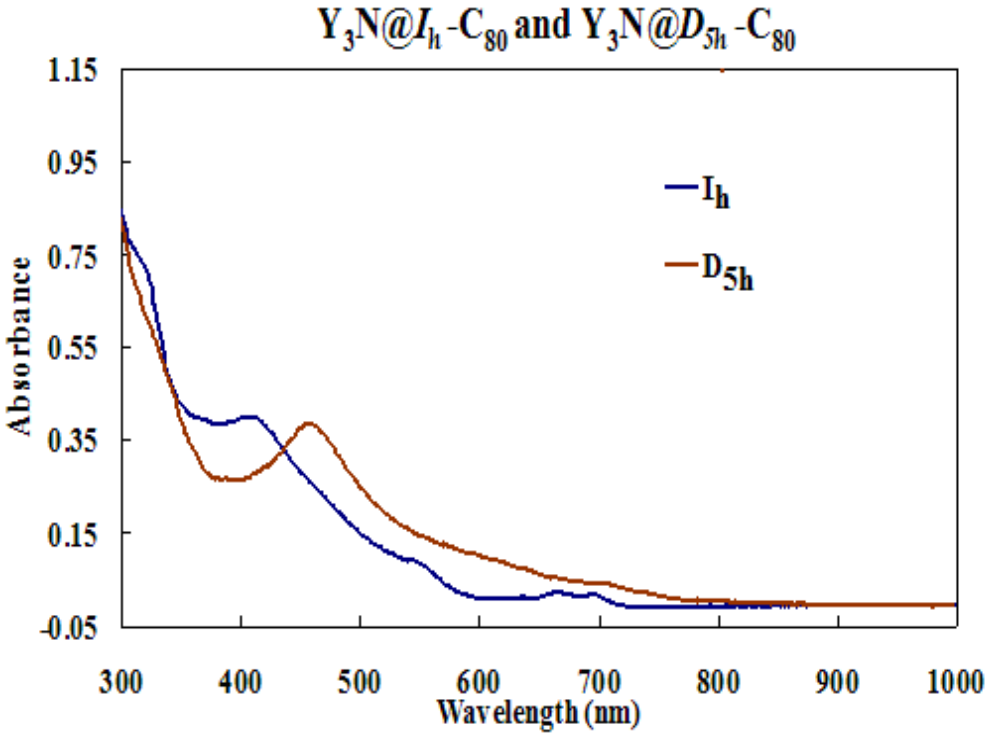

Figure 3.26. UV-Vis spectra of purified $Y_3N@I_h$-C_{80} and $Y_3N@D_{5h}$-C_{80} in toluene solution

Theoretical calculations were conducted for $C_{80}^{6-}(I_h)$ and $C_{80}^{6-}(D_{5h})$ cages. As shown in Figure 3.27, the $C_{80}^{6-}(I_h)$ is 0.0375 Hartree (23.53 kcal/mol) more stable than the $C_{80}^{6-}(D_{5h})$ isomer. The HOMO-LUMO gap of $C_{80}^{6-}(I_h)$ is also larger than that of $C_{80}^{6-}(D_{5h})$, suggesting that $C_{80}^{6-}(I_h)$ isomer is both thermodynamically and kineticly more stable than $C_{80}^{6-}(D_{5h})$. These results are consistent with the dominant yield of $Y_3N@I_h$-C_{80} (the relative yield ratio of $Y_3N@I_h$-C_{80} and $Y_3N@D_{5h}$-C_{80} is approximately 95:5).

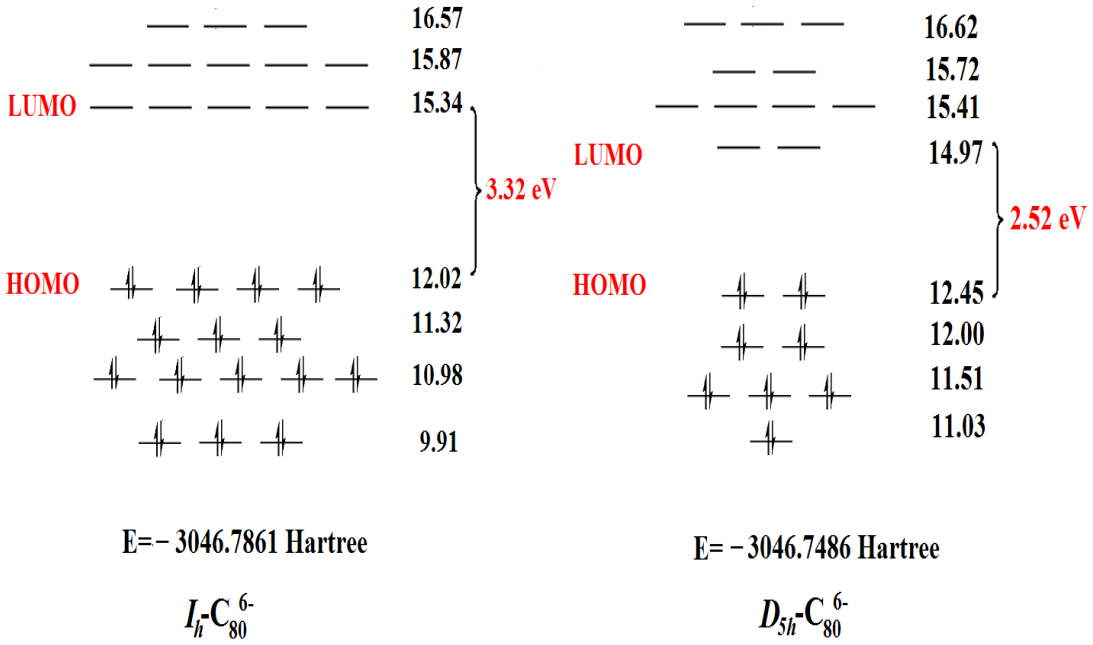

Figure 3.27. Theoretical calcultions for C_{80}^{6-} (I_h) and C_{80}^{6-} (D_{5h}) of $Y_3N@C_{80}$

3.2.3.2. $Y_3N@C_{82}$:

It was predicted that $M_3N@C_{82}$ is a non-IPR structure because of the small gap in the molecular orbital energy in the hexa-anion of the empty C_{82} cage.[42] Popov and Dunsch[43] suggested that the most plausible isomers for the TNT EMFs with C_{82} cages are $M_3N@C_{2v}(39705)$-C_{82} and $M_3N@C_s(39663)$-C_{82} by computational approaches. Remarkably, Echegoyen and Balch[29] recently reported the egg-shaped structure of $Gd_3N@C_s(39663)$-C_{82} obtained using single-crystal X-ray diffraction study, consistent with the earlier predictions of Popov and Dunsch.

There are 39,709 possible non-IPR isomeric structures and among them are 27 isomers with C_s symmetry. The simulated structure of $Y_3N@C_s(39663)$-C_{82} is shown in Figure 3.28, where the two fused pentagon are displaied in purple. The UV-Vis of $Y_3N@C_s(39663)$-C_{82} is shown in Figure 3.29.

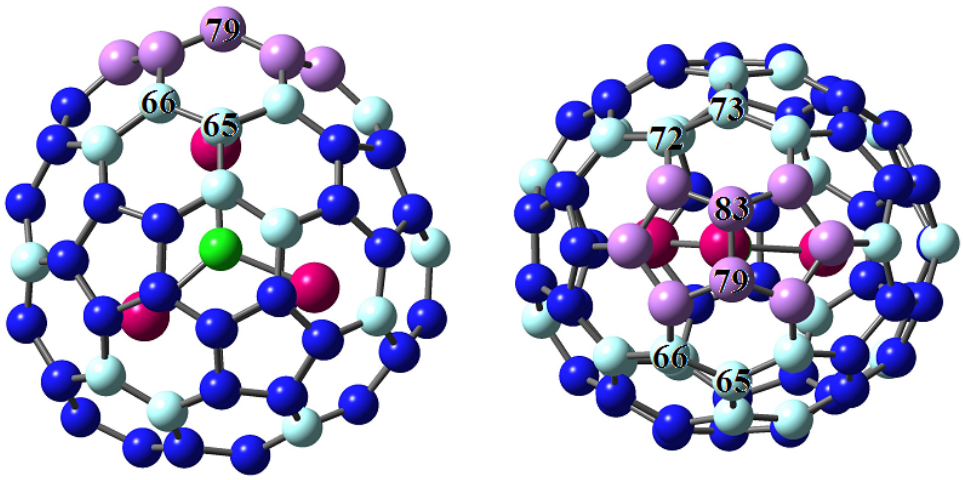

Figure 3.28. Structure of $Y_3N@C_s(39663)\text{-}C_{82}$ in toluene solution

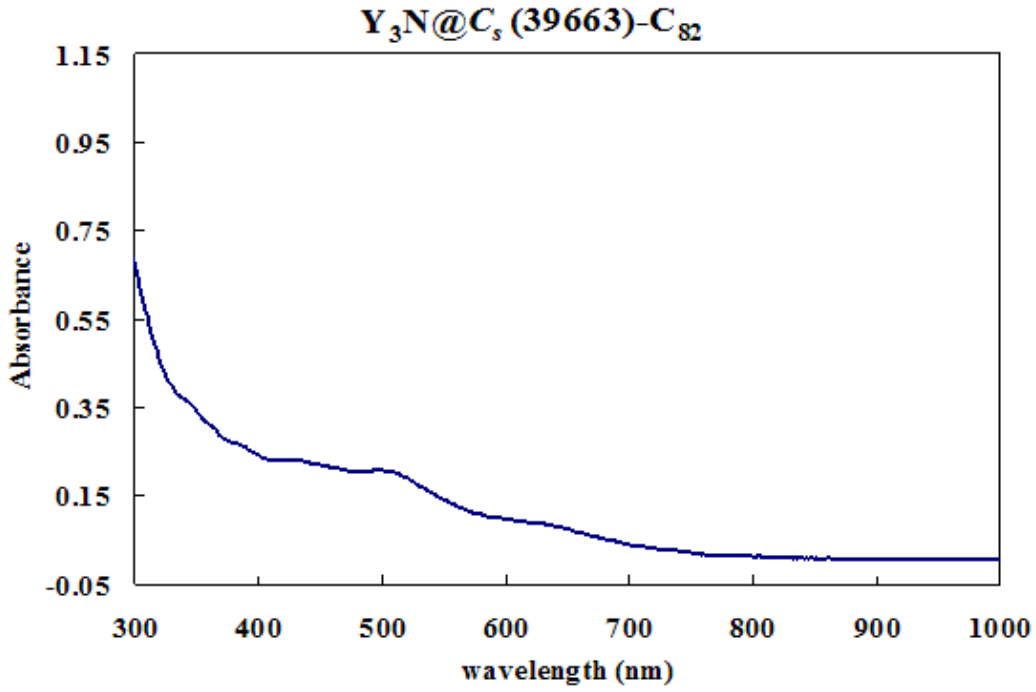

Figure 3.29. UV-Vis spectrum of purified $Y_3N@C_s(39663)\text{-}C_{82}$ in toluene solution

The ^{13}C NMR spectrum (Figure 3.30) for $Y_3N@C_{82}$ exhibits 45 lines, 37 of full intensity and 8 of half of intensity consistent with C_s symmetry structure (a 37×2, 8×1 pattern). The observed spectral line at 165.7 ppm (171.7 ppm by DFT prediction) is

also consistent with the pentalene carbons (C79 and C83, as shown in Figure 3.27) for this non-IPR structure. This peak is significantly more deshielded than most pentalene carbons reported to date, presumably due the greater strain of the pentalene motif in this case.[14] The half intensity signals at 153.7, 144.37, 143.87, and 143.81 are consistent with the 4 pyracylene 6,6,5 junction carbons in the plane of the C_s(39663)-C_{82} cage. Assuming that the 2 half-intensity corannulene 6,6,5 carbons are the signals at 140.3 and 139.7 ppm, that leaves 2 half-intensity 6,6,6 pyrene signals at 137.77 and 136.76 ppm. The DFT computed values for these half intensity signals are typically 3-5 ppm more deshielded than the experimental values. There are 11 pyrene type 6,6,6 carbons for the C_s(39663)-C_{82} structure tentatively assigned to the 11 (2×1) ^{13}C NMR signals below 138 ppm. Especially interesting are two highly shielded pyrene carbon 6,6,6 signals (127.52 and 126.55 ppm) that are spatially located over the Y atom complexed to the pentalene site (C65, C66, C72, C73, as shown in Figure 3.28). These two appear to be 2-3 ppm more shielded, but are clearly identified by the DFT results. The correlation of experimental and computational values is shown in Figure 3.31. Although a ^{13}C NMR INADEQUATE study is necessary to completely define the carbon-carbon connectivity and corresponding structure, the current study confirms that the ^{13}C NMR spectrum for $Y_3N@C_{82}$ is consistent with the cage reported for $Gd_3N@C_s$(39663)-C_{82}.[29] The experimental and computational ^{13}C values match well, as shown in the correlation between them in Figure 3.31.

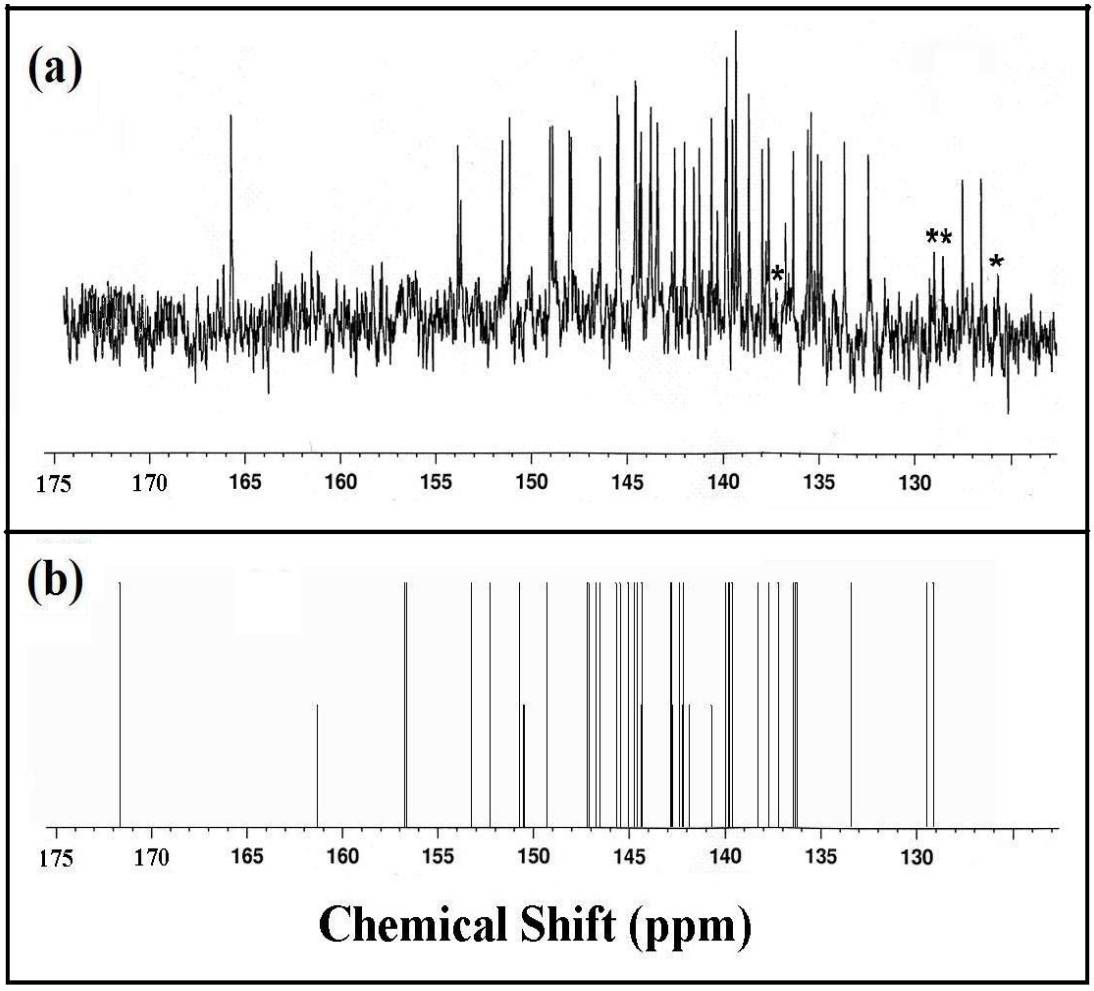

Figure 3.30. (a) ^{13}C NMR spectrum of $Y_3N@C_s(39663)\text{-}C_{82}$ in CS_2 with 10 mg $Cr(acac)_3$ relaxant and acetone-d_6 lock after 120,000 scan at 25 ºC, 37×2, 8×1 pattern (number of NMR lines × relative intensity). The chemical shifts for the forty-five lines are at δ: 165.69, 153.84, 153.70 (half-intensity), 151.51, 151.14, 149.03, 148.89, 148.03, 147.93, 146.43, 145.53, 145.45, 144.59, 145.55, 144.37 (half-intensity), 144.28, 143.81 (half-intensity), 143.77, 143.43, 143.41 (half-intensity), 142.53, 142.01, 141.53, 141.25, 140.61, 140.30 (half-intensity), 139.87, 139.82, 139.52, 139.34, 139.17 (half-intensity), 138.66, 137.96, 137.77 (half-intensity), 137.63, 136.76 (half-intensity), 136.35, 135.58, 135.42, 135.07, 134.89, 133.67, 132.40, 127.52, 126.55 ppm. The * corresponds to signals which came from the residual toluene in the sample. (b) Theoretical ^{13}C NMR spectrum of $Y_3N@C_s(39663)\text{-}C_{82}$

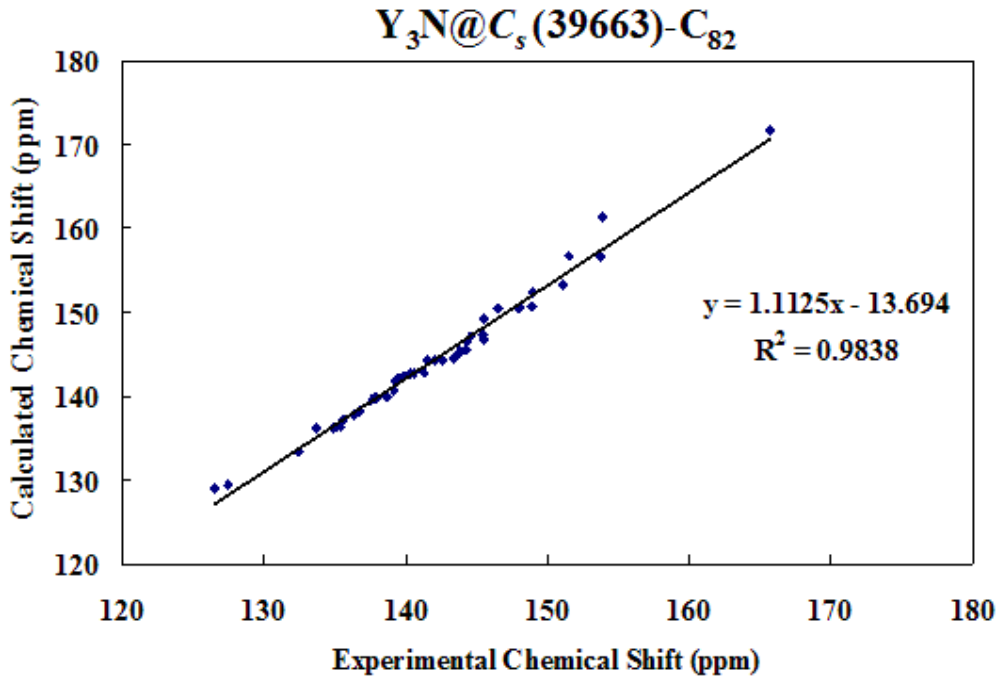

Figure 3.31. Correlation of experimental and computational ^{13}C NMR shift of $Y_3N@C_s(39663)\text{-}C_{82}$

There are nine IPR-satisfying isomers (three C_2 isomers, three C_s isomers, two C_{3v} isomers and one C_{2v} isomer) for the C_{82} cage.[44] For the mono- and di-EMFs reported so far, all fullerene cages are IPR-satisfying structure. For example, the major C_{2v} isomer has been established for $M@C_{82}$ type (M=La, Y, Ca) fullerene[45] and C_s and C_{3v} structures have been crystallographically determined for $Er_2@C_{82}$.[46, 47] However, for the TNT EMFs, the TNT clusters are encapsulated in a non-IPR cage. Theoretical calculations in Figure 3.32 demonstrated that the neutral non-IPR $C_s(39663)\text{-}C_{82}$ has a small HOMO-LUMO gap, suggesting the instability of $C_s(39663)\text{-}C_{82}$ cage. However, upon accepting six electrons, the HOMO-LUMMO gap becomes very large, increase the stability of $Y_3N@C_s(39663)\text{-}C_{82}$.

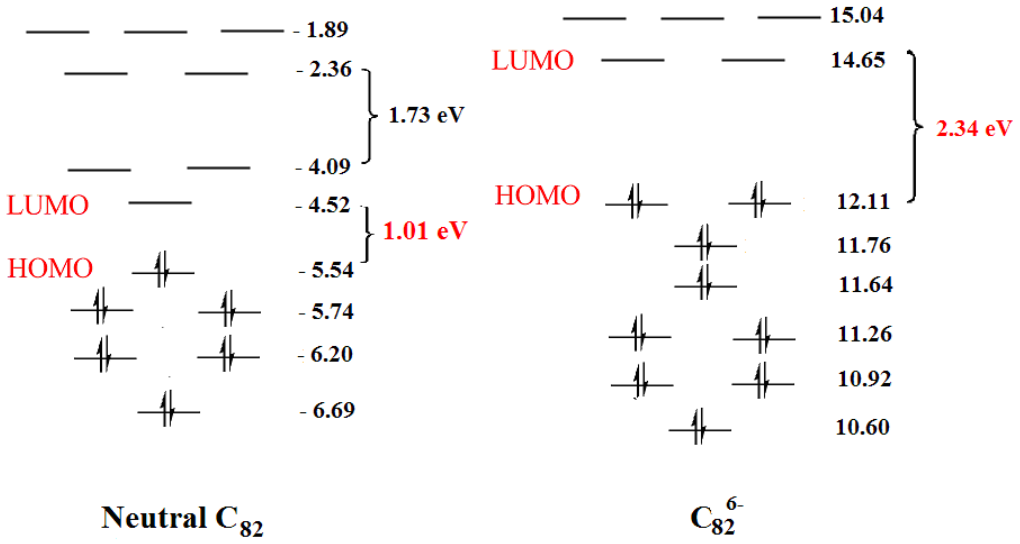

Figure 3.32. Illustration of the stabilization of the neutral C_s(39663)-C_{82} by accepting six electrons from Y_3N cluster

3.2.3.3. $Y_3N@C_{84}$:

Although there are 51,568 non-IPR and 24 IPR structures for C_{84}, the most abundant $M_3N@C_{84}$ (M=Tb, Tm, Gd) isomer has been confirmed as an egg-shaped structure with non-IPR C_s symmetry by an X-ray diffraction study.[22, 30] The C_{84} cage in $M_3N@C_s$(51365)-C_{84} (M=Tb, Tm, Gd) closely resembles the cage of the $Gd_3N@C_s$(39663)-C_{82}. The cage has a single pentalene, and a symmetry plane bisects this motif. Our study suggested that $Y_3N@C_{84}$ is another bucky-egg EMF utilizing the same non-IPR cage structure as the $M_3N@C_s$(51365)-C_{84} (M=Tb, Tm, Gd), as shown in Figure 3.33. The UV-Vis of $Y_3N@C_s$(51365)-C_{84} is shown in Figure 3.34.

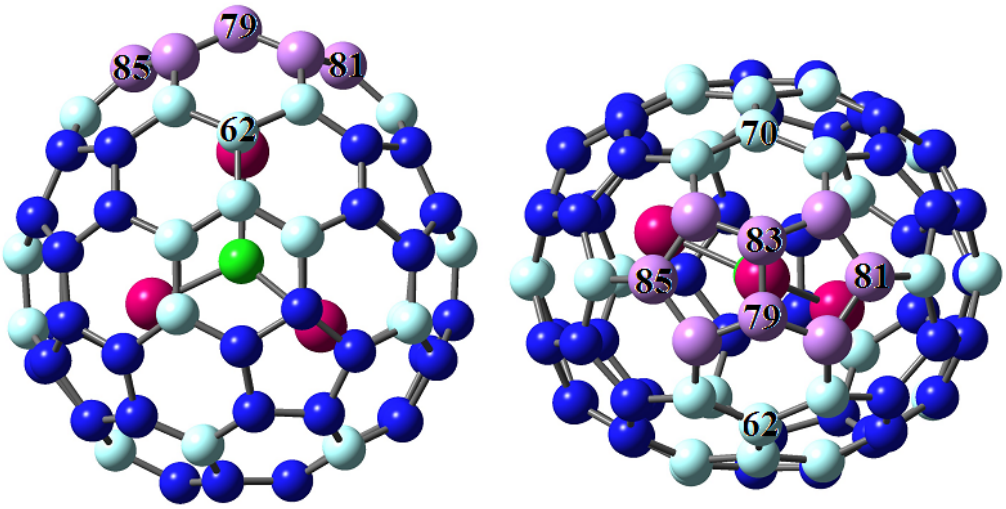

Figure 3.33. Structure of $Y_3N@C_s(51365)$-C_{84}

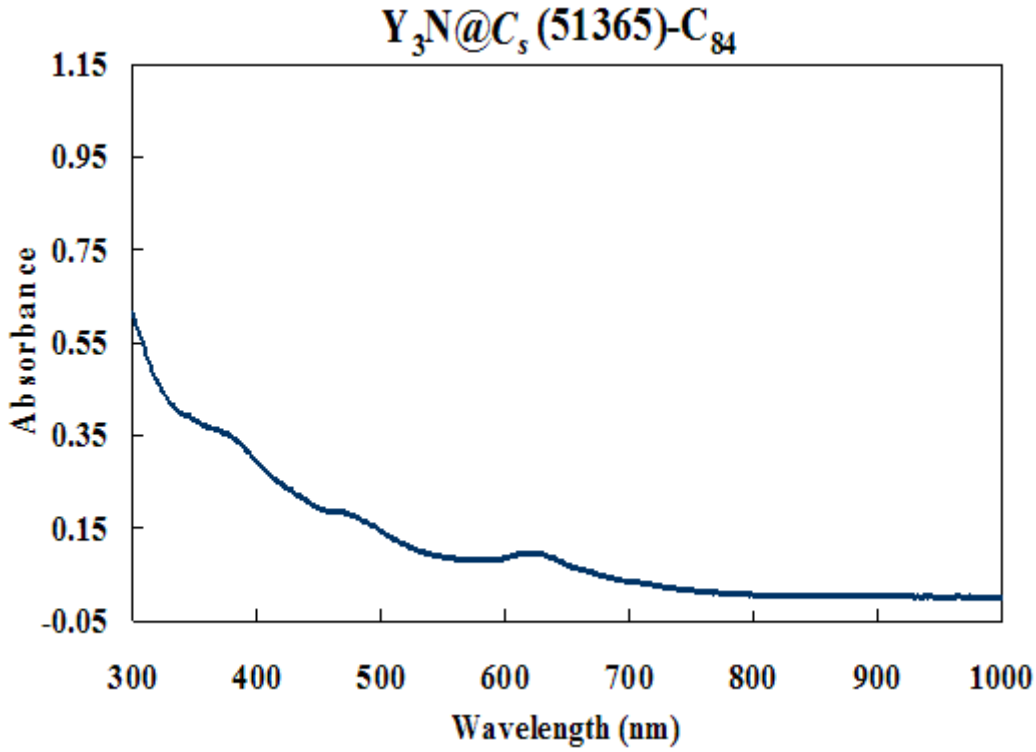

Figure 3.34. UV-Vis spectrum of purified $Y_3N@C_s(51365)$-C_{84} in toluene solution

As indicated in HPLC chromatogram (Figure 3.17), the retention time of $Y_3N@C_{84}$ is around 60 minutes, which is even longer than that of its neighboring higher TNT endohedral metallofullerenes, $Y_3N@C_{86}$, indicating the low symmetry of C_{84} cage. The high dipole moment is probably caused by a non-spherical charge

distribution due to the elliptical cage which is presumably responsible for the retention behavior of $Y_3N@C_{84}$.[48]

Figure 3.35 shows the high resolution experimental and theoretical ^{13}C NMR spectra for the $Y_3N@C_{84}$. The experimental spectrum consists of 47 lines, 37 of full intensity and 10 of half of intensity consistent with C_s symmetry structure (37 × 2, 10 ×1 pattern). The wide range of chemical shifts is from 124.01 to 160.24 ppm. There is one highly deshielded resonance at 160.24 ppm, confirming the presence of the pentalene motif with carbons (C79 and C83, as shown in Figure 3.32) for this non-IPR structure. The theoretical ^{13}C NMR chemical shift range, 127.39 to 159.71 ppm, is in excellent agreement with the experimental spectrum. Two nonequivalent half intensity 6,6,5 pyracylene carbons (C81 and C85, as shown in Figure 3.32) can be assigned to the experimental values at 149.5 and 146.98 ppm. These values are significantly more deshielded than the corresponding DFT computational values at 153.36 and 150.31 ppm. One isolated peak in the downfield region of the spectrum is due to pyrene carbon 6,6,6 signals (124.01 ppm) which matches the DFT calculated spectrum. In similar fashion to the $Y_3N@C_s(39663)\text{-}C_{82}$ isomer, this corresponds to the highly shielded pyrene carbon signals (C62 and C70, as shown in Figure 3.32) that are spatially located over the Y atom complexed to the pentalene site. Due to the large numbers of peaks, a one-to-one assignment for all the NMR peaks is impossible. The correlation of experimental and computational values is shown in Figure 3.36. To summarize, the ^{13}C NMR spectrum for $Y_3N@C_s(51365)\text{-}C_{84}$ is consistent with the carbon cage reported for the corresponding Tb, Tm and Gd isomers previously reported.[21, 30]

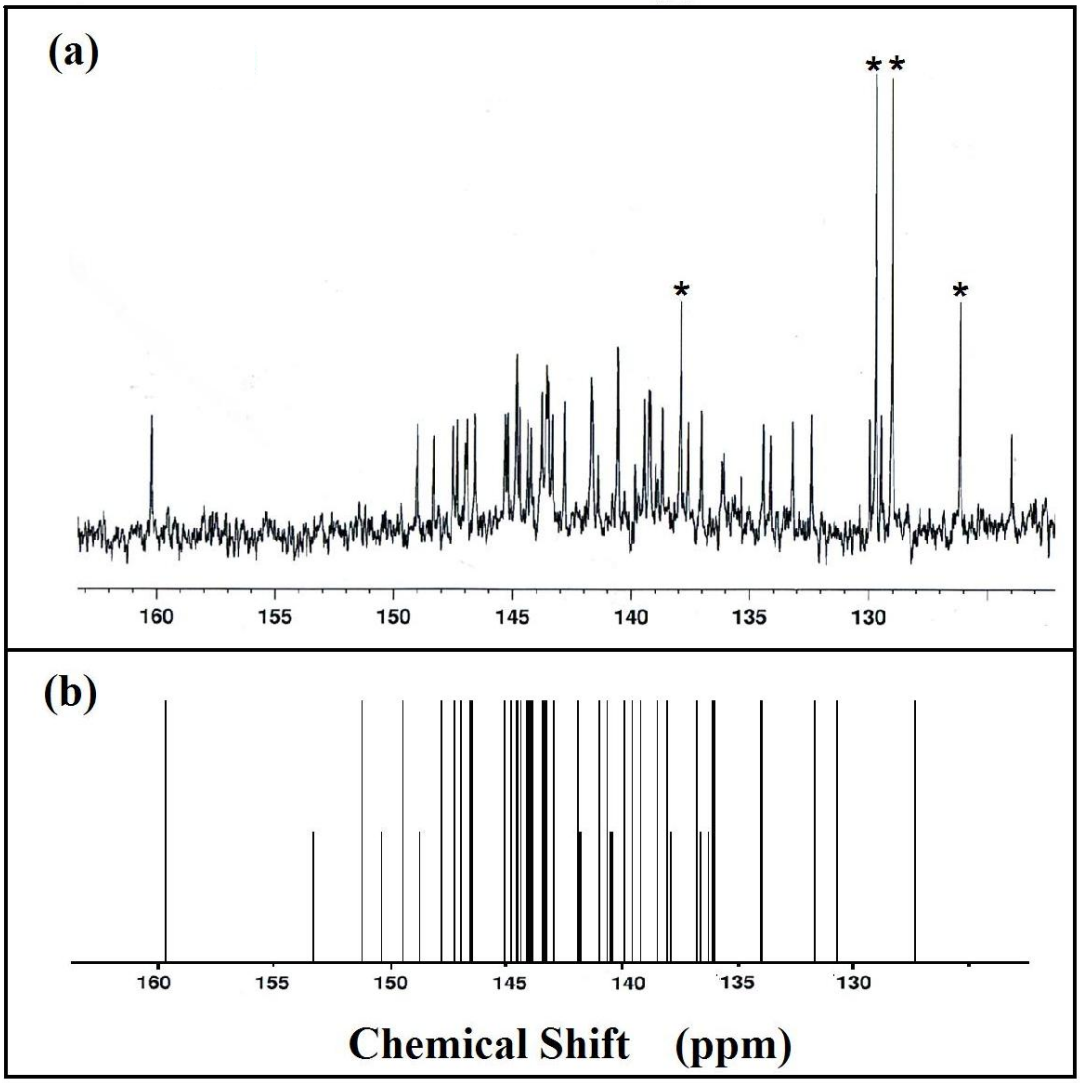

Figure 3.35. (a) ^{13} C NMR spectrum of $Y_3@C_s(51365)$-C_{84} in CS_2 with 10 mg $Cr(acac)_3$ relaxant and acetone-d_6 lock after 106,000 scan at 25 ºC, 2×37, 1×10 pattern (number of NMR lines x relative intensity). The chemical shifts for the forty-four lines are at δ: 160.24, 149.00, 148.32, 147.49, 147.33, 146.98. 146.91, 146.59, 145.31, 145.21, 144.86 (one and half intensity), 144.83 (one and half intensity) , 144.7, 144.37, 144.23, 143.78, 143.61, 143.56, 143.5, 143.34, 142.81, 141.68, 141.63, 141.40 (half-intensity), 140.58, 139.86, 139.46, 139.25, 139.20, 138.96 (half-intensity) , 138.86 (half-intensity), 138.70, 137.62, 137.02, 136.18 (half-intensity), 136.12 (half-intensity), 135.35 (half-intensity), 134.44, 134.12, 133.18, 132.39, 129,96, 129.49, 124.01 ppm. The * corresponds to signals which came from the residual toluene in the sample. (b) Theoretical ^{13}C NMR spectrum of $Y_3N@C_s(51365)$-C_{84}

Figure 3.36 shows the correlation between experimental and computational ^{13}C values. It is clear that these two series of values match pretty well.

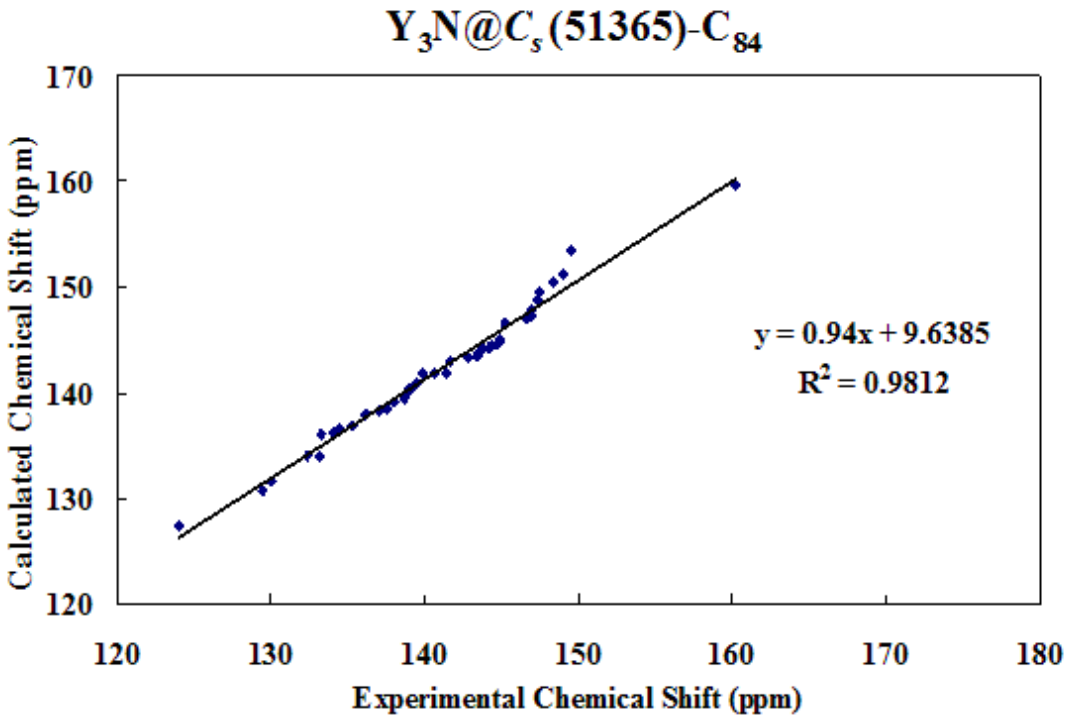

Figure 3.36. Correlation of experimental and computational ^{13}C NMR shift of $Y_3N@C_s(51365)\text{-}C_{84}$

Among all the non-IPR EMFs reported so far, the pentalene fold always coordinated with a metal ion of the cluster inside the cage.[14, 21, 30] As expected for $Y_3N@C_s(51365)\text{-}C_{84}$, the coordination of one Y atom with the pentalene motif (Figure 3.32) and the more restricted internal cage surface should yield 3 different electronic environments for the yttrium atoms of the $(Y_3N)^{6+}$ cluster at ambient temperatures. As shown in Figure 3.37, three ^{89}Y NMR signals are observed at 104.32, 65.33, and -19.53 ppm (relative to external YCl_3). In previous solution ^{89}Y NMR studies, it has been observed that there is a strong shielding effect for Y^{3+} ions complexed to

pentamethylcyclopentadienyl moieties. Hanusa[49] has reported that this ^{89}Y chemical shielding effect is ~100 ppm per cyclopentadienyl unit in organometalic complexes. Based on this additivitve effect, we tentatively assign the ^{89}Y NMR signal at -19.53 ppm to the Y atom (Labeled as **"a"** in Figure 3.37) complexed to the pentalene moiety in $Y_3N@C_s(51365)$-C_{84}. The DFT computational study suggests the chemical shifts for three Yttrium ions are 146.84, 102.08 and 14.95, which match the experimental values well.

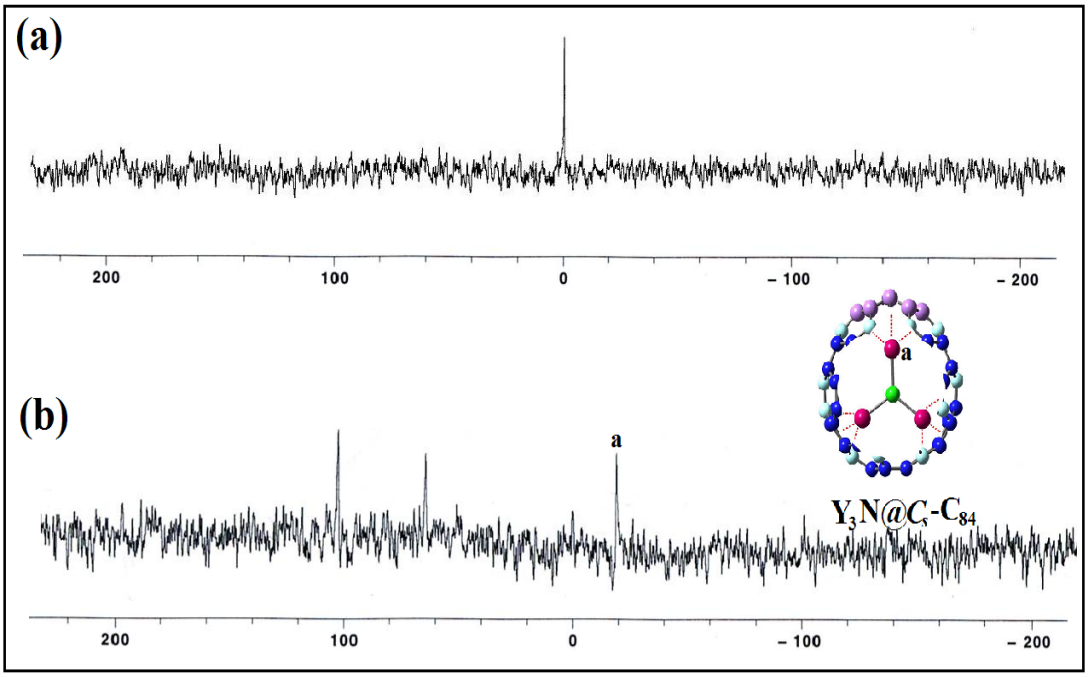

Figure 3.37. (a) ^{89}Y NMR of YCl_3 in D_2O after 32 scans (external reference); (b) ^{89}Y NMR of $Y_3N@C_{84}$ in 1,2-dichlorobenzene with 20 mg $Cr(acac)_3$ relaxant and 1,2-dichlorobenzene-d_4 lock after 41,200 scan. The chemical shifts for the three line are at δ: 104.32, 65.33, -19.53 ppm. (all spectra at 25 ºC)

As the third most abundant empty cage fullerenes, all empty C_{84} isomers are IPR-obeying structures and C_{84} cages with D_2 and D_{2d} symmetry have been separated and characterized successfully.[50] Theoretical calculations in Figure 3.38 suggest that the neutral non-IPR $C_s(51365)$-C_{84} has a small HOMO-LUMO gap and the instability

of this isomer, which is consistent the fact there is no non-IPR C_{84} isolated to date. However, upon accepting six electrons, the HOMO-LUMO gap becomes very large, thereby increasing the stability of the $Y_3N@C_s(51365)$-C_{84} molecule.

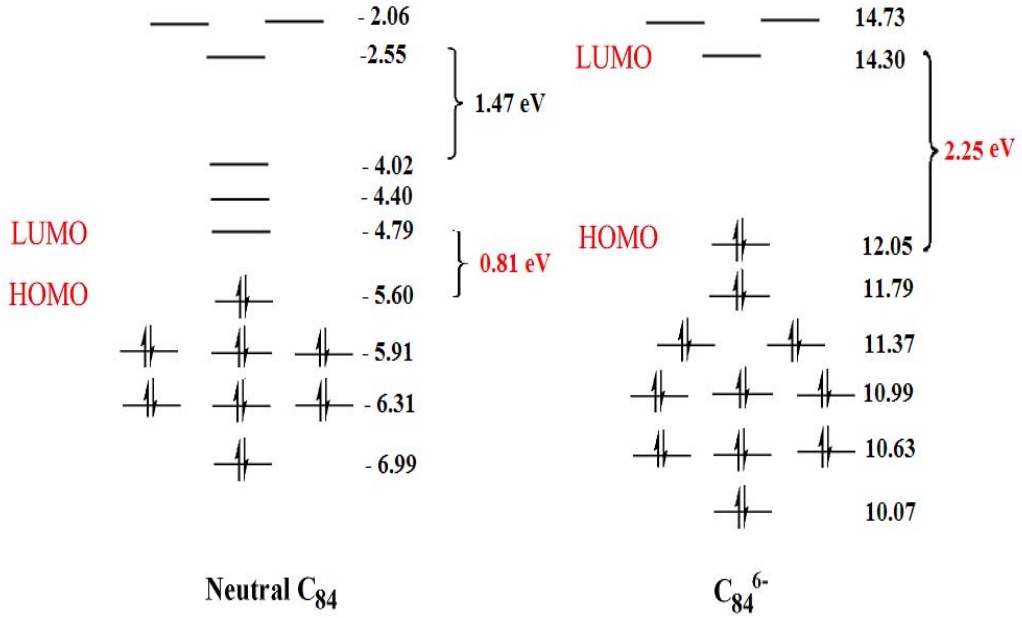

Figure 3.38. Illustration of the stabilization of the neutral $C_s(51365)$-C_{84} by accepting six electrons from Y_3N cluster

3.2.3.4. $Y_3N@C_{86}$:

There are 19 IPR allowed C_{86} isomers, of these two neutral isomers with C_2 and C_s symmetry are reported to be stable from experimental and computational studies.[51] However, another TNT metallofullerene, $Tb_3N@D_3(19)$-C_{86}, exhibits a carbon cage with D_3 symmetry as determined by previous single-crystal X-ray diffraction studies.[22] The ^{13}C NMR study suggests that $Y_3N@C_{86}$ has the same structure of $Tb_3N@D_3(19)$-C_{86}. The simulated structure and the Uv-Vis of $Y_3N@D_3(19)$-C_{86} are shown in Figure 3.39 and Figure 3.40.

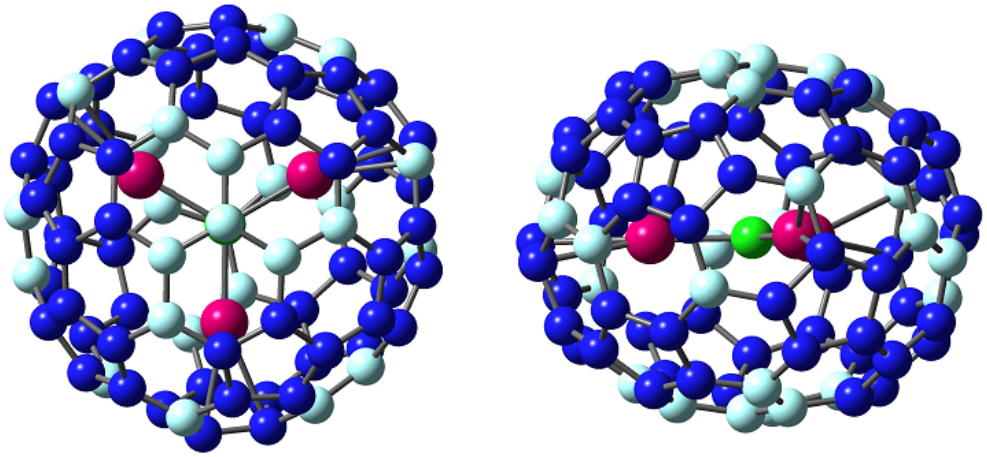

Figure 3.39. Structure of $Y_3N@D_3(19)\text{-}C_{86}$

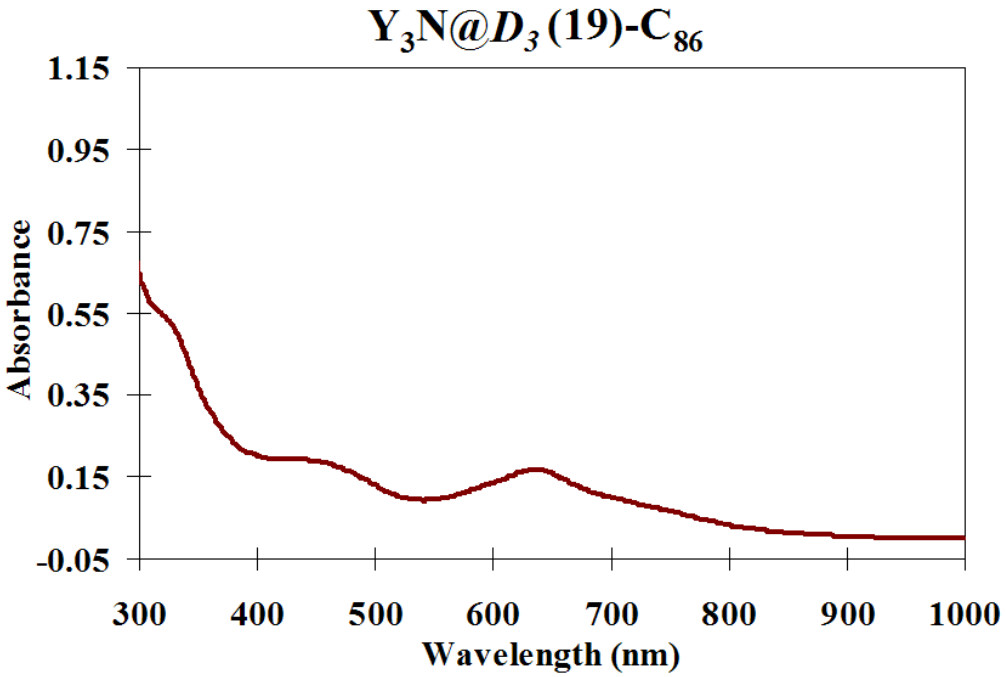

Figure 3.40. UV-Vis spectrum of purified $Y_3N@D_3(19)\text{-}C_{86}$ in toluene solution

The ^{13}C NMR spectrum (Figure 3.41) for $Y_3N@C_{86}$ exhibits a total of only 15 lines (14 full-intensity peaks, plus one 1/3-intensity peak) with a relatively small range of only ~15 ppm, in sharp contrast with the much larger spectral range for $Y_3N@C_s(39663)\text{-}C_{82}$ and $Y_3N@C_s(51365)\text{-}C_{84}$. The ^{13}C NMR spectrum for $Y_3N@C_{86}$ suggests an IPR allowed isomer because of the absence of a ^{13}C NMR signal at > 155 ppm that would be characteristic of a pentalene motif. Previously single-crystal X-ray

diffraction studies suggested that $Tb_3N@D_3(19)$-C_{86} exhibits a carbon cage with D_3 symmetry and this result is completely consistent with the 15 ^{13}C NMR signals observed for $Y_3N@C_{86}$. In addition, no other IPR allowed structure would exhibit fewer than 24 lines because these remaining structures all have lower symmetry. The ^{13}C NMR resonances for the carbons along the D_3 symmetry (2×1, 1/3 intensity) are easily identified (133.9 ppm) and are in excellent agreement with the DTF prediction, 136.81 ppm. In addition, there are 6 pyrene 6,6,6 type carbons that range from 131.6 to138.7 ppm in reasonable agreement with 6 DFT predicted values ranging from 132.5 -141.1 ppm. The correlation of experimental and computational values is shown in Figure 3.42.

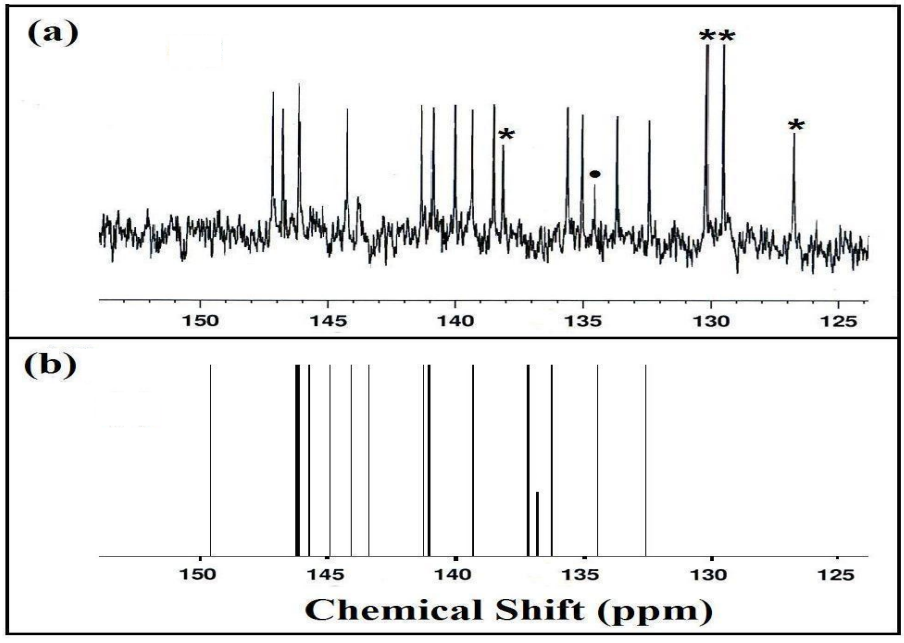

Figure 3.41. (a) ^{13}C NMR spectrum of $Y_3N@D_3$-C_{86} in CS_2 with 10 mg $Cr(acac)_3$ relaxant and acetone-d_6 lock after 108000 scan at 25 ºC, 14×6,1×2 pattern (number of NMR lines x relative intensity). The chemical shifts for the 15 lines are at δ:： 146.84, 146.42, 145.78, 145.72, 143.81, 140.79, 140.32, 139.42, 138.71, 137.87, 134.89, 134.31, 133.81 (one-third intensity), 132.92, 131.60 ppm. The * corresponds to signals which came from the residual toluene in the sample. The • corresponds to signal with 1/3 intensity. (b) Theoretical ^{13}C NMR spectrum of $Y_3N@D_3(19)$-C_{86}

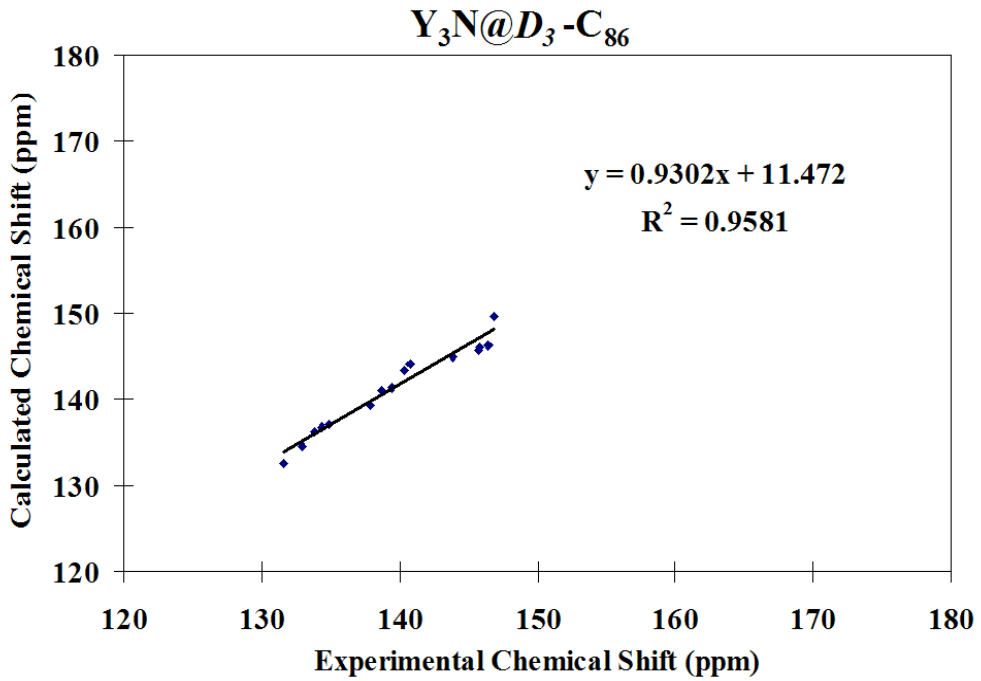

Figure 3.42. Correlation of experimental and computational ^{13}C NMR shift of $Y_3N@D_3(19)$-C_{86}

As shown in Figure 3.43, one single sharp ^{89}Y NMR signal is observed at 62.65 ppm (relative to external YCl_3), which suggests that the three Y atoms have the same chemical environment. However, due to the restricted motion of the $(Y_3N)^{6+}$ cluster, the signal is more highly deshielded than in the $Y_3N@I_h$-C_{80}.

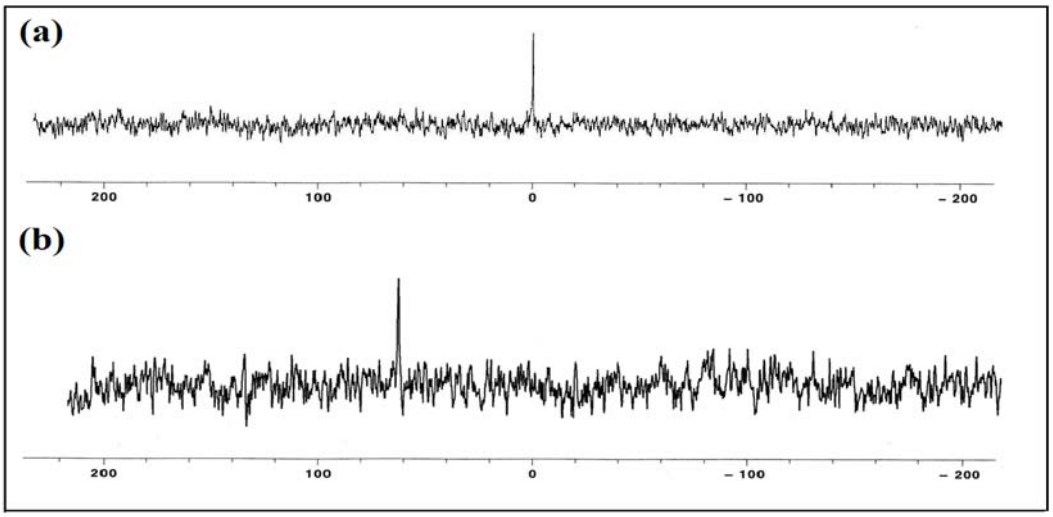

Figure 3.43. (a) ^{89}Y NMR of YCl_3 in D_2O after 32 scans (external reference); (b) ^{89}Y NMR of $Y_3N@D_3$-C_{86} in dichlorobenzene with 30 mg $Cr(acac)_3$ relaxant and 1,2-dichlorobenzene-d_4 lock after 51,920 scans. The chemical shifts for the one line is at δ: 62.65 ppm (all spectra at 25 ºC)

For the empty C_{86} cage, two IPR obeying isomers with C_2 and C_s symmetry have been proved to be stable from experimental and computational studies.[51] The neutral $D_3(19)$-C_{86} has not been separated and characterized so far due to the instability of this isomer, which is consistent with the DFT calculations in Figure 3.44. However, upon accepting six electrons, the HOMO-LUMO gap changes from 1.03 to 2.45 eV. The large HOMO-LUMO gap accounts for the stability of $Y_3N@D_3$-C_{86}.

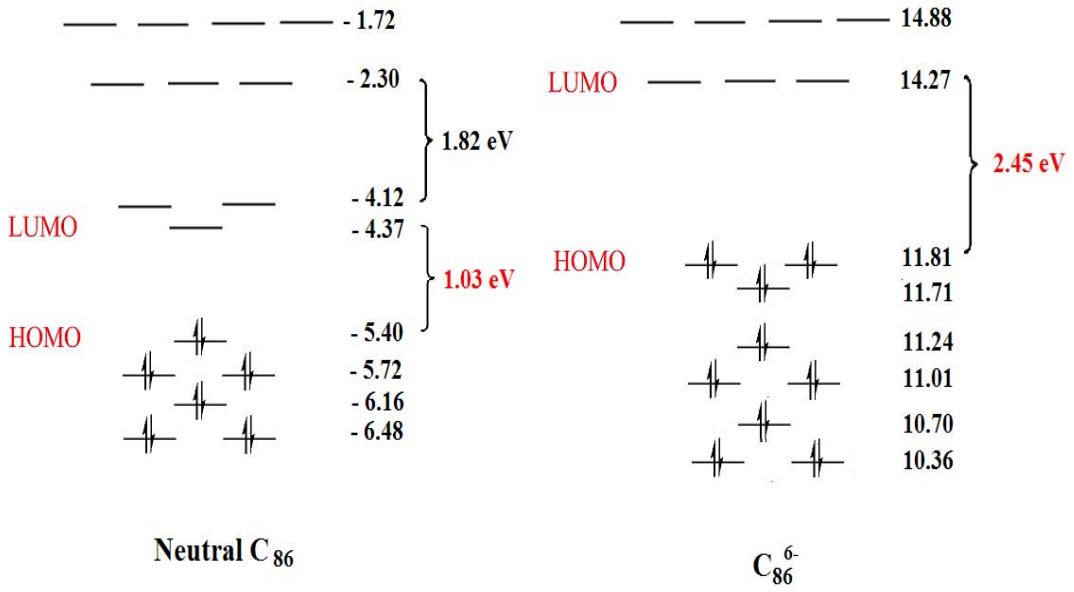

Figure 3.44. Illustration of the stabilization of the neutral $D_3(19)$-C_{86} by accepting six electrons from the Y_3N cluster

3.2.3.4. $Y_3N@C_{88}$:

The C_{88} fullerene has 35 IPR-satisfying isomers. Based on the theoretical calculations, Aihara *et al.* predicted that five isomers **5** (C_{2v}), **7** (C_2), **10** (C_{2v}), **11** (C_1), **17** (C_s), **23** (C_s) and **33** (C_2) are both thermodynamically and kinetically stable.[53] Among 35 isomers of C_{88}，these five isomers are most likely to be experimentally observed and isolated. However, recently a single-crystal X-ray diffraction study

discovered that $Tb_3N@C_{88}$ exhibits D_2 symmetry carbon cage, which is No. 35 of a total 35 IPR isomers of C_{88} in the list of Fowler and Manolopoulos' book.[22] The ^{13}C NMR study suggests that $Y_3N@C_{88}$ has the same structure as $Tb_3N@D_2(35)$-C_{88}. The simulated structure and the UV-Vis spectrum of $Y_3N@D_2(35)$-C_{88} are shown in Figure 3.45 and Figure 3.46.

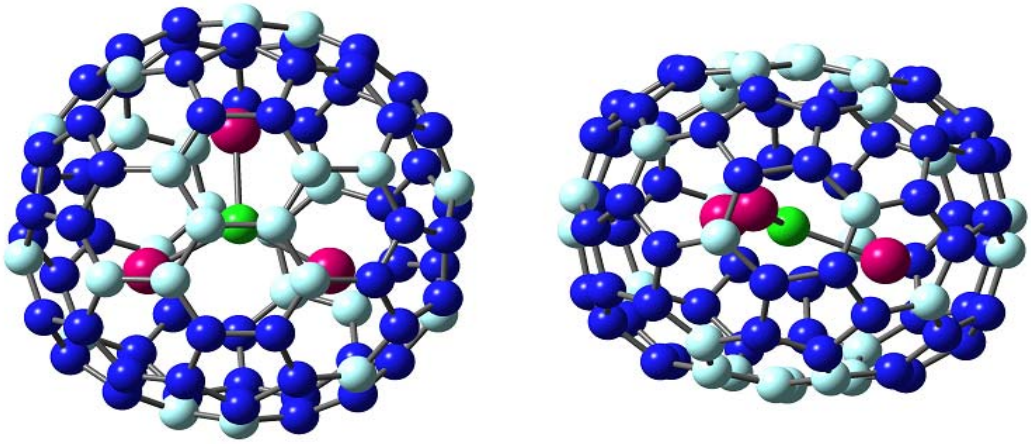

Figure 3.45. Structure of $Y_3N@D_2(35)$-C_{88}

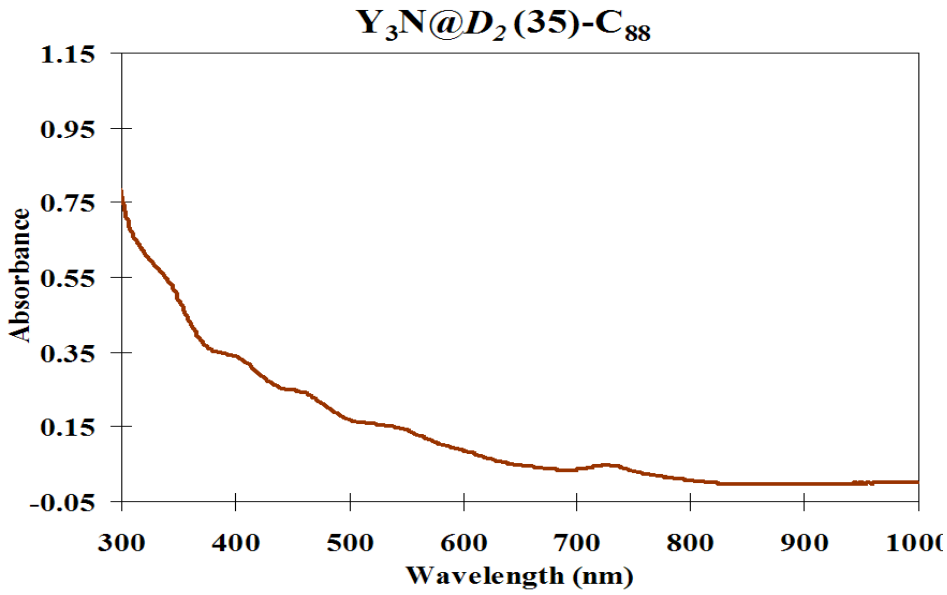

Figure 3.46. UV-Vis spectrum of purified $Y_3N@D_2(35)$-C_{88} in toluene solution

The ^{13}C NMR spectrum (Figure 3.47) for $Y_3N@C_{88}$ exhibits a total of 22 lines (lines at 139.10 and 139.69 ppm, double intensity) with a shift range from 131.0 to

150.0 ppm. In similar fashion to $Y_3N@C_{86}$, an IPR allowed isomer is suggested because of the absence of a ^{13}C NMR signal above 155 ppm. Among 35 IPR allowed C_{88} isomers, two of them (No.1 and 35) have D_2 symmetry (22 × 4 lines) which is consistent with the observed spectrum. One of these isomers, $Tb_3N@D_3(35)$-C_{88} exhibits D_2 symmetry carbon cage as previously determined. This result is completely consistent with the 22 ^{13}C NMR signals observed for $Y_3N@C_{88}$. In addition, no other IPR allowed structure would exhibits fewer than 22 lines except for isomer (34) with *T* symmetry that would exhibit 8 ^{13}C NMR resonances (1×4 and 7×12). All other C_{88} IPR isomers have lower symmetry and would exhibit more than 22 spectral lines.

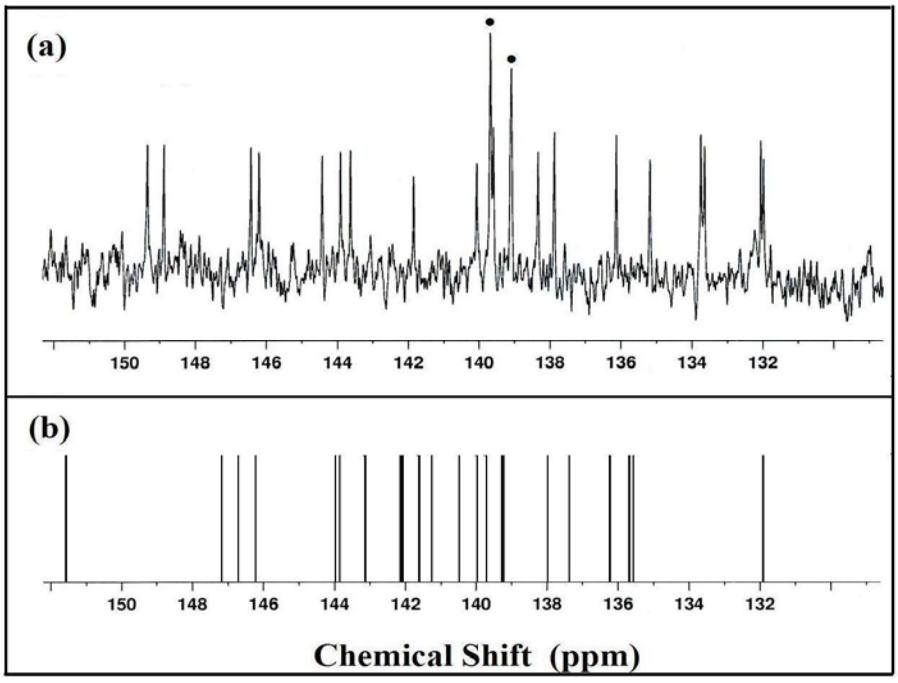

Figure 3.47. (a) ^{13}C NMR spectrum of $Y_3N@D_2$-C_{88} (Cs) in CS_2 with 10 mg $Cr(acac)_3$ relaxant and acetone-d_6 lock after 64000 scan at 25 ºC, 22 × 4 pattern (number of NMR lines x relative intensity). The chemical shifts for the 20 lines are at δ: 149.36, 148.89, 146.44, 146.21, 145.77, 144.44, 143.92, 143.64, 141.89,. 140.07, 139.69 (double intensity), 139.59, 139.10 (douoble intensity), 138.34, 137.88, 136.14, 135.19, 133.76, 133.65, 132.06, 131.99 ppm. The • corresponds to signal with double intensity (b) Theoretical ^{13}C NMR spectrum of $Y_3N@D_2$-C_{88}

Finally, there are 7 pyrene 6,6,6 type carbons that range from 132.0.-137.9 ppm in reasonably good agreement with 7 DFT predicted values ranging from 131.9 -139.2 ppm. The correlation between experimental and computational values is shown in Figure 3.48.

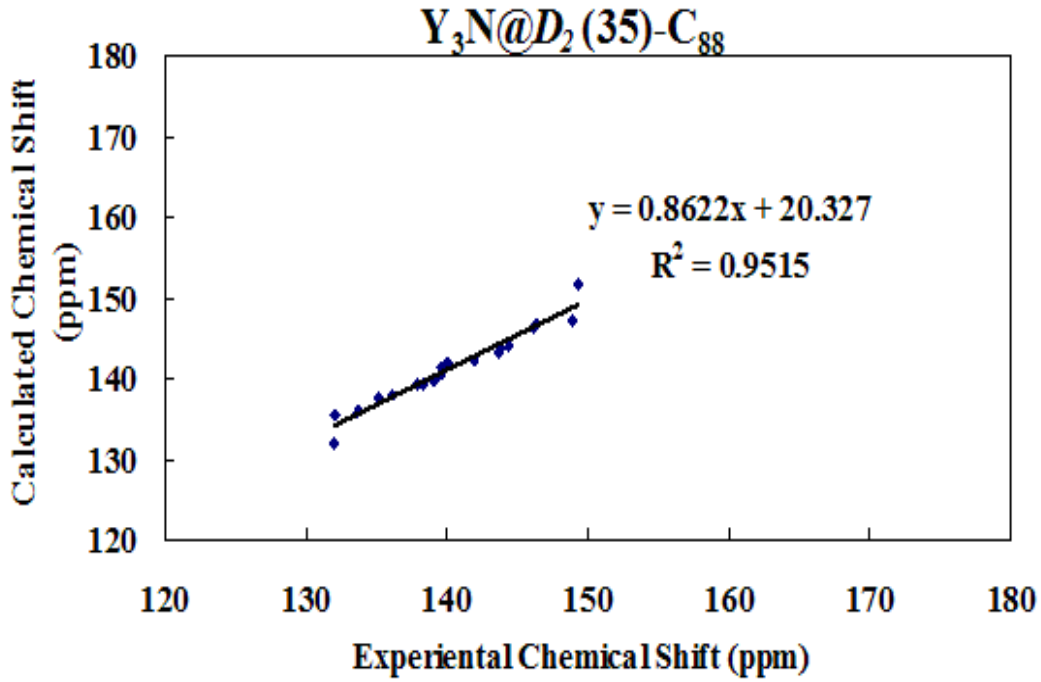

Figure 3.48. Correlation of experimental and computational ^{13}C NMR shift of $Y_3N@D_2(35)$-C_{88}

Figure 3.49 demonstrates the electronic structures of neutral $D_2(35)$-C_{88} and $D_2(35)$-C_{88}^{6-}. It is clear that after accepting six electrons, the small HOMO-LUMO gap of neutral cage becomes significantly larger, which leading to the stability of $Y_3N@D_2(35)$-C_{88}.

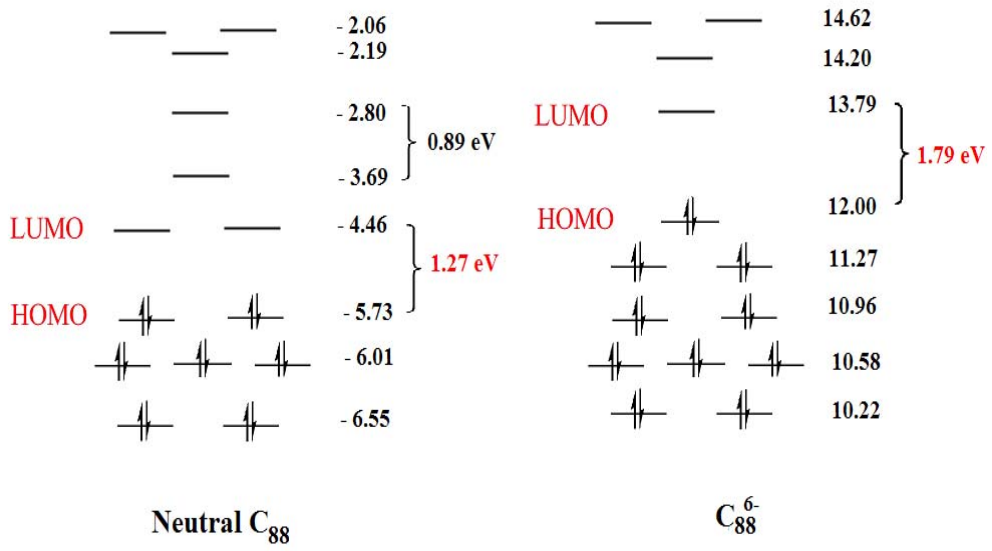

Figure 3.49. Illustration of the stabilization of the neutral *D*$_2$*(35)*-C_{88} by accepting six electrons from Y_3N cluster

3.4. Summary

In summary, a series of yttrium based TNT EMFs have been synthesized, isolated and characterized by HPLC, LD-TOF MS, Uv-Vis, single X-ray crystal study, experimental and computational ^{13}C and ^{89}Y NMR. These structures include $Y_3N@I_h$-C_{80}, $Y_3@D_{5h}$-C_{80}, $Y_3N@C_s$(39663)-C_{82}, $Y_3N@C_s$(51365)-C_{84}, $Y_3N@D_3$(19)-C_{86} and $Y_3N@D_2$(35)-C_{88}.

The first ^{89}Y NMR results have been obtained for $Y_3N@I_h$-C_{80}, $Y_3N@C_s$(51365)-C_{84} and $Y_3N@D_3$-C_{86} and these results suggest that the ^{89}Y NMR shift parameter is very sensitive to subtle changes in the carbon cage. The ^{89}Y and ^{13}C NMR spectrum at ambient temperatures also confirms isotropic motional averaging of the Y_3N cluster inside certain cages cage ($Y_3N@I_h$-C_{80}), but is certainly restricted in other cases, for example, $Y_3N@C_s$(51365)-C_{84}. The $[Y_3N]^{6+}$ motional freedom change

in different fullerene cages is shown in Figure 3.50.

The cage structure of yttrium-based TNT EMFs was determined by ^{13}C NMR. The DFT computational approach provides good agreement with the experimental ^{13}C results. Interestingly, the level of agreement appears to improve for cases where the $[Y_3N]^{6+}$ cluster is more restricted, for example, $Y_3N@C_s(39663)$-C_{82} and $Y_3N@C_s(51365)$-C_{84}. This is supported by the improved correlation between the DFT computational approach and experimental results for the latter restricted systems. This ^{13}C and ^{89}Y NMR study confirms the unique role of the trimetallic nitride $(Y_3N)^{6+}$ cluster template in forming a limited number of high symmetry isomers in the $Y_3N@C_{2n}$ (n=40-44) family.

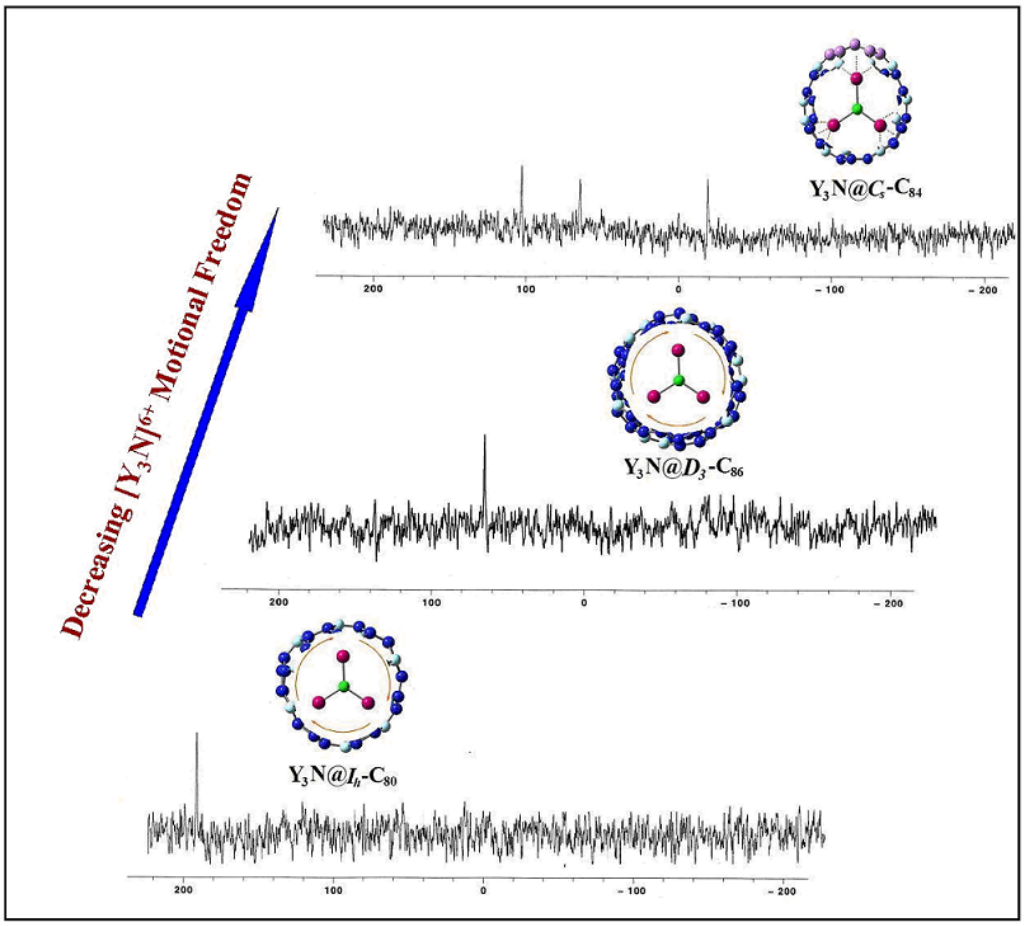

Figure 3.50. Illustration of motional freedom of $(Y_3N)^{6+}$ cluste in different fullerene cages

References:

(1) Shinohara, H., Endohedral metallofullerenes. *Rep. Prog. Phys.* **2000,** *63* (6), 843-892.

(2) Akasaka, T.; Nagase, T.; Eds.; Kluwer Academic Publishers: Dordrecht, T. N., *Endofullerenes: A New Family of Carbon Clusters* **2002**.

(3) Thompson Barry, C.; Frechet Jean, M. J., Polymer-fullerene composite solar cells. *Angew. Chem. Int. Ed.* **2008,** *47* (1), 58-77.

(4) Ross, R. B.; Cardona, C. M.; Guldi, D. M.; Sankaranarayanan, S. G.; Reese, M. O.; Kopidakis, N.; Peet, J.; Walker, B.; Bazan, G. C.; Van Keuren, E.; Holloway, B. C.; Drees, M., Endohedral fullerenes for organic photovoltaic devices. *Nature Mater.* **2009,** *8* (3), 208-212.

(5) Zhang, S. R.; Sun, D. Y.; Li, X. Y.; Pei, F. K.; Liu, S. Y., Synthesis and solvent enhanced relaxation property of water-soluble endohedral metallofullerenols. *Fullerene Sci. Technol.* **1997,** *5* (7), 1635-1643.

(6) Wilson, L. J., Medical Application of Fullerenes and Metallofullerenes. *The Electrochem. Soc. Interface•Winter* **1999**, 24-28.

(7) Wilson, L. J.; Cagle, D. W.; Thrash, T. P.; Kennel, S. J.; Mirzadeh, S.; Alford, J. M.; Ehrhardt, G. J., Metallofullerene drug design. *Coord. Chem. Rev.* **1999,** *192*, 199-207.

(8) Kato, H.; Kanazawa, Y.; Okumura, M.; Taninaka, A.; Yokawa, T.; Shinohara, H., Lanthanoid endohedral metallofullerenols for MRI contrast agents. *J. Am. Chem. Soc.* **2003,** *125* (14), 4391-4397.

(9) Iezzi, E. B.; Duchamp, J. C.; Fletcher, K. R.; Glass, T. E.; Dorn, H. C., Lutetium-based trimetallic nitride endohedral metallofullerenes: New contrast agents. *Nano. Letters* **2002,** *2* (11), 1187-1190.

(10) Shu, C. Y.; Ma, X. Y.; Zhang, J. F.; Corwin, F. D.; Sim, J. H.; Zhang, E. Y.; Dorn, H. C.; Gibson, H. W.; Fatouros, P. P.; Wang, C. R.; Fang, X. H., Conjugation of a water-soluble gadolinium endohedral fulleride with an antibody as a magnetic resonance imaging contrast agent. *Bioconjugate Chem.* **2008,** *19* (3), 651-655.

(11) Shu, C. Y.; Corwin, F. D.; Zhang, J. F.; Chen, Z. J.; Reid, J. E.; Sun, M. H.; Xu, W.; Sim, J. H.; Wang, C. R.; Fatouros, P. P.; Esker, A. R.; Gibson, H. W.; Dorn, H. C., Facile Preparation of a New Gadofullerene-Based Magnetic Resonance Imaging Contrast Agent with High H-1 Relaxivity. *Bioconjugate Chem.* **2009,** *20* (6), 1186-1193.

(12) Stevenson, S.; Rice, G.; Glass, T.; Harich, K.; Cromer, F.; Jordan, M. R.; Craft, J.; Hadju, E.; Bible, R.; Olmstead, M. M.; Maitra, K.; Fisher, A. J.; Balch, A. L.; Dorn, H. C., Small-bandgap endohedral metallofullerenes in high yield and purity. *Nature* **1999,** *401* (6748), 55-57.

(13) Duchamp, J. C.; Demortier, A.; Fletcher, K. R.; Dorn, D.; Iezzi, E. B.; Glass, T.; Dorn, H. C., An isomer of the endohedral metallofullerene $Sc_3N@C_{80}$ with D_{5h} symmetry. *Chem. Phys. Lett.* **2003,** *375* (5-6), 655-659.

(14) Stevenson, S.; Fowler, P. W.; Heine, T.; Duchamp, J. C.; Rice, G.; Glass, T.; Harich, K.; Hajdu, E.; Bible, R.; Dorn, H. C., A stable non-classical metallofullerene family. *Nature* **2000,** *408* (6811), 427-428.

(15) Olmstead, M. M.; Lee, H. M.; Duchamp, J. C.; Stevenson, S.; Marciu, D.; Dorn, H. C.; Balch, A. L., $Sc_3N@C_{68}$: Folded pentalene coordination in an endohedral fullerene that does not obey the isolated pentagon rule. *Angew. Chem. Int. Ed.* **2003,** *42* (8), 900-903.

(16) Olmstead, M. H.; de Bettencourt-Dias, A.; Duchamp, J. C.; Stevenson, S.; Marciu, D.; Dorn, H. C.; Balch, A. L., Isolation and structural characterization of the endohedral fullerene $Sc_3N@C_{78}$. *Angew. Chem. Int. Ed.* **2001,** *40* (7), 1223-1225.

(17) Stevenson, S.; Phillips, J. P.; Reid, J. E.; Olmstead, M. M.; Rath, S. P.; Balch, A. L., Pyramidalization of Gd_3N inside a C_{80} cage. The synthesis and structure of $Gd_3N@C_{80}$. *Chem.Commun.* **2004,** (24), 2814-2815.

(18) Krause, M.; Dunsch, L., Gadolinium nitride Gd_3N in carbon cages: The influence of cluster size and bond strength. *Angew. Chem. Int. Ed.* **2005,** *44* (10), 1557-1560.

(19) Krause, M.; Wong, J.; Dunsch, L., Expanding the world of endohedral fullerenes - The $Tm_3N@C_{2n}$ ($39 <= n <= 43$) clusterfullerene family. *Chem.-Eur. J.* **2005,** *11* (2), 706-711.

(20) Yang, S. F.; Dunsch, L., A large family of dysprosium-based trimetallic nitride endohedral fullerenes: $Dy_3N@C_{2n}$ ($39 <= n <= 44$). *J. Phys. Chem. B* **2005,** *109* (25), 12320-12328.

(21) Beavers, C. M.; Zuo, T.; Duchamp, J. C.; Harich, K.; Dorn, H. C.; Olmstead, M. M.; Balch, A. L., $Tb_3N@C_{84}$: an improbable, egg-shaped endohedral fullerene that violates the isolated Pentagon rule. *J. Am. Chem. Soc.* **2006,** *128* (35), 11352-11353.

(22) Zuo, T. M.; Beavers, C. M.; Duchamp, J. C.; Campbell, A.; Dorn, H. C.; Olmstead, M. M.; Balch, A. L., Isolation and structural characterization of a family of endohedral fullerenes including the large, chiral cage fullerenes $Tb_3N@C_{88}$ and $Tb_3N@C_{86}$ as well as the I_h and D_{5h} isomers of $Tb_3N@C_{80}$. *J. Am. Chem. Soc.* **2007,** *129* (7), 2035-2043.

(23) Melin, F.; Chaur, M. N.; Engmann, S.; Elliott, B.; Kumbhar, A.; Athans, A. J.; Echegoyen, L., The large $Nd_3N@C_{2n}$ ($40 <= n <= 49$) cluster fullerene family: preferential templating of a C_{88} cage by a trimetallic nitride cluster. *Angew. Chem. Int. Ed.* **2007,** *46*, 9032-9035.

(24) Chaur, M. N.; Melin, F.; Elliott, B.; Kumbhar, A.; Athans, A. J.; Echegoyen, L., New $M_3N@C_{2n}$ endohedral metallofullerene families (M = Nd, Pr, Ce; n=40-53): Expanding the preferential templating of the C_{88} cage and approaching the C_{96} cage. *Chem.-Eur. J.* **2008,** *14* (15), 4594-4599.

(25) Chaur, M. N.; Melin, F.; Ashby, J.; Elliott, B.; Kumbhar, A.; Rao, A. M.; Echegoyen, L., Lanthanum Nitride Endohedral Fullerenes $La_3N@C_{2n}$ ($43 <= n <= 55$): Preferential Formation of $La_3N@C_{96}$. *Chem.-Eur. J.* **2008,** *14* (27), 8213-8219.

(26) Yang, C. Y.; Hu, J. G.; Heeger, A. J., Molecular structure and dynamics at the interfaces within bulk heterojunction materials for solar cells. *J. Am. Chem. Soc.* **2006,** *128* (36), 12007-12013.

(27) Stevenson, S.; Lee, H. M.; Olmstead, M. M.; Kozikowski, C.; Stevenson, P.; Balch, A. L., Preparation and crystallographic characterization of a new endohedral, $Lu_3N@C_{80}$·5(o-xylene), and comparison with $Sc_3N@C_{80}$·5(o-xylene). *Chem.-Eur. J.* **2002,** *8* (19), 4528-4535.

(28) Zuo, T. M.; Olmstead, M. M.; Beavers, C. M.; Balch, A. L.; Wang, G. B.; Yee, G. T.; Shu, C. Y.; Xu, L. S.; Elliott, B.; Echegoyen, L.; Duchamp, J. C.; Dorn, H. C., Preparation and structural characterization of the I_h and the D_{5h} isomers of the endohedral fullerenes $Tm_3N@C_{80}$: Icosahedral C_{80} cage encapsulation of a trimetallic nitride magnetic cluster with three uncoupled Tm^{3+} ions. *Inorg. Chem.* **2008,** *47* (12), 5234-5244.

(29) Mercado, B. Q.; Beavers, C. M.; Olmstead, M. M.; Chaur, M. N.; Walker, K.; Holloway, B. C.; Echegoyen, L.; Balch, A. L., Is the isolated pentagon rule merely a suggestion for endohedral fullerenes? The structure of a second egg-shaped endohedral fullerene-$Gd_3N@C_s$(39663)-C_{82}. *J. Am. Chem. Soc.* **2008,** *130* (25), 7854-7855.

(30) Zuo, T.; Walker, K.; Olmstead, M. M.; Melin, F.; Holloway, B. C.; Echegoyen, L.; Dorn, H. C.; Chaur, M. N.; Chancellor, C. J.; Beavers, C. M.; Balch, A. L.; Athans, A. J., New egg-shaped fullerenes: non-isolated pentagon structures of $Tm_3N@C_s$(51365)-C_{84} and $Gd_3N@C_s$(51365)-C_{84}. *Chem. Commun.* **2008,** (9), 1067-1069.

(31) Diederich, F.; Whetten, R. L., Beyond C_{60} - the Higher Fullerenes. *Accounts Chem. Res.* **1992,** *25* (3), 119-126.

(32) Johnson, R. D.; Meijer, G.; Bethune, D. S., C_{60} Has Icosahedral Symmetry. *J. Am. Chem. Soc.* **1990,** *112* (24), 8983-8984.

(33) Ajie, H.; Alvarez, M. M.; Anz, S. J.; Beck, R. D.; Diederich, F.; Fostiropoulos, K.; Huffman, D. R.; Kratschmer, W.; Rubin, Y.; Schriver, K. E.; Sensharma, D.; Whetten, R. L., Characterization of the Soluble All-Carbon Molecules C_{60} and C_{70}. *J. Phys. Chem.* **1990,** *94* (24), 8630-8633.

(34) Fu, W. J.; Xu, L. S.; Azurmendi, H.; Ge, J. C.; Furher, T.; Zuo, T. M.; Reid, J.; Shu, C. Y.; Harich, K.; Dorn, H. C., ^{89}Y and ^{13}C NMR Cluster and Carbon Cage Studies of an Yttrium Metallofullerene Family, $Y_3N@C_{2n}$ (n = 40-43). *J. Am. Chem. Soc.* **2009,** *131* (33), 11762-11769.

(35) Merritt, M. E.; Harrison, C.; Kovacs, Z.; Kshirsagar, P.; Malloy, C. R.; Sherry, A. D., Hyperpolarized ^{89}Y offers the potential of direct imaging of metal ions in biological systems by magnetic resonance. *J. Am. Chem. Soc.* **2007,** *129* (43), 12942-12943.

(36) Ge, Z. X.; Duchamp, J. C.; Cai, T.; Gibson, H. W.; Dorn, H. C., Purification of endohedral trimetallic nitride fullerenes in a single, facile step. *J. Am. Chem. Soc.* **2005,** *127* (46), 16292-16298.

(37) Frisch, M. J.; Trucks, G. W.; Schlegel, H. B.; Scuseria, G. E.; Robb, M. A.; Cheeseman, J. R.; Montgomery, J. A.; Vreven, Jr., T.; Kudin, K. N.; Burant, J.

C.; Millam, J. M.; Iyengar, S. S.; Tomasi, J.; Barone, V.; Mennucci, B.; Cossi, M.; Scalmani, G.; Rega, N.; Petersson, G. A.; Nakatsuji, H.; Hada, M.; Ehara, M.; Toyota, K.; Fukuda, R.; Hasegawa, J.; Ishida, M.; Nakajima, T.; Honda, Y.; Kitao, O.; Nakai, H.; Klene, M.; Li, X. ; Knox, J. E.; Hratchian, H. P.;. Cross, J. B; Adamo, C.; Jaramillo, J.; Gomperts, R.; Stratmann, R. E.; Yazyev, O.; Austin, A. J.; Cammi, R.; Pomelli, C.; Ochterski, J. W.; Ayala, P. Y. ; Morokuma, K.; Voth, G. A.; Salvador, P.; Dannenberg, J. J.; Zakrzewski, V. G.; Dapprich, S.; Daniels, A. D.; Strain, M. C.; Farkas, O.; Malick, D. K.; Rabuck, A. D.; Raghavachari, K.; Foresman, J. B.; Ortiz, J. V.; Cui, Q.; Baboul, A. G.; Clifford, S.; Cioslowski, J; Stefanov, B. B.; Liu, G.; Liashenko, A ; Piskorz, P.; Komaromi, I.; Martin, R. L.; Fox, D. J.; Keith, T.; Al-Laham, M. A.; Peng, C. Y.; Nanayakkara, A.; Challacombe, M.; Gill, P. M. W.; Johnson, B.; Chen, W.; Wong, M. W.; Gonzalez, C.; and Pople, J. A.; Gaussian, Inc.: Wallingford, CT, 2004.

(38) Zuo, T. M.; Xu, L. S.; Beavers, C. M.; Olmstead, M. M.; Fu, W. J.; Crawford, D.; Balch, A. L.; Dorn, H. C., $M_2@C_{79}N$ (M = Y, Tb): Isolation and characterization of stable endohedral metallofullerenes exhibiting M-M bonding interactions inside aza[80]fullerene cages. *J. Am. Chem. Soc.* **2008,** *130* (39), 12992-12997.

(39) Yang, S. F.; Popov, A. A.; Dunsch, L., Carbon Pyramidalization in Fullerene Cages Induced by the Endohedral Cluster: Non-Scandium Mixed Metal Nitride Clusterfullerenes. *Angew. Chem. Int. Ed.* **2008,** *47* (43), 8196-8200.

(40) Wang, X.; Zuo, T.; Olmstead, M. M.; Duchamp, J. C.; Glass, T. E.; Cromer, F.; Balch, A. L.; Dorn, H. C., Preparation and structure of $CeSc_2N@C_{80}$: an icosahedral carbon cage enclosing an acentric $CeSc_2N$ unit with buried f electron spin. *J. Am. Chem. Soc.* **2006,** *128* (27), 8884-9.

(41) Shannon, R. D., Revised Effective Ionic-Radii and Systematic Studies of Interatomic Distances in Halides and Chalcogenides. *Acta Crystallogr. Sect. A* **1976,** *32*, 751-767.

(42) Campanera, J. M.; Bo, C.; Poblet, J. M., General rule for the stabilization of fullerene cages encapsulating trimetallic nitride templates. *Angew. Chem. Int. Ed.* **2005,** *44* (44), 7230-7233.

(43) Popov, A. A.; Dunsch, L., Structure, stability, and cluster-cage interactions in nitride clusterfullerenes $M_3N@C_{2n}$ (M = Sc, Y; 2n=68-98): a density functional theory study. *J. Am. Chem. Soc.* **2007,** *129* (38), 11835-11849.

(44) Fowler, P. W.; Manolopoulos, D. E., *An Atlas of fullerenes*. Oxford University: New York: 1995.

(45) Feng, L.; Wakahara, T.; Tsuchiya, T.; Maeda, Y.; Lian, Y. F.; Akasaka, T.; Mizorogi, N.; Kobayashi, K.; Nagase, S.; Kadish, K. M., Structural characterization of $Y@C_{82}$. *Chem. Phys. Lett.* **2005,** *405* (4-6), 274-277.

(46) Olmstead, M. M.; de Bettencourt-Dias, A.; Stevenson, S.; Dorn, H. C.; Balch, A. L., Crystallographic characterization of the structure of the endohedral fullerene [$Er_2@C_{82}$ isomer I] with C_s cage symmetry and multiple sites for erbium along a band of ten contiguous hexagons. *J. Am. Chem. Soc.* **2002,** *124* (16), 4172-4173.

(47) Olmstead, M. M.; Lee, H. M.; Stevenson, S.; Dorn, H. C.; Balch, A. L., Crystallographic characterization of Isomer 2 of $Er_2@C_{82}$ and comparison with Isomer 1 of $Er_2@C_{82}$. *Chem. Commun.* **2002,** (22), 2688-2689.

(48) Fuchs, D.; Rietschel, H.; Michel, R. H.; Fischer, A.; Weis, P.; Kappes, M. M., Extraction and chromatographic elution behavior of endohedral metallofullerenes: Inferences regarding effective dipole moments. *J. Phys. Chem.* **1996,** *100*(2), 725-729.

(49) White, R. E.; Hanusa, T. P., Prediction of ^{89}Y NMR chemical shifts in organometallic complexes with density functional theory. *Organometallics* **2006,** *25* (23), 5621-5630.

(50) Sun, G. Y.; Kertesz, M., Isomer identification for fullerene C_{84} by ^{13}C NMR spectrum: A density-functional theory study. *J. Phys. Chem. A* **2001,** *105* (21), 5212-5220.

(51) Miyake, Y.; Minami, T.; Kikuchi, K.; Kainosho, M.; Achiba, Y., Trends in structure and growth of higher fullerenes isomer structure of C_{86} and C_{88}. *Mol. Cryst. Liq. Cryst.* **2000,** *340*, 553-558.

(52) Kiuchi, M.; Aihara, J., Localization energies and kinetic stability of C_{86} fullerene isomers. *Theochem-J. Mol. Struct.* **2004,** *685* (1-3), 97-100.

(53) Watanabe, M.; Ishimaru, D.; Mizorogi, N.; Kiuchi, M.; Aihara, J., Thermodynamically and kinetically stable isomers of the C_{88} and C_{90} fullerenes. *Theochem.-J. Mol. Struct.* **2005,** *726* (1-3), 11-16.

Chapter 4

Preparation, Separation and Characterization Yttrium based *Di*-metallic EMFs

4.1. Introduction

Endohedral metallofullerenes (EMFs) have attracted special interest during the past decade not only for their unique electronic and structural novelty,[1, 2] but also for their potential applications as MRI contrast agents[3-9] and photovoltaic devices.[10, 11] Endohedrals encapsulated in the fullerene cages include metal atoms,[12-14] metal clusters,[15, 16] metal nitride clusters[17-19] and metal-carbide clusters.[20-26] In particular, *di*-metallic EMFs, M_2C_{2n} have been studied widely during recent years.

Members of the M_2C_{2n} family may exist as the traditional EMFs, $M_2@C_{2n}$ or as the metal-carbide EMFs, $M_2C_2@C_{2n-2}$. A number of traditional EMFs, $M_2@C_{2n}$, have been purified and well characterized, such as $Er_2@C_s$-C_{82},[27] $Er_2@C_{3v}$-C_{82}[28] and $M_2@D_2$-C_{72} (M=La or Ce).[16, 29] The first metal-carbide EMF, $Sc_2C_2@C_{84}$ was previously reported as $Sc_2@C_{86}$.[30] The ^{13}C NMR and synchrotron X-ray structural analyses determined the endohedral characters of Sc_2C_2 unit inside a D_{2d}-C_{84} cage.[20] Soon after, a number of metal carbide EMFs, for example, $Ti_2C_2@D_{3h}$-C_{78},[21] $Y_2C_2@C_{82}$ with three geometries (C_s, C_{2v} and C_{3v}),[22] $Sc_3C_2@I_h$-C_{80},[23] $Sc_2C_2@C_{2v}$-C_{68}[24] were separated and structurally characterized. More recently, Liu and Balch reported a series of *di*-gadolinium endohedrals (Gd_2C_{90}-Gd_2C_{124}) and the single-crystal X-ray analysis of

one member of this series - $Gd_2C_2@D_3(85)$-C_{92}.[25]

For the metal-carbide EMFs, the crystallographic data and theoretical calculation suggested that the M_2C_2 unit within the carbon cage display a butterfly shape with the C_2 unit perpendicular to a line between the two metal atoms.[25] Poblet and co-workers suggested the electronic structure of metal carbide EMFs as $[M_2C_2]^{4+}@[C_{2n}]^{4-}$.[31] In this model, the encapsulated metal ions stay in their usual M^{3+} state and carbide C_2 exits as an acetylide ion, C_2^{2-}. As a result, four electrons transfer from M_2C_2 to a carbon cage and fill the LUMO-1 and/or LUMO-2 orbitals of the empty cage fullerenes. Attempts to detect the ^{13}C chemical shifts of the carbide were not successful until Nagase *et al.* reported the ^{13}C chemical shifts of the carbide of $Sc_2C_2@C_{3v}$-C_{82}, $Sc_2C_2@D_{2d}$-C_{84} and $Sc_3C_2@I_h$-C_{80} by using ^{13}C-enriched samples.[26]

Herein, we present the first preparation, separation and characterization of two *di*-yttrium EMFs and distinguish one of them is that a metal-carbide based EMF, $Y_2C_2@C_{92}$. The carbide in the C_{92} cage was successfully detected by ^{13}C NMR spectroscopy. Scalar $J_{Y\text{-}C}$ coupling between two magnetically equivalent yttrium atoms and the carbide was observed, which could lead to interesting studies of the electronic and magnetic properties of metal-carbide clusters inside the fullerene cage.

4.2. Experimental Section and Calculation

Preparation and separation: Two *di*-yttrium EMFs were prepared in a Krätschmer-Huffman generator described in Chapter 3. The hollow graphite rod was packed with the mixture of the Y_2O_3, graphite powder and metallic Cu with a weight

ratio of 1.1:1.0:2.1 and vaporized in a dynamic flow of He and N_2 (flow rate ratio of N_2/H_2=3:100). The resulting soot was then extracted with refluxing toluene and the soot extract was applied to the CPDE-MPR column for a chemical reactivity separation.[32] The eluent was further separated by two-stage HPLC.

Characterization of the Y_2C_{2n}: Mass spectrometry was performed on a Kratos Analytical Kompact SEQ LD-TOF mass spectrometer. The 150 MHz ^{13}C measurement of Y_2C_{90} was performed on a Bruker Avance spectrometer (600 MHz, ^1H). The 200 MHz ^{13}C measurement of the Y_2C_{94} was performed on a Bruker Avance spectrometer (800 MHz, ^1H) at 25 ºC. The samples were dissolved in carbon disulfide with chromium tris(acetylacetonate, $Cr(acac)_3$) as the relaxation agent and acetone-d_6 as an internal lock. Cyclic voltammetric measurements were conducted using a CH Instruments model 600A potentiostat (Austin, TX) and a single compartment microelectrochemical cell. A 2 mm glassy carbon disk electrode along with a Pt auxiliary was applied as working electrode using Ag/AgCl as a reference. Measurements were performed using *o*-dichlorobenzene solutions containing 0.100 M tetra-*n*-butylamonium tetrafluoroborate. Potentials are reported relative to the reversible ferrocene oxidation couple.

Computational Studies: DFT computations were performed using the Gaussian 03 program package.[33, 34] All molecules were geometry optimized using the UB3LYP/DZVP level for yttrium and the UB3LYP/6-31G* level for carbon and nitrogen atoms.[35] DFT energy optimized values were obtained starting from the X-ray crystallographic structures of the corresponding $Gd_2C_2@D_3(85)$-C_{92}.[25] The energy

minimized values and the same level of theory were used to calculate all ^{13}C NMR chemical shifts. Gaussian 03 keyword "opt" was used for the optimized structure and "opt=TS" was used for the transition state structure. Tim Fuhrer in Dorn's group kindly collaborated on the calculation work.

4.3. Results and Discussion

4.3.1. Preparation and Separation

The *di*-metallic EMF samples were prepared by the traditional Krätschmer-Huffman method described in the experimental section. To reiterate briefly, Y_2O_3, graphite powder and metallic Cu was packed in the hollow graphite rod. The packed graphite rods were vaporized in a dynamic flow of He and N_2. The resulting soot was then extracted in a Soxhlet extractor with refluxing toluene. The extract was applied to the cyclopentadiene-functionized Merrifield resin (CPDE-MPR) column.[32] After chemical separation, most of the empty cages and reactive EMFs are retained on the CPDE-MPR column. The eluent was further separated by two-stage HPLC. The first stage was carried out utilizing a PBB column (4.6 × 250 mm) and the second stage employed a PYE column (10 × 250 mm). The first stage HPLC chromatogram is shown in Figure 4.1.

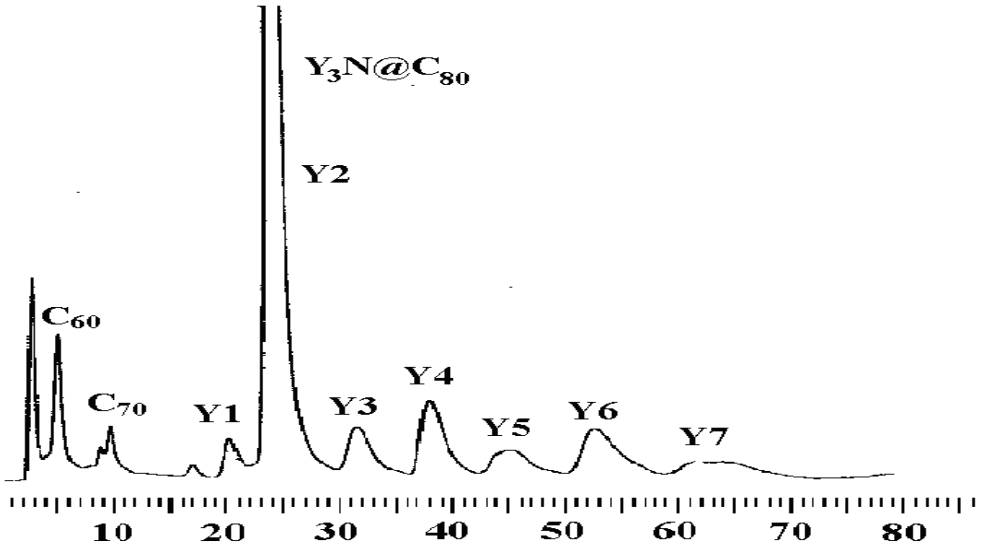

Figure 4.1. HPLC chromatogram of the eluent from CPDE-MPR column (4.6 × 250 mm PBB column; λ=390 nm; flow rate 2.0 mL/min; toluene as eluent; 25 ºC)

As we discussed in Chapter 3, there are seven fractions from Y1 to Y7 in the PBB column. Fraction Y5 contained $Y_3N@C_{86}$ and Y_2C_{90}. Fraction Y7 contained Y_2C_{94}. Fraction Y5 and Y7 were collected and further separated using a 5PYE column.

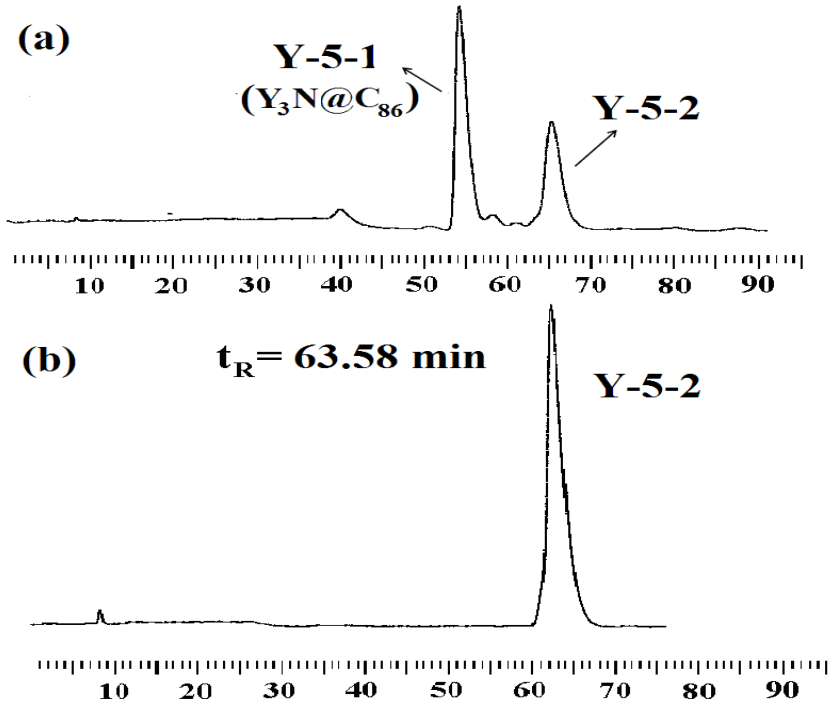

Figure 4.2. (a) HPLC chromatogram of fraction Y-5 in the first cycling process on a PYE column, (b) HPLC chromatogram of purified Y-5-2 on a PYE column, (10 × 250 mm PYE column; λ=390 nm; flow rate 2.0 mL/min; toluene as eluent; 25 ºC)

$Y_3N@C_{86}$ was easily separated from Y_2C_{90} since their retention times on a PYE column were so different (Figure 4.2a). The HPLC chromatogram of the pure Y_2C_{90} is shown in Figure 4.2b. The Y7 fraction contains mainly three peaks as illustrated on a PYE column, as shown in Figure 3a. We collected and purified the first two peaks, Y-7-1 and Y-7-2. The purity of these two fractions was confirmed by HPLC (Figure 4.3b and 4.3c).

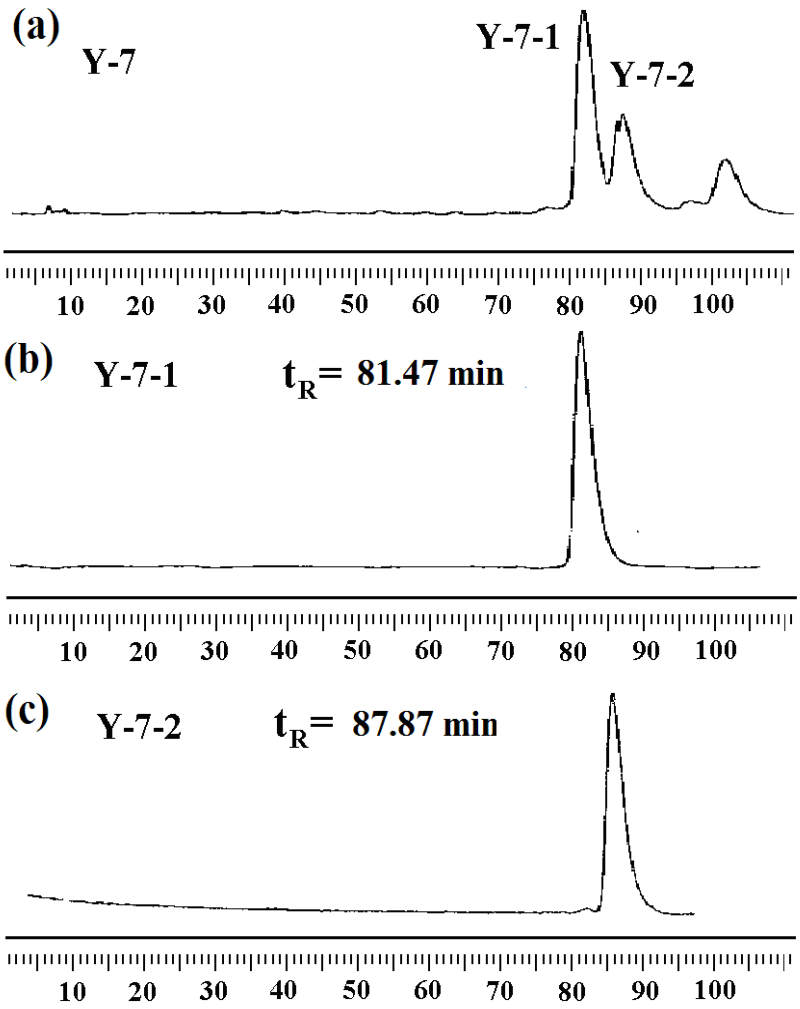

Figure 4.3. (a) HPLC chromatogram of fraction Y-7 in the first cycling process on a PYE column, (b) HPLC chromatogram of purified Y-7-1 on a PYE column, (c) HPLC chromatogram of purified Y-7-2 on a PYE column (10 x 250 mm PYE column; λ=390 nm; flow rate 2.0 mL/min; toluene as eluent; 25 ºC)

4.3.2. Characterization

4.3.2.1. Y_2C_{90}

The LD-TOF mass spectrum of the purified Y-5-2 fraction is shown in Figure 4.4. The peak at m/z=1258 suggests the production of Y_2C_{90}. Furthermore, the measured isotope distribution agrees well with the theoretical isotopic pattern of Y_2C_{90}. The UV-Vis of Y_2C_{90} in toluene is shown in Figure 4.5.

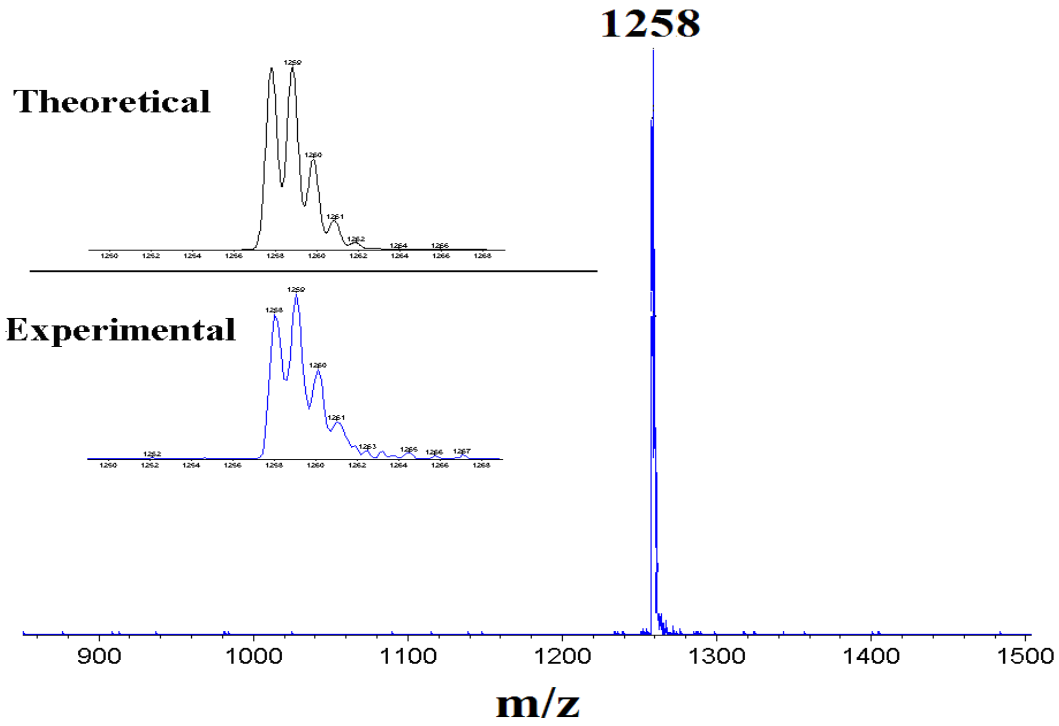

Figure 4.4. The LD-TOF mass spectrum of Y_2C_{90} with positive ionization

The structure of Y_2C_{90} needed to be further characterized by ^{13}C NMR or single-crystal X-ray analysis. We performed the ^{13}C NMR study, as shown in Figure 4.6. The ^{13}C chemical shift region is from 120 to 160 ppm, which is consistent with regular fullerenes. However, the structure of Y_2C_{90} cannot be assigned only based on this ^{13}C NMR study because of the featureless spectrum. The poor spectrum is possibly due to the following reasons: 1) the limited amount of sample; 2) low symmetry of Y_2C_{90}; 3)

possible multiple isomers for Y_2C_{90}. We are trying to get a single crystal of Y_2C_{90} for future X-ray analysis.

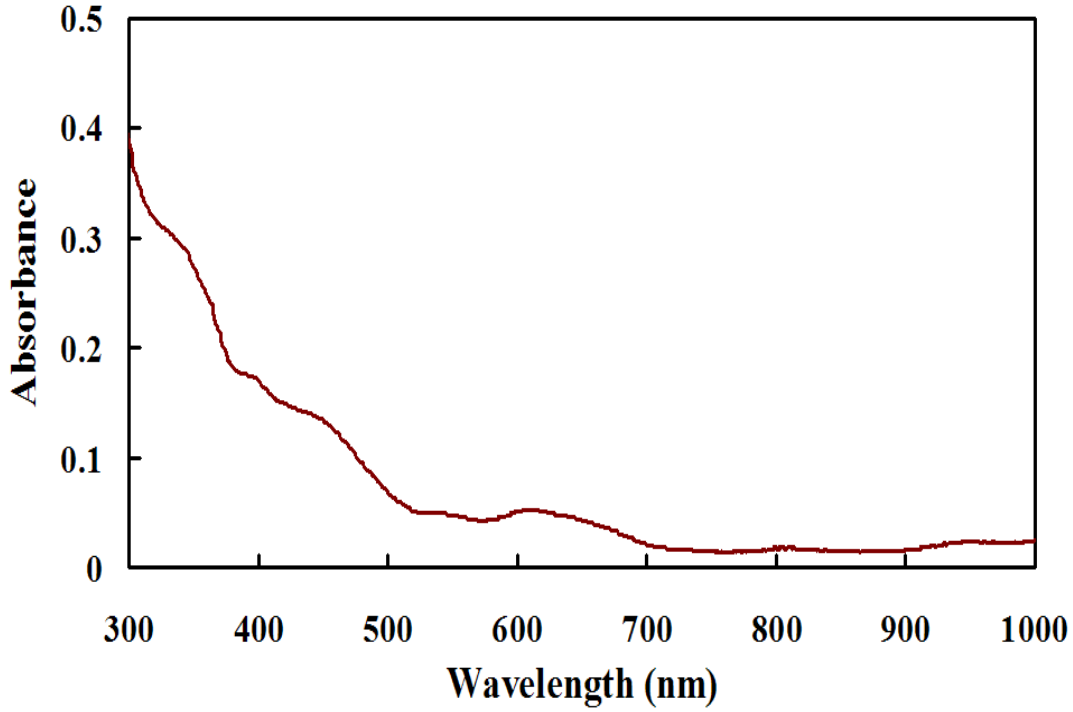

Figure 4.5. UV-Vis spectrum of purified Y_2C_{90} in toluene solution

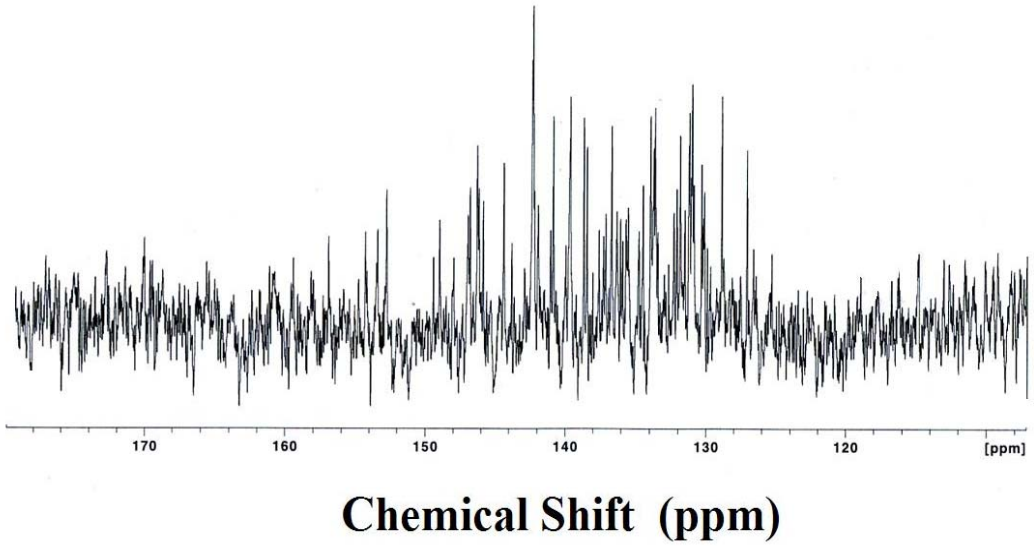

Figure 4.6. ^{13}C NMR spectrum of Y_2C_{90} in CS_2 with 5 mg $Cr(acac)_3$ relaxant and acetone-d_6 lock after 64, 000 scans

4.3.2.2. Y_2C_{94}

The LD-TOF mass spectrum of Y-7-1 is shown in Figure 4.7. The m/z =1307 peak indicates the component of Y-7-1 is Y_2C_{94}. The Y-7-2 peak has the same the mass with the Y-7-1, suggesting these two fractions are different isomers of Y_2C_{94}. The UV-Vis of Y-7-1 fraction is shown in Figure 8.

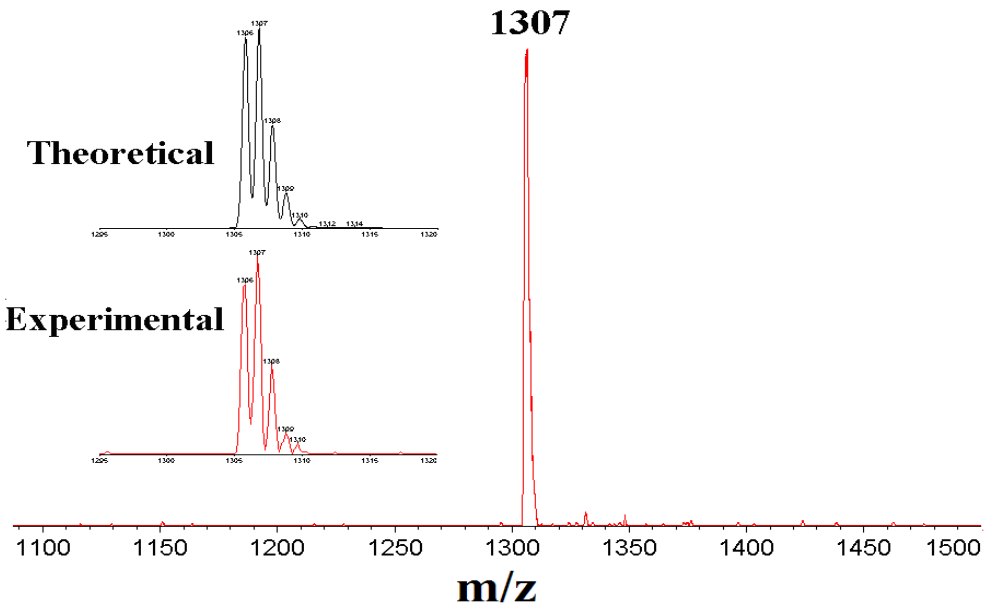

Figure 4.7. The LD-TOF Mass spectrum of Y-7-1 with positive ionization

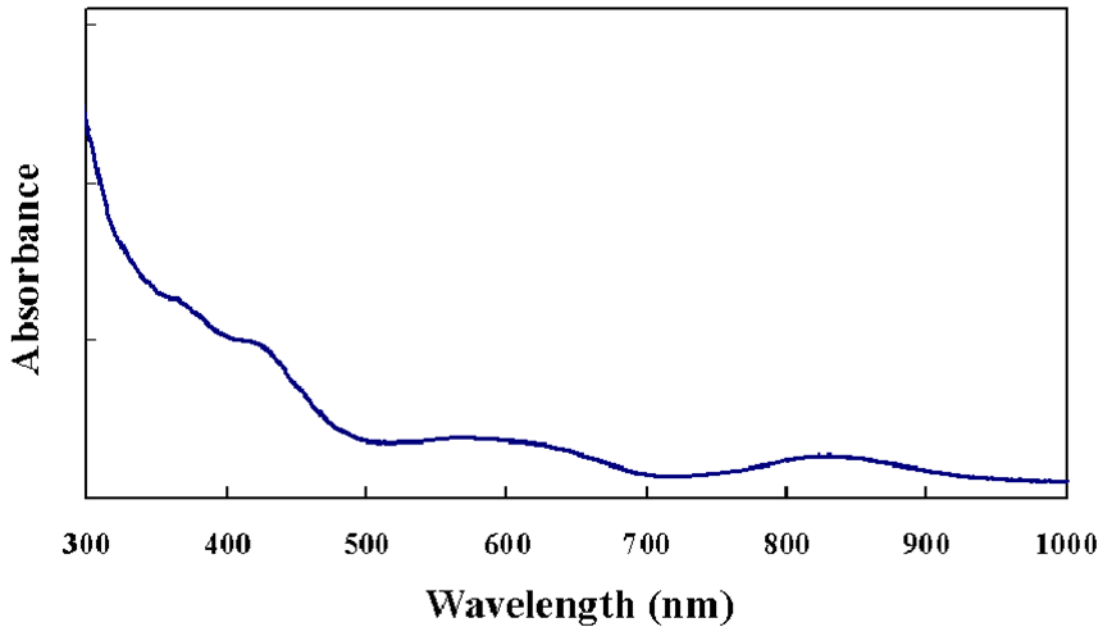

Figure 4.8. UV-Vis spectrum of purified Y-7-1 in toluene solution

The ^{13}C NMR spectrum of purified Y-7-1 fraction in CS_2 solution at room temperature consists of a series of 15 distinct lines between δ =128 to 152 ppm (Figure 4.9). There are 1 double intensity, 13 full intensity and one 1/3 intensity signals, indicating a 15 × 6, 1 × 2 (number of NMR lines × relative intensity) pattern. With respect to the structure of Y_2C_{94}, we considered the simple endohedral $Y_2@C_{94}$ first. However, of the 134 IPR-satisfying and 153,494 non-IPR C_{94} isomers,[36] none match the present ^{13}C NMR spectral pattern. Instead, the observed ^{13}C NMR pattern is consistent with the ^{13}C NMR pattern of a C_{92} cage with D_3 symmetry, suggesting that Y_2C_{94} are metal-carbide endohedral fullerenes, in which a Y_2C_2 cluster is encapsulated by the C_{92} cage. There are five C_{92}-D_3 isomers (i.e., #28, #71, #78, #83, #85) in the 86 IPR-satisfying isomers of C_{92} which can produce the 15×6, 1×2 pattern in ^{13}C NMR spectrum.[36] We suggest the Y_2C_{94} is $Y_2C_2@D_3(85)$-C_{92} by considering the previously reported $Gd_2C_2@D_3(85)$-C_{92} structure.[25]

The theoretical range of ^{13}C NMR chemical shift, 129.47 to 153.15 ppm, is in good agreement with the range of the experimental spectrum, 128.97 to 151.69 ppm. The chemical shift of the C_3 axis carbon, 141.20 ppm (labeled as **11**), is not consistent with regular corannulene-type 6,6,6 carbon shifts, which should be within 130-139 ppm. However, our calculated result (140.31 ppm) agrees with the experimental result very well. This unusual chemical shift may be due to the two Yttrium atoms which are spatially located over the C_3 axis carbon. The experimental and computational values match well, as shown in the correlation between them in Figure 4.10.

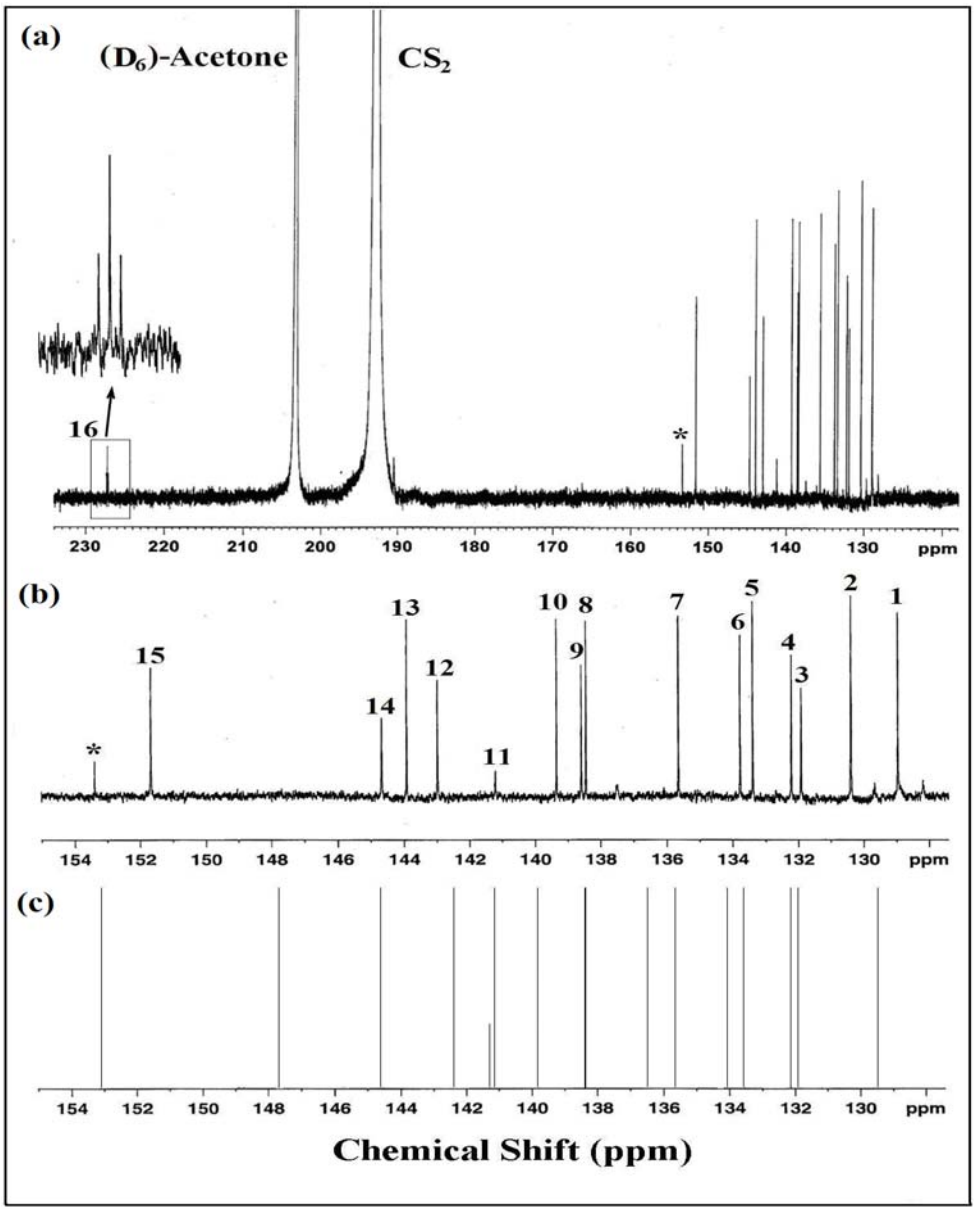

Figure 4.9. 800MHz ^{13}C NMR spectrum of $Y_2C_2@D_3(85)$-C_{92} in CS_2 with 10 mg $Cr(acac)_3$ relaxant and acetone-d_6 lock after 32,768 scan at 25 ºC. The chemical shifts for the sixteen lines are at δ: 227.26 (1/3 intensity), 151.69, 144.67, 143.92, 142.99, 141.20 (1/3 intensity), 139.38, 138.59, 138.45, 135.67, 133.78, 133.42, 132.23, 131.93, 130.40 (double intensity), 128.97 ppm. (a) The whole range of ^{13}C NMR spectrum of $Y_2C_2@D_3(85)$-C_{92} (b) Expand range (from 128 to 154 ppm) of ^{13}C NMR spectrum of $Y_2C_2@D_3(85)$-C_{92}. The signal marked with * is assigned to impurities because of its unreasonable chemical shifts; we didn't see this signal in 600 MHz ^{13}C NMR. (c) Calculated ^{13} C NMR spectrum of $Y_2C_2@D_3(85)$-C_{92}

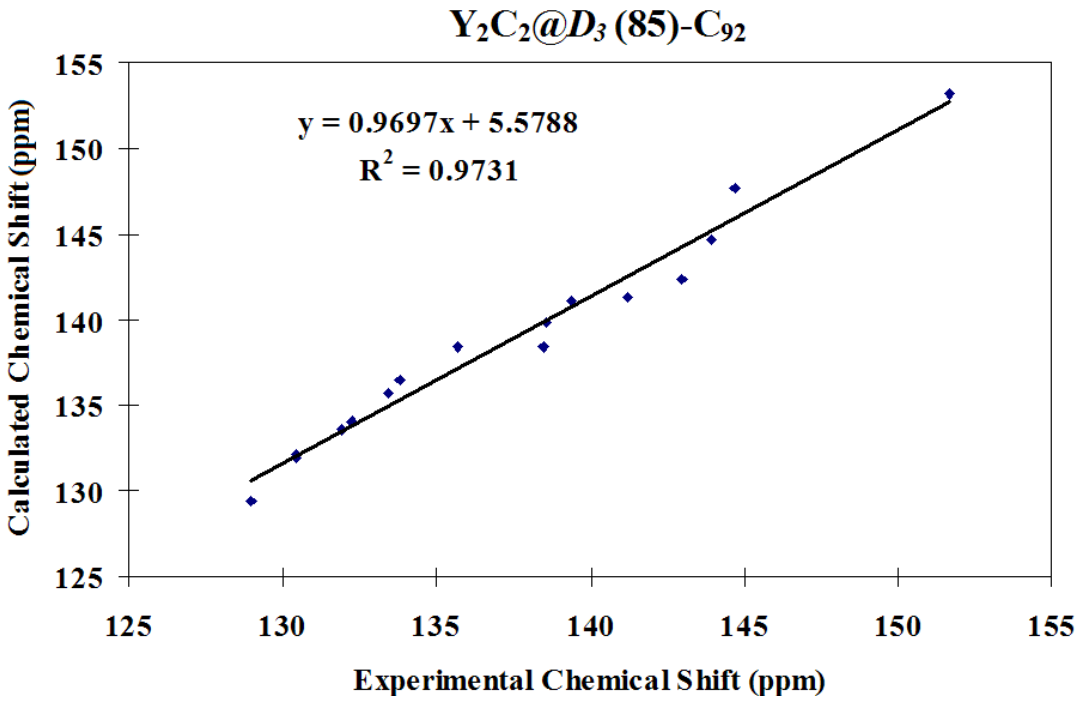

Figure 4.10. Correlation of experimental and computational ^{13}C NMR shift of $Y_2C_2@D_3(85)$-C_{92}

One highly deshielded signal was detected at chemical shift δ = 227.3 ppm in the both proton-decoupled and proton-coupled modes, which suggests that it originates from a quaternary carbon atom. This signal is due to the carbide in $Y_2C_2@D_3(85)$-C_{92}, which is consistent with Nagase's results.[26] Clair *et al.*[37] reported a ^{13}C NMR study of the scandium acetylide compound, Cp_2*ScC ≡ CScCp$_2$* (Cp*=pentamethylcyclopentadienyl). The chemical shift for the acetylenic carbon is also at relatively low field (δ = 178.4 ppm). The unusual deshielding of the carbide unit in the fullerene could be related to the positive charge of the Y atom and dianion character of the carbide within the cage. The average of the two calculated values, 189.27 ppm, is consistent with the deshielding trend of the carbide inside the C_{92} cage. An interesting triplet with 1:2:1 pattern (Figure 4.9) was observed because the two magnetically equivalent yttrium atoms are coupled to the carbide carbons. The $J_{Y\text{-}C}$

coupling of 25 Hz is consistent with previously reported values.[38] Since there is no direct covalent bonding between yttrium and carbon, the coupling is more interesting. To our best knowledge, this is the first observation of coupling between metallic atoms and a carbide within the fullerene cage.

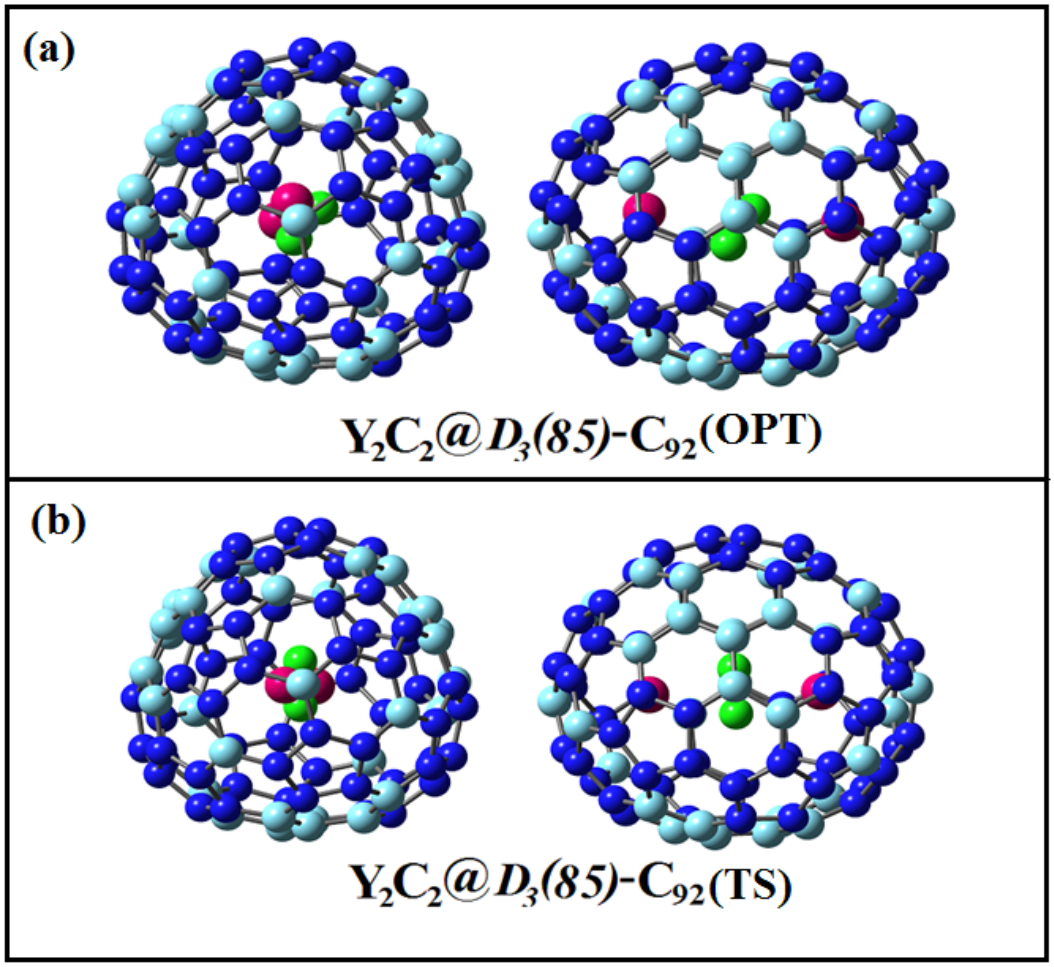

Figure 4.11. The simulated structure of $Y_2C_2@D_3(85)$-C_{92} in (a) optimized (OPT) and (b) transition state (TS)

The structure of $Y_2C_2@D_3(85)$-C_{92}, optimized by density functional theory (DFT) calculations, is shown in Figure 4.11a. The simulated structural result indicates that Y_2C_{94} contains a Y_2C_2 unit inside a C_{92} cage. In this conformation, the carbon-carbon bond distance of the C_2 unit inside the cage is 0.126 nm, corresponding to a triple bond distance, which is consistent with the formal electronic structure $[Y_2C_2]^{4+}@C_{92}^{4-}$.[26] We

performed the DFT calculation on D_3(85)-C_{92} as a neutral molecule, dianion, tetra-anion and hexa-anion, as shown in Figure 4.12. The small HOMO-LUMO gap of neutral D_3(85)-C_{92} suggests the instability of the molecule. There is a large gap between LUMO-1 and LUMO-2 of neutral D_3(85)-C_{92} so it is difficult to fill the LUMO-2 and higher orbitals. After encapsulation of the endohedrals, the electrons of the yttrium atoms are transferred to the D_3(85)-C_{92} cage. DFT calculations suggest when four electrons are transferred to the cage, the resulting tetra-anion of D_3(85)-C_{92} has the largest HOMO-LUMO gap, which is consistent with the electronic structure $[Y_2C_2]^{4+}@C_{92}^{4-}$ that is predicted.

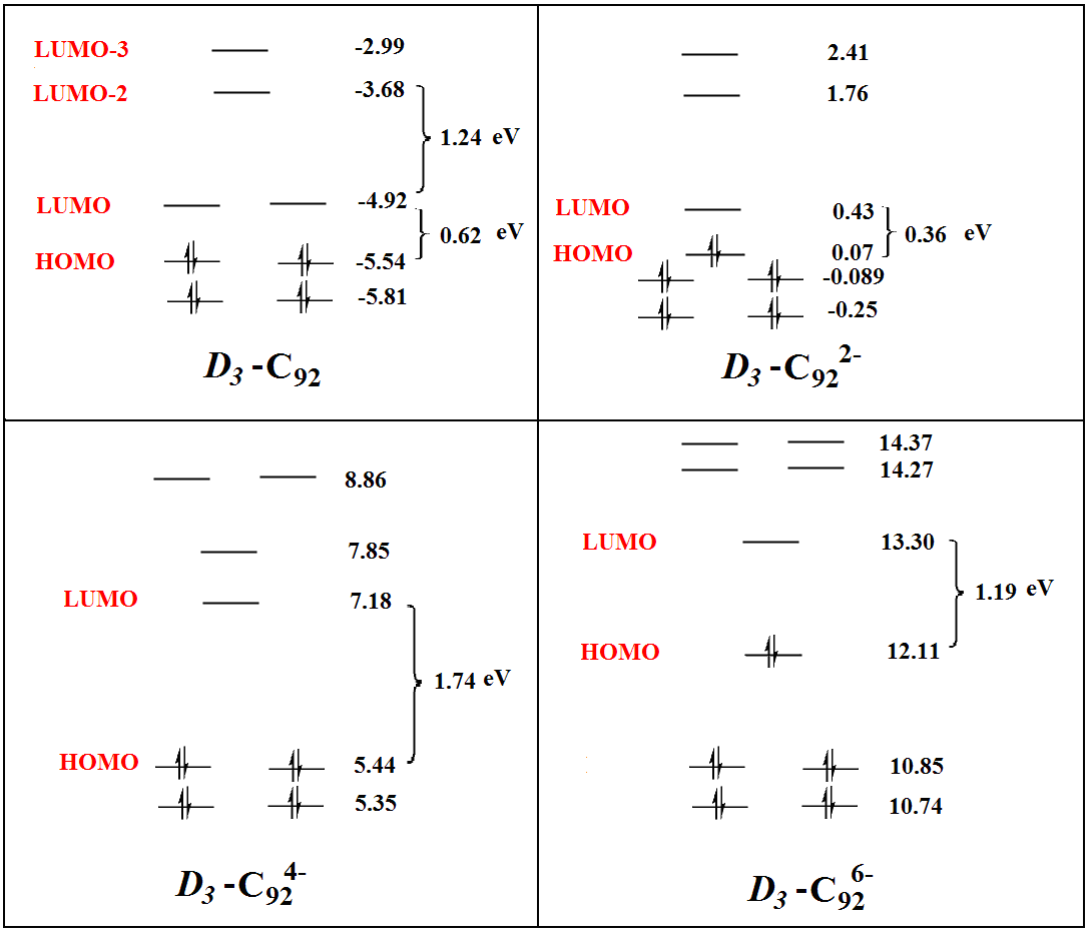

Figure 4.12. Molecular orbital energy levels for empty cage D_3(85)-C_{92} as a neutral molecule, dianion, tetra-anion and hexa-anion

The simulated structure of $Y_2C_2@D_3(85)$-C_{92} indicates that the two carbons of carbide are not chemically and magnetically equivalent, which seems contradictory to the $J_{Y\text{-}C}$ coupling observed in ^{13}C NMR spectrum (1:2:1 triplet). We performed the DFT calculation of $Y_2C_2@D_3(85)$-C_{92} with a transition state (TS) structure. As shown in Figure 11b, the TS structure of $Y_2C_2@D_3(85)$-C_{92} shows the "ideal butterfly shape", where the C_2 unit lies perpendicular to a line between the two metal atoms. The energy difference between the optimized structure and the ideal butterfly structure is very small, only 1.83 kcal/mol, as shown in Figure 4.13.

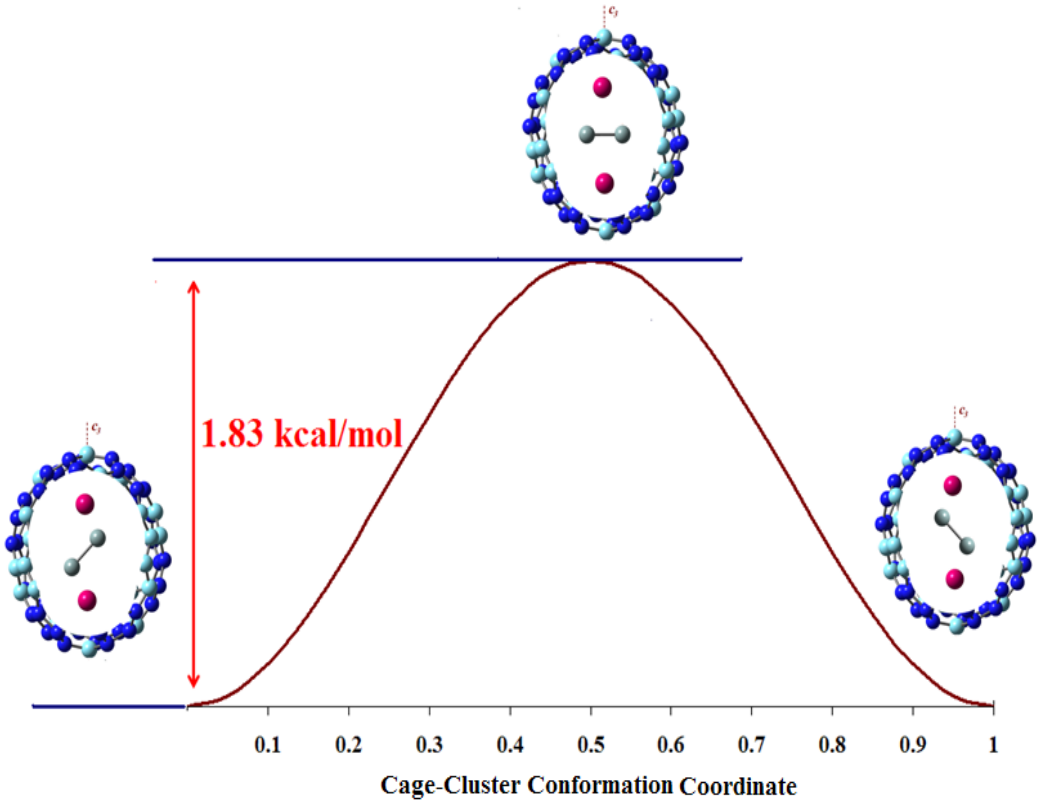

Figure 4.13. The small barrier between simulated structure of $Y_2C_2@D_3(85)$-C_{92} in optimized (OPT) and transition state (TS)

The small energy difference between the transition and optimized structure suggests that the barrier between these two states is very small and the carbide unit inside the cage may rotate rapidly around the yttrium atoms, as shown in Figure 4.14.

Thus, an equivalent environment would be created for this carbide on the NMR time scale, which accounts for the triplet observed in the ^{13}C NMR spectrum.

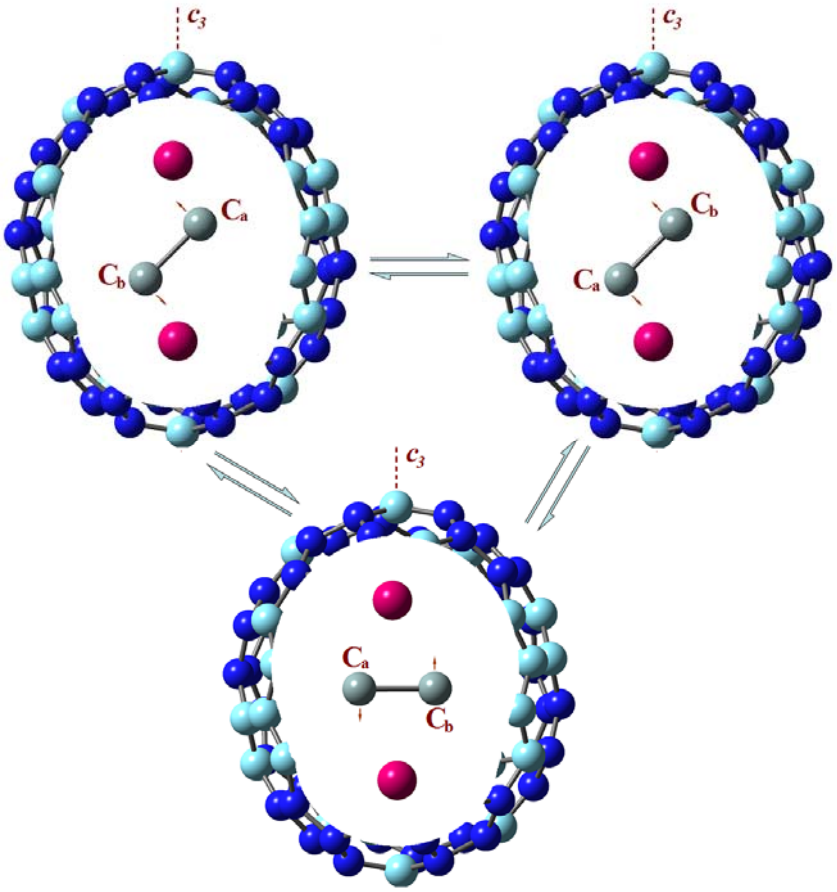

Figure 4.14. Schematic rotation process of the carbide in the C_{92} cage

The electrochemical behavior of $Y_2C_2@D_3(85)$-C_{92} was determined by cyclic voltammetry, as shown in Figure 4.15. Two reduction peaks and one oxidation peak were observed. The first and second reduction potentials ($^{red}E_1$ and $^{red}E_2$) are -1.51 and -1.76 V, respectively. The oxidation potential ($^{ox}E_1$) is 0.46 V. The resulting electrochemical bandgap ($^{ox}E_1$-$^{red}E_1$) for the $Y_2C_2@D_3(85)$-C_{92} is 1.97 V. This bandgap is larger than that of other metal carbide endohedral fullerenes shown in Table 4.1, such as $Sc_2C_2@C_{3v}$-C_{82} (1.11 V)[39] and $Sc_3C_2@I_h$-C_{80} (0.44 V),[40] and it is comparable to TNT EMFs, such as $Sc_3N@I_h$-C_{80} (1.88 V)[41] and $Y_3N@I_h$-C_{80} (2.05 V).[41] The large

electrochemical bandgap is also consistent with the DFT predicted HOMO-LUMO value, 1.74 eV. This large electrochemical bandgap suggests the high stability of this unique EMF.

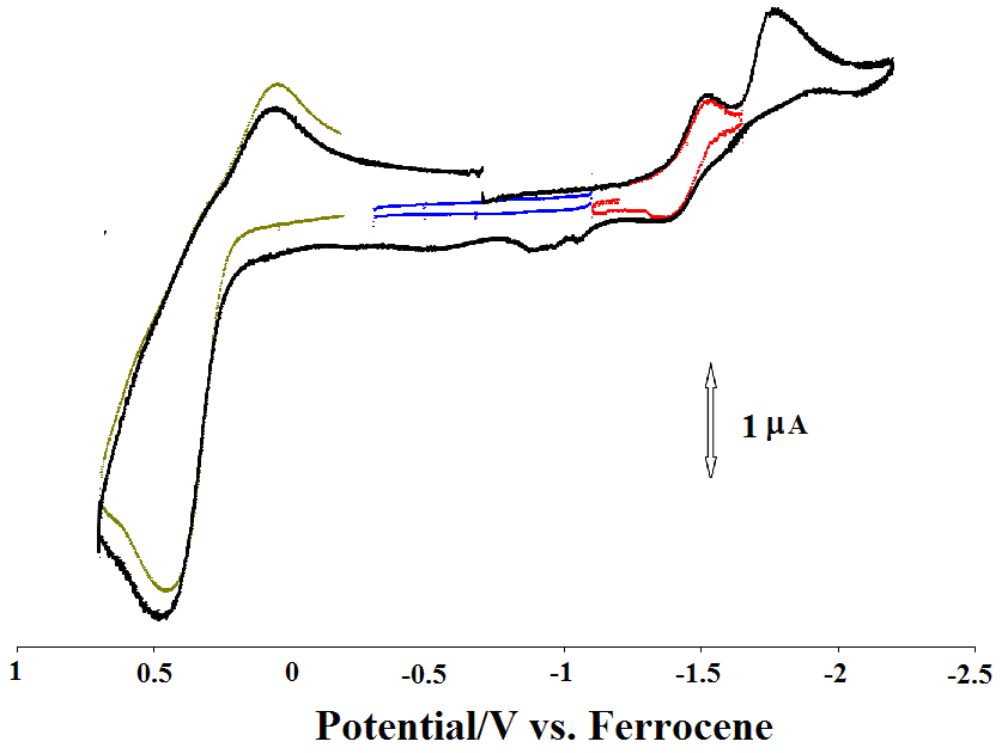

Figure 4.15. Cyclic voltammogram of the $Y_2C_2@D_3(85)$-C_{92}

Table 4.1. The redox potentials of $Y_2C_2@D_3(85)$-C_{92} and related EMFs

Compound	$^{ox}E_1$ (V)	$^{red}E_1$ (V)	$^{red}E_2$ (V)	$^{red}E_3$ (V)	Bandgap (V)
$Y_2C_2@D_3(85)$-C_{92}	0.46	-1.51	-1.76		1.97
$Sc_2C_2@C_{3v}$-C_{82} [39]	0.16	-0.95	-1.38		1.11
$Sc_3C_2@I_h$-C_{80} [40]	-0.06	-0.50	-1.64	-1.82	0.44
$Sc_3N@I_h$-C_{80} [41]	0.59	-1.29	-1.56		1.88
$Y_3N@I_h$-C_{80} [41]	0.64	-1.41	-1.83		2.05

4.4. Summary

In summary, we have prepared, separated and characterized two *di*-metallic EMFs, Y_2C_{90} and Y_2C_{94}. We successfully distinguished one of the *di*-metallofullerenes Y_2C_{94} as a metal carbide based EMF, $Y_2C_2@D_3(85)$-C_{92}. The carbide within the cage was successfully detected by ^{13}C NMR. Yttrium-carbon scalar coupling of a motional averaged cluster inside the C_{92} cage is reported. It is the first time to observe the coupling between a metal atom and a carbide for EMFs. However, the structures of Y_2C_{90} and isomer II of Y_2C_{94} remain to be established since these compounds may exists as either the traditional EMFs, $M_2@C_{2n}$ or the metal carbide based EMFs, $M_2C_2@C_{2n-2}$.

References:

(1) Shinohara, H., Endohedral metallofullerenes. *Rep. Prog. Phys.* **2000,** *63* (6), 843-892.

(2) Akasaka, T.; Nagase, T.; Eds.; Kluwer Academic Publishers: Dordrecht, T. N., *Endofullerenes: A New Family of Carbon Clusters* **2002**.

(3) Wilson, L. J.; Cagle, D. W.; Thrash, T. P.; Kennel, S. J.; Mirzadeh, S.; Alford, J. M.; Ehrhardt, G. J., Metallofullerene drug design. *Coord. Chem. Rev.* **1999,** *192*, 199-207.

(4) Iezzi, E. B.; Duchamp, J. C.; Fletcher, K. R.; Glass, T. E.; Dorn, H. C., Lutetium-based trimetallic nitride endohedral metallofullerenes: New contrast agents. *Nano. Lett.* **2002,** *2* (11), 1187-1190.

(5) Okumura, M.; Mikawa, M.; Yokawa, T.; Kanazawa, Y.; Kato, H.; Shinohara, H., Evaluation of water-soluble metallofullerenes as MRI contrast agents. *Acad. Radiol.* **2002,** *9*, S495-S497.

(6) Kato, H.; Kanazawa, Y.; Okumura, M.; Taninaka, A.; Yokawa, T.; Shinohara, H., Lanthanoid endohedral metallofullerenols for MRI contrast agents. *J. Am. Chem. Soc.* **2003,** *125* (14), 4391-4397.

(7) Bolskar, R. D.; Benedetto, A. F.; Husebo, L. O.; Price, R. E.; Jackson, E. F.; Wallace, S.; Wilson, L. J.; Alford, J. M., First soluble M@C_{60} derivatives provide enhanced access to metallofullerenes and permit in vivo evaluation of Gd@C_{60}[$C(COOH)_2$]$_{10}$ as a MRI contrast agent. *J. Am. Chem. Soc.* **2003,** *125* (18), 5471-5478.

(8) Shu, C. Y.; Ma, X. Y.; Zhang, J. F.; Corwin, F. D.; Sim, J. H.; Zhang, E. Y.; Dorn, H. C.; Gibson, H. W.; Fatouros, P. P.; Wang, C. R.; Fang, X. H., Conjugation of a water-soluble gadolinium endohedral fulleride with an antibody as a magnetic resonance imaging contrast agent. *Bioconjugate Chem.* **2008,** *19* (3), 651-655.

(9) Shu, C. Y.; Corwin, F. D.; Zhang, J. F.; Chen, Z. J.; Reid, J. E.; Sun, M. H.; Xu, W.; Sim, J. H.; Wang, C. R.; Fatouros, P. P.; Esker, A. R.; Gibson, H. W.; Dorn, H. C., Facile Preparation of a New Gadofullerene-Based Magnetic Resonance Imaging Contrast Agent with High H-1 Relaxivity. *Bioconjugate Chem.* **2009,** *20* (6), 1186-1193.

(10) Thompson Barry, C.; Frechet Jean, M. J., Polymer-fullerene composite solar cells. *Angew. Chem. Int. Ed.* **2008,** *47* (1), 58-77.

(11) Ross, R. B.; Cardona, C. M.; Guldi, D. M.; Sankaranarayanan, S. G.; Reese, M. O.; Kopidakis, N.; Peet, J.; Walker, B.; Bazan, G. C.; Van Keuren, E.; Holloway, B. C.; Drees, M., Endohedral fullerenes for organic photovoltaic devices. *Nature Mater.* **2009,** *8* (3), 208-212.

(12) Chai, Y.; Guo, T.; Jin, C. M.; Haufler, R. E.; Chibante, L. P. F.; Fure, J.; Wang, L. H.; Alford, J. M.; Smalley, R. E., Fullerenes with Metals Inside. *J. Phys. Chem.* **1991,** *95* (20), 7564-7568.

(13) Wakahara, T.; Okubo, S.; Kondo, M.; Maeda, Y.; Akasaka, T.; Waelchli, M.;

Kako, M.; Kobayashi, K.; Nagase, S.; Kato, T.; Yamamoto, K.; Gao, X.; Van Caemelbecke, E.; Kadish, K. M., Ionization and structural determination of the major isomer of Pr@C_{82}. *Chem. Phys. Lett.* **2002,** *360* (3-4), 235-239.

(14) Akasaka, T.; Kono, T.; Takematsu, Y.; Nikawa, H.; Nakahodo, T.; Wakahara, T.; Ishitsuka, M. O.; Tsuchiya, T.; Maeda, Y.; Liu, M. T. H.; Yoza, K.; Kato, T.; Yamamoto, K.; Mizorogi, N.; Slanina, Z.; Nagase, S., Does Gd@C_{82} have an anomalous endohedral structure? Synthesis and single crystal X-ray structure of the carbene adduct. *J. Am. Chem. Soc.* **2008,** *130* (39), 12840-12841.

(15) Kato, H.; Taninaka, A.; Sugai, T.; Shinohara, H., Structure of a missing-caged metallofullerene: La_2@C_{72}. *J. Am. Chem. Soc.* **2003,** *125* (26), 7782-7783.

(16) Lu, X.; Nikawa, H.; Nakahodo, T.; Tsuchiya, T.; Ishitsuka, M. O.; Maeda, Y.; Akasaka, T.; Toki, M.; Sawa, H.; Slanina, Z.; Mizorogi, N.; Nagase, S., Chemical understanding of a non-IPR metallofullerene: Stabilization of encaged metals on fused-pentagon bonds in La_2@C_{72}. *J. Am. Chem. Soc.* **2008,** *130* (28), 9129-9136.

(17) Stevenson, S.; Rice, G.; Glass, T.; Harich, K.; Cromer, F.; Jordan, M. R.; Craft, J.; Hadju, E.; Bible, R.; Olmstead, M. M.; Maitra, K.; Fisher, A. J.; Balch, A. L.; Dorn, H. C., Small-bandgap endohedral metallofullerenes in high yield and purity. *Nature* **1999,** *401* (6748), 55-57.

(18) Olmstead, M. M.; de Bettencourt-Dias, A.; Duchamp, J. C.; Stevenson, S.; Dorn, H. C.; Balch, A. L., Isolation and crystallographic characterization of $ErSc_2N$@C_{80}: an endohedral fullerene which crystallizes with remarkable internal order. *J. Am. Chem. Soc.* **2000,** *122* (49), 12220-12226.

(19) Stevenson, S.; Fowler, P. W.; Heine, T.; Duchamp, J. C.; Rice, G.; Glass, T.; Harich, K.; Hajdu, E.; Bible, R.; Dorn, H. C., A stable non-classical metallofullerene family. *Nature* **2000,** *408* (6811), 427-428.

(20) Wang, C. R.; Kai, T.; Tomiyama, T.; Yoshida, T.; Kobayashi, Y.; Nishibori, E.; Takata, M.; Sakata, M.; Shinohara, H., A scandium carbide endohedral metallofullerene: (Sc_2C_2)@C_{84}. *Angew. Chem. Int. Ed.* **2001,** *40* (2), 397-399.

(21) Tan, K.; Lu, X., Ti_2C_{80} is more likely a titanium carbide endohedral metallofullerene (Ti_2C_2)@C_{78}. *Chem. Commun.* **2005,** (35), 4444-4446.

(22) Inoue, T.; Tomiyama, T.; Sugai, T.; Okazaki, T.; Suematsu, T.; Fujii, N.; Utsumi, H.; Nojima, K.; Shinohara, H., Trapping a C_2 radical in endohedral metallofullerenes: Synthesis and structures of (Y_2C_2)@C_{82} (Isomers I, II, and III). *J. Phys. Chem. B* **2004,** *108* (23), 7573-7579.

(23) Iiduka, Y.; Wakahara, T.; Nakahodo, T.; Tsuchiya, T.; Sakuraba, A.; Maeda, Y.; Akasaka, T.; Yoza, K.; Horn, E.; Kato, T.; Liu, M. T. H.; Mizorogi, N.; Kobayashi, K.; Nagase, S., Structural Determination of Metallofullerene Sc_3C_{82} Revisited: A Surprising Finding. *J. Am. Chem. Soc.* **2005,** *127* (36), 12500-12501.

(24) Shi, Z. Q.; Wu, X.; Wang, C. R.; Lu, X.; Shinohara, H., Isolation and characterization of Sc_2C_2@C_{68}: A metal-carbide endofullerene with a non-IPR carbon cage. *Angew. Chem. Int. Ed.* **2006,** *45* (13), 2107-2111.

(25) Yang, H.; Lu, C.; Liu, Z.; Jin, H.; Che, Y.; Olmstead, M. M.; Balch, A. L.,

Detection of a Family of Gadolinium-Containing Endohedral Fullerenes and the Isolation and Crystallographic Characterization of One Member as a Metal-Carbide Encapsulated inside a Large Fullerene Cage. *J. Am. Chem. Soc.* **2008,** *130* (51), 17296-17300.

(26) Yamazaki, Y.; Nakajima, K.; Wakahara, T.; Tsuchiya, T.; Ishitsuka, M. O.; Maeda, Y.; Akasaka, T.; Waelchli, M.; Mizorogi, N.; Nagase, S., Observation of ^{13}C NMR chemical shifts of metal carbides encapsulated in fullerenes: $Sc_2C_2@C_{82}$, $Sc_2C_2@C_{84}$, and $Sc_3C_2@C_{80}$. *Angew. Chem. Int. Ed.* **2008,** *47* (41), 7905-7908.

(27) Olmstead, M. M.; de Bettencourt-Dias, A.; Stevenson, S.; Dorn, H. C.; Balch, A. L., Crystallographic characterization of the structure of the endohedral fullerene [$Er_2@C_{82}$ isomer I] with C_s cage symmetry and multiple sites for erbium along a band of ten contiguous hexagons. *J. Am. Chem. Soc.* **2002,** *124* (16), 4172-4173.

(28) Olmstead, M. M.; Lee, H. M.; Stevenson, S.; Dorn, H. C.; Balch, A. L., Crystallographic characterization of Isomer 2 of $Er_2@C_{82}$ and comparison with Isomer 1 of $Er_2@C_{82}$. *Chem. Commun.* **2002,** (22), 2688-2689.

(29) Yamada, M.; Wakahara, T.; Tsuchiya, T.; Maeda, Y.; Akasaka, T.; Mizorogi, N.; Nagase, S., Spectroscopic and theoretical study of endohedral dimetallofullerene having a Non-IPR fullerene cage: $Ce_2@C_{72}$. *J. Phys. Chem. A* **2008,** *112* (33), 7627-7631.

(30) Wang, C. R.; Inakuma, M.; Shinohara, H., Metallofullerenes $Sc_2@C_{82}$(I, II) and $Sc_2@C_{86}$(I, II): isolation and spectroscopic studies. *Chem. Phys. Lett.* **1999,** *300* (3-4), 379-384.

(31) Valencia, R.; Rodriguez-Fortea, A.; Poblet, J. M., Understanding the stabilization of metal carbide endohedral fullerenes $M_2C_2@C_{82}$ and related systems. *J. Phys. Chem. A* **2008,** *112* (20), 4550-4555.

(32) Ge, Z. X.; Duchamp, J. C.; Cai, T.; Gibson, H. W.; Dorn, H. C., Purification of endohedral trimetallic nitride fullerenes in a single, facile step. *J. Am. Chem. Soc.* **2005,** *127* (46), 16292-16298.

(33) Frisch, M. J.; Trucks, G. W.; Schlegel, H. B.; Scuseria, G. E.; Robb, M. A.; Cheeseman, J. R.; Montgomery, J. A.; Vreven, Jr., T.; Kudin, K. N.; Burant, J. C.; Millam, J. M.; Iyengar, S. S.; Tomasi, J.; Barone, V.; Mennucci, B.; Cossi, M.; Scalmani, G.; Rega, N.; Petersson, G. A.; Nakatsuji, H.; Hada, M.; Ehara, M.; Toyota, K.; Fukuda, R.; Hasegawa, J.; Ishida, M.; Nakajima, T.; Honda, Y.; Kitao, O.; Nakai, H.; Klene, M.; Li, X. ; Knox, J. E.; Hratchian, H. P.;. Cross, J. B; Adamo, C.; Jaramillo, J.; Gomperts, R.; Stratmann, R. E.; Yazyev, O.; Austin, A. J.; Cammi, R.; Pomelli, C.; Ochterski, J. W.; Ayala, P. Y. ; Morokuma, K.; Voth, G. A.; Salvador, P.; Dannenberg, J. J.; Zakrzewski, V. G.; Dapprich, S.; Daniels, A. D.; Strain, M. C.; Farkas, O.; Malick, D. K.; Rabuck, A. D.; Raghavachari, K.; Foresman, J. B.; Ortiz, J. V.; Cui, Q.; Baboul, A. G.; Clifford, S.; Cioslowski, J; Stefanov, B. B.; Liu, G.; Liashenko, A ; Piskorz, P.; Komaromi, I.; Martin, R. L.; Fox, D. J.; Keith, T.; Al-Laham, M. A.; Peng, C. Y.; Nanayakkara, A.; Challacombe, M.; Gill, P. M. W.; Johnson, B.; Chen, W.;

Wong, M. W.; Gonzalez, C.; and Pople, J. A.; Gaussian, Inc.: Wallingford, CT, 2004.

(34) Fu, W. J.; Xu, L. S.; Azurmendi, H.; Ge, J. C.; Furher, T.; Zuo, T. M.; Reid, J.; Shu, C. Y.; Harich, K.; Dorn, H. C., ^{89}Y and ^{13}C NMR Cluster and Carbon Cage Studies of an Yttrium Metallofullerene Family, $Y_3N@C_{2n}$ (n = 40-43). *J. Am. Chem. Soc.* **2009,** *131* (33), 11762-11769.

(35) Zuo, T. M.; Xu, L. S.; Beavers, C. M.; Olmstead, M. M.; Fu, W. J.; Crawford, D.; Balch, A. L.; Dorn, H. C., $M_2@C_{79}N$ (M = Y, Tb): Isolation and characterization of stable endohedral metallofullerenes exhibiting M-M bonding interactions inside aza[80]fullerene cages. *J. Am. Chem. Soc.* **2008,** *130* (39), 12992-12997.

(36) Fowler, P. W.; Manolopoulos, D. E., *An Atlas of fullerenes*. Oxford University: New York: 1995.

(37) St.Clair, M.; Schaefer, W. P.; Bercaw, J. E., Reactivity of Permethylscandocene Derivatives with Acetylene - Structure of Acetylenediylbis(Permethylscandocene), (η5-C5Me5)2ScC≡CSc(η5-C5Me5)2. *Organometallics* **1991,** *10* (3), 525-527.

(38) Denhaan, K. H.; Wielstra, Y.; Teuben, J. H., Reactions of Yttrium Carbon Bonds with Active Hydrogen-Containing Molecules - a Useful Synthetic Method for Permethylyttrocene Derivatives. *Organometallics* **1987,** *6* (10), 2053-2060.

(39) Anderson, M. R.; Dorn, H. C.; Stevenson, S. A., Making connections between metallofullerenes and fullerenes: electrochemical investigations. *Carbon* **2000,** *38* (11-12), 1663-1670.

(40) Wakahara, T.; Sakuraba, A.; Iiduka, Y.; Okamura, M.; Tsuchiya, T.; Maeda, Y.; Akasaka, T.; Okubo, S.; Kato, T.; Kobayashi, K.; Nagase, S.; Kadish, K. M., Chemical reactivity and redox property of $Sc_3@C_{82}$. *Chem. Phys. Lett.* **2004,** *398* (4-6), 553-556.

(41) Cardona, C. M.; Elliott, B.; Echegoyen, L., Unexpected chemical and electrochemical properties of $M_3N@C_{80}$ (M = Sc, Y, Er). *J. Am. Chem. Soc.* **2006,** *128* (19), 6480-6485.

Chapter 5

Two Paramagnetic Endohedral Metalloheterofullerenes, $Y_2@C_{79}N$ and $Gd_2@C_{79}N$

5.1. Introduction

Since the discovery of macroscopic production of fullerenes, chemists have been fascinated by the idea of modifying the all-carbon fullerene network and replacing the carbon atoms with one or more other atoms.[1-3] The substitution of a carbon atom by a heteroatom may result in significant change of fullerene geometry, electronic character and chemical functionality, leading to formation of the heterofullerenes with unusual physico-chemical properties.[1-3]

One of these heterofullerenes, $C_{59}N$, is derived from C_{60} by substituting a nitrogen atom for one of the carbon atoms.[3-5] Since the $C_{59}N$ is an odd-electron species and is energetically unstable, the stable form of this heterofullerenes is a dumbbell-like dimmer $[C_{59}N]_2$ with a single C-C bond connecting two cages.[4]

Fullerenes can be encapsulated with metal atoms or clusters. The resulting endohedral metallofullerenes (EMFs) could have novel electronic and magnetic properties. Therefore, their potential applications in various areas are expected. For example, EMFs with gadolinium (Gd) ions trapped inside have been considered promising candidates as the next magnetic resonance imaging (MRI) contrast agents.[6-10]

Similar to the regular fullerene cages, heterofullerenes also have the ability to host endohedrals and form endohedral metalloheterofullerenes. Unfortunately, only very limited work have been reported in the field of endohedral metalloheterofullerenes. The first experimental detection is the formation of $[La_2@C_{79}N]^+$ and the $[La_2@C_{81}N]^+$ by fast atom bombardment mass fragmentation.[11] However, these species can not be isolated and further characterized due to their instability. So far, only two *di*-metallic endohedral metalloheterofullerenes, $Y_2@C_{79}N$ and $Tb_2@C_{79}N$, were isolated successfully and characterized preliminarily.[12] Herein, we report the preparation and isolation of a new endohedral metalloheterofullerene with two paramagnetic metal ions trapped, $Gd_2@C_{79}N$. In addition, we discuss the characterizations of $Y_2@C_{79}N$.

5.2. Experimental Section

Preparation and Separation: The procedures for the preparation and purification of $Y_2@C_{79}N$ and $Gd_2@C_{79}N$ were analogous to those used for TNT-EMFs and metallic carbide EMFs described in Chapter 3 and 4. To reiterate briefly, a hollow graphite rod was packed with a mixture of Y_2O_3 or Gd_2O_3, graphite powder and Cu with weight ratios 1.1:1.0:2.1 (Y_2O_3:C:Cu) and 2:1.0:2.1(Gd_2O_3:C:Cu) respectively. These rods were then vaporized in a Krätschmer and Huffman generator under a dynamic flow of He and N_2 (flow rate ratio of N_2/H_2=3:100). The resulting soot was then extracted with refluxing toluene and applied to the cyclopentadiene-functionized Merrifield resin (CPDE-MPR) column.[13] The eluent was further separated using a two-stage HPLC approach.

Characterization of the $M_2@C_{79}N$: Mass spectrometry was performed on a Kratos Analytical Kompact SEQ LD-TOF mass spectrometer. Cyclic voltammetric measurements were conducted using a CH Instruments model 600A potentiostat (Austin, TX) and a single compartment microelectrochemical cell. A 2 mm glassy carbon disk electrode along with a Pt auxiliary was applied as working electrode using Ag/AgCl as a reference. Measurements were performed using *o*-dichlorobenzene solutions containing 0.100 M tetra-*n*-butylamonium tetrafluoroborate. Potentials were reported relative to the reversible ferrocene oxidation couple. The x-band EPR spectrum of $Gd_2@C_{79}N$ at 4K was obtained by using a Bruker E500 spectrometer. The w-band EPR spectrum of $Gd_2@C_{79}N$ at 30K was obtained by using a Bruker E680 spectrometer. Other EPR spectra were recorded with a Bruker D200 ER IBM-Bruker spectrometer.

5.3. Results and Discussion

5.3.1. Preparation and Separation

The preparation of $Y_2@C_{79}N$ and $Gd_2@C_{79}N$ was through the traditional Krätschmer-Huffman generator method, as discussed in experimental section. The eluent after CPDE-MPR column[13] was furthered separated by the two stage HPLC technique. The first stage was carried out on a PBB column (4.6 × 250 mm) and the HPLC chromatogram is shown in Figure 5.1. The Gd-based sample after chemical separation displays a similar HPLC trace with seven fractions from Gd1 to Gd7 (Figure 1a). The fractions Y1 and Gd1 from the PBB column were collected and further

purified by using a PYE column (10 × 250 mm).

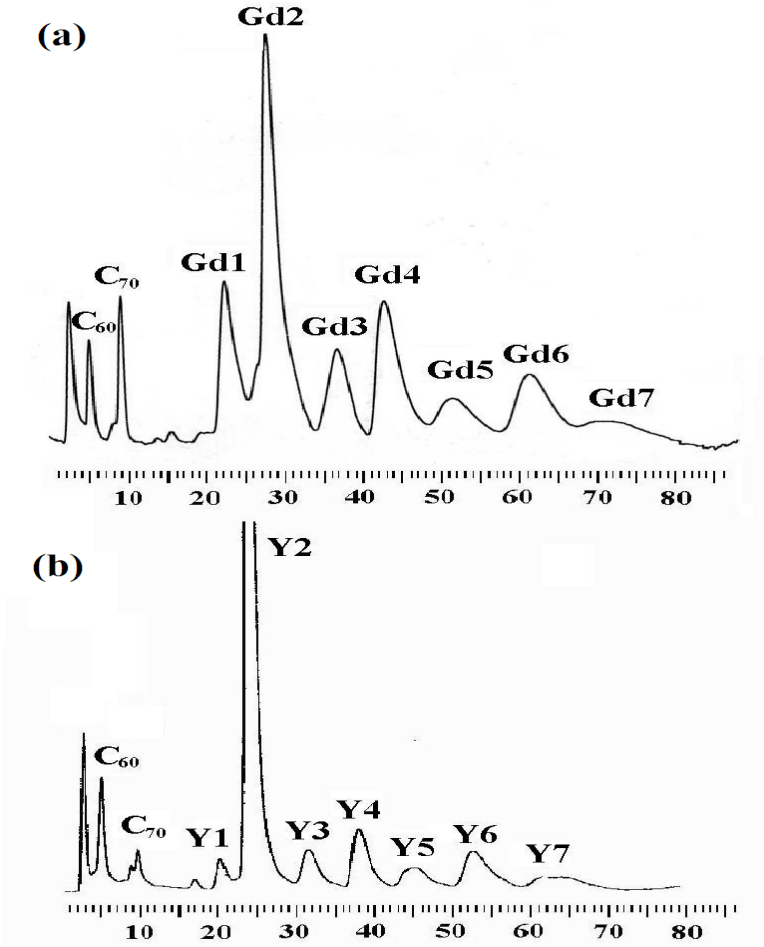

Figure 5.1. HPLC chromatograms of the eluent from CPDE-MPR column (a) Yttrium-based EMFs, (b) Gadolinium-based EMFs (4.6 × 250 mm 5PBB column; λ=390 nm; flow rate 2.0 mL/min; toluene as eluent; 25 ºC)

Figure 5.2 shows the HPLC chromatogram of fractions Gd1 and Y1 on a PYE column. There are two main fractions on the PYE column and they are empty cage fullerene C_{84} and $M_2@C_{79}N$ (M=Y, Gd). Since the retention time of C_{84} and $M_2@C_{79}N$ are very different on a PYE column, C_{84} can be easily separated from $M_2@C_{79}N$. The HPLC chromatograms of the pure $Gd_2@C_{79}N$ and $Y_2@C_{79}N$ samples are shown in Figure 5.3.

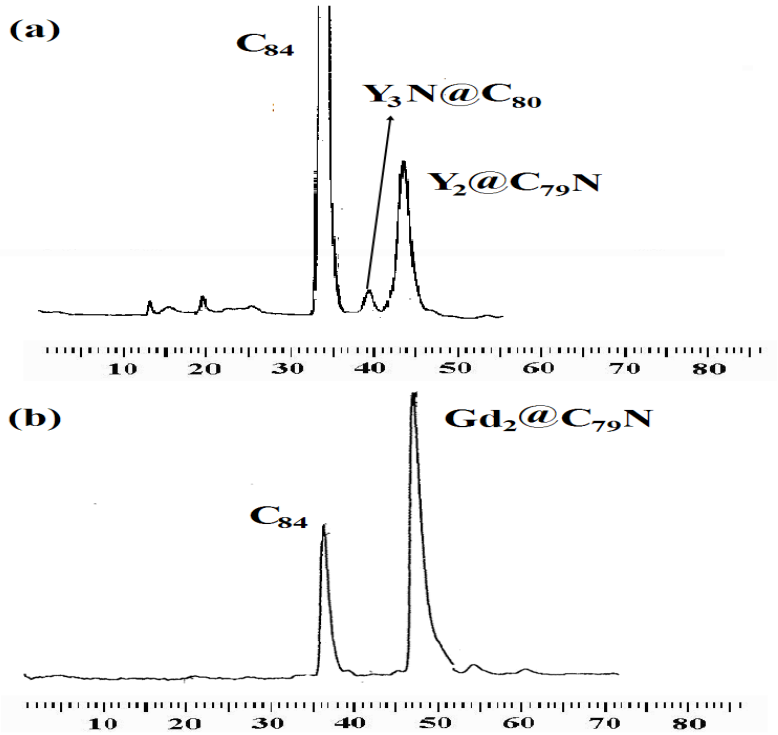

Figure 5.2. HPLC chromatograms on a PYE column (a) Separation of $Y_2@C_{79}N$ from C_{84}, (b) Separation of $Gd_2@C_{79}N$ from C_{84} (10 × 250 mm 5PBB column; λ=390 nm; flow rate 2.0 mL/min; toluene as eluent; 25 ºC)

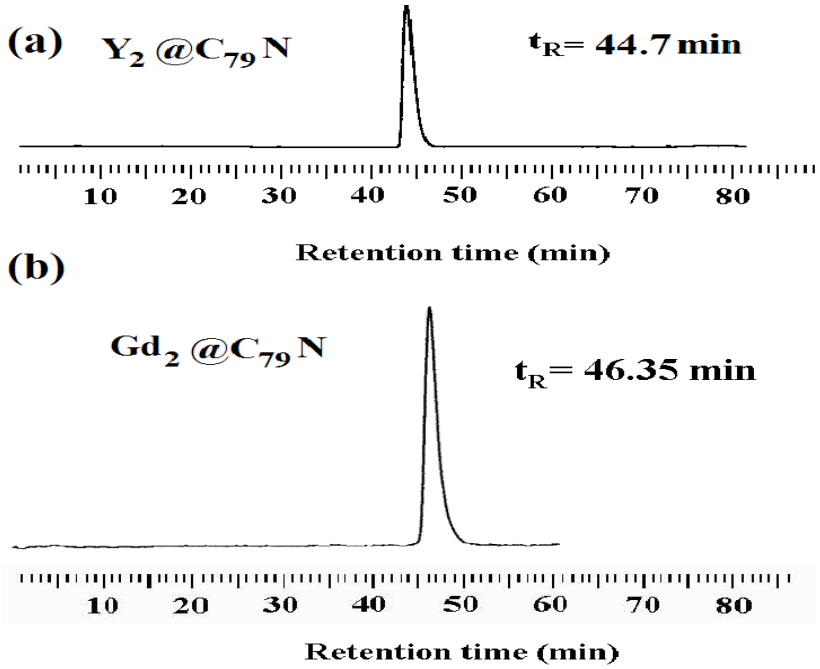

Figure 5.3. HPLC chromatograms of purified $M_2@C_{79}N$ (M=Y, Gd) on a PYE column. (a) $Y_2@C_{79}N$ (b) $Gd_2@C_{79}N$ (10 × 250 mm 5PBB column; λ=390 nm; flow rate 2.0 mL/min; toluene as eluent; 25 ºC)

5.3.2. Characterization

5.3.2.1 $Y_2@C_{79}N$

The mass spectrum of $Y_2@C_{79}N$ confirms the identity and purity of sample, as shown in Figure 5.4. The inset of Figure 4 shows the satisfactory comparison of the computed and observed isotopic distributions. The UV-Vis spectrum of $Y_2@C_{79}N$ is shown in Figure 5.5.

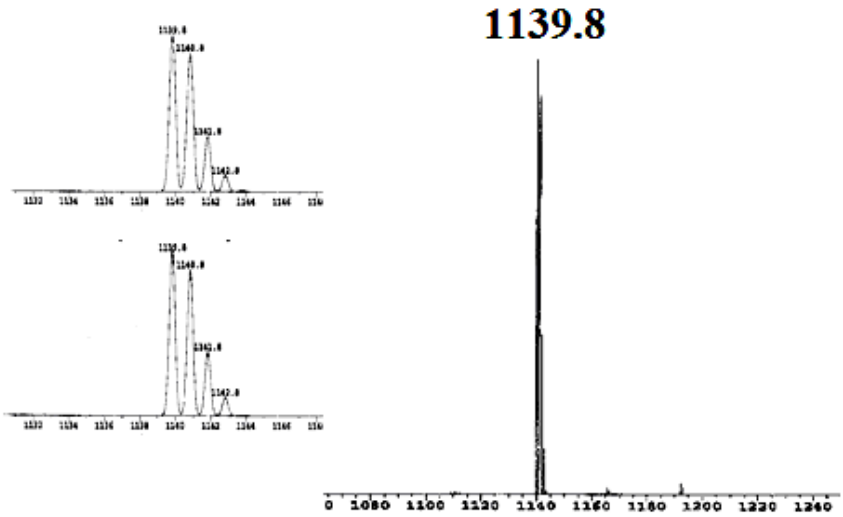

Figure 5.4. The LD-TOF mass spectrum of $Y_2@C_{79}N$ with positive ionization

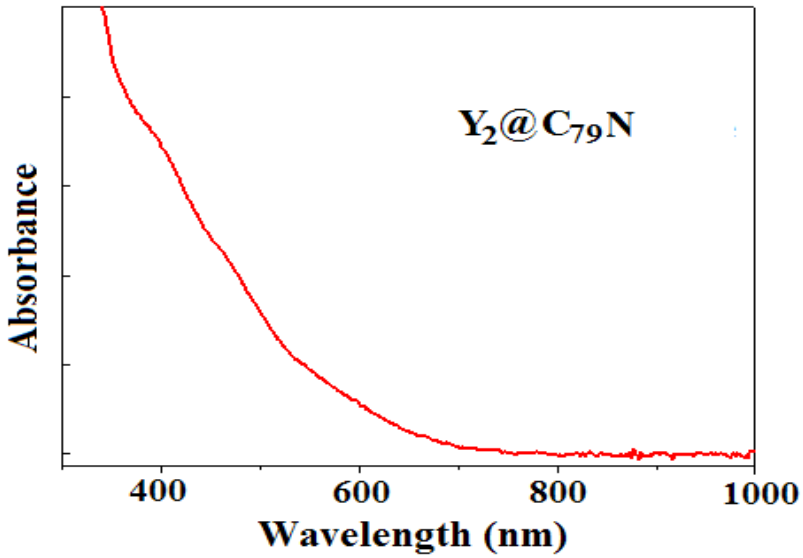

Figure 5.5. UV-Vis spectrum of purified $Y_2@C_{79}N$ in toluene solution

The DFT calculation suggested a $[M_2]^{5+}@[C_{79}N]^{5-}$ electronic model for the $M_2@C_{79}N$ molecule.[12] Thus, there is an unpaired electron in this molecule. The unpaired electron of $Y_2@C_{79}N$ molecule was shared by the two yttrium atoms and formed a single-electron chemical bond between them. This prediction was confirmed by X-band EPR solution measurements at 298K, as illustrated in Figure 5.6. For dilute $Y_2@C_{79}N$ in nitrobenzene, three symmetric peaks with a 1:2:1 ratio of intensity were observed. The nuclear spin number of ^{89}Y is I=1/2 and the sum of the spin number of the two Y atoms is 1. If the hyperfine splitting results from two equivalent ^{89}Y, the EPR signals will yield 3 peaks with 1:2:1 ratio according to the ($2I+1$) rule. This pattern is consistent with the experimental observation, suggesting the spin density mainly located between two equivalent ^{89}Y nuclides. The observed g-factor (g_0=1.973) and large yttrium coupling (a= 83.18 G) also indicate that the hyperfine splitting results from two equivalent ^{89}Y nuclides.[14] These observations are in sharp contrast to the g-factor (g_0=2.007) and hyperfine coupling (a= 14.216) of 2,2,6,6-tetramethyl-1-piperidinyl-oxy (TEMPO), where the hyperfine structure is due to the ^{14}N nuclides.

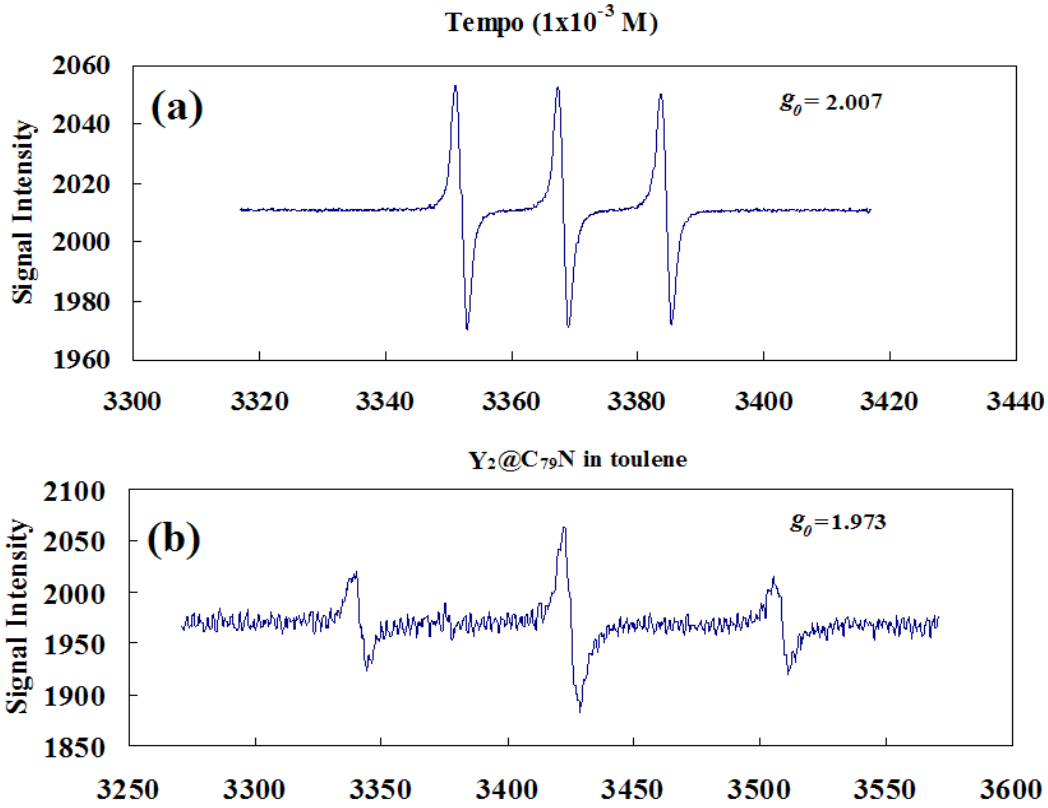

Figure 5.6. EPR spectra of (a) 2,2,6,6-tetramethyl-1-piperidinyl-oxy (Tempo) and (b) $Y_2@C_{79}N$ in toulene at 298 K

Electron transfer between organic donors and paramagnetic EMFs has been widely examined.[15-17] For example, as we discussed in Chapter 1, Nagase *et al.* have found the spin-site exchange system constructed between paramagnetic $La@C_{82}$ and *N*,*N*,*N*',*N*'-tetramethyl-*p*-phenylendiamine (TMPD).[15] Because the endohedral metalloheterofullerene $Y_2@C_{79}N$ has similar paramagnetic character as $La@C_{82}$, it is reasonable to question whether similar electron transfer could take place between $Y_2@C_{79}N$ and organic donor TMPD, as shown in Scheme 1.

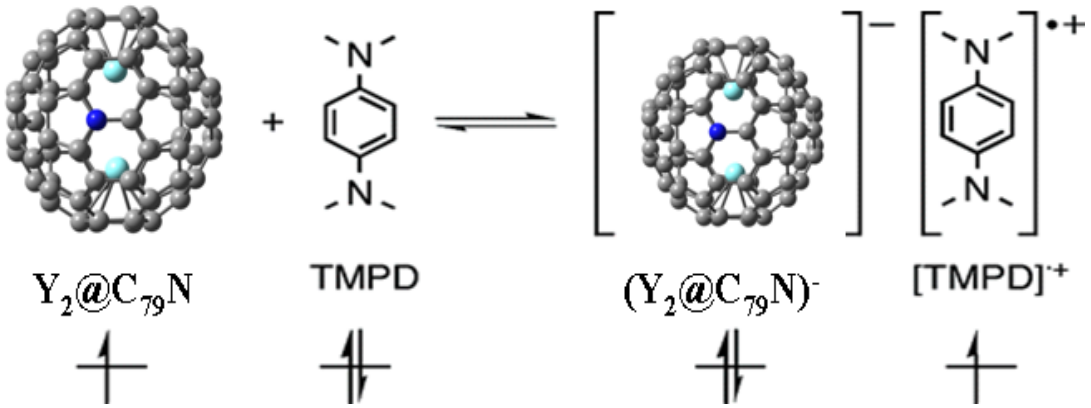

Scheme 5.1. Spin-site exchange system constructed from $Y_2@C_{79}N$ and TMPD.

Herein, we tried to monitor the electron transfer process between $Y_2@C_{79}N$ and TMPD in nitrobenzene by EPR measurements at various temperatures, as shown in Figure 5.7 and 5.8. Figure 5.7a shows the EPR spectrum of purified $Y_2@C_{79}N$ at 290 K. After addition of the TMPD ($Y_2@C_{79}N$: TMPD=1:1), the intensity of the EPR signal of $Y_2@C_{79}N$ is weakened and the signal of $[TMPD]^{\bullet+}$ appeared, suggesting the spin-site exchange between $Y_2@C_{79}N$ and TMPD. EPR spectra of $Y_2@C_{79}N$ with TMPD from 280 to 240 K are shown in Figure 5.7b to 5.7d. There was no obvious $[TMPD]^{\bullet+}$ EPR signal when the temperature is 280 K. When the temperature was decreased to 260 K, the strong $[TMPD]^{\bullet+}$ EPR signal appeared, indicating the equilibrium shifts to the formation of the ion pair. However, when the temperature was further decreased to 240 K, the intensity of $[TMPD]^{\bullet+}$ EPR signal was weakened, indicating the equilibrium shifts to the formation of the $Y_2@C_{79}N$/TMPD pair.

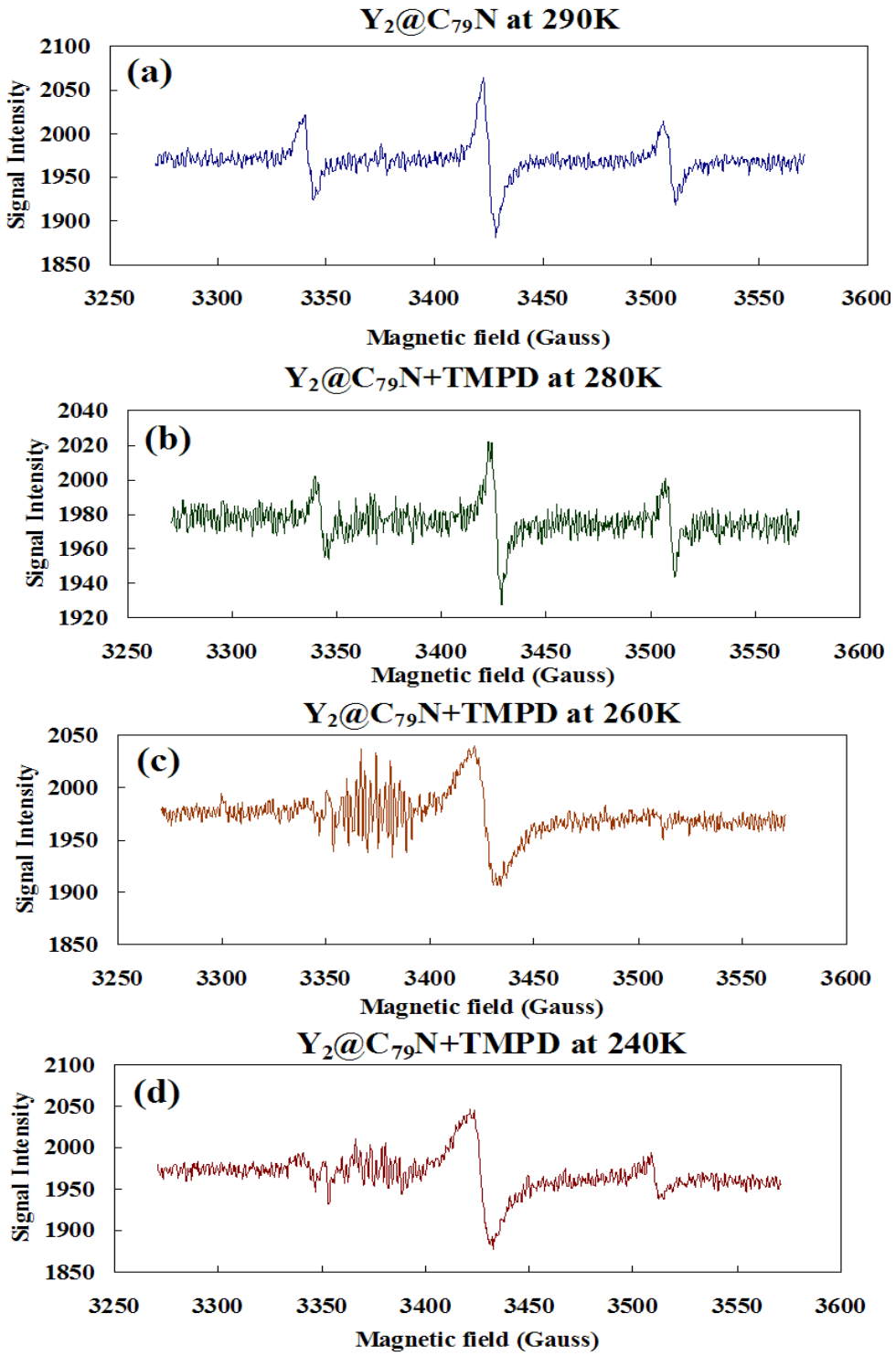

Figure 5.7. EPR spectra of (a) Pure $Y_2@C_{79}N$ in nitrobenzene at 290K and (b) $Y_2@C_{79}N$ in the presence of 1 equiv. of TMPD in nitrobenzene at 280 K and (c) $Y_2@C_{79}N$ in the presence of 1 equiv. of TMPD in nitrobenzene at 260 K and (d) $Y_2@C_{79}N$ in the presence of 1 equiv. of TMPD in nitrobenzene at 240 K

EPR measurements at 300 K and 320 K were also performed (Figure 5.8). There was no obvious EPR signal detected at 320 K. However, if the temperature was decreased to 260 K, the EPR signal due to $[TMPD]^{\bullet+}$ radical cation and $Y_2@C_{79}N$ appeared again, suggesting this electron transfer process is reversible.

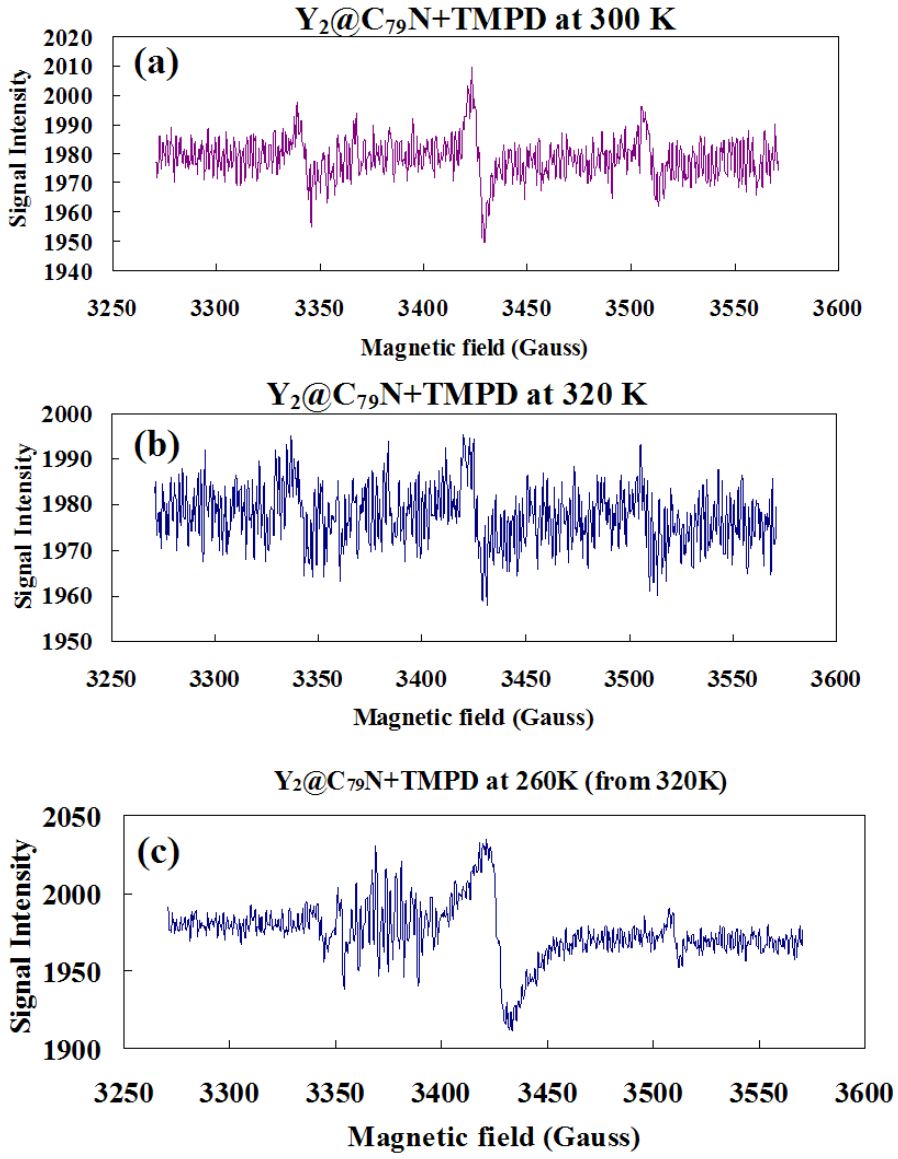

Figure 5.8. EPR spectra of (a) $Y_2@C_{79}N$ in the presence of 1 equiv. of TMPD in nitrobenzene at 300 K and (b) $Y_2@C_{79}N$ in the presence of 1 equiv. of TMPD in nitrobenzene at 320 K and (c) $Y_2@C_{79}N$ in the presence of 1 equiv. of TMPD in nitrobenzene at 260 K(from 320 K)

The electrochemical properties of the $Y_2@C_{79}N$ were studied by cyclic

voltammetry, as shown in Figure 5.9. Three reduction peaks and one oxidation peak were observed. The first and second reduction potentials ($^{red}E_1$, $^{red}E_2$, $^{red}E_3$) are -1.47, -1.76 and -2.23 V, respectively. The oxidation potential ($^{ox}E_1$) is 0.55 V. The resulting electrochemical bandgap ($^{ox}E_1$-$^{red}E_1$) for the $Y_2@C_{79}N$ is 2.02 V. This large bandgap is consistent with the HOMO-LUMO gap predicted by DFT calculations.[12]

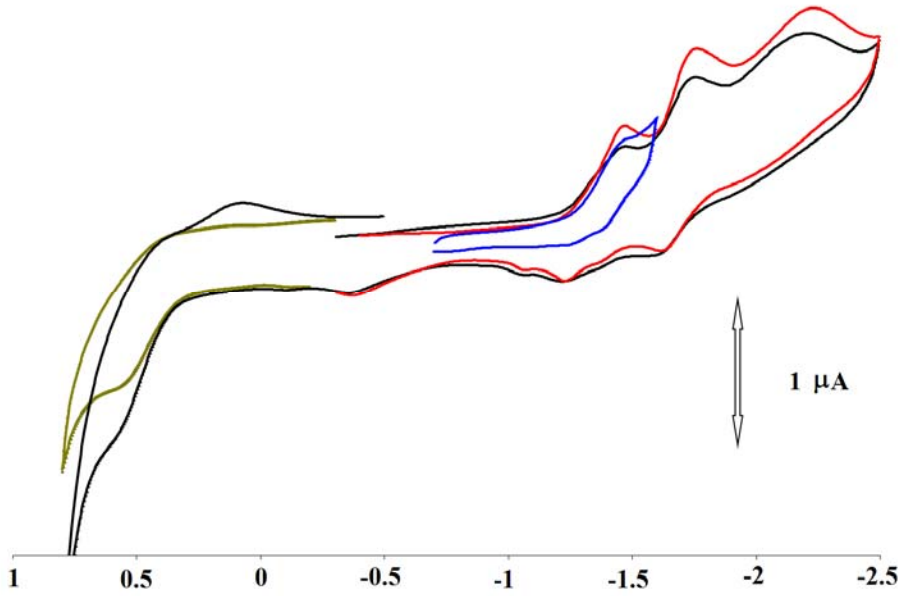

Figure 5.9. Cyclic voltammogram of the $Y_2@C_{79}N$

5.3.2.2. $Gd_2@C_{79}N$

As shown in Figure 10, the LD-TOF mass spectrum shows a strong signal at m/Z=1278, confirming the formation of $Gd_2@C_{79}N$. The inset of Figure 5.10 shows the satisfactory match of the calculated and experimental isotopic distributions.

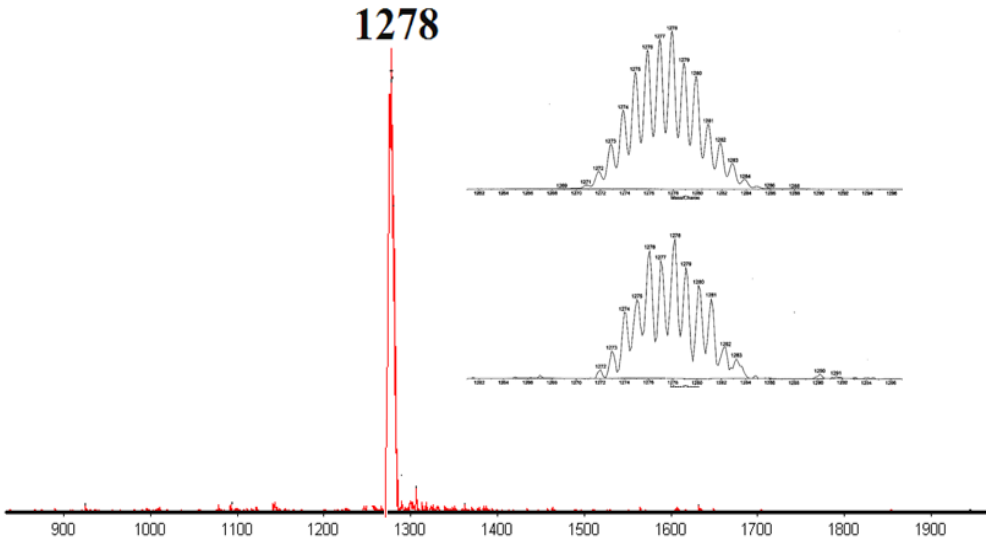

Figure 5.10. The LD-TOF mass spectrum of $Gd_2@C_{79}N$ with positive ionization

The UV-Vis spectrum of $Gd_2@C_{79}N$ is shown in Figure 5.11. Compared with the UV-Vis of $Y_2@C_{79}N$ (Figure 5), the similarity suggested that they have the same fullerene cage structure. The simulated structure of $Gd_2@C_{79}N$ is shown in Figure 5.12.

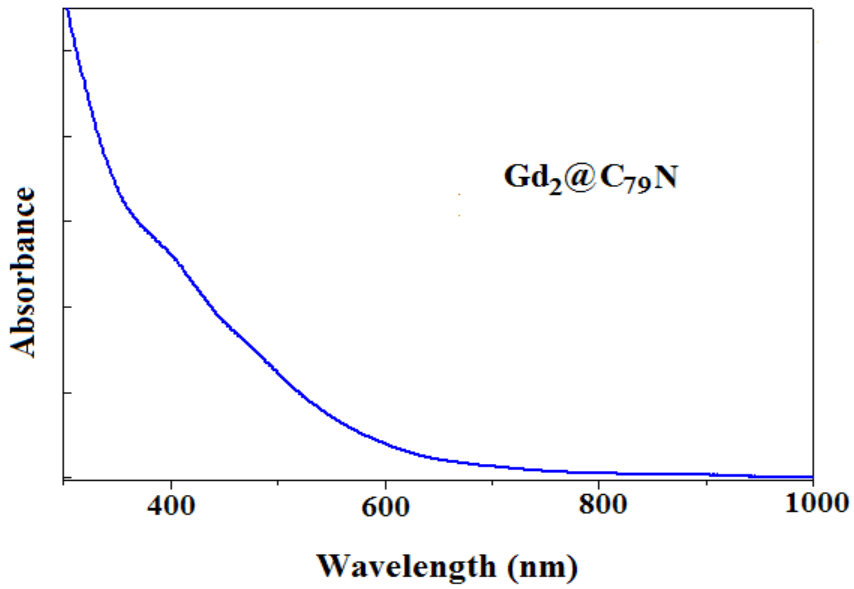

Figure 5.11. UV-Vis spectrum of purified $Gd_2@C_{79}N$ in toluene solution

It has been predicted that the formal electronic structure of $M_2@C_{79}N$ is described as $[M_2]^{5+}@[C_{79}N]^{5-12}$ which results from the charge transfer from the two metal atoms to the $C_{79}N$ cage. The electronic configuration of a Gd atom is

[Xe]$6s^2 4f^7 5d^1$. During the encapsulation process, the three electrons on the outer 6s and 5d orbital of one Gd atom and two electrons on the outer 6s orbital of the other Gd atom are transferred to the $C_{79}N$ cage. In a similar fashion, one electron is shared by two Gd ions. As a result, a radical spin is localized between the two Gd ions. However, for the Gd-based complex, it is well known that the EPR signal is not easily detected because of the extremely fast relaxation rates of Gd and rather broad EPR line widths.[18] Usually, extremely low temperature (for example, 4 K) is required to observe the hyperfine coupling.[19] However, for $Gd_2@C_{79}N$ case, the radical spin between two Gd ions plays an important role in the spin structure, resulting in an unusual long spin relaxation time, which enables the detection of EPR even at room temperature.

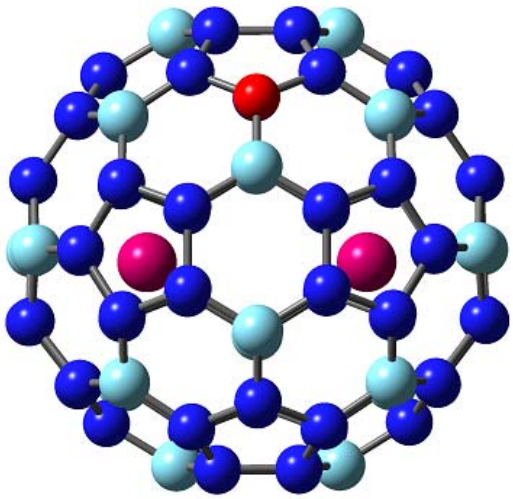

Figure 5.12. Structure of $Gd_2@C_{79}N$

The EPR spectra of $Gd_2@C_{79}N$ in toluene and solid state at room temperature are shown in Figure 5.13. It is surprising that the EPR signal of $Gd_2@C_{79}N$ was detected at room temperature in toluene and solid states, since it is normally invisible in other gadolinium complexes and fullerenes. For example, the Figure 5.13b is the EPR spectrum of pure $Gd_3N@C_{80}$ in toluene and there is no EPR signal detected. Thus EPR

signal of the $Gd_2@C_{79}N$ is due to the spin density located between two Gd ions not the Gd ions themselves. The spectra in toluene and in solid state are symmetrical. The reason is that the radical is in the center of two Gd ions and thus it experiences the same crystal field in all directions.

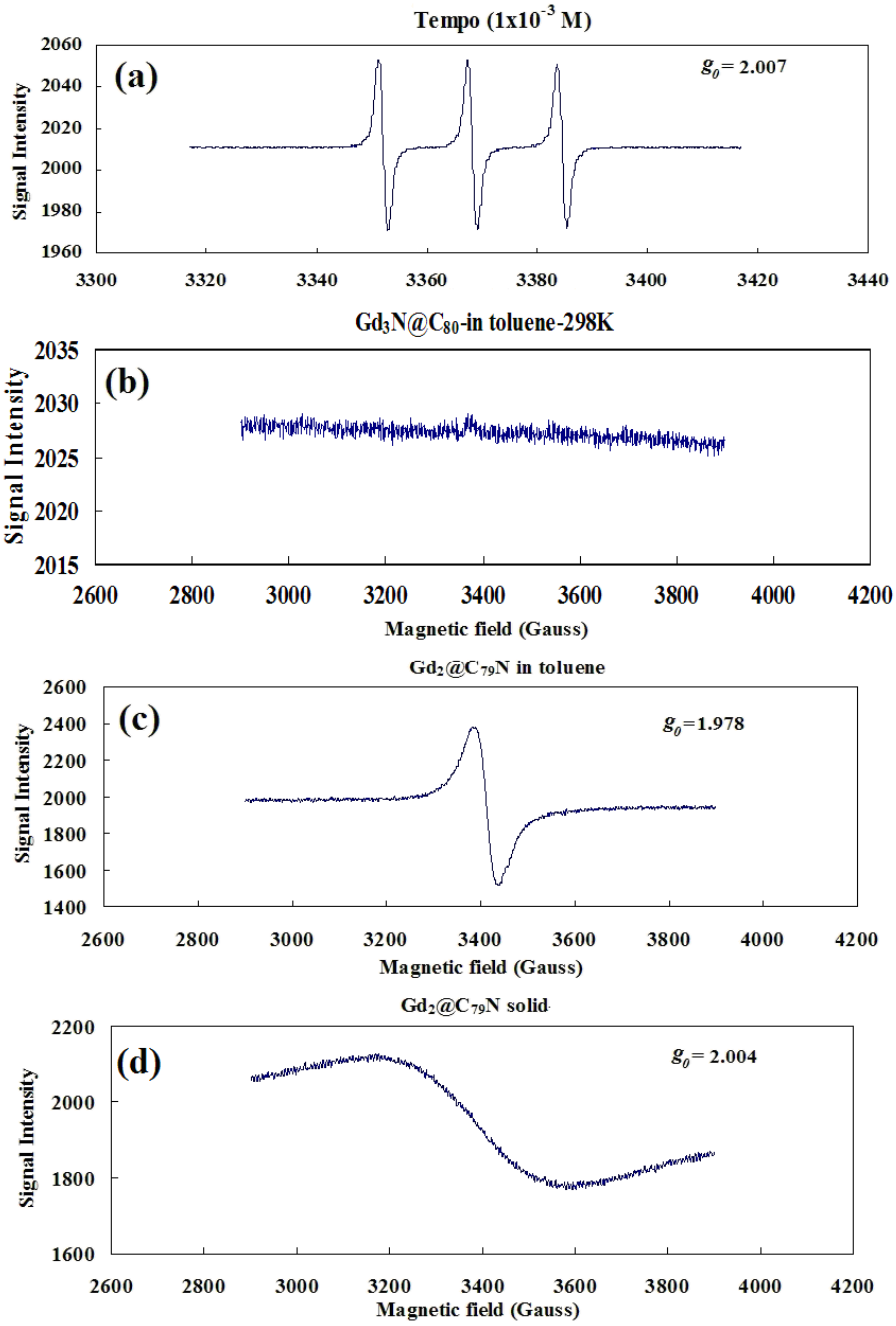

Figure 5.13. EPR spectra of (a) Tempo at 298 K and (b) $Gd_3N@C_{80}$ in toluene at 298 K and (c) $Gd_2@C_{79}N$ in toluene at 298 K (d) $Gd_2@C_{79}N$ in solid state at 298K

$Gd_2@C_{79}N$ in toluene exhibits an EPR spectrum consisting of a sharp single line; the observed g-factor (g_0=1.978), confirms that the EPR signal is due to the spin density localized between two Gd ions not the nitrogen atom (as g_0=2.007 in the TEMPO sample). The EPR spectrum of a solid $Gd_2@C_{79}N$ sample shows a broadened single line, which is due to Heisenberg exchange. The observed g-factor of the solid sample is g_0=2.004, suggesting that the spin density may transfer from the two Gd ions center to the $C_{79}N$ cage.

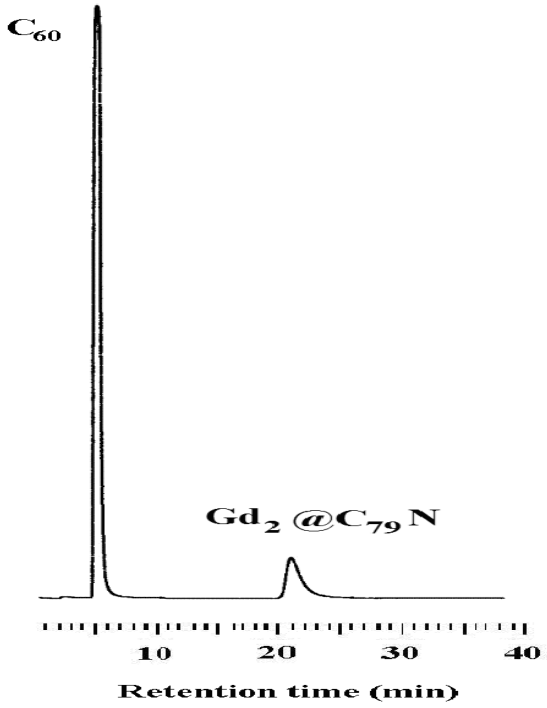

Figure 5.14. HPLC chromatogram of mixture of C_{60} and $Gd_2@C_{79}N$ (10 ×250 mm 5PBB column; λ=390 nm; flow rate 2.0 mL/min; toluene as eluent; 25 ºC)

The effect of Heisenberg exchange was confirmed by a solid-state dilution experiment where the $Gd_2@C_{79}N$ sample was mixed with C_{60}. The ratio of C_{60}: $Gd_2@C_{79}N$ was around 9:1, as shown in Figure 5.14. In the EPR of the C_{60}: $Gd_2@C_{79}N$ mixture, a sharp single line was observed, as illustrated in Figure 5.15a. The g-factor, g_0=1.978, was same as obtained in toluene solution. The EPR spectrum of the mixed

solid sample suggests nearly isotropic motion of the $Gd_2@C_{79}N$ molecule and/or Gd-Gd cluster motional averaging in the C_{60} solid matrix. There is a small sharp peak with the observed g-factor (g_0=2.001), which is due to the defective C_{60} radical,[20] as shown in Figure 5.15b.

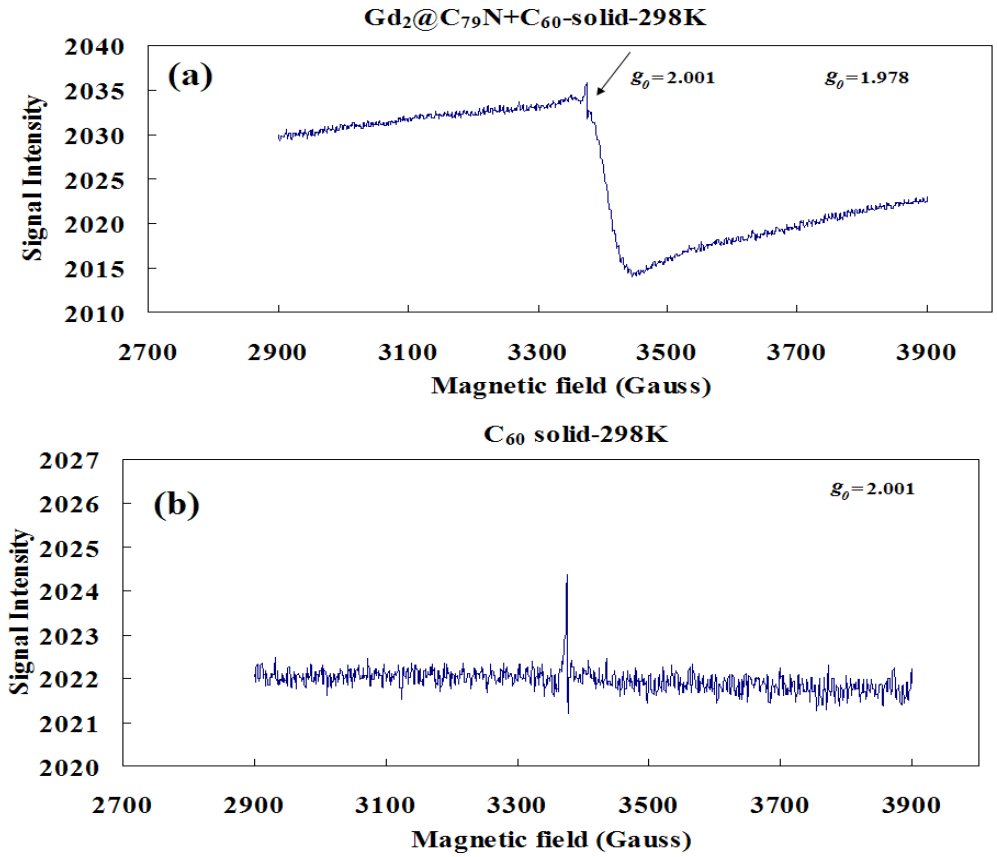

Figure 5.15. EPR spectra of (a) $Gd_2@C_{79}N$ samples in a solid solution with C_{60} at 298 K and (b) Pure C_{60} in solid state at 298 K

We also obtained the EPR spectra of $Gd_2@C_{79}N$ in the solid state in a wide range of temperatures, from 148 K to 388 K, to see the temperature dependence of EPR spectra (Figures 5.16 and 5.17). The signal at around 1600 Gauss is due to the glass tube used for EPR measurement. It was observed that when the temperature was low (148 K), the spectrum was more broadened than the spectrum measured at higher temperature, which may be due to random orientations at low temperatures.

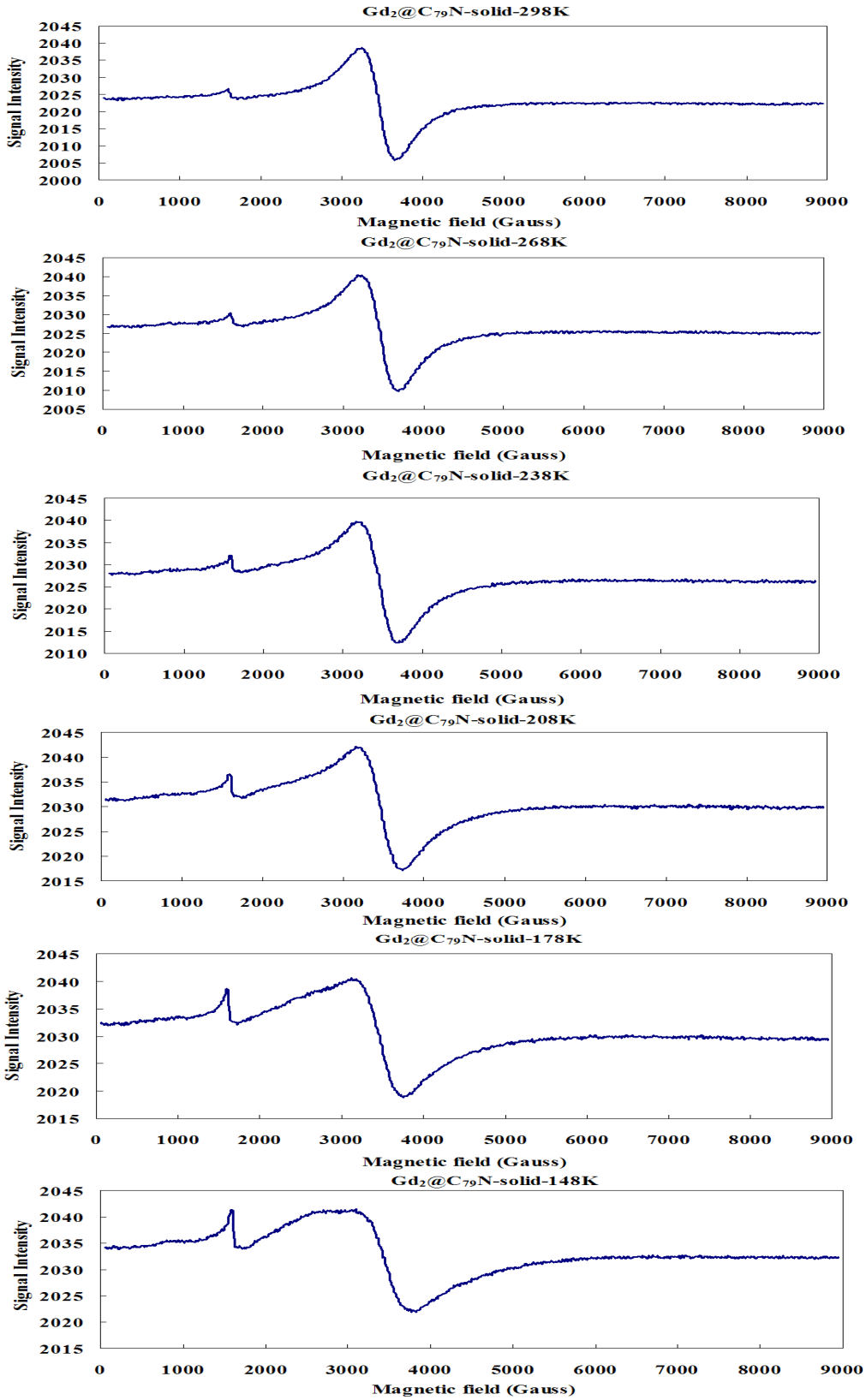

Figure 5.16. EPR spectra of $Gd_2@C_{79}N$ in solid state in a wide range of temperatures (from 148 K to 298 K)

The EPR spectra of $Gd_2@C_{79}N$ in the solid state at higher temperatures were also obtained. As shown in Figure 5.17, the EPR signal was still observed at higher temperature (up to 388 K); when the temperature returned to 298 K, the EPR signal was still observed. This suggests that this paramagnetic endohedralheterofullerene is very stable and can survive a wide range of temperatures.

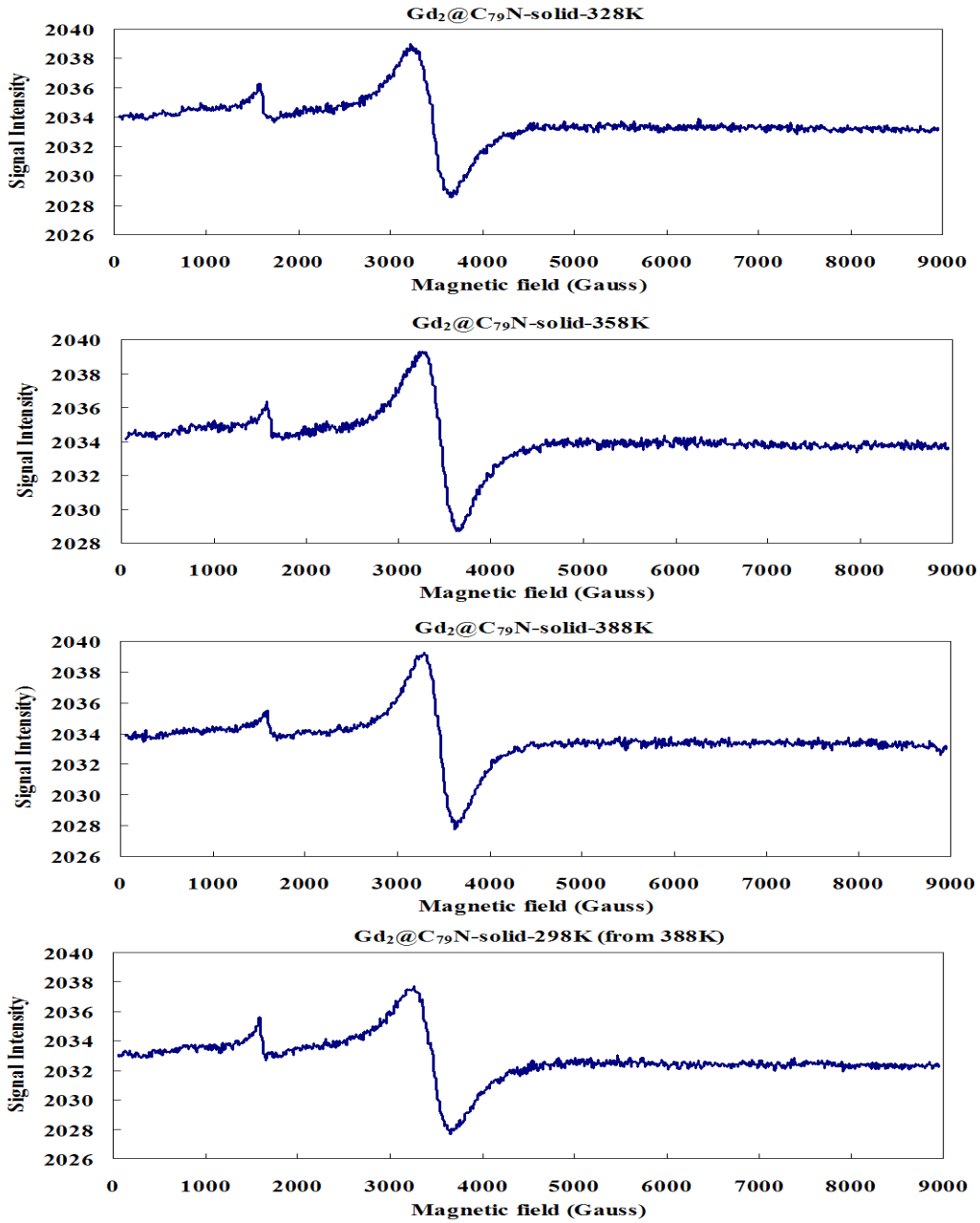

Figure 5.17. EPR spectra of $Gd_2@C_{79}N$ in solid state in a wide range of temperatures (from 298 K to 388 K)

The 5,5-Dimethyl-1-pyrroline N-oxide (DMPO) is a well known spin trap.[21, 22] We mixed DMPO with $Gd_2@C_{79}N$ in toluene to check whether the radical between the Gd ions can be trapped. The EPR measurement indicated that no reactions happened between DMPO and $Gd_2@C_{79}N$, as shown in Figure 5.18. This is consistent with the location of the radical, which is between two Gd ions within the fullerene cage and is not easily trapped.

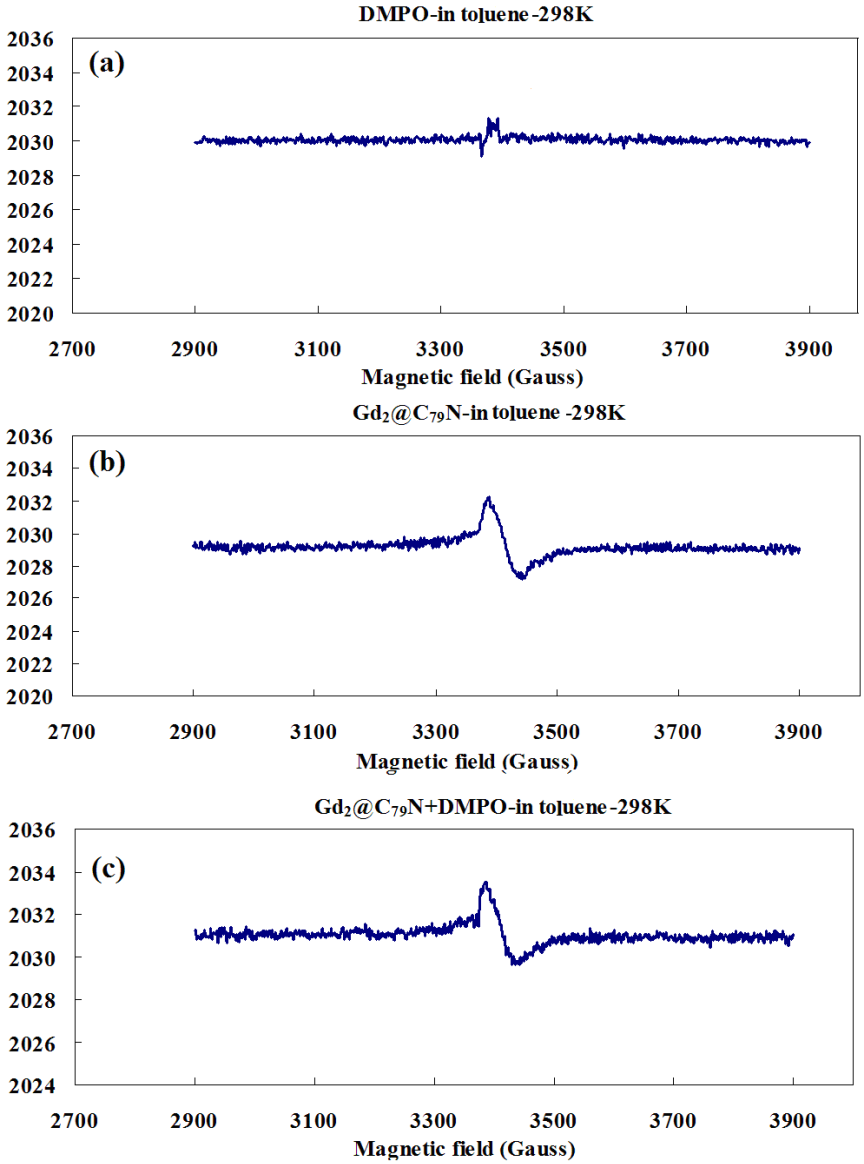

Figure 5.18. EPR spectra of (a) Pure DMPO in toluene at 298 K and (b) $Gd_2@C_{79}N$ in toluene at 298 K and (c) $Gd_2@C_{79}N$ and DMPO mixture in toluene at 298 K.

The hyperfine coupling between unpaired electron and two gadoliniums was observed at extremely low temperature X-band and W-band EPR measurement, as shown in Figure 5.19. Both spectra are featured by the fine structure of high spin state. The w-band measurement (Figure 5.19b) gave a more simplified spectrum, which was almost symmetric around the intense central line. Seven peaks on both side of the central line at equidistant intervals could be recognized and totally 15 peaks can be counted (inset of the Figure 5.19b). The 15 peaks suggest the spin quantum number of 15/2 for the spin state of $Gd_2@C_{79}N$. As previously reported,[19] the ground spin state of $Gd@C_{82}$-I was characterized by an integer spin quantum number of $S = 3$. The spin ($S = 1/2$) on the π orbital of the fullerene cage is coupled with the octet spin ($S = 7/2$) of the encapsulated gadolinium in an antiferromagnetic manner with the exchange coupling constant of $J = -1.8$ cm^{-1}. In the case of $Gd_2@C_{79}N$, however, the spin state is characterized by a half-integer spin quantum number of $S = 15/2$. The spin ($S = 1/2$) between two gadoliniums and two octet spins ($S = 7/2$) of two encapsulated gadoliniums was coupled with each other in a ferromagnetic manner. Because the central line of $Gd_2@C_{79}N$ was due to the Kramer's doublet in the state with a half-integer spin quantum number of $S = 15/2$, the sharpness of the line was prominent and the anisotropic nature of the line was weak.

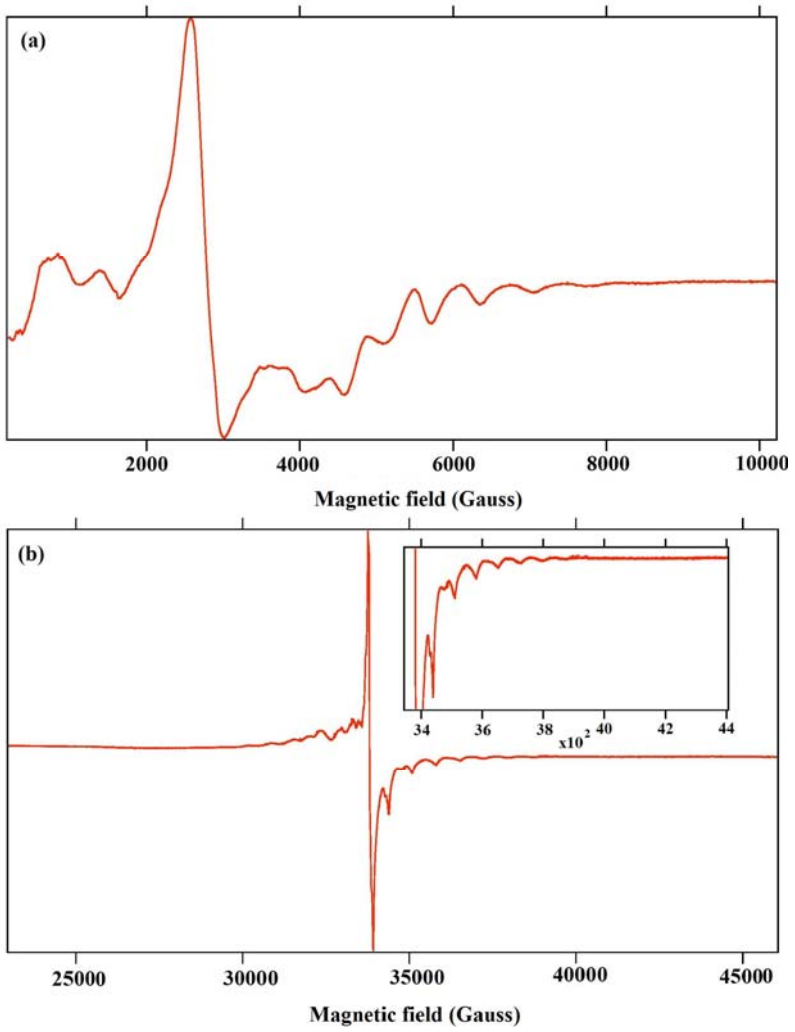

Figure 5.19. (a) X-band EPR spectrum of $Gd_2@C_{79}N$ sample at in CS_2 at 4 K (b) W-band EPR spectrum of $Gd_2@C_{79}N$ sample in CS_2 at 30 K

The electrochemical properties of $Gd_2@C_{79}N$ were studied by cyclic voltammetry, as shown in Figure 5.20 and are very similar to $Y_2@C_{79}N$. There are also three reduction peaks and one oxidation peak observed. The first and second reduction potentials ($^{red}E_1$, $^{red}E_2$, $^{red}E_3$) are -1.52, -1.79 and -2.24 V, respectively. The oxidation potential ($^{ox}E_1$) is 0.54 V. The resulting electrochemical bandgap ($^{ox}E_1$- $^{red}E_1$) for $Gd_2@C_{79}N$ is 2.06 V. This large electrochemical bandgap suggests the high stability of this unique material.

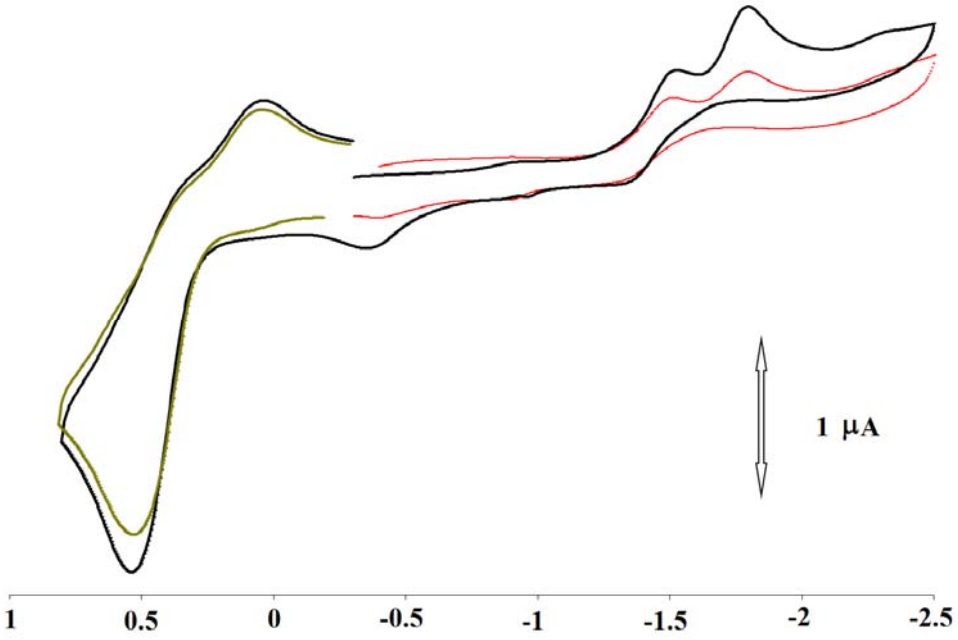

Figure 5.20. Cyclic voltammogram of the $Gd_2@C_{79}N$.

5.4. Summary

In summary, we have successfully prepared and characterized two paramagnetic endohedral metalloheterofullerenes, $Y_2@C_{79}N$ and $Gd_2@C_{79}N$. Based on the EPR study, the spin density of two paramagnetic samples is mainly located between two metallic ions. A spin-site exchange system can be constructed from $Y_2@C_{79}N$ and the organic donor TMPD. $Gd_2@_{79}N$ is a very stable paramagnetic material and the radical inside can survive over a wide range of temperatures. This unique property may be important to develop new materials useful for optical and magnetic applications. We are currently trying to obtain single crystals of these compounds for X-ray structural analysis to identify the position of nitrogen atom on the fullerene cage.

References:

(1) Vostrowsky, O.; Hirsch, A., Heterofullerenes. *Chem. Rev.* **2006,** (106), 5191-5207.

(2) Andreoni, W.; Curioni, A.; Holczer, K.; Prassides, K.; KeshavarzK, M.; Hummelen, J. C.; Wudl, F., Unconventional bonding of azafullerenes: Theory and experiment. *J. Am. Chem. Soc.* **1996,** *118* (45), 11335-11336.

(3) Hirsch, A.; Nuber, B., Nitrogen heterofullerenes. *Acc. Chem. Res.* **1999,** *32* (9), 795-804.

(4) Hummelen, J. C.; Knight, B.; Pavlovich, J.; Gonzalez, R.; Wudl, F., Isolation of the heterofullerene $C_{59}N$ as its dimer $(C_{59}N)_2$. *Science* **1995,** *269* (5230), 1554-1556.

(5) Kim, K. C.; Hauke, F.; Hirsch, A.; Boyd, P. D. W.; Carter, E.; Armstrong, R. S.; Lay, P. A.; Reed, C. A., Synthesis of the $C_{59}N^+$ carbocation. A monomeric azafullerene isoelectronic to C_{60}. *J. Am. Chem. Soc.* **2003,** *125* (14), 4024-4025.

(6) Wilson, L. J., Medical Application of Fullerenes and Metallofullerenes. *Electrochem. Soc. Interface•Winter* **1999**, 24-28.

(7) Okumura, M.; Mikawa, M.; Yokawa, T.; Kanazawa, Y.; Kato, H.; Shinohara, H., Evaluation of water-soluble metallofullerenes as MRI contrast agents. *Acad. Radiol.* **2002,** *9*, S495-S497.

(8) Bolskar, R. D.; Alford, J. M.; Benedetto, A. F.; Huesbo, L. O.; Wilson, L. J., Development of $Gd@C_{60}$ based MRI contrast agents. *Abstracts of Papers of the American Chemical Society* **2002,** *223*, U660-U661.

(9) Shu, C. Y.; Corwin, F. D.; Zhang, J. F.; Chen, Z. J.; Reid, J. E.; Sun, M. H.; Xu, W.; Sim, J. H.; Wang, C. R.; Fatouros, P. P.; Esker, A. R.; Gibson, H. W.; Dorn, H. C., Facile Preparation of a New Gadofullerene-Based Magnetic Resonance Imaging Contrast Agent with High H-1 Relaxivity. *Bioconjugate Chem.* **2009,** *20* (6), 1186-1193.

(10) Shu, C. Y.; Ma, X. Y.; Zhang, J. F.; Corwin, F. D.; Sim, J. H.; Zhang, E. Y.; Dorn, H. C.; Gibson, H. W.; Fatouros, P. P.; Wang, C. R.; Fang, X. H., Conjugation of a water-soluble gadolinium endohedral fulleride with an antibody as a magnetic resonance imaging contrast agent. *Bioconjugate Chem.* **2008,** *19* (3), 651-655.

(11) Akasaka, T.; Okubo, S.; Wakahara, T.; Yamamoto, K.; Kobayashi, K.; Nagase, S.; Kato, T.; Kako, M.; Nakadaira, Y.; Kitayama, Y.; Matsuura, K., Endohedrally metal-doped heterofullerenes: $La@C_{81}N$ and $La_2@C_{79}N$. *Chem. Lett.* **1999,** (9), 945-946.

(12) Zuo, T. M.; Xu, L. S.; Beavers, C. M.; Olmstead, M. M.; Fu, W. J.; Crawford, D.; Balch, A. L.; Dorn, H. C., $M_2@C_{79}N$ (M = Y, Tb): Isolation and characterization of stable endohedral metallofullerenes exhibiting M-M bonding interactions inside aza[80]fullerene cages. *J. Am. Chem. So.c* **2008,** *130* (39), 12992-12997.

(13) Ge, Z. X.; Duchamp, J. C.; Cai, T.; Gibson, H. W.; Dorn, H. C., Purification of

endohedral trimetallic nitride fullerenes in a single, facile step. *J. Am. Chem. Soc.* **2005,** *127* (46), 16292-16298.

(14) Knight, L. B.; Woodward, R. W.; Vanzee, R. J.; Weltner, W., Properties of Sc_3,Y_3, and Sc_{13}(Questionable) Molecules at Low-Temperatures, as Determined by Electron-Spin-Resonance. *J. Chem. Phys.* **1983,** *79* (12), 5820-5827.

(15) Tsuchiya, T.; Sato, K.; Kurihara, H.; Wakahara, T.; Maeda, Y.; Akasaka, T.; Ohkubo, K.; Fukuzumi, S.; Kato, T.; Nagase, S., Spin-site exchange system constructed from endohedral metallofullerenes and organic donors. *J. Am. Chem. Soc.* **2006,** *128* (45), 14418-14419.

(16) Tsuchiya, T.; Sato, K.; Kurihara, H.; Wakahara, T.; Nakahodo, T.; Maeda, Y.; Akasaka, T.; Ohkubo, K.; Fukuzumi, S.; Kato, T.; Mizorogi, N.; Kobayashi, K.; Nagase, S., Host-guest complexation of endohedral metallofullerene with azacrown ether and its application. *J. Am. Chem. Soc.* **2006,** *128* (20), 6699-6703.

(17) Tsuchiya, T.; Kurihara, H.; Sato, K.; Wakahara, T.; Akasaka, T.; Shimizu, T.; Kamigata, N.; Mizorogi, N.; Nagase, S., Supramolecular complexes of La@C_{82} with unsaturated thiacrown ethers. *Chem. Comm.* **2006,** (34), 3585-3587.

(18) Atsarkin, V. A.; Demidov, V. V.; Vasneva, G. A.; Odintsov, B. M.; Belford, R. L.; Raduchel, B.; Clarkson, R. B., Direct measurement of fast electron spin-lattice relaxation: Method and application to nitroxide radical solutions and Gd^{3+} contrast agents. *J. Phys. Chem. A* **2001,** *105* (41), 9323-9327.

(19) Furukawa, K.; Okubo, S.; Kato, H.; Shinohara, H.; Kato, T., High-field/high-frequency ESR study of Gd@C_{82}-I. *J. Phys. Chem. A* **2003,** *107* (50), 10933-10937.

(20) Kempinski, W.; Piekara-Sady, L.; Katz, E. A.; Shames, A. I.; Shtutina, S., C_{60}^{+} defect centers: effect of rubidium intercalation into C_{60} studied by EPR. *Solid State Commun.* **2000,** *114* (3), 173-176.

(21) Hashimoto, M.; Nakai, Y.; Kohno, M.; Tajima, K.; Kanaori, K.; Endo, N.; Makino, K., DMPO spin trapping of superoxide anion in strong alkaline DMSO solution. *Chem. Lett.* **1997,** (1), 71-72.

(22) Reszka, K. J.; McCormick, M. L.; Buettner, G. R.; Hart, C. M.; Britigan, B. E., Nitric oxide decreases the stability of DMPO spin adducts. *Nitric Oxide-Biol. Chem.* **2006,** *15* (2), 133-141.

Chapter 6

Preparation and characterization of Hydrogenated Scandium-based TNT EMF

6.1. Introduction

Since the discovery and isolation of fullerenes in macroscopic amounts,[1] the chemical modification of these new material has attracted wide interest because of their potential applications in various areas, such as photovoltaic devices,[2, 3] molecular electronics[4, 5] and energy storage materials.[6, 7] Hydrogenation of fullerenes is of fundamental interest, particularly in relation to their potential use as hydrogen storage materials. Various theoretical and experimental studies have been devoted to carbon nanomaterials (nanotubes, fullerenes and nanofibers) for their storage capacities for hydrogen.[8-12] Fullerenes are considered to be one form of carbon that can be conveniently hydrogenated and dehydrogenated reversibly due to their unique curved molecular structure.[13] Established routes for hydrogenation of fullerenes include Birch reduction,[14] hydroboration,[15] solid phase hydrogenation,[16] electrochemical reduction[17] as well as dissolving metal reductions[18] and hydrogen radical induced hydrogenation.[19]

The first hydrogenated fullerene was prepared by Birch reduction in 1990 and $C_{60}H_{36}$ was described as the main product.[14] Despite early skepticism, this experiment has been repeated successfully in several laboratories.[20, 21] These extensive studies, both computational and experimental, have been applied to determine the structure of

this unique product.[22-24] Soon after, similar routines were applied to hydrogenate other empty fullerene cages, such as C_{70}, C_{76} and C_{84}.[25, 26] However, the structures of the most of the hydrogenated fullerenes remain unclear because of multiple isomers and instabilities of the samples. All hydrogenation reactions to date reported have focused on empty-cages fullerenes and only partially hydrogenated products have been obtained. Darwish *et al.* have reported that the attempted reduction of $C_{60}H_{36}$ over rhodium/alumina catalysts for ten days did not reveal any further hydrogenation of the C_{60} cage.[18]

In this chapter, we report the preparation and characterization of a hydrogenated TNT EMF, specially, $Sc_3N@C_{80}$ by the Benkeser reduction.[6, 27] Our study demonstrated that a highly reduced TNT EMF can be synthesized. Analysis of the hydrogenated product by MALDI-TOF mass spectrometry indicated the formation of $Sc_3N@C_{80}H_{80}$. In addition, as a by-product, a water-soluble $Sc_3N@C_{80}$ derivative containing amino functional groups was also prepared and characterized.

6.2. Experimental Section

Preparation and Separation: The hydrogenation of TNT EMF was carried out by the Benkeser reduction,[6, 27] which is the modification of the classic Birch reduction by replacing the ammonia solvent with a low-molecular-weight amine, as shown in Scheme 6.1. $Sc_3N@C_{80}$ (6.0 mg, 0.0054 mmol) were dissolved in 12 mL of ethylenediamine (0.5 mg/mL concentration) and 404 mg (5.5 mmol) of tert-butanol was added. The resulting solution was deoxygenated with bubbling argon for 30 min, and

38 mg (5.5 mmol) of lithium metal was added. The mixture was stirred vigorously under a N_2 atmosphere. The dark brown solution changed to yellow and then blue. The blue color disappeared quickly due to the decay of the solvated electrons. After 24 hours, the solution turned pale yellow. The resulting solution was then poured into 10 mL of ice water to destroy the excess lithium metal. The mixture was extracted with toluene, and the two layers separated. The toluene layer was washed with brine and dried over anhydrous Na_2SO_4 and evaporated under reduced pressure to obtain hydrogenated product.

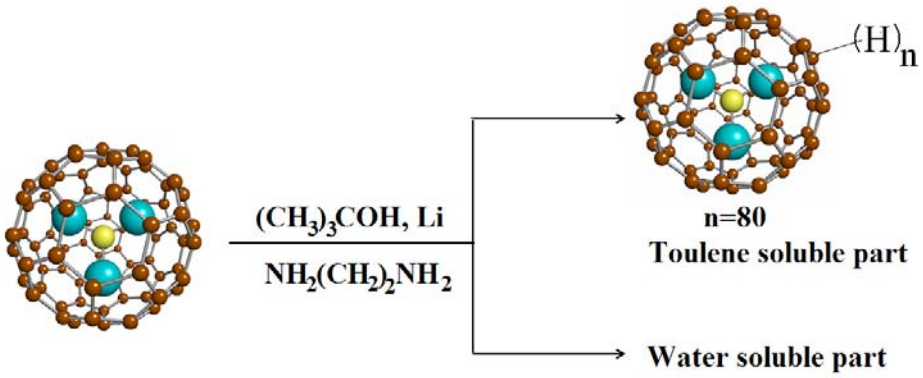

Scheme 6.1. Hydrogenation of $Sc_3N@C_{80}$ via Benkeser Reduction

The water layer contains amino functionalized water-soluble $Sc_3N@C_{80}$. However, the water solubility is not very good. In order to increase the water solubility of the amino functionalized $Sc_3N@C_{80}$, further treatment was carried out. The water layer was concentrated to 4 ml and then 50 % NaOH (4 ml) and few drops of H_2O_2 were added. The mixture was stirred at room temperature overnight, and then dialyzed via an egg membrane to remove excess NaOH, t-butanol and other impurities. The resultant solution was concentrated and then chromatographed on a Sephadex G-25

size-exclusion gel column with distilled water as eluent. The brown fractions were collected and characterized by MALDI-TOF mass spectrometry. The detailed process is shown in Scheme 6.2.

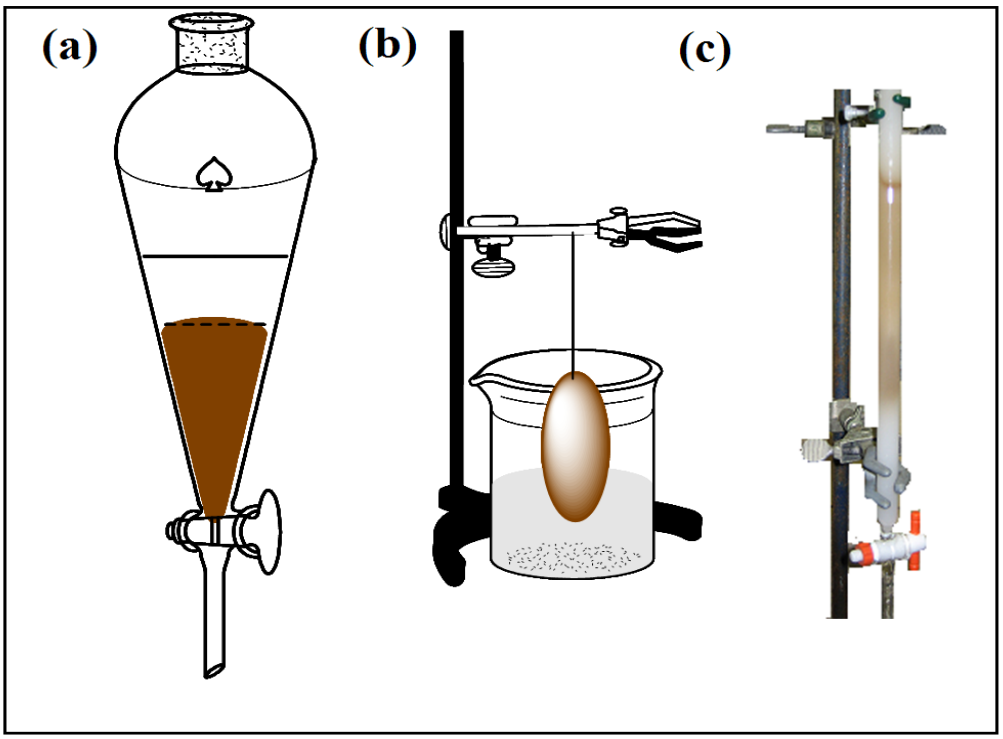

Scheme 6.2. Treatment of water-soluble $Sc_3N@C_{80}$.derivatives containing amino functional groups. (a) separation of hydrogenated product and water-soluble $Sc_3N@C_{80}$.derivatives; (b) dialyzed via an egg membrane; (c) chromatographed on a Sephadex G-25 size-exclusion gel column

Characterization: HPLC investigations were carried out on a PYE column (250 x 10 mm) at ambient temperature using toluene as mobile phase, at a flow rate of 1.0 mL/min. A JEOL ECP 500 MHz instrument was used for all NMR measurements. Mass spectrometry was performed on a Kratos Analytical Kompact SEQ MALDI-TOF mass spectrometer. XPS measurements were taken with a 5400 XPS from Perkin-Elmer using 250 W Mg Kα (1253.6) radiation. The X-Ray power supply was 13 kv and vacuum was 1×10^{-7} Torr.

6.3. Results and Discussion

6.3.1. Hydrogenated $Sc_3N@C_{80}$

Typical high-performance liquid chromatography (HPLC) traces of $Sc_3N@C_{80}$ and hydrogenated product are presented in Figure 6.1. After the reaction was complete, the brown color of the starting $Sc_3N@C_{80}$ disappeared, suggesting the $Sc_3N@C_{80}$ was completely consumed. This is consistent with the HPLC chromatogram. As shown in Figure 6.1b, there is no $Sc_3N@C_{80}$ left and one main peak eluting at 15.5 min is due to the pale yellow hydrogenated product.

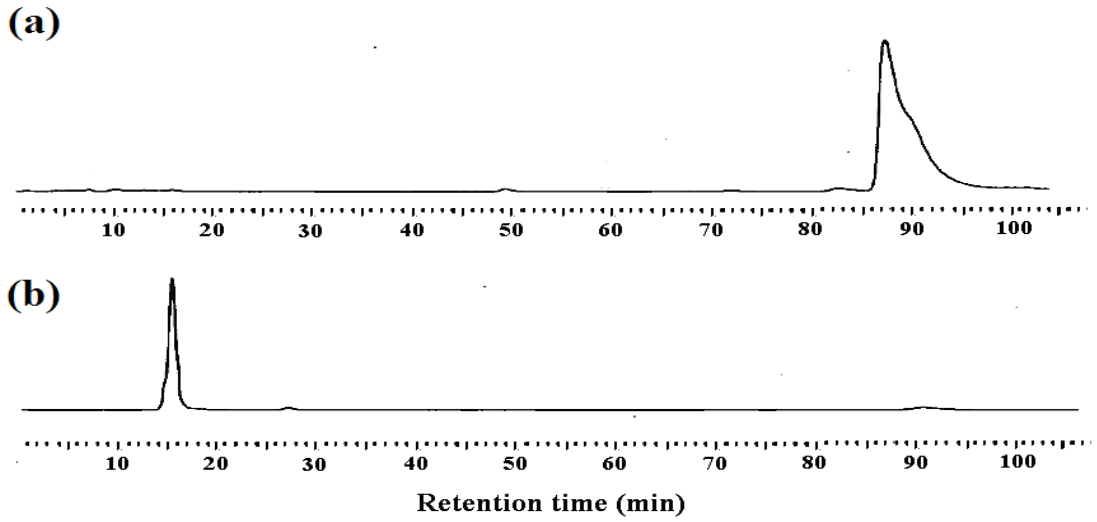

Figure 6.1. (a) HPLC chromatogram of purified $Sc_3N@C_{80}$; (b) HPLC chromatogram of hydrogenated $Sc_3N@C_{80}$ (10 x 250 mm PYE column; λ=335 nm; flow rate 1.0 mL/min; toluene as eluent; 25 ºC)

The mass spectrum of the hydrogenated product detected strong signals at m/z 1190, indicating the formation of $Sc_3N@C_{80}H_{80}$. Simultaneously, because of the sensitivity of the hydrogenated fullerene to light and oxygen, a small satellite peak at m/z 1206 was observed, which was assigned to be $Sc_3N@C_{80}H_{80}O$.[28] In addition, the

peak at m/z 1110 is attributed to the fragment of $Sc_3N@C_{80}$ formed by loss of the hydrogen from hydrogenated $Sc_3N@C_{80}$ under laser desorption.

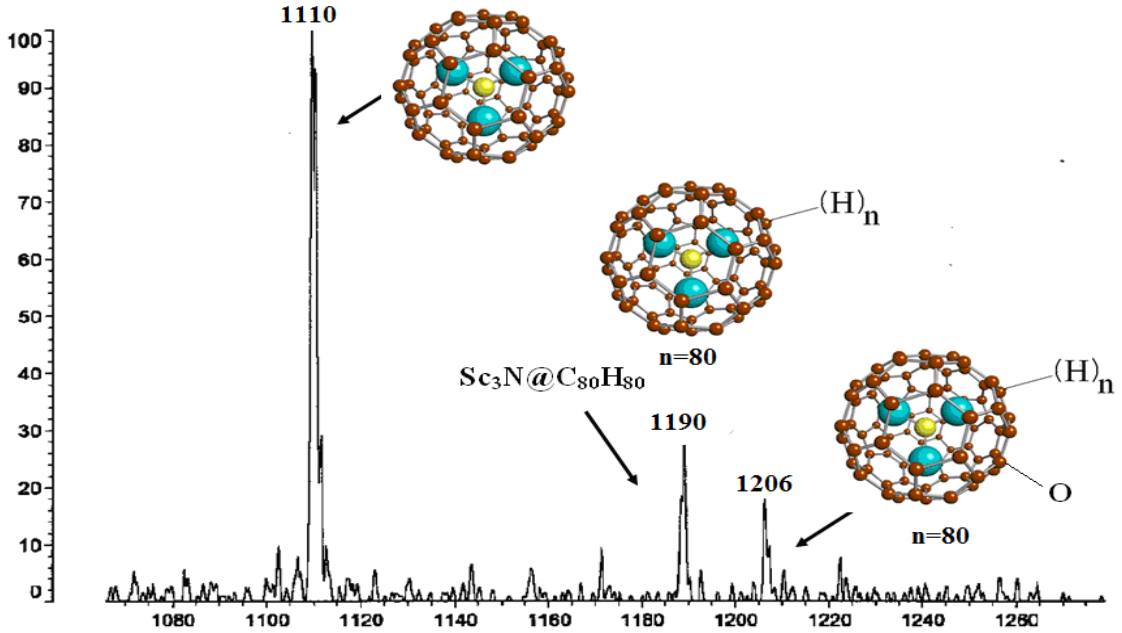

Figure 6.2. The MALDI-TOF mass spectrum of hydrogenated $Sc_3N@C_{80}$ using a 9-nitroanthracene matrix with positive ionization

As discussed in Chapter 1, obtaining a satisfying ^1H NMR spectrum for hydrogenated fullerenes has proved to be difficult due to the existence of multiple isomers and instability of the hydrogenated fullerene, especially for highly hydrogenated fullerenes.[24, 28, 29] The reported ^1H spectra of $C_{60}H_{36}$ exhibited the broad, featureless signals between 2.5 and 4.2 ppm.[24, 28] The 500 MHz ^1H spectrum of the hydrogenated $Sc_3N@C_{80}$ sample is shown in Figure 6.3. This spectrum showed one broad signal, which is centered at δ = 1.25 ppm. The peaks at 7.26 ppm are from solvent ($CDCl_3$). Other peaks are possibly due to the impurities in the sample. Compared with ^1H spectra of hydrogenated C_{60} reported previously, a steady upfield shift was observed because of the increasing content of hydrogen.[24, 30] This result could

be reproduced over the course of several different synthesis and purification procedures.

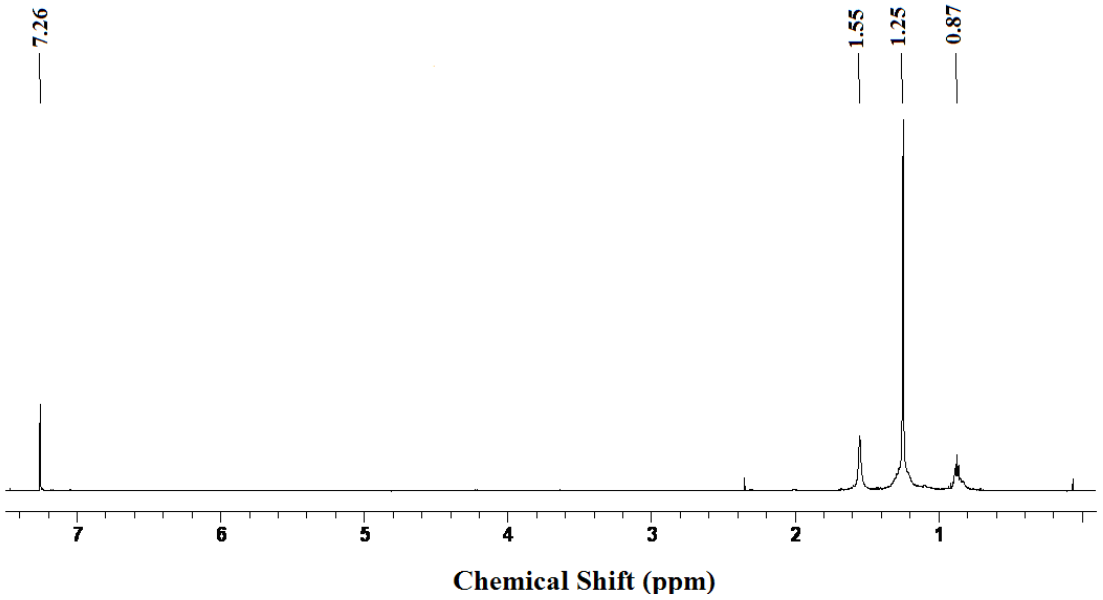

Figure 6.3. 500MHz ^{1}H NMR spectrum of the $Sc_3N@C_{80}H_{80}$ in d-chloroform at 25 ºC

The heteronuclear multiple quantum coherence (HMQC) spectrum of hydrogenated $Sc_3N@C_{80}$ reveals that the broad hydrogen peak at 1.25 ppm is related with the carbons with chemical shift around 30 ppm, which is within the sp^2 hybridized carbons region. As discussed in Chapter 3, the ^{13}C NMR shift of sp^2 hybridized carbons for fullerenes and EMFs is normally within 125-170 ppm range.[31] The broad carbon signals observed in the sp^3 region were ascribed to sp^3 hybridized carbons formed by hydrogenation of $Sc_3N@C_{80}$.[24] HMQC also indicated the hydrogen attached on the two different types of carbon and the ratio is 3:1, which is consistent with the "in-out" isomerism of $C_{80}H_{80}$.[32] Similar broad signals have been previously observed in a ^{13}C spectrum of $C_{60}H_{36}$ prepared by Birch reduction.[24]

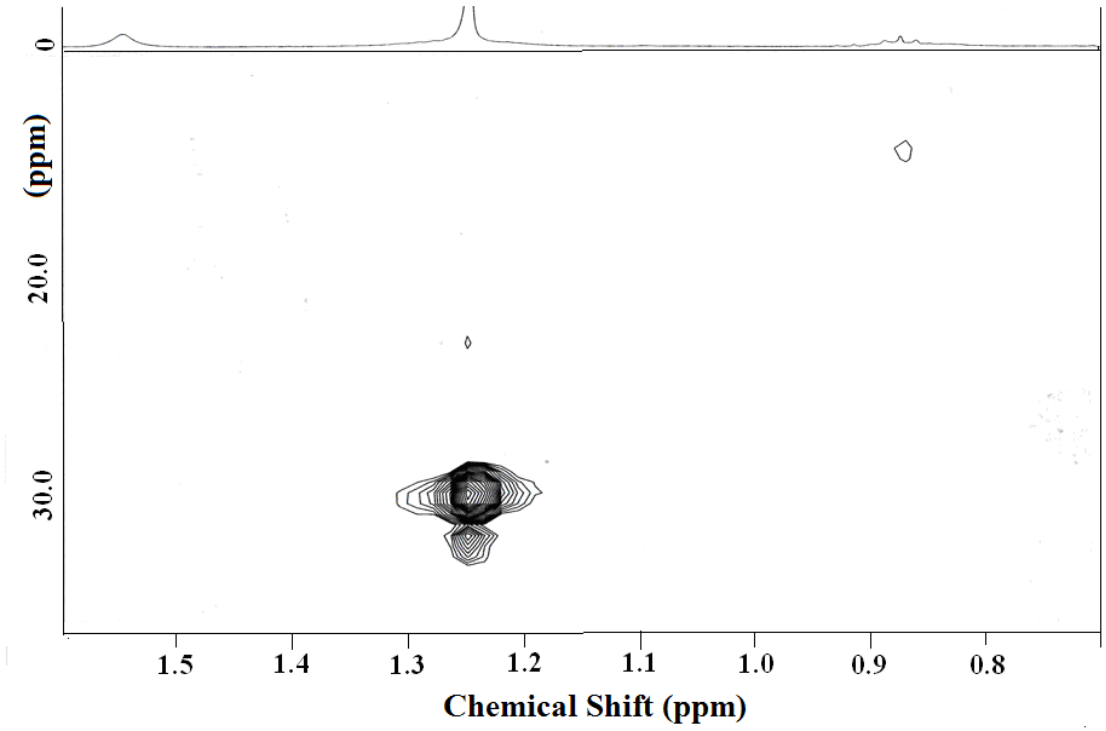

Figure 6.4. The 500 MHz HMQC spectrum of $Sc_3N@C_{80}H_{80}$ in d-chloroform at 25 ºC

The FT-IR spectrum of hydrogenated $Sc_3N@C_{80}$ is shown in Figure 6.5. The strong absorptions at 2922 and 2852 cm^{-1} suggest the presence of C-H bonds. The peaks around 2300 cm^{-1} are due to the asymmetric stretch of CO_2 from the air. The peaks ranging from 1700 cm^{-1} to 1000 cm^{-1} indicate that the spherical fullerene cage is still present but distorted.[27] The presence of bands at 600 cm^{-1} may be due to the strong Sc-N cluster stretching frequency.[33]

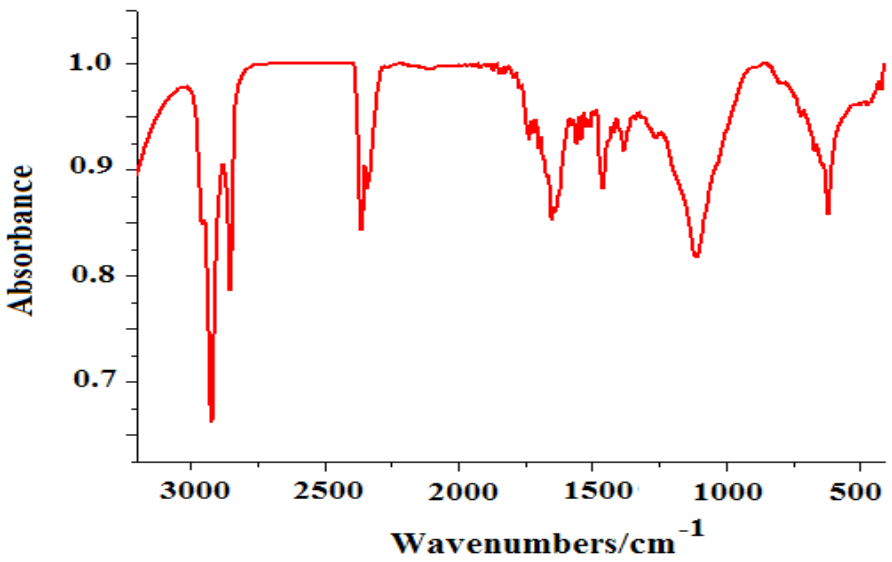

Figure 6.5. FTIR spectrum (KBr) of $Sc_3N@C_{80}H_{80}$

As shown in Figure 6.6, the UV-Vis absorption spectrum of $Sc_3N@C_{80}H_{80}$ is drastically different from that of the original $Sc_3N@C_{80}$, consistent with a much less extended π system. In addition, $Sc_3N@C_{80}H_{80}$ in toluene is very lightly colored even at high concentration, consistent with a highly altered chromophore.

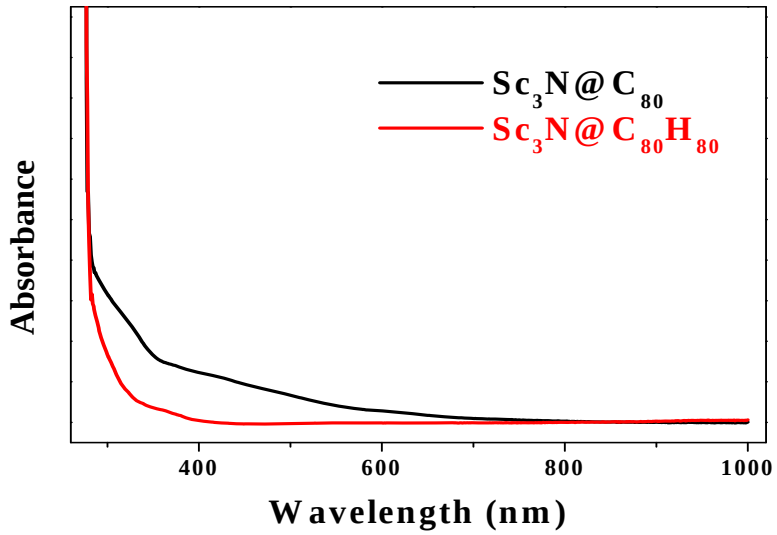

Figure 6.6. UV-Vis spectra of $Sc_3N@C_{80}$ and hydrogenated $Sc_3N@C_{80}$ in toluene solution

The thermal decomposition of hydrogenated product was performed in a sealed, vacuumed quartz tube. After 12 hours heating at 500 °C, the sample color changed from light yellow to black (Figure 6.7). HPLC and MALDI-TOF MS for the toluene

soluble portion of the heat treated sample confirmed the presence of the $Sc_3N@C_{80}$ (Figure 6.8). In addition, a small amount of residual insoluble black material was also observed. Temperature programmed desorption (TPD) thermograms for hydrogen desorption detected the molecular hydrogen released.

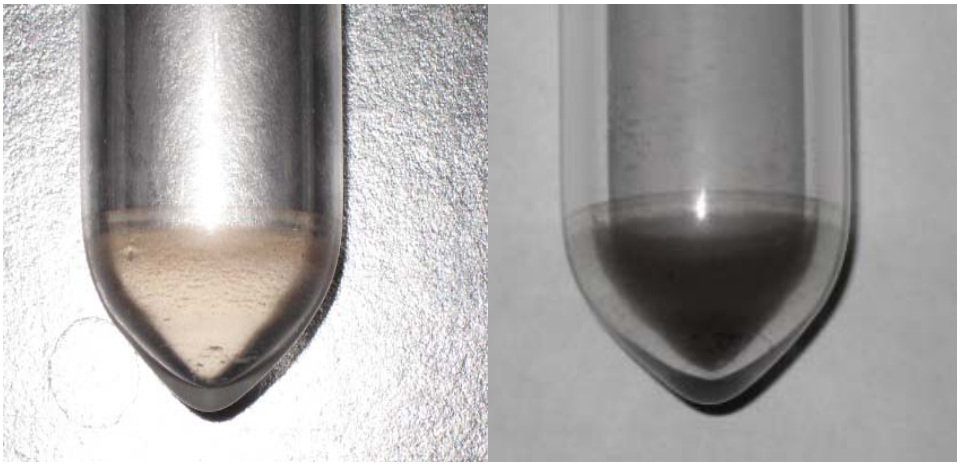

(a) (b)

Figure 6.7. Decomposition of hydrogenated $Sc_3N@C_{80}$ at 500 ºC (a) before heating; (b) after heating

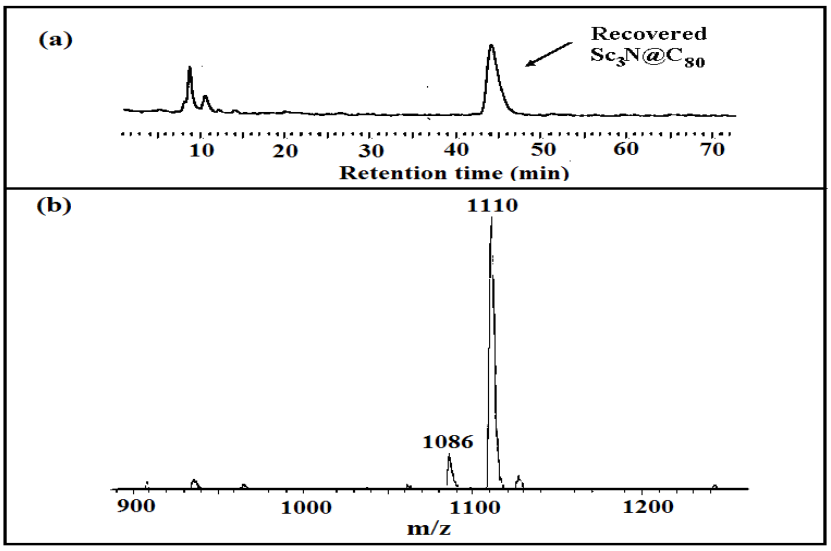

Figure 6.8. (a) HPLC chromatogram for the thermally treated hydrogenated $Sc_3N@C_{80}$ (10 x 250 mm PYE column; λ=335 nm; flow rate 2.0 mL/min; toluene as eluent; 25 ºC) (b) MALDI-TOF mass spectrum of thermally treated hydrogenated $Sc_3N@C_{80}$ using a 9-nitroanthracene matrix with positive ionization

The mass spectrometric data indicates the formation of the fully hydrogenated $Sc_3N@C_{80}$ and the subsequent characterization indicated that thermal treatment causes reversion to molecular and $Sc_3N@C_{80}$. However, the structure of $Sc_3N@C_{80}H_{80}$ is not well described. Based on DFT theoretical calculation, Linnolahti and co-workers[32] postulated an interesting "in-out" isomerism. When 20 interconnecting carbons were hydrogenated inside and the remaining 60 carbons was hydrogenated outside, remarkably stable I_h-symmetric $C_{80}H_{80}$ will be produced, whose energy per CH unit is even lower than that of dodecahedrane, which was optimal for sp^3 hybridization. This "in-out" isomer of $C_{80}H_{80}$ allows each carbon to adopt the tetrahedral configuration, which is optimal for sp^3 hybridization. More recently, Zhao *et. al.*[34] predicted the encapsulated metals in the fullerene cage can increase the hydrogenation capacity and improve the energy efficiency for hydrogen storage because the C-H binding is strengthened at higher H densitities (X>36): this prediction is complete with complete hydrogenation of the present TNT EMF structure.

6.3.2. Water-soluble $Sc_3N@C_{80}$ Derivative

As unique types of molecules, EMFs exhibit a wide range of exciting biological properties and display special promise in medical and life sciences.[35-40] For example, metallofullerenes with paramagnetic metals inside can be used as magnetic resonance imaging (MRI) contrast agents,[37, 38] those with heavy metals inside may be utilized as contrast agents in X-ray,[39] and those will be good radiotracers if encapsulated is a radio-active metal.[40] However, the strongly hydrophobic nature of the EMFs is a

serious drawback for the development of biological application. Intense effort has focused on preparing and characterizing "truly" water-soluble EMFs derivatives.[41, 42]

As discussed in the experimental section, there are two fractions resulting from hydrogenation reaction. One is a light yellow toluene layer and the other is a brown water-soluble layer. The toluene soluble fraction is hydrogenated $Sc_3N@C_{80}$ and the water layer contains amino functionalized water-soluble $Sc_3N@C_{80}$.

Similar to other water-soluble fullerene derivatives, it is difficult to analyze the fullerene derivatives directly by mass spectroscopy,[43] but the data serves to establish a good understanding of the components of sample. As shown in Figure 6.9, mass spectral analyses of the water-soluble derivative reveal a series of fragments of the amino derivatives having fewer adduct groups per $Sc_3N@C_{80}$ sphere than the supposed parent compound, which was most likely due to the intense laser stripping off the functional groups on the EMF cage. The signal at 1109 also indicated the existence of the intact $Sc_3N@C_{80}$, which validates the successfully modification of $Sc_3N@C_{80}$, since the bare $Sc_3N@C_{80}$ itself is completely insoluble in water.

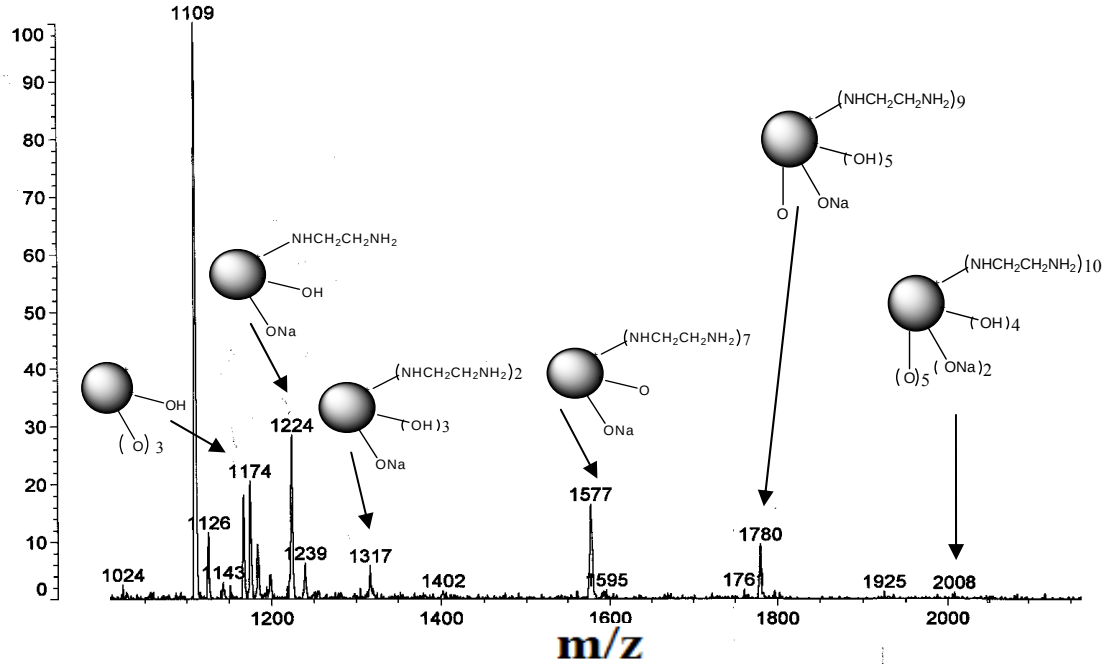

Figure 6.9. MALDI-TOF mass spectrum of water-soluble $Sc_3N@C_{80}$ derivatives using a S8 as matrix with positive ionization

The XPS spectrum of the water-soluble $Sc_3N@C_{80}$ derivative shows three main peaks in the regions of C1s，O1s, and N1s. There is no Sc metal observed because of the shielding by the carbon cage and low sensitivity. The XPS pattern of fraction 1 in the core level region of Cls is shown on Figure 6.10. A simple curve-fitting analysis showed that C1s feature of fraction 1 can be split to four peaks, in which the main peak at a binding energy of 285.2 eV (46.5%) is assigned to the non-oxygenated carbon, the second peak at 286.7 eV (32.6%) is assigned to the carbons linked with a single hydroxyl group or amino group, the third peak at 288.4 eV (18.8 %) is due to the existence of carbonyl groups, and the fourth peak located at 289.92 eV(2.2 %) is nearly 4 eV higher than that of the main peak, indicating the existence of carboxyl group. By calculating the C/O/N ratio from the XPS peak areas, the molecular formula of

water-soluble $Sc_3N@C_{80}$ Derivatives can be estimated as $Sc_3N@C_{80}(OH)_mO_n(NHCH_2CH_2NH_2)_l$ (m ≈13, n ≈26, l ≈10).

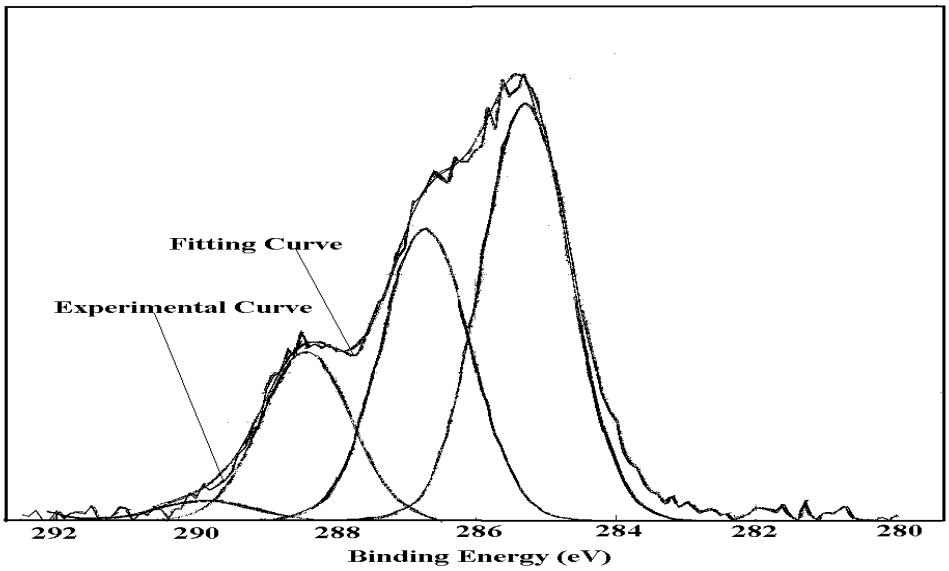

Figure 6.10. XPS spectrum of the C1s binding energy of water-soluble $Sc_3N@C_{80}$ derivative

The UV-Vis spectra of $Sc_3N@C_{80}$ and water-soluble $Sc_3N@C_{80}$ derivative are shown in Figure 6.11. The difference between the two spectra indicates that the cage structure of $Sc_3N@C_{80}$ was largely changed after chemical modification.

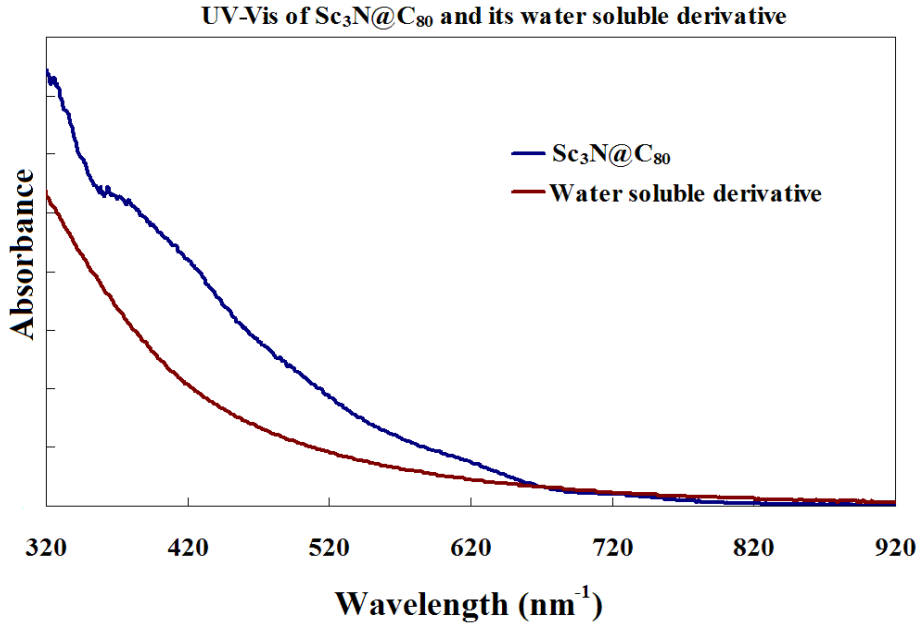

Figure 6.11. UV-Vis spectra of $Sc_3N@C_{80}$ in toluene solution and its water-soluble derivative in H_2O

6.4. Summary

In summary, we have synthesized and characterized hydrogenated $Sc_3N@C_{80}$ and a corresponding water-soluble $Sc_3N@C_{80}$ derivative containing amino functional groups. A remarkable result is the high degree of hydrogenation of metallofullerene C_{80} cage that is achieved. Thermal treatment in a sealed, vacuum quartz tube demonstrate that the hydrogen is released 500 ^{o}C and pristine $Sc_3N@C_{80}$ is recovered in this reversion process. This study indicates that TNT EMFs could be promising hydrogen storage materials. However, the detail structure of the hydrogenated and water soluble derivatives is still unknown and further characterization is needed.

References:

(1) Kroto, H. W.; Heath, J. R.; Obrien, S. C.; Curl, R. F.; Smalley, R. E., C_{60} - Buckminsterfullerene. *Nature* **1985,** *318* (6042), 162-163.

(2) Thompson Barry, C.; Frechet Jean, M. J., Polymer-fullerene composite solar cells. *Angew. Chem. Int. Ed.* **2008,** *47* (1), 58-77.

(3) Ross, R. B.; Cardona, C. M.; Guldi, D. M.; Sankaranarayanan, S. G.; Reese, M. O.; Kopidakis, N.; Peet, J.; Walker, B.; Bazan, G. C.; Van Keuren, E.; Holloway, B. C.; Drees, M., Endohedral fullerenes for organic photovoltaic devices. *Nature Mater.* **2009,** *8* (3), 208-212.

(4) Dunsch, L.; Yang, S., Metal nitride cluster fullerenes: Their current state and future prospects. *Small* **2007,** *3* (8), 1298-1320.

(5) Kitaura, R.; Shinohara, H., Endohedral metallofullerenes and nano-peapods. *Jpn. J. Appl. Phys.* **2007,** *46* (3A), 881-891.

(6) Peera, A. A.; Alemany, L. B.; Billups, W. E., Hydrogen storage in hydrofullerides. *Appl. Phys. A: Mater. Sci. Process.* **2004,** *78* (7), 995-1000.

(7) Sankaran, M.; Muthukumar, K.; Viswanathan, B., Boron-substituted fullerenes - Can they be one of the options for hydrogen storage? *Fullerenes Nanotubes and Carbon Nanostructures* **2005,** *13* (1), 43-52.

(8) Chambers, A.; Park, C.; Baker, R. T. K.; Rodriguez, N. M., Hydrogen storage in graphite nanofibers. *J. Phy. Chem. B* **1998,** *102* (22), 4253-4256.

(9) Park, C.; Anderson, P. E.; Chambers, A.; Tan, C. D.; Hidalgo, R.; Rodriguez, N. M., Further studies of the interaction of hydrogen with graphite nanofibers. *J. Phys. Chem. B* **1999,** *103* (48), 10572-10581.

(10) Liu, C.; Fan, Y. Y.; Liu, M.; Cong, H. T.; Cheng, H. M.; Dresselhaus, M. S., Hydrogen storage in single-walled carbon nanotubes at room temperature. *Science* **1999,** *286* (5442), 1127-1129.

(11) Hirscher, M.; Becher, M.; Haluska, M.; Quintel, A.; Skakalova, V.; Choi, Y. M.; Dettlaff-Weglikowska, U.; Roth, S.; Stepanek, I.; Bernier, P.; Leonhardt, A.; Fink, J., Hydrogen storage in carbon nanostructures. *J. Alloys Compd.* **2002,** *330*, 654-658.

(12) Nossal, J.; Saini, R. K.; Alemany, L. B.; Meier, M.; Billups, W. E., The synthesis and characterization of fullerene hydrides. *Eur. J. Org. Chem.* **2001,** (22), 4167-4180.

(13) Withers, J. C.; Loutfy, R. O.; Lowe, T. P., Fullerene commercial vision. *Fullerene Sci. Technol.* **1997,** *5* (1), 1-31.

(14) Haufler, R. E.; Conceicao, J.; Chibante, L. P. F.; Chai, Y.; Byrne, N. E.; Flanagan, S.; Haley, M. M.; Obrien, S. C.; Pan, C.; Xiao, Z.; Billups, W. E.; Ciufolini, M. A.; Hauge, R. H.; Margrave, J. L.; Wilson, L. J.; Curl, R. F.; Smalley, R. E., Efficient Production of C_{60} (Buckminsterfullerene), $C_{60}H_{36}$, and the Solvated Buckide Ion. *J. Phys. Chem.* **1990,** *94* (24), 8634-8636.

(15) Henderson, C. C.; Cahill, P. A., $C_{60}H_2$ - Synthesis of the Simplest C_{60} Hydrocarbon Derivative. *Science* **1993,** *259* (5103), 1885-1887.

(16) Jin, C. M.; Hettich, R.; Compton, R.; Joyce, D.; Blencoe, J.; Burch, T., Direct Solid-Phase Hydrogenation of Fullerenes. *J. Phys. Chem.* **1994,** *98* (16), 4215-4217.

(17) Cliffel, D. E.; Bard, A. J., Electrochemical Studies of the Protonation of C_{60}^- and C_{60}^{2-}. *J. Phys. Chem.* **1994,** *98* (33), 8140-8143.

(18) Darwish, A. D.; AbdulSada, A. K.; Langley, G. J.; Kroto, H. W.; Taylor, R.; Walton, D. R. M., Polyhydrogenation of [60]- and [70]fullerenes with Zn/HCl and Zn/DCl. *Synth. Met.* **1996,** *77* (1-3), 303-307.

(19) Attalla, M. I.; Vassallo, A. M.; Tattam, B. N.; Hanna, J. V., Preparation of Hydrofullerenes by Hydrogen Radical-Induced Hydrogenation. *J. Phys. Chem.* **1993,** *97* (24), 6329-6331.

(20) Billups, W. E.; Gonzalez, A.; Gesenberg, C.; Luo, W. M.; Marriott, T.; Alemany, L. B.; Saunders, M.; JimenezVazquez, H. A.; Khong, A., ^{3}He NMR spectra of highly reduced C_{60}. *Tetrahedron Lett.* **1997,** *38* (2), 175-178.

(21) Vasil'ev, Y.; Wallis, D.; Nuchter, M.; Ondruschka, B.; Lobach, A.; Drewello, T., From major to minor and back - a decisive assessment of $C_{60}H_{36}$ with respect to the Birch reduction of C_{60}. *Chem. Commun.* **2000,** (14), 1233-1234.

(22) Dunlap, B. I.; Brenner, D. W.; Schriver, G. W., Symmetrical Isomers of $C_{60}H_{36}$. *J. Phys .Chem.* **1994,** *98* (7), 1756-1757.

(23) Clare, B. W.; Kepert, D. L., Structures and Stabilities of Hydrofullerenes - Completion of a Tetrahedral Fused Quadruple Crown Structure and a Double Crown Structure at $C_{60}H_{36}$. *Theochem.-J. Mol. Struc.* **1994,** *110* (3), 181-189.

(24) Nossal, J.; Saini, R. K.; Sadana, A. K.; Bettinger, H. F.; Alemany, L. B.; Scuseria, G. E.; Billups, W. E.; Saunders, M.; Khong, A.; Weisemann, R., Formation, isolation, spectroscopic properties, and calculated properties of some isomers of $C_{60}H_{36}$. *J. Am. Chem. Soc.* **2001,** *123* (35), 8482-8495.

(25) Henderson, C. C.; Rohlfing, C. M.; Gillen, K. T.; Cahill, P. A., Synthesis, Isolation, and Equilibration of 1,9-$C_{70}H_2$ and 7,8-$C_{70}H_2$. *Science* **1994,** *264* (5157), 397-399.

(26) Darwish, A. D.; Kroto, H. W.; Taylor, R.; Walton, D. R. M., Hydrogenation of [76]-, [78]- and [84]-fullerenes: Cage degradation. *J. Chem. Soc., Perkin Trans. 2* **1996,** (7), 1415-1418.

(27) Zhang, J. P.; Wang, N. X.; Yang, Y. X.; Yu, A. G., Hydrogenation of [60]fullerene with lithium in aliphatic amines. *Carbon* **2004,** *42* (3), 675-676.

(28) Darwish, A. D.; Abdulsada, A. K.; Langley, G. J.; Kroto, H. W.; Taylor, R.; Walton, D. R. M., Polyhydrogenation of [60]-Fullerenes and [70]-Fullerenes. *J. Chem. Soc., Perkin Trans. 2* **1995,** (12), 2359-2365.

(29) Taylor, R.; Walton, D. R. M., The Chemistry of Fullerenes. *Nature* **1993,** *363* (6431), 685-693.

(30) Wang, C. R.; Shi, Z. Q.; Wan, L. J.; Lu, X.; Dunsch, L.; Shu, C. Y.; Tang, Y. L.; Shinohara, H., $C_{64}H_4$: Production, isolation, and structural characterizations of a stable unconventional fulleride. *J. Am. Chem. Soc.* **2006,** *128* (20), 6605-6610.

(31) Fu, W. J.; Xu, L. S.; Azurmendi, H.; Ge, J. C.; Furher, T.; Zuo, T. M.; Reid, J.; Shu, C. Y.; Harich, K.; Dorn, H. C., ^{89}Y and ^{13}C NMR Cluster and Carbon Cage

Studies of an Yttrium Metallofullerene Family, $Y_3N@C_{2n}$ (n = 40-43). *J. Am. Chem. Soc.* **2009,** *131* (33), 11762-11769.

(32) Linnolahti, M.; Karttunen, A. J.; Pakkanen, T. A., Remarkably stable icosahedral fulleranes: $C_{80}H_{80}$ and $C_{180}H_{180}$. *ChemPhysChem* **2006,** *7* (8), 1661-1663.

(33) Krause, M.; Dunsch, L., Isolation and characterisation of two $Sc_3N@C_{80}$ isomers. *ChemPhysChem* **2004,** *5* (9), 1445-1449.

(34) Zhao, Y. F.; Heben, M. J.; Dillon, A. C.; Simpson, L. J.; Blackburn, J. L.; Dorn, H. C.; Zhang, S. B. B., Nontrivial tuning of the hydrogen-binding energy to fullerenes with endohedral metal dopants. *J. Phys. Chem. C* **2007,** *111* (35), 13275-13279.

(35) Wilson, L. J.; Cagle, D. W.; Thrash, T. P.; Kennel, S. J.; Mirzadeh, S.; Alford, J. M.; Ehrhardt, G. J., Metallofullerene drug design. *Coord. Chem. Rev.* **1999,** *192*, 199-207.

(36) Wilson, L. J., Medical Application of Fullerenes and Metallofullerenes. *Electrochem. Soc. Interface•Winter* **1999**, 24-28.

(37) Kato, H.; Kanazawa, Y.; Okumura, M.; Taninaka, A.; Yokawa, T.; Shinohara, H., Lanthanoid endohedral metallofullerenols for MRI contrast agents. *J. Am. Chem. Soc.* **2003,** *125* (14), 4391-4397.

(38) Shu, C. Y.; Corwin, F. D.; Zhang, J. F.; Chen, Z. J.; Reid, J. E.; Sun, M. H.; Xu, W.; Sim, J. H.; Wang, C. R.; Fatouros, P. P.; Esker, A. R.; Gibson, H. W.; Dorn, H. C., Facile Preparation of a New Gadofullerene-Based Magnetic Resonance Imaging Contrast Agent with High H-1 Relaxivity. *Bioconjugate Chem.* **2009,** *20* (6), 1186-1193.

(39) Wharton, T.; Wilson, L. J., Toward fullerene-based X-ray contrast agents: design and synthesis of non-ionic, highly-iodinated derivatives of C_{60}. *Tetrahedron Lett.* **2002,** *43* (4), 561-564.

(40) Cagle, D. W.; Alford, J. M.; Kennel, S. J.; Mirzadeh, S. B.; Thrash, T. P.; Wilson, L. J., $^{166}Ho@C_{82}$: Exploring the use of metallofullerenes in nuclear medicine. *Abstr. Am. Chem. Soc.* **1998,** *215*, U959-U959.

(41) Zhang, S. R.; Sun, D. Y.; Li, X. Y.; Pei, F. K.; Liu, S. Y., Synthesis and solvent enhanced relaxation property of water-soluble endohedral metallofullerenols. *Fullerene Sci. Technol.* **1997,** *5* (7), 1635-1643.

(42) Iezzi, E. B.; Cromer, F.; Stevenson, P.; Dorn, H. C., Synthesis of the first water-soluble trimetallic nitride endohedral metallofullerols. *Synth. Met.* **2002,** *128* (3), 289-291.

(43) Sun, D. Y.; Liu, Z. Y.; Guo, X. H.; Liu, S. Y., Unusual polymerization behavior of water-soluble fullerenols in laser desorption ionization time-of-flight mass spectrometry. *Rapid Commun. Mass Spectrom.* **1997,** *11* (1), 114-116.